

STRUCTURAL INVESTIGATION OF G-PROTEIN SIGNALING IN PLANTS

by
BURCU KAPLAN TÜRKÖZ

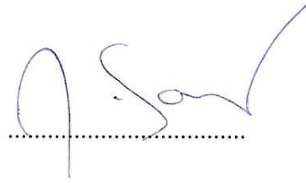
Submitted to the Graduate School of Engineering and Natural Sciences
in partial fulfillment of
the requirements for the degree of
Doctor of Philosophy

Sabancı University
2009

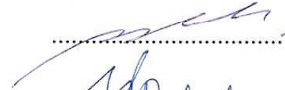
STRUCTURAL INVESTIGATION OF G-PROTEIN SIGNALING IN PLANTS

APPROVED BY:

Prof. Dr. Zehra SAYERS
(Dissertation Supervisor)



Prof. Dr. Beki KAN



Assoc. Prof. Hikmet BUDAK



Prof. Dr. Michel KOCH



Assoc. Prof. Uğur SEZERMAN



DATE OF APPROVAL: 10.08.2009

© BURCU KAPLAN TÜRKÖZ 2009

All Rights Reserved

STRUCTURAL INVESTIGATION OF G-PROTEIN SIGNALING IN PLANTS

Burcu KAPLAN TÜRKÖZ

Biological Sciences and Bioengineering, PhD Dissertation, 2009

Supervisor: Prof. Dr. Zehra Sayers

Keywords: Heterotrimeric G protein, *Arabidopsis thaliana*, recombinant protein, biophysics, X-ray scattering

ABSTRACT

Heterotrimeric G proteins, composed of alpha, beta and gamma subunits, are a major group of signaling molecules in eukaryotic organisms. There is lack of direct biophysical and structural data for the plant heterotrimer unlike its mammalian counterparts.

Heterotrimeric G protein subunits from *Arabidopsis* were cloned and purified. The alpha subunit, GPA1 was purified from *Pichia*, with a GTP binding ratio of 0.3 mole GTP/ mole protein. The recombinant beta (AGB1) and gamma (AGG1 and AGG2) subunits were isolated from *E.coli* and preliminary purification strategies were optimized. This is to our knowledge, the first study to report recombinant production of a plant beta subunit and in vitro dimerization of purified AGB1-AGG2 subunits.

GPA1 was purified in two different biophysical states, as characterized by UV-spectroscopy, dynamic light scattering, circular dichroism spectropolarimetry and mass spectrometry. The stable oligomeric form had higher GTP hydrolysis activity and a GDP binding ratio of 1.4 mole GDP/mole protein. Indirect biophysical evidence points to interaction of GPA1 with receptor mimetic compounds, membrane fractions of yeast

cells and the recombinant AGB1-AGG2 dimer. This is to our knowledge, the first study showing the expression and purification of the plant alpha subunit from a eukaryotic expression system and its detailed biophysical characterization.

Small angle solution X-ray scattering (SAXS) measurements verified the oligomeric nature of the protein, which was stabilized via detergent micelles. The detergent content was verified by proton nuclear magnetic resonance spectroscopy. SAXS patterns were consistent with dimeric protein complexing with micelles. Rigid body modeling was used for further modeling.

BİTKİ G-PROTEİN SİNYAL İLETİMİNİN YAPISAL ARAŞTIRMALARI

Burcu KAPLAN TÜRKÖZ

Biyoloji Bilimleri ve Biyomühendislik, Doktora Tezi, 2009

Tez Danışmanı: Prof. Dr. Zehra Sayers

Anahtar kelimeler: Heterotrimerik G protein, Arabidopsis thaliana, rekombinant protein, biyofizik, X-ışını saçılımı

ÖZET

Heterotrimerik G proteinleri alfa, beta ve gamma altbirimlerinden oluşan ve ökaryot organizmalarda bulunan sinyal iletim molekülleridir. Memeli heterotrimerinin biyofiziksel ve yapısal özellikleri üzerine kapsamlı incelemeler olmasına rağmen bitki proteinleri üzerine çalışmalar sayılıdır.

Bu çalışma kapsamında, Arabidopsis heterotrimerik G protein altbirimleri klonlandı ve saflaştırıldı. Pichia hücrelerinden saflaştırılan alfa altbiriminde (GPA1) bir mol proteine 0.3 mol GTP bağlandığı gösterildi. Rekombinant beta (AGB1) ve gama (AGG1 ve AGG2) altbirimleri E.coli hücrelerinde üretildi ve ilk saflaştırma aşamaları optimize edildi. Bu tez bitki beta altbiriminin rekombinant olarak üretilmesi ve saflaştırılmış AGB1-AGG2 etkileşimini gösteren ilk çalışmadır.

GPA1 proteinin iki farklı biyofiziksel formda saflaştırıldığı UV spektroskopisi, dinamik ışık saçılımı, dairesel dikroizm spektroskopisi ve kütle spektrometrisi ile gösterildi. Kararlı oligomerik formun GTP hidroliz aktivitesi daha yüksek ve GDP bağlama oranı da 1.4 mol GDP/mol protein'dir. Biyofiziksel bulgular GPA1 proteinin reseptör benzeri bileşikler, maya hücrelerinin zar kesimleri ve rekombinant AGB1-AGG2 dimeri ile etkileştiğini dolaylı olarak göstermiştir. Bu tez, bitki alfa altbiriminin bir ökaryot ekspresyon sistemi kullanılarak saflaştırılması ve detaylı biyofiziksel karakterizasyonu üzerine ilk çalışmadır.

Küçük açı X-ışını saçılımı (SAXS) ölçümleri oligomerik proteinin deterjan miselleriyle birarada saflaştırıldığını göstermiştir. Deterjan misellerinin miktarı proton nükleer magnetik rezonans spektroskopisi ile tespit edildi. SAXS sonuçları GPA1 proteinin dimerik protein-misel kompleksi halinde olduğunu gösterdi. Yapısal modeller katı cisim modellemesi kullanılarak hesaplandı.

To my family and to the ones who “became my family” with their love

℘

To the memory of my beloved aunt Hanife Abay

Aileme ve sevgileriyle “aileden” olanlara

℘

Sevgili halam Hanife Abay’ın anısına

ACKNOWLEDGEMENTS

I would like to thank my supervisor, Prof. Dr. Zehra Sayers for all her motivation, encouragement, and support. She taught me how to learn, how to teach, how to plan and perform experiments and how to conclude on results. She was with us in the lab, in her office and at EMBL during long, cold, sleepless, tiring hours and thus taught us how to be patient and resistant. She helped me very much on writing this thesis and I will appreciate this all my life. We were together for the last 6 years and I know we have much more time to share. I believe the best way to thank her truly; is to continue to do research improving myself everyday.

I would like to thank all committee members, Prof Dr. Michel Koch, Prof. Dr, Beki Kan, Dr. Hikmet Budak, Dr. Uğur Sezerman, Prof. Dr. İsmail Çakmak and Dr. Alimet Özen for their valuable comments and revisions on the dissertation draft.

Prof.Dr. Michel Koch gave his precious time to read and correct my drafts, to guide me in science and in life. I am very lucky that I had the chance to meet him; I shaked hands with Michel Koch ☺. He always has an answer to my questions; I know I need to work very hard to have some of the answers one day. I would like to thank him deeply for everything.

I would like to thank Prof Dr. Beki Kan for being in my thesis comitte, for her help in data analysis and for allowing me to use lab facilities of Marmara University Biophysics Department.

I want to thank to Dr. Alpay Taralp, he was always there for me when I needed an idea or just to take a breathe. His encouragement and support will always be appreciated and will be needed.

I would like to express my special thanks to Dr. Alimet Özen. I had the chance to work with her in teaching NS 102 nearly every spring and summer semester during my

PhD. I was very lucky that I could learn the tips of teaching and communicating with students from her. I will always respect and remember her patience and enthusiasm in teaching.

I also want to thank very much to all the “hoca”s of our faculty, for their smiling faces and for asking how things are going. My special thanks will go to Dr. Wilfried Meidl, Dr. Selim Çetiner, Dr. Mehmet Ali Gülgün, Dr. Clewa Ow-Yang, Dr. Canan Atılğan, Dr. Gürdal Ertek, Dr. Emrah Kalemci, Dr. Zafer Gedik, Dr. Ünal Ertan, Dr. Hüveyda Başağa, Dr. Levent Öztürk, Dr. Batu Erman, Dr. Mehmet Ali Alpar, Dr. Alev Topuzoğlu, Dr. Yusuf Menceloğlu, Dr. Yuda Yürüm and Dr. Albert Erkip.

I want to thank to all my friends for their support and love.

Some friends, we met here but they left SU. Yet, they were always with me, supporting and cheering me up. Thank you my dear friends, Elanur Şireli, Burcu Dartan, Çetin Baloğlu and Özgür Kütük.

Some of my friends, they were not in the lab with me, nor do they belong to SU. But we shared a lot during this long and difficult path. Some of them are very old friends, thank you staying with me so long, some I met later, thank you for choosing to stay near. Thank you my friends Özge İnce, Ufuk Kara, Burcu İnce, Bahar Karaoğlu, Çetin Meriçli, Yeşim-Onur Sarioğlu, Deniz-Osman Yokarıbaş, Ezgi Ozan, Alkım Eren, Levent-Sakine Uslu Yaşam-Selahattin Okur, Selin-Ersin Özdemir, Zeynep-Erhan Ermişoğlu, Güner Türköz, Barış Kılınç, Seda-Murat Üner and Banu Bozlu.

It was not always easy to keep up in the lab. I want to thank for the ones who helped me to breathe in the lab; Bahar Soğutalmaz Özdemir, Özgür Gül, Mert Balkan, Kaan Yılcıoğlu, Tuğsan Tezil. Nalan Liv, Elif Damla Arışan, Emel Durmaz, Esen Doğan, Zeynep Işık, Ebru Kaymak, Özge Canlı, Özge Cebeci, Geraldine Mitou, Çağrı Bodur, Gözde Korkmaz, İzzet Akçay, Devrim Özarslan, Gamze Günal, Can Timuçin, Yekta Yamaner and Derin Demiroğlu. I want to thank very much to my little lab sisters, who always had smiling and asking eyes, Deniz Uğur and Ceren Saygı.

There were always smiling faces around in SU, sometimes I was feeling that you were waiting for me when I needed a warm voice. Thank you all my friends, İbrahim İnanç, Ayça Çeşmeliolu, İstem Özen, Çınar Öncel, Özgür Bozat, Alper Küçükural, Aydın and Isumi Albayrak, Alp Bassa, Emel Yeşil, Murat Mülayim, Özlem Aykut, Burcu Saner, Kazim Acatay, Ilknur Durgar El-Kahlout, Yasser Ibrahim Ahmed El Kahlout, Mustafa Parlak, Mehmet Ozdemir, Esen Aksoy, Yunus Sarıkaya and Mehmet Karaca.

I want to thank to members of Marmara University Biophysics department, Dr. Oya Orun, Dr. Pınar Tiber and Dr. Cevdet Nacar for sharing their experience, lab equipment and friendship with me. They are the ones who made me convince myself that I am not the only one.

The hardest times were probably the endless x-ray nights at the beamline, waiting for the good data and trying not to sleep. I want to thank Filiz Yeşilirmak, Filiz Çollak, Onur Gökçe, Gizem Dinler and Elif Alpoge for the motivation and group work. At the end we had lots of data which we tried to fit to something logical. I want to thank very much to Dr. Dimitri Svergun, Dr. Peter Konarev, Dr. Maxim Pethukov, Dr. Manfred Roessle, Alexey Kikhney, and Adam Round for their efforts in data analysis and all EMBL Hamburg members for their hospitality and coffee room.

I want to thank to all the laboratory specialists; Tuğba Baytekin Birkan, Burçin Yıldız, Bülent Köroğlu, Mehmet Güler, Atilla Yazıcı, Veli Bayır and Sibel Pürçüklü for their generous help about all the equipment puzzles that I could not solve. I know everything would be a mess without the presence of Tuğba, she had magical hands, with one touch she was making the equipment (which we thought was broken) work. I want to thank very much to Burçin Yıldız for her generous help in proton NMR data collection and analysis.

I also want to thank all the administrative staff, Zuhul Bakkal Yazıcı, Işıl Önal Karabudak, Zehra Öner and Esen Çetinkaya for their patience on my endless questions starting with “How can I...”

Last but not the least, some people deserve special thanks, Mustafa abi his tea and chitchat, Dr.Zehra Kalkan for keeping me healthier, Nurcan for making the food bearable with her smile.

Thank you all SU members for making me happy and strong at the hardest times.

I will always remember the good times in happiness.

3 reasons why I did not quit;

Teaching

The lovely, curious and happy faces of all my students. I want to thank to all students whom I had the chance to teach and work together, and especially the ones who were always right behind me; Sedef İskit (my right flipper), Simin Öz (happy and cheerful), Duygu Öztürk, Berk Baysan, Sine Yağanoğlu, Anıl Aktürk (gel machine), Mert Aydın (soldier), Avdar Şan and Ali Fuat Kısakürek. It is a great pleasure to see them becoming successful scientists.

Friendly conversations

The supporting, motivating and winding lunches, after lunches and coffee sessions with Tuğba Baytekin Birkan, Zuhale Bakkal Yazıcı, Bülent Köroğlu, Burak Birkan, Atilla Yazıcı and Ali Kasal. I want to thank deeply to my friends for being with me not only at the good times but also at the bad times.

Love, support and much more

The inner faith and strength in me, which I assume developed through living with my family.

I want to thank to every single member of my big family; all of my relatives from my mother's and father's families for always loving and supporting me.

I want to thank especially to;

Muammer Kaplan, my father for teaching me to be proud, strong and determined,

Sevgi Kaplan, my mother for raising me surrounded with love but still teaching me how to stand on my own legs and to be independent,

Yigitcan Kaplan, my brother for always showing me the other side of the mirror and for raising the feeling of responsibility in me,

Ali Kaplan, my uncle, for being a role model as an engineer and a teacher,

Hanife Abay, my aunt for always supporting and encouraging me,

Hatice Kaplan, my grandmother for her endless will in learning and wondering about the universe

Mehmet Türköz; my husband, besides all his love and support, I want to thank him for being the devils advocate in all the issues and decisions in my life.

Burcu Kaplan Türköz

August 2009, Istanbul

TABLE OF CONTENTS

CHAPTER 1	1
1 INTRODUCTION	1
CHAPTER 2	6
2 BACKGROUND	6
2.1 The Mammalian Heterotrimer	6
2.2 Structure- function relations of heterotrimeric G proteins.....	7
2.3 The plant heterotrimeric G proteins	19
2.3.1 GPA1	20
2.3.2 AGB1 and AGG1/AGG2.....	24
2.3.3 Signaling Components	28
2.4 The plant heterotrimer	29
2.5 Biophysical Approach.....	32
2.5.1 Circular Dichorism Spectropolarimetry.....	32
2.5.2 The use and detection of detergents in membrane protein purification..	34
2.5.3 Small Angle Solution X-ray Scattering	35
CHAPTER 3	36
3 MATERIALS AND METHODS.....	36
3.1 Materials	36
3.1.1 Chemicals.....	36

3.1.2	Molecular biology kits	36
3.1.3	Other materials.....	37
3.1.4	Equipment.....	37
3.1.5	Genes	37
3.1.6	Buffers and solutions	37
3.1.7	Culture medium	38
3.1.8	Sequencing.....	39
3.2	Methods	39
3.2.1	Culture growth	39
3.2.2	PCR.....	40
3.2.3	Cloning.....	41
3.2.4	Transformation.....	42
3.2.5	Agarose gel electrophoresis	42
3.2.6	Verification and Sequencing.....	42
3.2.7	Expression screen for GST-AGB1 and GST-AGG1	43
3.2.8	Expression screen for RGS-his-AGB1 and RGS-his-AGG2.....	44
3.2.9	Large Scale Expression from <i>E.coli</i> cultures.....	44
3.2.10	Purification of recombinant AGB1 and AGG2	44
3.2.11	Large Scale Expression of GPA1-myc-his	46
3.2.12	Purification of recombinant GPA1	46
3.2.13	SDS-PAGE	51

3.2.14	Native-PAGE /TCA Stain.....	51
3.2.15	Western blotting.....	52
3.2.16	Protein Concentration Determination.....	52
3.2.17	GTP Binding Assay.....	53
3.2.18	GTPase activity Assay.....	54
3.2.19	Biophysical characterization.....	55
CHAPTER 4.....		59
4	RESULTS.....	59
4.1	Optimization of Expression of GPA1.....	59
4.2	Nickel-Affinity Purification of GPA1.....	65
4.2.1	Small scale purifications: HisTrap™ HP.....	65
4.2.2	Large Scale GPA1 Purification.....	69
4.2.3	Affinity Purification with Detergents.....	78
4.3	Anion Exchange.....	85
4.3.1	Obtaining two biophysically different GPA1 pools.....	87
4.3.2	Anion Exchange, load with detergent.....	91
4.4	Size Exclusion Chromatography.....	100
4.5	Functional Assays.....	115
4.5.1	GDP Binding.....	115
4.5.2	GTP Binding.....	119
4.5.3	GTP Hydrolysis.....	121

4.6	Biophysical Characterization.....	128
4.6.1	Membrane Localization.....	128
4.6.2	Interaction with AGB1/AGG2 Dimer.....	129
4.6.3	Analysis for presence of detergents.....	130
4.6.4	MALDI-TOF MS.....	137
4.7	Structural Characterization of GPA1.....	140
4.7.1	Secondary Structure Analysis.....	140
4.7.2	SAXS data analysis.....	149
4.8	Expression of AGB1 and AGG1 / 2 subunits.....	163
4.8.1	Cloning into pGEX-4T-2 vector.....	163
4.8.2	Cloning into pQE-80L vector.....	166
4.8.3	Expression and Purification of AGB1.....	168
4.8.4	Expression and Purification of GST-AGG1.....	176
4.8.5	Expression and Purification of RGS-his-AGG2.....	177
4.8.6	Dimerization.....	185
CHAPTER 5.....		187
5	DISCUSSION.....	187
5.1	Purification of GPA1.....	189
5.2	Expression and Purification of AGB1, AGG1 and AGG2.....	196
5.2.1	Dimerization.....	198
5.3	Heterotrimer Formation.....	198

CHAPTER 6	199
6 CONCLUSIONS	199
REFERENCES	201
APPENDIX A	209
APPENDIX B	211
APPENDIX C	212
APPENDIX D	215
APPENDIX E	217
APPENDIX F	221
APPENDIX G	229
APPENDIX H	231
APPENDIX I	236
APPENDIX J	242
APPENDIX K	244
APPENDIX L	249
APPENDIX M	255
APPENDIX N	256

LIST OF FIGURES

Figure 2.1 The classical model for receptor mediated G protein activation [13].	7
Figure 2.2: 2.0 Å structure of the heterotrimeric complex 1GOT.	8
Figure 2.3: The models for rhodopsin-transducin heterotrimer complex.	16
Figure 2.4: Unrooted tree from CLUSTALW alignment of all human G α and GPA1.	21
Figure 2.5: CLUSTALW alignment of human G α i family members and GPA1.	22
Figure 2.6: CLUSTALW alignment of human and arabidopsis G β protein sequences.	25
Figure 2.7: CLUSTALW alignment of human gamma subunits, AGG1 and AGG2.	26
Figure 2.8: 1GOT (A) and the homology modeled Arabidopsis complex (B) [113].	30
Figure 2.9: Far-UV CD spectral analysis of secondary structural elements.	33
Figure 2.10: The near UV CD spectrum for type II dehydroquinase from <i>Streptomyces coelicolor</i> . Figure taken from [116].	33
Figure 4.1 Growth of GS115 cells expressing GPA1 in MMH or BMMY.	60
Figure 4.2: Comparison of growth of GS115 cells with the empty vector (pPICZC), the LacZ gene (pPICZC-LacZ) and the GPA1 gene (pPICZC-GPA1).	60

Figure 4.3: Comparison of growth of GS115 cells expressing GPA1 in BMMY medium after induction with 0.5 % (---) or 1 % (-) methanol.	61
Figure 4.4: Pellet weight as function of methanol induction time.	62
Figure 4.5: Optical densities of cell cultures as a function of methanol addition time.	62
Figure 4.6: Affinity (HisTrap™ HP column) purified GPA1 amount as function of methanol addition time.	63
Figure 4.7: Comparison of pellet weight for cultures with methanol addition at 24 hours and at 6 th and 24 th hours after induction.	64
Figure 4.8: Amount of Ni-affinity purified GPA1 as function of the methanol addition time.	64
Figure 4.9: Growth of GPA1-GS115 cells in induction medium.	65
Figure 4.10: Elution of GPA1 from HisTrap™ HP column.	67
Figure 4.11: 12% SDS-PAGE analysis of HisTrap™ HP fractions.	67
Figure 4.12: Elution of GPA1 from HisTrap™ HP column.	68
Figure 4.13: 12% SDS-PAGE analysis of HisTrap™ HP fractions.	68
Figure 4.14: 12% SDS-PAGE analysis of Ni-affinity fractions.	70
Figure 4.15: Comparison of UV spectra of Ni-affinity elutions; E1 and E2.	71
Figure 4.16: Western analysis of Ni-affinity elutions after storage at -20 °C.	71
Figure 4.17: DLS, size distributions by intensity (A) and number (B) of Ni-affinity GPA1.	72
Figure 4.18: Comparison of UV spectra of Ni-affinity elutions; before and after dialysis.	73

Figure 4.19: Comparison of fresh and -20 °C stored samples with different additives.	74
Figure 4.20: 12% SDS-PAGE (A) and Western (B) analysis of Ni-affinity elutions.	75
Figure 4.21: A: HiPrep™ 26/10 Desalting chromatogram. B: 12% SDS-PAGE analysis.	76
Figure 4.22: Comparison of UV-Vis spectra of desalting column load and desalted pool.	77
Figure 4.23: DLS size distributions by intensity (A) and number (B) of fresh desalted pool, without additives.	77
Figure 4.24: 12% SDS-PAGE analysis of Ni-affinity (Triton X-100) fractions.	79
Figure 4.25: UV spectra of Ni-affinity pool (Triton X-100 and AlF_4^-).	79
Figure 4.26: DLS size distributions by intensity (A) and volume (B) of Ni-affinity purified GPA1 (Triton X-100).	80
Figure 4.27: 12% SDS-PAGE analysis of Ni-affinity (Triton X-100) fractions.	81
Figure 4.28: DLS size distributions by intensity (A) and volume of Ni-affinity pool after dialysis.	82
Figure 4.29: 12% SDS-PAGE analysis of Ni-affinity (Lubrol-PX) fractions.	83
Figure 4.30: Western analysis of Ni-affinity (Lubrol-PX) elution E2.	83
Figure 4.31: DLS size distributions by intensity (A) and volume (B) of concentrated Ni-NTA pool.	84
Figure 4.32: DLS size distributions by intensity (A) and volume (B) of N-affinity pool after dialysis.	84
Figure 4.33: Elution of GPA1 from a HiTrap Q HP column with NaCl gradient.	88
Figure 4.34: 12% SDS-PAGE analysis of anion exchange fractions.	88

Figure 4.35: DLS size distributions by intensity (A) and number (B) of anion exchange pool 3 before dialysis.	89
Figure 4.36: DLS size distributions by intensity (A) and number (B) of anion exchange pool 4 before dialysis.	89
Figure 4.37: DLS size distribution by intensity (A) and number (B) for pool 3 after dialysis.	89
Figure 4.38: DLS size distribution by intensity (A) and number (B) for pool 4 after dialysis.	90
Figure 4.39: 12% SDS-PAGE and Silver stain analysis of anion exchange pools.	90
Figure 4.40: Elution of GPA1 from a HiTrap Q HP column with NaCl gradient.	92
Figure 4.41: 12% SDS-PAGE analysis of anion exchange fractions.	92
Figure 4.42: Comparison of UV spectra for pool 3, 4 and 5 (after dialysis).	93
Figure 4.43: DLS size distributions by intensity (A), volume (B) and number (C) of fresh pool 3 in final dialysis buffer.	94
Figure 4.44: DLS size distributions by intensity (A) and volume (B) of fresh pool 4 in final dialysis buffer.	94
Figure 4.45: 12% SDS-PAGE analysis of anion exchange pools with Silver stain.	95
Figure 4.46: Western analysis of Ni-affinity and anion exchange fractions.	95
Figure 4.47: DLS size distributions by intensity (A), volume (B) and number (C) of lyophilized and resuspended pool 3 in final dialysis buffer.	96
Figure 4.48: DLS size distributions by intensity (A), volume (B) and number (C) of lyophilized and resuspended pool 4 in final dialysis buffer.	96
Figure 4.49: Elution of GPA1 from a HiTrap Q HP column with NaCl gradient.	97
Figure 4.50: 12% SDS-PAGE analysis of anion exchange pools.	98

Figure 4.51: UV-vis spectra of pool 3 and pool 4 GPA1 and corresponding filtrates.	98
Figure 4.52: DLS size distributions by intensity (A) and number (B) of pool 3 GPA1.	99
Figure 4.53: DLS size distributions by intensity (A) and number (B) of pool 4 GPA1.	99
Figure 4.54: Elution pattern of GPA1 from S-300 HR 16/60 column with Buffer A.	102
Figure 4.55: 12% SDS-PAGE analysis of S-300 (Buffer A) fractions.	103
Figure 4.56: Comparison of UV spectra of GPA1 eluted in different elution volumes.	104
Figure 4.57: DLS size distributions by intensity (A) and volume (B) of concentrated GPA1 (column load).	104
Figure 4.58: DLS size distributions by intensity (A) and volume (B) of peak 1 fraction 32 ml.	104
Figure 4.59: DLS size distributions by intensity (A) and volume (B) of peak 2 fraction 44 ml.	105
Figure 4.60: DLS size distributions by intensity (A) and number (B) of peak 3 fraction 54 ml.	105
Figure 4.61: DLS size distributions by intensity (A) and volume (B) of peak 4 fraction 60 ml.	105
Figure 4.62: Elution pattern of GPA1 from S-300 HR 16/60 column with Buffer B.	106
Figure 4.63: 12% SDS-PAGE analysis of S-300 HR 16/60 column peak 2 fractions.	106
Figure 4.64: UV-vis spectra of S-300 peak 2 fractions.	107
Figure 4.65: DLS size distributions by intensity (A) and volume (B) of a S-300 peak 2 pool. Samples was stored at -80 °C.	107
Figure 4.66: Elution pattern of GPA1 from S-300 HR 16/60 column with Buffer C.	108

Figure 4.67: 12% SDS-PAGE analysis of Ni-affinity and S-300 (Buffer C) fractions.	109
Figure 4.68: Western analysis of S-300 eluted GPA1 before and after dialysis.	109
Figure 4.69: DLS size distribution by intensity (A) and volume (B) of 57 ml (top) fraction stored at +4 °C.	110
Figure 4.70: DLS size distribution by intensity (A) and volume (B) of 57.5 ml fraction stored at -80 °C.	110
Figure 4.71: Elution pattern of GPA1 from S-200 HR 16/60 column with Buffer D.	111
Figure 4.72: 12% SDS-PAGE analysis of S-200 (Buffer D) fractions.	111
Figure 4.73: UV spectra of S 200 fractions.	112
Figure 4.74: DLS size distributions by intensity (A) and volume (B) of void top fraction.	112
Figure 4.75: DLS size distributions by intensity (A) and volume (B) of 52 ml fraction.	112
Figure 4.76: Comparison of UV spectra of GPA1 (stg. 3---) and desalted pool (stg. 3.2-).	115
Figure 4.77: Comparison of UV spectra of GPA1 (stg 2.2) measured against different buffers.	116
Figure 4.78: Comparison of UV spectra of GPA1 (stg. 3.2) measured against different buffers.	117
Figure 4.79: Dependence of absorbance at 254 nm on GDP concentration in 50 mM Tris HCl, pH 8.0.	117
Figure 4.80: The UV spectra of different concentrations of GDP in Tris buffer.	119
Figure 4.81: UV-Vis Spectra of GDP filtrates of GPA1 from stg. 2.2 and 3.2.	119
Figure 4.82: Dependence of [³⁵ S]GTPγS binding to GPA1 (stg. 2.2) concentration.	120

Figure 4.83: Dependence of [³⁵ S]GTPγS binding to pool 3 (stg. 3.1.1) concentration.	120
Figure 4.84: Dependence of released ³² P on protein purity.	121
Figure 4.85: Time course of GTPase activity of 290 nM pool 3 GPA1 (stg 3.1.1).	122
Figure 4.86: Concentration dependence of GTPase activity of pool 3 GPA1 (stg. 3.1.1).	123
Figure 4.87: Concentration dependence of GTPase activity of pool 4 GPA1 (stg. 3.1.1).	123
Figure 4.88: Effect of detergent and MgCl ₂ on GTPase activity of pool 4 (stg. 3.1.1).	124
Figure 4.89: Time course of GTPase activity of 70 nM GPA1 (stg 3.2.1).	124
Figure 4.90: Concentration dependence of GTPase activity of GPA1 (stg. 3.2.1).	125
Figure 4.91 Effect of nucleotide competition on GTPase activity of GPA1 (stg.3.2.1).	126
Figure 4.92: Effects of receptor mimetics compound (MP) on GTPase activity of GPA1 (stg. 3.2.1.).	126
Figure 4.93: Western detection of GPA1 in membrane fractions of <i>P.pastoris</i> .	128
Figure 4.94: Western blot analysis of S-200 GPA1 (stg. 3.2.1, Lubrol-PX) fractions.	129
Figure 4.95: NMR spectrum for HND buffer (ppm values are given).	130
Figure 4.96: NMR spectrum of HND buffer (A) and 0.1% Lubrol-PX in HND (B).	131
Figure 4.97: NMR spectrum of HND buffer (A) and 0.1% Lubrol-PX in HND (B).	131
Figure 4.98: NMR spectrum of BSA in HND, with (A) or without (B) 0.1 % Lubrol.	132
Figure 4.99: NMR spectrum of GPA1 (stg. 3.2.1) (A) and 0.1% Lubrol (B) in HND.	132

Figure 4.100: Calculation of Lubrol-PX concentration from NMR spectrum of 0.1% Lubrol-PX in HND.	133
Figure 4.101: Calculation of Lubrol-PX concentration from NMR spectrum of GPA1 in HND.	134
Figure 4.102 NMR spectrum of 0.02 % Triton X-100 (A) and HND-GGM (B).	134
Figure 4.103: NMR spectrum of GPA1 (stg. 3.1.1) (A) and 0.02% Triton X-100 (B) in HND-GGM (B).	135
Figure 4.104: TCA stained 8% Native-PAGE analysis for detergents and GPA1.	136
Figure 4.105: 8% Native-PAGE analysis of GPA1 from different stages.	137
Figure 4.106: 12% SDS-PAGE analysis of samples used in native gel (Figure 4.105).	137
Figure 4.107: MALDI-TOF result and data analysis for pool 3 (stg. 2.2.1).	138
Figure 4.108: MALDI-TOF result and data analysis for pool 4 (stg. 2.2.1).	139
Figure 4.109: Far (A) and Near-UV (B) spectra of GPA1 (stg.2.1).	141
Figure 4.110: Far (A) and near -UV (B) spectra for GPA1 (stg.3.1, Triton X-100).	141
Figure 4.111: Far-UV (A) and Near-UV (B) CD spectra of pool 3 and pool 4 (stg.2.2.1).	142
Figure 4.112: Far-UV (A) and Near-UV (B) CD spectra of pool 3 and pool 4 (stg.3.1.1, Triton X-100).	143
Figure 4.113: Far-UV (A) and Near-UV (B) CD spectra of pool 3 and pool 4 (stg.3.1.1, Triton X-100 and AlF_4^-).	144
Figure 4.114: Far-UV (A) and Near-UV (B) CD spectra of pool 3 and pool 4 (stg. 3.1.1, Lubrol-PX).	144

Figure 4.115: Far-UV (A) and Near-UV (B) CD spectra for pool 3 with and without GTP γ S and MgCl $_2$.	146
Figure 4.116: Ellipticity of pool 3 with and without C48/80.	147
Figure 4.117: Ellipticity of pool 3 with and without 100 μ M of MP.	147
Figure 4.118: Ellipticity for pool 3 with and without 100 μ M Mas 7.	148
Figure 4.119: Intensity plot (A) and Guinier plot (B) of BSA.	150
Figure 4.120: The distance distribution function of BSA.	150
Figure 4.121: Intensity plot for anion exchange GPA1 pool 3.	151
Figure 4.122: Guinier plot for anion exchange GPA1 pool 3.	152
Figure 4.123: Comparison of scattering plots of GPA1 with different molecular masses.	154
Figure 4.124: A: Scattering pattern of S-200 pool 1 GPA1 (two consecutive measurements). B: Guinier plot for pool 1 GPA1, sR $_g$ limits 0.732-1.297.	154
Figure 4.125: Scattering plot (A) and Guinier plot (B) for S-200 pool 2. sR $_g$ limits: 0.808 to 1.202.	155
Figure 4.126: Scattering plot (A) and Guinier plot (B) for S-200 pool 3. sR $_g$ limits: 0.81-1.297.	155
Figure 4.127: Scattering plot (A) and Guinier plot (B) for S-200 pool 4. sR $_g$ limits: 0.867-1.302.	156
Figure 4.128: Scattering plot (A) and Guinier plot (B) of BSA (3.91 mg/ml). sR $_g$ limits 0.597-1.255.	156
Figure 4.129: DLS size distributions by intensity of GPA1 pool 1 (stg.3.2.1).	158
Figure 4.130: DLS size distributions by intensity of GPA1 pool 2 (stg.3.2.1).	158

Figure 4.131:DLS size distributions by intensity (A) and volume (B) GPA1 pool 4 (stg.3.2.1).	158
Figure 4.132: SASREF fit (g111e) to scattering curve.	159
Figure 4.133: SASREF fit (g111h) to scattering curve.	160
Figure 4.134: SASREF models.g111e (A) and g111h (B).	160
Figure 4.135: SUPCOMB superimposed model, g111er	161
Figure 4.136: Overlay of g111er (gray) with g111e (A) and g111h (B).	161
Figure 4.137: Crystal structure of 1GFI (Galphai bound to GDP and AlF_4^-).	161
Figure 4.138: Unit cell structure of 1GFI (Gi with GDP and AlF_4^-).	162
Figure 4.139: 1% Agarose gel electrophoresis analysis of PCR amplification of <i>AGBI</i> and <i>AGGI</i> fragments.	164
Figure 4.140: 1% Agarose gel electrophoresis analysis of restriction enzyme digestion for insertion into pGEX-4T-2. Lane 1: 100 bp. DNA Ladder Plus ®.	164
Figure 4.141: 1% Agarose gel electrophoresis analysis of colony PCR for pGEX-4T-2 constructs.	165
Figure 4.142: 1% Agarose gel electrophoresis analysis of restriction enzyme digestion.	165
Figure 4.143: 1% Agarose gel electrophoresis analysis of PCR amplification of <i>AGBI</i> and <i>AGG2</i> with primers designed for pQE-80L.	166
Figure 4.144: 1% Agarose gel electrophoresis analysis of colony PCR with <i>AGBI</i> primers.	167
Figure 4.145: 1% Agarose gel electrophoresis analysis of colony PCR with <i>AGG2</i> primers.	167

Figure 4.146: 1% Agarose gel electrophoresis analysis of restriction enzyme digestion of selected plasmids. Lane 5: O'GeneRuler Mix ®.	168
Figure 4.147: 12% SDS-PAGE analysis of GST-AGB1 expression at 18 ° C.	169
Figure 4.148: Western analysis of RGS-his-AGB1 expression.	170
Figure 4.149: HisTrap HP column chromatogram of elution of RGS-his-AGB1 with linear imidazole and pH gradient.	172
Figure 4.150: 12% SDS-PAGE analysis of HisTrap HP column fractions.	172
Figure 4.151: 12% SDS-PAGE analysis of HisTrap HP column fractions.	173
Figure 4.152: Western analysis of HisTrap HP column fractions.	173
Figure 4.153 HisTrap HP column chromatogram of elution of RGS-his-AGB1 with a linear imidazole gradient.	174
Figure 4.154: 12% SDS-PAGE analysis of HisTrap HP column fractions.	174
Figure 4.155: Western analysis of HisTrap HP column fractions.	175
Figure 4.156: Western analysis RGS-his-AGB1 expression from Rosetta 2 (DE3) cells.	176
Figure 4.157: 12% SDS-PAGE analysis of GST-AGG1 expression at 18 ° C.	177
Figure 4.158: Western analysis of RGS-his-AGG2 expression at 25 ° C.	178
Figure 4.159: 15% SDS-PAGE analysis of Ni-NTA RGS-his-AGG2 fractions.	180
Figure 4.160: Western analysis of Ni-NTA RGS-his-AGG2 fractions.	180
Figure 4.161: DLS size distributions by intensity of RGS-his-AGG2 (A) and (B) PBS buffer.	181

Figure 4.162: 15% SDS-PAGE analysis of batch purification RGS-his-AGG2 fractions.	181
Figure 4.163: UV spectra of RGS-his-AGG2.	182
Figure 4.164: DLS size distributions by volume of RGS-his-AGG2 (elution 2).	182
Figure 4.165: HisTrap HP chromatogram of RGS-his-AGG2 elution with a linear imidazole gradient.	183
Figure 4.166: 15% SDS-PAGE analysis of RGS-his-AGG2 fractions.	183
Figure 4.167: UV spectra of RGS-his-AGG2.	184
Figure 4.168: DLS size distributions by intensity of RGS-his-AGG2 after dialysis.	184
Figure 4.169: Western analysis of complexes of RGS-his-AGB1 and RGS-his-AGG2.	185

LIST OF TABLES

Table 3.1 Plasmids purchased from TAIR	37
Table 3.2: Thermal cycle conditions for <i>AGB1</i> , <i>AGG1</i> and <i>AGG2</i> .	41
Table 4.1: Purification Conditions for GPA1 HisTrap™ HP Affinity.	66
Table 4.2: Absorbance values and concentration estimates after affinity and dialysis.	73
Table 4.3: Absorbance values and concentration estimates of GPA1 with additives.	74
Table 4.4: The absorbance values after Ni-affinity and desalting.	76
Table 4.5: Absorbance values and concentration estimation for Ni-affinity elutions	80
Table 4.6: Absorbance values and concentration estimations for Ni-affinity fractions.	81
Table 4.7 Comparison of NaCl concentrations and elution volumes for anion exchange in the presence of different additives.	86
Table 4.8: Absorbances and concentration estimates for pool 3 and 4.	88
Table 4.9 Comparison of absorbance values of dialyzed pools 3, 4 and 5	93
Table 4.10: Purification Conditions for GPA1 Gel Filtration	101
Table 4.11 Molecular mass estimations for S-300 (Buffer A) peaks.	103

Table 4.12 Molecular mass for S-300 (Buffer B) peak 2 fractions.	106
Table 4.13 Molecular mass for S-300 peak 2 (Buffer C) fractions.	108
Table 4.14: Estimation of GDP content of GPA1 at different stages of the purification.	118
Table 4.15: CPM values of 290 nM pool 3 GPA1 (stg 3.1.1).	122
Table 4.16: CPM values of pool 3 GPA1 (stg. 3.1.1) as a function of concentration.	122
Table 4.17: CPM values of pool 4 GPA1 (stg. 3.1.1) as a function of concentration.	123
Table 4.18: CPM values of GPA1 (stg. 3.2.1) as a function of concentration.	125
Table 4.19: Concentration estimations for pool 3 (stg.2.2.1).	151
Table 4.20: Summary of SAXS measurements and MM estimations.	152
Table 4.21: Molecular mass estimations from column calibration curve.	153
Table 4.22: Concentration estimations for GPA1 pools (stg. 3.2.1).	153
Table 4.23: MM estimations from SAXS data of BSA and S-200 pools.	156
Table 4.24: Comparison of R _g (Guinier), volume (Porod) and diameter (DLS).	157
Table 4.25: SASREF Parameters and error values.	159
Table 4.26: Primers designed for cloning into pGEX-4T-2.	163
Table 4.27: Primers designed for cloning into pQE-80L.	166
Table 4.28 Expression of GST-AGB1 in inclusion body fractions at different induction parameters. UP: urea soluble, IP: urea insoluble.	169
Table 4.29: Purification Conditions for RGS-his-AGB1	171

Table 4.30: Expression of GST-AGG1 in inclusion body fractions at different induction parameters. UP: urea soluble, IP: urea insoluble.	177
Table 4.31: Purification conditions for RGS-his-AGG2	179
Table 4.32: Absorbance values and concentration estimations for RGS-his-AGG2	182

LIST OF SYMBOLS AND ABBREVIATIONS

ABA: Abscisic acid

AGB1:G β protein from *A. thaliana*

AGG1/AGG2: G γ proteins from *A. thaliana*

ATP:Adenosine triphosphate

CD: Circular dichroism spectropolarimetry

CL: Cleared Lysate

C-terminus: Carboxyl terminus

DLS: Dynamic Light Scattering

DTT: 1,4-Dithio-DL-threitol

EFPI: EDTA-free protease inhibitor cocktail

ER: Endoplasmic reticulum

FT: Flow through

GAP: GTPase activating protein

G α : G-protein alpha subunit

G β : G-protein beta subunit

G $\beta\gamma$: Protein dimer consisting of G β and G γ subunits

GDI: Guanine nucleotide dissociation inhibitor

GDP: Guanosine di-phosphate

G γ : G-protein gamma subunit

GPA1: G α protein from *A. thaliana*

GPCR: G-protein coupled receptor

GTP: Guanosine tri-phosphate

GTP γ S: non-hydrolyzable GTP analog

GTPase: enzyme converting GTP into GDP

G α -GDP: G α bound to GDP, in its inactive state

G α -GTP: G α bound to GTP, in its active state

GGM: GDP (30 μ M) Glycerol (10 %) MgCl₂ (5 mM)

HEPES: 4-(2-hydroxyethyl)-1-piperazineethanesulfonic acid

HND: HEPES (20 mM, pH 8.0) NaCl (150 mM) DTT (1 mM)

IPTG: Isopropyl β -D-1-thiogalactopyranoside

MCS: Multiple cloning site

MM: Molecular Mass

NMR: Nuclear magnetic resonance

N-terminus: Amino terminus

PM: Plasma membrane

Ras: Family of monomeric GTPases

RGS: Regulators of G-protein signaling

SAXS: Small Angle X-ray Scattering

SDS: Sodium Dodecyl Sulfate

TAIR: The Arabidopsis Information Resource

TM: Trans membrane

TND: Tris HCl (50 mM, pH 8.0), NaCl (150 mM), DTT (1 mM)

WD40 repeat: Tryptophane-Aspartate repeat consisting of 40 residues

CHAPTER 1

1 INTRODUCTION

Heterotrimeric G proteins are mediators that transmit the external signals via receptor molecules to effector molecules and play a crucial role in signal transduction in mammalian, plant and lower eukaryotic cells. The mammalian heterotrimeric G proteins are composed of three subunits, α , β and γ . The α subunit by binding /dissociation from $\beta\gamma$ dimer, transmits signals from receptor to effector molecules. Availability of high-resolution structural data led to a comprehensive understanding of the mechanism of signaling in mammalian systems. The α subunits have posttranslational lipid modifications which allow them to attach to the plasma membrane and interact with the hydrophobic regions of the receptor. Following receptor activation heterotrimer dissociation or loosening occurs and the α subunit and the $\beta\gamma$ dimer interact with downstream effector molecules to transmit the signal. The α subunit can bind and hydrolyze GTP and this enzymatic activity serves as an on/off switch for the heterotrimeric signaling cycle.

There are 16 $G\alpha$ genes in the human genome, which encode 21 known $G\alpha$ proteins of molecular mass ranging from 39 to 52 kDa. These proteins can be divided into four major classes based on sequence similarity: $G\alpha$ (s /olf), $G\alpha$ (i1/i2/i3/o/t-rod / t-cone /gust /z), $G\alpha$ (q / 11 / 14 / 16) and $G\alpha$ (12 / 13). Despite the high number of $G\alpha$ subunits there are up to date only 6 $G\beta$ and 14 $G\gamma$ subunits identified in humans. There are, however, more than 800 genes encoding for GPCRs only in the human genome. Each $G\alpha$ has a distinct function, the specificity determined by the poorly conserved C-terminal receptor-binding domain. The signaling diversity in mammalian systems

probably results from this specific GPCR- $G\alpha$ coupling. The heterotrimeric G proteins are involved in various signaling mechanisms including visual perception (Gt-rod), olfactory system (Golf), nervous system (Gi/o/z), taste (Ggust) and many others. The signaling specificity may not be directly related to $G\beta\gamma$, since most β and γ isoforms are functionally interchangeable with each other and different $G\beta\gamma$ can interact with the same $G\alpha$. Still not all $\beta\gamma$ or heterotrimer combinations occur; for example $G\beta 1\gamma 1$ always couples to Gt (transducin) and functions in rhodopsin directed light dependent signaling [1].

Plant heterotrimeric G proteins are identified in several higher plants. The plant heterotrimer was shown to be involved in signaling pathways directing cell and plant growth, development and differentiation, ion channel regulation and drought tolerance and biotic stress resistance. These processes are mediated by several plant hormones. Plants have one or two isoforms of $G\alpha$ subunit as opposed to the high number in mammalian systems. Similarly there is only one $G\beta$ and two $G\gamma$ isoforms identified in different plants [2].

Studies revealed the presence of the three subunits in the *A. thaliana* genome. The G protein α subunit, GPA1 was first to be isolated [3] followed by the β - subunit AGB1 [4] and the two γ -subunits; AGG1, AGG2 [5, 6].

Current research on plant heterotrimeric G proteins is mainly focused on null mutant / overexpression studies performed in model organisms, i.e. *A. thaliana* and *O. sativa*. These studies provide information about the pathways involving the heterotrimeric G proteins, however, the mechanism of G protein activation via signaling molecules and mechanisms of interactions with different partners in pathways remain unknown. Current literature is especially poor from the perspective of structural analyses on the plant heterotrimeric G-proteins, whereas for the mammalian counterparts, such studies have contributed unique insights to understanding of their functional roles. Structural characterization of the plant heterotrimer and the individual subunits would reveal the level of similarity with the mammalian complexes and may allow prediction of the nature of interactions of the proteins with up/down stream signaling components.

The overall aim of this work is to understand the structural constraints of the heterotrimeric G protein signaling mechanism(s) in plant species. To achieve this objective, the corresponding genes from the model plant *A.thaliana* are cloned in different expression systems. The specific aims can be summarized as:

- Recombinant expression of *A.thaliana* heterotrimeric G protein subunits.
- Purification of recombinant GPA1.
- Characterization of the GDP / GTP binding and GTPase activity of recombinant GPA1 by UV spectrophotometry and radioactive assays.
- Biophysical characterization of GPA1 by Western analysis, receptor mimetics interaction, ¹H NMR and MALDI-TOF.
- Structural characterization of GPA1 by CD, DLS and SAXS.
- Purification of AGB1 and AGG1/2.
- Reconstitution of the plant heterotrimer.

GPA1 was expressed as a C-terminal myc epitope and 6 his fusion using *Pichia pastoris* from a genome integrated expression construct that leads to intracellular production of recombinant protein [7]. The presence of G α or G $\beta\gamma$ is not yet identified in *P.pastoris* but is reported from other yeast including *S.cerevisiae* [8]. *P.pastoris* is shown to perform co-and post-translational lipid modifications myristoylation and palmitoylation [9].

In this study, GPA1 was isolated with or without the presence of detergents using his-tag affinity chromatography with yields of 10 or 20 mg/L culture, respectively. The protein was further purified by either anion exchange or size exclusion chromatography. Purified recombinant protein was routinely analyzed by using UV spectrophotometry

and circular dichroism (CD) spectropolarimetry and western detection to assure protein quality, monodispersity and size were analyzed by dynamic light scattering (DLS). Anion exchange resulted in separation of two biophysically different forms of GPA1; one an oligomeric but stable form, the other one a heterogenous mixture with monomeric sized particles and prone to both aggregation and degradation. In contrast, gel filtration column purified GPA1, on the other hand, appeared to be homogeneous with a molecular mass higher than that expected from the monomer. NMR analysis showed that this protein was purified together with detergent/lipid micelles. It was shown that all three forms of GPA1 had comparable GTP binding and hydrolysis activity. The oligomeric form had higher tendency to bind GDP. CD measurements indicated helical secondary structure elements resembling that observed in the native proteins. Attempts to collect small angle solution X-ray scattering (SAXS) data from the anion exchange purified forms of GPA1 were not successful. SAXS measurements from the gel filtration purified protein were consistent with the presence of high molecular mass structures, which may be oligomeric GPA1 alone or protein-micelle complexes (PMC). The molecular mass was estimated to be about 2.5 fold of GPA1.

Mass spectrometry analyses were different for the oligomeric and monomeric forms. The N-terminus of the monomeric form did not contain any lipid modifications, whereas the 6 N-terminal amino acids could not be detected at all for the oligomeric GPA1. Furthermore the trypsin digestion patterns were different, the lysines in the putative nucleotide and receptor binding domains of oligomeric GPA1 were not digested. The recombinant protein was expressed in cytosolic fractions and was also present in membrane fractions of *P.pastoris*. The interaction of oligomeric GPA1 with receptor mimetic compounds was shown by CD analysis.

AGB1 and AGG1/2 could not be expressed in *P.pastoris* (data not shown). Hence, the genes were inserted into different *E.coli* expression vectors and several strains were screened for protein production. AGB1 expression was very low in each case and AGG1 was expressed in inclusion body fractions. AGG2 was expressed in soluble fractions and initial purification strategy was optimized with yield approximately 1-4 mg/150 ml culture.

The interaction of AGB1 and AGG2 was shown by a non-denaturing SDS-PAGE-Western detection strategy. Interaction of GPA1 with partially purified β and γ subunits was demonstrated by PAGE analysis. This interaction appeared to reverse the aggregation observed for GPA1 after storage and protected from degradation.

These results show that the biophysical properties of the oligomeric form and the PMC form of GPA1 are similar and correspond to a stable state which may resemble the membrane-bound form of native GPA1. These studies highlight the tendency of GPA1 to form complexes. It appears that meaningful studies directed to develop an understanding of the signaling mechanism in plants would require additionally the presence of the $\beta\gamma$ dimer. Purification of the plant β and γ subunits for reconstitution of the recombinant heterotrimer is being investigated.

CHAPTER 2

2 BACKGROUND

2.1 The Mammalian Heterotrimer

Heterotrimeric G proteins are mediators that transmit external signals arriving at receptor molecules to effector molecules and play a crucial role in signal transduction in mammalian and plant systems.

Most information on heterotrimeric G-proteins is from studies on the mammalian complex. The mammalian heterotrimeric G proteins are composed of three subunits; α , β and γ . The $G\alpha$ subunit is the site of GTP binding and GTPase activity and β and γ subunits remain as a tight complex during the signal transduction process. In the general mechanism of signal transmission from receptor to effector molecules the state of association of the α subunit with the $\beta\gamma$ dimer acts as a switch (Figure 2.1). Signal transduction occurs via G-protein coupled receptors (GPCRs) which are identified as 7 TM domain proteins in mammals; the extracellular amino-terminal extension determining the ligand specificity [10]. Activation of the GPCR upon ligand binding leads to an interaction with the membrane bound $G\alpha$ inside the cell. This interaction, occurring between the cytoplasmic loop of the receptor and the amino- and carboxy-terminal domains of $G\alpha$ catalyses the nucleotide exchange. The nucleotide exchange, GDP to GTP, releases $G\alpha$ from $G\beta\gamma$, allowing both the $G\alpha$ and $G\beta\gamma$ to interact with their downstream effector molecules. $G\beta$, released from $G\alpha$, remains strictly bound to

the γ subunit, which anchors the heterotrimer/dimer to the lipid bilayer via a lipid modification at its carboxy terminus. The intrinsic GTPase activity of $G\alpha$ eventually results in GTP hydrolysis and in the re-formation of the heterotrimer. RGS (Regulator of G protein signaling) proteins, which are GTPase activating factors (in the case of $G\alpha$ GAPs), bind to $G\alpha$ and accelerate the rate of GTP hydrolysis to GDP, shortening the lifetime of $G\alpha$'s active, GTP-bound state. GAPs lead to reduced signal strength and/or accelerated termination of the signal after ligand removal from the GPCR [11]. There are other regulatory proteins which have GDI (guanine nucleotide dissociation inhibitor) activity, these associate with the $G\alpha$ subunits in their GDP bound state preventing GDP release, one of them being the $G\beta\gamma$ dimer itself [12].



Figure 2.1 The classical model for receptor mediated G protein activation [13].

R: GPCR, R*: activated GPCR.

2.2 Structure- function relations of heterotrimeric G proteins

It is well known that key structural domains regulate the function of the heterotrimeric G proteins complex. All three subunits have characteristic functional regions conserved among structurally characterized mammalian proteins. There are

experimentally-determined structures for two different mammalian G protein heterotrimers, a 2.0 Å structure of the heterotrimer Gt- α (bovine) /Gi- α (rat) chimera (expressed in *E.coli*), Gi- β 1 γ 1 (isolated from bovine rod outer segment) PDB accession code 1GOT [14] and a 2.3 Å structure of the Gi- α 1 (rat, expressed in *E.coli*), Gi- β 1 (bovine), Gi- γ 2 (C68S) (bovine, coexpressed with G β in insect cells) PDB accession code 1GP2 [15].

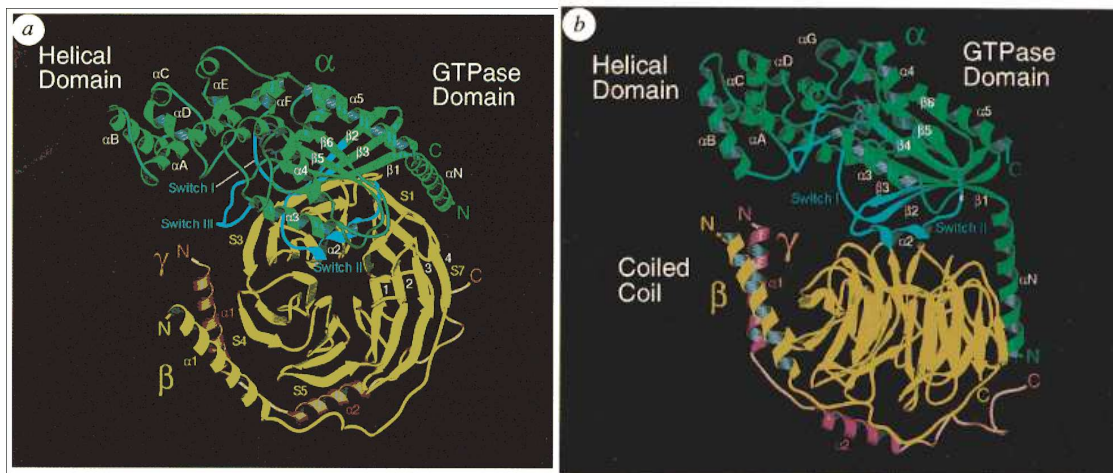


Figure 2.2: 2.0 Å structure of the heterotrimeric complex 1GOT.

Gt α / Gi α (green) chimera and the G β (yellow) G γ (brown in a and pink in b) subunits GDP in magenta, and the switch I-III regions are colored in cyan. Residues 216-294 of bovine Gt α replaced with residues 220-298 of rat Gi α , expressed in *E.coli*. G β γ dimer isolated from photolysed bovine retinal rod segments. a: Ribbon drawing of the complex b: Rotated 70° about the horizontal axis compared with the view in a [14].

The mammalian α subunit has two domains; one with an α helical secondary structure which buries the nucleotide in the core of the protein and the other a ras (GTPase) domain, where nucleotide binding and hydrolysis occurs [16]. Structure of transducin (isolated from bovine rod) bound to GTP γ S (a non hydrolyzable analog of GTP), 1TND [17], revealed many important features for GTP binding and hydrolysis, including the active site arginine and glutamine residues. These residues were later shown to have a key function in GTP hydrolysis and mutating these abolishes hydrolysis creating constitutively active G α [18]. Many other crystal structures at different resolutions and with different ligands and/or effectors; the AlF $_4^-$ -GDP bound

G α (GTP hydrolysis transition state), GTP γ S stabilized G α and RGS bound G α [19-21] also contributed to the understanding of G α structure and function. GTPase domain contains the GTP/GDP binding site, the Mg⁺²-binding domain, the threonine and glycine residues needed for GTP hydrolysis, the covalently attached lipid anchoring the subunit to the bilayer and sites for binding receptors, effector molecules, and the $\beta\gamma$ subunit.

The G β subunits have a molecular mass of approximately 36 kDa, all share 7 WD-40 repeats and thus fold in to a 7 blade β -propeller structure. The γ subunits are disordered helical coils and interact with beta subunits through an N-terminal coiled-coil. Upon this interaction the γ subunit makes extensive contacts all along the base of β and this interaction is not dissociable except under denaturing conditions [22]. These structural features are conserved in both the heterotrimer and the dimer form (PDB accession code 1TBG [23]) and the conformation of free dimer is identical to that in the heterotrimer. The amino acid sequences of β 1- β 4 are highly homologous (~80%), β 5 is less similar and was shown to interact with some RGS proteins which have G γ similar (GGL) domains [1].

The mammalian G γ subunits are small proteins with molecular mass around 7-8 kDa. The overall sequence homology among G γ 's is lower as compared to G α and G β , and these are grouped according to their C-terminus amino acid sequence. The G γ subunits with identical C-terminus sequence interact with the same receptor, thus this sequence also plays a role in heterotrimer-receptor specificity [24].

The crystals of G $\beta\gamma$ (1TBG) or the heterotrimer 1GOT were produced from proteins isolated from bovine rod outer segments. The β and γ subunits were also produced with *in vitro* translation [25] or using baculovirus expression systems [26]. These studies contribute to understanding some important biochemical properties of both the individual subunits and the dimer itself. G β is not stable without the presence of its dimerizing partner and forms high molecular mass aggregates. Co-expression /co-translation is not required, however, for dimerization of β and γ . Trypsin proteolysis was used to detect dimerization as shown by the discrete pattern of purified bovine

brain G $\beta\gamma$ [27]. The G β 1 subunit has only one site available for tryptic digestion in the dimer form (Arg-129) which results in 2 fragments of size ~25 and 14 kDa [28].

The high resolution crystal structures for transducin in heterotrimeric and GTP γ S bound forms reveal some conformational differences which may result in heterotrimer dissociation. The G $\beta\gamma$ dimer binds to a hydrophobic pocket present in G α -GDP. GTP binding to G α removes the hydrophobic pocket and reduces the affinity of G α for the G $\beta\gamma$ dimer. In the GDP bound heterotrimeric form 1GOT [14], the G β interface is mainly formed by the exposed hydrophobic amino acid residues and switch regions are flexible allowing the interaction. In the GTP γ S bound Gt crystal structure; 1TND [17], these hydrophobic amino acids side chains are rather buried inside and basic and polar amino acids are located at the interface. The key structural rearrangement upon activation occurs in the backbone loops of G α which act as switches depending on the bound nucleotide. Switches position themselves depending on whether GDP or GTP occupies the nucleotide binding site. When GDP is bound, the switches orient to permit tight association of G α to the β subunit, but upon GTP binding, these switches reorient such that the G α / G $\beta\gamma$ interaction is disrupted permitting a slightly different interaction at the same interface with membrane-localized enzyme, i.e. effectors. Switch I is a loop connecting helix α 4 to strand β 6, switch II, corresponds to the loop preceding the α 2 helix, and the helix itself and switch III corresponds to the loop that connects helix α 3 to strand β 5 (Figure 2.2a). Almost the entire length of the switch II region is buried in the contact with β subunit and also forms the binding site for the γ phosphate of GTP. Both the switch II and the amino-terminal parts of G α are dynamic components of GTP hydrolysis. Upon GTP-hydrolysis, the switch II helix rotates approximately 120°, exposing the hydrophobic residues, including Trp-211, to interact with complementary nonpolar pockets in the β subunit. The same rotation also creates two ionic interactions between the α and β subunit [29]. Conformational changes within switch II region are coordinated with a complementary shift of the switch I peptide that ultimately traps GDP in the catalytic site of α subunit. Switch I also contributes an oxygen ligand to the Mg⁺² in the GTP bound state [19]. The structural changes occurring in switch I and II are directly due to GTP binding, whereas switch III does not have a binding site for GTP. Switch III indirectly undergoes structural rearrangements by responding to the changes occurring in switch II and this coupling was shown to play a role in effector

activation [30]. The N-terminal helical region is exposed only in the GDP bound form, which is another interaction site for the dimer. The N terminal helical region of $G\alpha$ is ordered by its interaction with the beta-propeller domain of $G\beta$ (Figure 2.2b). These data support the classical view of heterotrimer dissociation upon receptor activation. Recently, an alternative mechanism for heterotrimeric G protein activity involving subunit structural rearrangement rather than dissociation was also suggested for G_i family based on FRET analyses [31]. Several biochemical data suggest that subunit dissociation may not be necessary for effector interaction after nucleotide exchange [32]. It is argued that the mode of activation may depend on the type of receptor and alpha subunit; for example dissociation is a more favorable mechanism in case of transducin- $G\beta 1\gamma 1$ heterotrimer due to the requirement of movement of transducin from rod outer segments to other cellular compartments in order to respond to varying light sources [33].

The mammalian $G\alpha$ subunits share high sequence homology especially for the amino acids in the GTPase domain; P binding loop (GXGESGKS), Mg^{+2} -binding domain (RXXTXGI and DXXG) and guanine ring binding motifs (NKXD and TCAT). The helical domain is, however, not conserved and this divergence might be the reason of interaction with different effectors [18].

The GTP binding activity of mammalian G protein α subunits have been established through both radioactive assays [34] and intrinsic fluorescence measurements [35-37]. The radioactive assay allows direct measurement of the amount of bound radioactive $GTP\gamma S$, whereas intrinsic fluorescence measurements rely on the conformational change that occurs in switch II. GTP binding assays not only reveal the kinetic properties of the individual subunit but also give valuable information about the effect of other proteins; activators, GDIs and other interactor proteins. These studies showed that the dissociation of bound GDP is the rate-limiting step for GTP binding and the requirement for a cation, especially Mg^{+2} for irreversible binding to $GTP\gamma S$. In the absence of Mg^{+2} $GTP\gamma S$ binding is freely reversible and GDP binding is largely unaffected [38]. The GTPase activity of each mammalian $G\alpha$ was shown to be different, with *in vitro* k_{cat} values (first order reaction rate constant); $G\alpha s$ 3.5 min^{-1} and $G\alpha i$ $1.8-$

2.4 min⁻¹ at 20 °C, Gα_q 0.8 min⁻¹, Gα₁₂ 0.2 min⁻¹, and the lowest for Gα_z 0.05 min⁻¹ at 30 °C [18].

Circular dichroism was also used to investigate the effect of bound nucleotide on recombinant (*E.coli*) Gα_i and no significant spectral change was observed in the presence of GDP or non-hydrolyzable GTP analog [39]. Yet receptor activation was shown to decrease the helical content of non-myristoylated Gα_i and this maybe explained by the interaction of helical Gα C terminus with the receptor upon activation [40]. Similarly conformational changes are also expected to take place also in the helical N-terminal region. Furthermore CD was used as a tool for verification of the intactness of the recombinant Gα subunits [41].

The N-terminus amino acids were either cleaved in order to obtain crystal quality protein or these amino acids were not visible in the electron density maps. Structural features of N-terminus are not clear in crystal structures of Gα transducin (27 and 26 amino acids missing for 1TND and 1TAG respectively, protein isolated from bovine rod) or Gα_{i1} (33 amino acids missing; 1GIA, 1GIL, 1GFI; recombinant rat Gα_i expressed in *E.coli*, [19]). Although the N-terminus of Gα is more ordered in the heterotrimeric state, still 5 and 4 amino acids are missing in 1GOT and 1GP2 crystal structures respectively.

The N-terminus of Gα plays significant role when membrane, receptor and Gβγ interactions are considered. The mammalian alpha subunits all have at least one lipid modification at the immediate N-terminus that would facilitate to locate the heterotrimer in close contact to receptor, which is in the plasma membrane (PM). The presence of hydrophobic fatty acids increases the overall hydrophobicity of the proteins.

Gα_i (α_{i1}, α_{i2}, α_{i3}, α_o, α_z, α_t) family members are myristoylated as the result of co-translational addition of the saturated 14-C fatty acid myristate to the glycine residue by a stable amide bond at the new N-termini following the removal of the initiator methionine. The addition of myristate also depends on the 4th residue following glycine, which has to be either a serine or threonine for the myristoylation to occur. This residue

is a serine in case of $G\alpha_i$ family members. Mutating the glycine residue results in cytosolic $G\alpha_i$ which can not bind to PM. All $G\alpha$ families except $G\alpha_t$ and $G\alpha_{\text{gust}}$ are posttranslationally modified by the addition of 16-C fatty acid palmitate attached through a reversible thioester linkage to cysteine residue(s) [42]. The palmitoylation site is one (or more) cysteine residue(s) in the N terminal 20 amino acid region [33], with the exception of $G\alpha_s$ which was recently shown to have two palmitate moieties at glycine 2 and cysteine 3 [43].

Palmitoylation site is the cysteine following the myristoylated glycine for $G\alpha_i$ family members and requires presence of myristic acid and/or the $G\beta\gamma$ dimer. The presence of $G\beta\gamma$ is enough for palmitoylation to occur for the myristoylation mutants (G2A) of $G\alpha_i$ and $G\alpha_z$, and the heterotrimeric form was shown to be a better substrate for palmitoylation for $G\alpha_i$ and $G\alpha_s$ [44]. This suggests that palmitoylation occurs after membrane attachment of $G\alpha$ by its increased hydrophobicity, either through the myristic acid or the hydrophobic $G\beta\gamma$ [42]. On the other hand the mutating the 3rd cysteine of $G\alpha_o$ results in high amount of cytosolic protein, even though the protein is myristoylated [45]. Thus the presence of myristate is a transient hydrophobic anchor that allows the protein to be placed near the PM, where palmitoylation may take place and the more hydrophobic palmitate anchors the protein more strongly to the PM.

Palmitate is attached through a reversible covalent bond and the palmitoylation/depalmitoylation cycle contributes to the dynamic nature of $G\alpha$ activation and oligomerization. The GDP bound form of myristoylated $G\alpha_o$ was shown by native continuous gel electrophoresis; to be in oligomeric form (dimer, trimer, tetramer and pentamer), which was disintegrated to monomers upon $GTP\gamma S$ binding and addition of Lubrol-PX. In vitro palmitoylation resulted in a stable oligomeric form, which was not completely reversed by the addition of $GTP\gamma S$. Furthermore the palmitoylated $G\alpha_o$ had lower $GTP\gamma S$ binding [46]. Depalmitoylation was shown to occur upon agonist stimulation of receptor for $G\alpha_o$ [47] and $G\alpha_s$ [48, 49]. Palmitoylation was also shown to effect protein-protein interactions; palmitoylated $G\alpha_s$ had higher affinity to $G\beta\gamma$ and $G\beta\gamma$ protected GDP- $G\alpha_s$ from depalmitoylation but not $GTP\gamma S$ - $G\alpha_s$ [50] and palmitoylated $G\alpha_z$ and $G\alpha_{i1}$ had lower affinity to RGS proteins

[51]. It is clear that this reversible lipid modification affects the functioning of $G\alpha$ subunits, yet the exact mechanism of this cycle is unclear; is palmitoylation favored by interaction with $G\beta\gamma$ (or does palmitoylation favors $G\beta\gamma$ interaction), by returning to GDP bound form by GTP hydrolysis or by recruitment to the PM with GDP bound heterotrimeric form (if $G\alpha$ was ever translocated to cytosol). The precise order of events in this cycle will clarify the different observations for various $G\alpha$ subunits localization (internalization) upon activation considering that palmitoylation may take place in any cellular membrane, PM and although at a lower extent at Golgi or endoplasmic reticulum (ER) [18].

The overall hydrophobicity of $G\beta\gamma$ is already high and furthermore the γ subunits are prenylated. 20-C isoprenoid group geranyl geranyl or 15-C isoprenoid farnesyl is posttranslationally attached through a stable thioether linkage to a cysteine in the so called CAAX motif in the C terminus of $G\gamma$ subunits, where A represent an aliphatic amino acid residue. The last amino acid X of CAAX box determines the isoprenoid to be attached, farnesyl in case of serine or methionine and geranyl geranyl in case of leucine. $G\gamma_{1,9,11}$ are farnesylated and remaining $G\gamma$ subunits are geranyl geranylated. Prenylation occurs in the cytosol followed by $G\beta\gamma$ dimerization, and then the dimer is translocated to ER where AAX amino acids are cleaved off and the new C-terminus is carboxyl methylated. Prenylation is not required for the formation of the $G\beta\gamma$ dimer as shown by limited proteolysis [52]; but dimerization was shown to be necessary for proteolytic cleavage and methylation of the $G\gamma$ C –terminus [33].

Prenylation of $G\gamma$ increases the affinity of dimer to $G\alpha$ [52] and allows its attachment to the PM. Cysteine mutant studies show that without prenylation the dimer is not attached to the PM even in the presence of the $G\alpha$ subunit [53]. Some $G\beta\gamma$ dimers were shown to be localized to inner cellular membranes upon heterotrimer interaction, to Golgi complex $G\gamma_{1,9,11}$ rapidly and $G\gamma_{5,10}$ slowly and to ER, $G\gamma_{13}$. The activated dimers of $G\gamma_{2,3,4,7,8,12}$ stay attached to PM [54].

The presence of both the lipid modifications and the $G\beta\gamma$ assure $G\alpha$ membrane attachment and thus receptor proximity. The exact mode of membrane attachment and the effect of fatty acids on the structure of the heterotrimer is not known.

There is no crystal structure of a heterotrimer with myristoylated and palmitoylated $G\alpha$. Especially an understanding of the effect of myristate on the $G\alpha$ - $G\beta$ interface will be crucial, ie does myristate directly interact with $G\beta$ or does it allow a favorable conformation of $G\alpha$ to bind $G\beta\gamma$. In a recent study of $G\alpha_t$ in living cells, a very small fraction of the myristoylation deficient protein was shown to be localized to PM and interact with $G\beta\gamma$, but had severely reduced GTPase activity in vivo [55]. There are studies investigating the dynamics of the N-terminus helix by use of site directed fluorescent labelling and EPR. The N-terminal helix solvent exposed residues of $G\alpha_i$ that are placed on $G\beta\gamma$ interface (as judged from the $G\beta\gamma$ bound crystal structure) were mutated to cysteine either in the presence or absence of myristate. In the non myristoylated protein the N-terminus is more solvent exposed in the GDP bound form and is placed in a more hydrophobic environment in GTP or GDP- AlF_4^- bound form [56]. On the other hand myristoylated cysteine labeled N-terminus was more immobile in the hydrophobic environment and the immobility was not significantly altered in conformations with different nucleotides [57]. Both studies verified that N-terminus was present as a more ordered helix in the presence of $G\beta\gamma$. The presence of $G\beta\gamma$ may have a stabilizing effect on the N-terminus helix of $G\alpha$ which becomes a disordered random coil in the absence of $G\beta\gamma$ (either by dissociation or by increased distance). There may be a binding pocket on GPA1 where the disordered N-terminus helix is hidden by hydrophobic interactions, which are stronger in the presence of myristate.

The mode of membrane attachment is another important issue in heterotrimeric G protein cycle. The $G\alpha_i/s$ subunits were shown to prefer lamellar membrane structures, whereas the heterotrimeric $G\alpha_i$ prefers non-lamellar hexagonal structures [33]. The presence of $G\beta\gamma$ was shown to be the driving force of the heterotrimer to be recruited to nonlamellar phase [58]. The α helical transmembrane peptides can induce formation of nonlamellar membrane structures, thus GPCR may have a similar effect [33]. A recent study gives insight to the membrane-heterotrimer interaction by use of electron

microscopy. The transducin-G $\beta\gamma$ heterotrimer was crystallized on the surface of a 2-D lipid bilayer and the results show that the membrane interacting portion of the protein is only the 2% of the total heterotrimer surface. The crystal structure fit on the surface reveals that the membrane interacting residues are from *Gat* β 2- β 3 loop and its N-terminal helix [59]. Still the absence of receptor (rhodopsin would be in this case) and the missing portions of N- and C-terminal helices of G α in the heterotrimer crystal structure limits further conclusion.

All GPCRs has 7 transmembrane alpha helices with an extracellular N-terminus, an intracellular C-terminus and 3 interhelical loops on each side of the membrane. The only crystal resolution native structure up to date is that of rhodopsin and this structure revealed that the C-terminal helix had an eighth α -helix and a fourth intracellular loop which is a palmitoylation site [60]. The attempts to crystallize other receptors failed and only engineered receptors could be crystallized [61]. Much information about the receptor-heterotrimer interaction is from rhodopsin (1GZM)-transducin-G β 1 γ 1 (1GOT) complex.

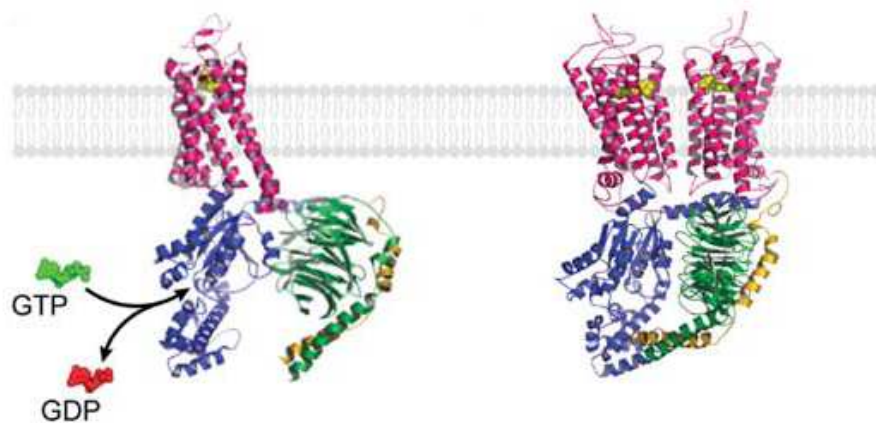


Figure 2.3: The models for rhodopsin-transducin heterotrimer complex. A: Superimposed models of 1GZM and 1GOT. B: The superimposed models of inactive rhodopsin dimmers (1GZM packed into unit cell constraints from atomic force microscopy data) [62] and 1GOT. Figure taken from [18].

Both the $G\alpha$ and $G\beta\gamma$ dimer binds to receptor; the later through the C-terminal region of $G\gamma$ [16]. The receptor interacting sites on $G\alpha$ were shown with different biochemical approaches and were found to be C-terminus, N-terminal helix and the $\alpha4 / \beta6$ loop which are all distant from the nucleotide pocket. There is some evidence highlighting the movement of $\alpha5$ helix, switch I and switch II regions upon receptor activation, yet the mechanism how GDP release can be achieved with such distant interaction sites is unknown [63]. A mechanism for liganded receptor enhancement of the GDP release from $G\alpha$ subunit was recently suggested and points out the importance of $\alpha5$ helix. This helical region connects the C terminus receptor binding region to the nucleotide binding pocket. Upon receptor binding structural changes occur in $\alpha5$ helix simultaneously with GDP release [64].

The classical view of receptor-heterotrimer interaction is the “collision coupling” model in which only the activated receptor can couple with the heterotrimer. Dark (inactive) rhodopsin was also shown to bind $G\alpha_t$, but the affinity of activated receptor is much higher. Similarly $G\alpha_i$ co-purified with $\alpha2$ adrenergic receptor and the unactivated δ -opoid receptor can bind to $G\alpha_o$. The presence of $GTP\gamma S$ did not cause dissociation in the later case, which may be explained by the presence of a receptor- $G\alpha(GDP)G\beta\gamma$ complex. All these data support the presence of a precoupled system; the receptor is already bound to the heterotrimer prior to activation [63] as given in Figure 2.3A. The recent findings suggest that GPCRs can dimerize [65] as supported by the findings from atomic force microscopy analysis of inactive rhodopsin (Figure 2.3B), but there is also opposing data suggesting that only monomeric receptors are active [66].

The receptor-heterotrimer specificity is another important issue in understanding heterotrimeric G protein function. There is high number of GPCRs in mammalian systems, yet every receptor does not activate every heterotrimer. There is evidence that the $G\alpha$ subunits have receptor specificity, especially in C-terminus; chimeric $G\alpha_q$ protein with C-terminus replaced with that of $G\alpha_i$ results in activation by the receptor specific to $G\alpha_i$ but the effector specificity is that of $G\alpha_q$. The C-terminal 5-7 amino acids of $G\alpha$ are disordered in the heterotrimeric G protein crystal structures, which were shown to be interacting with receptor using a peptide screen approach [67]. On the other hand receptors activating the same $G\alpha$ subunits have very low sequence homology and not

much is known about if there is a receptor-specific sequence for selecting the heterotrimer isoform (s) [63].

The primary effectors of heterotrimeric G proteins are either attached to PM or transmembrane proteins such as phospholipase C, adenylyl cyclase (AC) and ion channels [59]. The crystal structures for effector complexes for different G α subunits all reveal a localized hydrophobic effector-binding surface on G α which is structurally conserved among different G α subunits. The hydrophobic residues inserted into a pocket formed between switch II and α -3 helix; α 2/ β 4 and α 3/ β 5 loops were shown to be involved in effector specificity. The involvement of N-terminus and myristoylation of G α i in effector binding was also shown. The number of effectors identified is low as compared to the possible heterotrimer combinations, some G α subunits were shown to interact with only one effector and others with many effectors. The numbers of effectors are expected to be high since even highly homologous G α subunits interact with different effectors. Some effectors were shown to increase the GTP hydrolysis rate of their respective G α subunits; PLC β 1 for G α q and PDE γ for G α t. Thus, these effectors can act as GAPs and control the duration of the signal in which they are involved. A specific family of GAPs are called RGS due to their conserved RGS domain which forms a bundle of nine α -helices which is the binding site to G α switch regions [18]. The binding of RGS to switch regions was shown to stabilize the transition state conformation and thus increase GTP hydrolysis rate. The transition state was mimicked with the presence of AlF $_4^-$ ion, which increases RGS binding [21]. The structural constraints of G α N-terminal helix interaction with the RGS are not identified, yet it was shown that the presence of myristoylation increased the affinity of G α (z/i) to RGS proteins whereas palmitoylation decreased [18].

The G $\beta\gamma$ dimer also interacts with effector molecules including PLC β , AC, β -adrenergic receptor kinase, MAP kinase pathway components, K $^+$ and Ca $^{+2}$ channels, crystal structures are available for some of them. The G $\beta\gamma$ interacts with these effector molecules and G α using a similar mechanism but different residues are involved for interactions with known effectors. Most of the interaction is through the central structure around the cavity formed by blades. The G $\beta\gamma$ dimer has effector specificity

similar to $G\alpha$ different $G\beta\gamma$ subunits interact with different effector molecules. The specificity is considered to be mainly due the hydrophobicity and tight structural constrains of $G\beta$ and also the involvement of lipid moiety on the $G\gamma$ was shown. [18]

Recently new signaling components functioning in heterotrimeric signal transduction pathway were identified, which are non-receptor GEF proteins. These soluble proteins (AGS1, Ric8A) act as receptors and promote GDP release /GTP binding to $G\alpha i/q$. The involvement of $G\alpha$ subunits in cell division was shown to be receptor independent and Ric-8 was shown to prefer the GDP bound state and increase $GTP\gamma S$ binding in *C.elegans* [68]. There are also GDI proteins that act on $G\alpha i$ family to prevent GDP release by their conserved GoLoco domain to help formation of a salt bridge between the P-loop and switch I [69]. This salt bridge is also observed in the heterotrimer structure and locks GDP inside $G\alpha$. These proteins are suggested to promote $G\alpha$ dissociation from heterotrimer without nucleotide release/exchange [33].

2.3 The plant heterotrimeric G proteins

In plants studies revealed the presence of the three subunits in the *A. thaliana* and *Oryza sativa* (rice) genomes; $G\alpha$; GPA1 [3] and RGA1 [70], $G\beta$; AGB1 [4] and RGB1 [71], and finally the two $G\gamma$; AGG1, AGG2 [5, 6] and RGG1, RGG2 [72], respectively. For other cereals, α subunits were identified from *Triticum aestivum*; TaGA1, TaGA2 [73], *Hordeum vulgare* (accession: AF267485.2) and β subunits from *Triticum avestivum* (accession: BAC10503) and *Zea mays*, ZGB1 [4]. Sequence homologies show that plant G proteins contain the functional domains seen in mammalian counterparts. Recombinant expression studies show that plant $G\alpha$ subunits can bind specifically to GTP and have GTPase activity [74-77].

The signaling pathways involving heterotrimeric G proteins in *A.thaliana* were shown mainly by analyses on mutant plants. The phenotypic differences in the absence or with the overexpression of the subunits are well characterized for *A. thaliana* and

O.sativa [78]. These studies point to involvement of G proteins in important plant processes such as regulation of ion channels (stomatal regulation and drought stress), cell division, seed germination, plant growth and development and pathogen response which are regulated by plant hormones abscisic acid (ABA), auxin, brassinolide, gibberellin [78-81], ethylene, salicylic acid and jasmonic acid [82]. Many other signaling pathways including; light [73, 83], sphingolipid [84], oxidative stress response to ozone [85] and response to metal toxicity [86] also appear to be mediated by plant heterotrimeric G proteins. Furthermore the presence of heterotrimeric G protein subunits in diverse plant species highlights their importance in plant systems [2].

2.3.1 GPA1

GPA1 is detected in all organs and cell types, being most abundant in vegetative tissues including leaves and roots, less in floral stems and least in floral buds and floral meristems [87]. Results of localization studies of $G\alpha$ are consistent with the classical heterotrimer model where the protein immunolocalizes at the PM and ER membrane [88].

GPA1 is encoded by a 1149 bp gene resulting in a protein of 383 amino acids, corresponding to a molecular mass of 44,482 Da. GPA1 is 36% identical to rat $G\alpha i1-3$ and bovine rod transducin ($G\alpha t$) at the amino acid level [3].


```

H_Gi_3      MGCTLS----AEDKAAVERSKMIDRNLRDGEKAAAEVKKLLLLGAGESGKSTIVKQMKI
H_Gi_1      MGCTLS----AEDKAAVERSKMIDRNLRDGEKAAAEVKKLLLLGAGESGKSTIVKQMKI
H_Gi_2      MGCTVS----AEDKAAERSKMIDRNLRDGEKAAAEVKKLLLLGAGESGKSTIVKQMKI
H_Gs        MGCRQS----SEEKAAARRSRIDRHLRSESQQRREIKLLLLGTSNSGKSTIVKQMKI
H_Go        MGCTLS----AEPRAALERSKAIERKNLKEDGISAAADVKKLLLLGAGESGKSTIVKQMKI
H_Gt_2      MGSGAS----AEDKELAKRSKELKKLQEDADREARTVKLLLLGAGESGKSTIVKQMKI
H_Gt_1      MGAGAS----AEEK----HSRELKKLKEDAERDARTVKLLLLGAGESGKSTIVKQMKI
GPA1        MGLLCSRSRHHTEDTDENTQAAEIRRRIQAKAAEKHIRKLLLLGAGESGKSTIVKQIKI
           1 21          3 3 3          4444444
           9999
           ** *      *:      ::      :::::.....      :      *****:*****:**:

H_Gi_3      IHEDGYSEDECKQYKVVVYSNTIQSIIAIIIRAMGRKIDFGGEAARADDARQLFVLGSAE
H_Gi_1      IHEAGYSEEECKQYKAVVYSNTIQSIIAIIIRAMGRKIDFGDSARADDARQLFVLGAAE
H_Gi_2      IHEDGYSEEECRQYRAVVVYSNTIQSIIAIVKAMGNLQIDFADPSRADDARQLFALSCTAE
H_Gs        IHSGGFNLEACKYKPLIIYNADISLTRIIRALAAALRIDFHNPDRAVDVQLFALTGPAE
H_Go        IHEDGFSGEDVQYKPVVYSNTIQSLAAVRAMDTLGIEYDGRERKADARVCDVVSRME
H_Gt_2      IHQDGYSPPEECLEFKAIIYGNVLQSIILAIRAMTTLGIDYAEFSCADDGRQLNLADSIE
H_Gt_1      IHQDGYSLPEECLEFIAIIYGNTLQSIILAIVRAMTTLNIQYGDSARQDDARKLMHMADTIE
GPA1        LFQTGFDEGELKSYVVIHANVYQTIKLLHDGTREFAQNETDSAKYMLSESTAIGEKLS
           9 9 9 9 99          9 9
           ...*:.      .:      ::      *.      :::      :      .      :      :      .      :      .

H_Gi_3      E-G-----VMTPELAGVIKRLWRDGGVQACFSRSREYQLNDSASYYLNDLDRISQSNYI
H_Gi_1      E-G-----FMTAELAGVIKRLWKDSGVQACFNRSREYQLNDSAAYYLNDLDRIAQPNYI
H_Gi_2      EQG-----VLPDDLSGVIRRLWADHGVQACFGRSREYQLNDSAAYYLNDLERIAQSDYI
H_Gs        SKG-----EITPELLGVMRRLWADPGAQACFSRSSEYHLDNAAYYLNDLERIAAADYI
H_Go        DTE-----PFSAELLSAMRRLWGDSGIQCFNRSREYQLNDSAKYYLDSLDRIGADYQ
H_Gt_2      E-G-----TMPPELVEVIRRLWADHGVQACFERAAEYQLNDSASYYLQLERITPEYL
H_Gt_1      E-G-----TMPKEMSDIQRLWKDSGIQACFERASEYQLNDSAGYYLSDLERLVTPGVY
GPA1        EIGRLDYPRLTKDIAEGIETLWKDPAIQETCARGNELQVPDCTKYLMENLKRLSDINYI
           9
           .      .:      ::      :      **      .      *      *      .:      :      *      .:      *      *

H_Gi_3      FTQQDVLTRVKTFGIVTHTFFKDLY-----FKMFDVGGQRSERKKWIHCFBGVTAII
H_Gi_1      FTQQDVLTRVKTFGIVTHTFFKDLH-----FKMFDVGGQRSERKKWIHCFBGVTAII
H_Gi_2      FTQQDVLTRVKTFGIVTHTFFKDLH-----FKMFDVGGQRSERKKWIHCFBGVTAII
H_Gs        FTVEDILRSRDMTFGIVTKTFFKELT-----FKMVDVGGQRSERKKWIHCFBGVTAII
H_Go        PTEQDILRTRVKTFGIVTHTFFKNLH-----FRLFDVGGQRSERKKWIHCFBGVTAII
H_Gt_2      PSEQDVLRSRVKTFGIITKFSVKDLN-----FRMFDVGGQRSERKKWIHCFBGVTCII
H_Gt_1      PTEQDVLRSRVKTFGIITKFSFKDLN-----FRMFDVGGQRSERKKWIHCFBGVTCII
GPA1        PTKEDVLYARVRTFGVVIQFSPVGNKKSGEVYRLFDVGGQRSERKKWIHLFPGVTAVI
           6 5 3          3 3 763 3 33 3 33
           Switch I/Mg42 binding          switch II/ Mg42 binding
           *:      **:      *      *      *      *      *      *      *      *      *      *      *      *      *
           *:      **:      *      *      *      *      *      *      *      *      *      *      *      *      *

H_Gi_3      FCVALSDYDLVLANDEMNRMHESSMKLFDSICNNKWFTETSIILFLNKKDLFEEKIRSP
H_Gi_1      FCVALSDYDLVLANDEMNRMHESSMKLFDSICNNKWFTETSIILFLNKKDLFEEKIRSP
H_Gi_2      FCVALSAYDLVLANDEMNRMHESSMKLFDSICNNKWFTETSIILFLNKKDLFEEKITSP
H_Gs        FCVELSGYDLKLYNDNQTSRMAESLRLFDSICNNWFINTSLILFLNKKDLLAEKIRIP
H_Go        FCVALSGYDQVLHEDTTRNRMHESSLMLFDSICNNKFIDTSIILFLNKKDLFEEKIRSP
H_Gt_2      FCAALSAYDMVLVDDEVNRMHESSLHLFNSICNNKFFAATSIVLFLNKKDLFEEKIRKVH
H_Gt_1      FIAALSAYDMVLVDDEVNRMHESSLHLFNSICNNRYFATSIVLFLNKKDVFEEKIRKAH
GPA1        FCAAISEYDQVLFEDBQKNRMETKELFDVLKQPCFEKTSFMLFLNKKFDIFEPKVLDVP
           Switch III          7777
           *      .      *      *      *      *      *      *      *      *      *      *      *      *      *
           *      .      *      *      *      *      *      *      *      *      *      *      *      *      *

H_Gi_3      LTIC--YPEYT----GSNTYEEAAAYIQCQFEDLNR-----KDTKMIYTHFTCATDT
H_Gi_1      LTIC--YPEYA----GSNTYEEAAAYIQCQFEDLNKR-----KDTKMIYTHFTCATDT
H_Gi_2      LTIC--FPEYT----GANKYDEAASYIQSKFEDLNKR-----KDTKMIYTHFTCATDT
H_Gs        LTIC--FPEYK----GQNTYEEAAVYIQRQFEDLNRN-----RETKMIYSHFTCATDT
H_Go        LTIC--FPEYT----GPNTYEDAAAYIQAQFESKNRS-----P-NKMIYCHMFTCATDT
H_Gt_2      LSIC--FPEYD----GNNSYDDAGNYIKSQFLDLNMR-----KDVKMIYSHMFTCATDT
H_Gt_1      LSIC--FPDYD----GPNTYEDAGNYIKVQFLELNMR-----RDVKMIYSHMFTCATDT
GPA1        LNVCEFRDYQPVSSGRQELEHAYEFVKKKFELYQNTAPDRVDRVFKIYRTALDQ
           7777
           p.receptor bin
           .:      .:      *      *      *      *      *      *      *      *      *      *      *      *      *

H_Gi_3      KNVQFVDAVTDVIKNNLKECGLY
H_Gi_1      KNVQFVDAVTDVIKNNLKDCGLF
H_Gi_2      KNVQFVDAVTDVIKNNLKDCGLF
H_Gs        SNIQFVDAVTDVIQNNLKYIGLC
H_Go        NNIQVFDAVTDIIANNLRGCGLY
H_Gt_2      QNVKFVDAVTDIIKENLKDCGLF
H_Gt_1      QNVKFVDAVTDIIKENLKDCGLF
GPA1        KLVKKTFKLVDETLRRRNLLEAGLL
           p.receptor bin
           .:      .:      *      *      *      *      *      *      *      *      *      *      *      *      *

```

Figure 2.5: CLUSTALW alignment of human Gαi family members and GPA1. Completely conserved (blue), identical (green) and conserved domains (bold face) are shown. Important residues are numbered and indicated in text.

Multiple alignment with all human G α shows that GPA1 is most similar to G α i family (Figure 2.4). The heterotrimeric G α specific residues and motifs are conserved in GPA1 (Figure 2.5); palmitoylated cysteine (2), G $\beta\gamma$ contact sites (3), P-loop (4), RGS contact site (5) and nucleotide binding residues (7). The critical residues for GTP hydrolysis are also identical in GPA1, arginine and glutamine (6). Considering the conserved residues GPA1 is most similar to G α i subfamily and similarity results from the G α i subfamily specific N-terminus myristoylation motif; glycine (1) and serine (1), GoLoco binding residues (9) and within this subfamily the absence of the carboxy-terminal cysteine (8) is unique to only G α z, which is known to play a role in cell proliferation and death via its control of potassium channels [89]. The evolutionary connection between plant and mammalian G α was investigated using bioinformatic tools and plant G α is found to be descended from G α o which was predicted to be the G α ancestor [90]. All residues of GoLoco motif are not conserved in GPA1, which is a good indicator that plants have different effector proteins possessing GDI activity. Switch regions and putative receptor binding sites are underlined in Figure 2.5 and these are not fully conserved as expected.

There is limited literature on recombinant expression of plant G α subunits. Cloning of *GPA1* has been reported by Wise et al., [76] and GPA1 was produced from *E.coli* in the presence of an arginine tRNA encoding plasmid with a yield of 1-2 mg per L culture. The recombinant protein bound 0.3 mol GTP γ S / mol protein with an apparent Kd of 0.34 nM assuming one binding site. Recombinant RGA1 was produced from *E.coli* and there are two significantly different kcat values reported; 0.44 min⁻¹ [75] and 0.0075 min⁻¹ [74]. The first kcat was calculated from the apparent binding constant (0.36 nM) and Mg⁺² was not required for GTP binding [75]. In another study GPA1 was expressed with an N-terminus 6 his tag in *E.coli* and purified protein had a very high GTP binding rate, 1.4 min⁻¹ and 14.4 min⁻¹ as shown by radioactive and fluorescent GTP γ S probes respectively. The kcat was reported to be 0.12 min⁻¹ and the bound GTP γ S was 0.91 mol GTP γ S/ mol protein and GPA1 was shown to prefer GTP γ S over GDP in a 5 minute nucleotide competition assay. According to these values the authors suggest that GPA1 has higher affinity to GTP over GDP and is found mostly as GTP bound due to its low GTPase activity [77].

RGA1 with mutations at active site arginine (R191L) or glutamine (Q223L) were shown to be GTPase dead (constitutively active) but they retained GTP binding ability [91]. Q222L mutant of GPA1 was also shown to be constitutively active. [92]. Total protein was isolated from Arabidopsis seedlings, native, overexpressing GPA1 and overexpressing Q222L GPA1 and applied to gel filtration column. The fractions were detected with α -GPA1 antibody and most of the protein was eluted as oligomers with molecular mass higher than 45kDa; even for the constitutively active form [93]. This may imply that GPA1 forms oligomers *in vivo*, with other proteins and/or itself.

There is no direct experimental evidence showing GPA1 or any other plant G α is myristoylated or palmitoylated upto date. As indirect evidence, a peptide consisting of the N-terminal 8 residues of GPA1 was synthesized and 2nd amino acid glycine was shown to be N- myristoylated by *A.thaliana* myristoyl transferase (AtNMT1) by an *in vitro* spectroscopic assay [94]. The putative lipid modifications sites; G2 and C5 were mutated and CFP (Cyan Fluorescent Protein) fusion single or double mutants were localized both on PM and cytosol, G2 mutants being more cytosolic. In the same study the Q222L mutant was localized to PM similar to GPA1 [95]. These results imply that GPA1 has sites for both myristoylation and another molecule (not proved to be palmitate) which increase the proteins affinity to PM.

2.3.2 AGB1 and AGG1/AGG2

AGB1 is encoded by a 1134 bp gene resulting in a protein with 377 amino acids; ~41 kDa. AGB1 contains the WD-40 domains and share 45% identity with mammalian G β subunits (Figure 2.6).

```

                                1   1
H_beta_4  M--SELEQLRQEAQ----LRNQIQDARKACNDATLVQITSNMDSVGRIQMRTTRTLRGH
H_beta_1  M--SELDQLRQEAQ----LKNQIRDARKACADATLSQITNNIDPVGRIQMRTTRTLRGH
H_beta_2  M--SELEQLRQEAQ----LRNQIRDARKACGDSTLTQITAGLDPVGRIQMRTTRTLRGH
H_beta_3  M--GEMEQLRQEAQ----LKKQIADARKACADVTLAEIVSGLEVGRVQMRTTRTLRGH
AGB1      MSVSELKERHAVATETVNNLRDQLRQRRLQLLDTDAAQGRTRVS-FGATDLVCCRTLQGH
          ..*::: : * :   **::: * * * :   : . * ::   ****:*
          2222          3333          333          222

H_beta_4  LAKIYAMHWGYDSRLLVSASQDGLIWDSYTTNKMHAIPLRSS  WVMTCAYAPSGNYVAC
H_beta_1  LAKIYAMHWGDSRLLVSASQDGLIWDSYTTNKVHAIPLRSS  WVMTCAYAPSGNYVAC
H_beta_2  LAKIYAMHWGDSRLLVSASQDGLIWDSYTTNKVHAIPLRSS  WVMTCAYAPSGNFVAC
H_beta_3  LAKIYAMHWATDSKLLVSASQDGLIWDSYTTNKVHAIPLRSS  WVMTCAYAPSGNFVAC
AGB1      TGKVYSLDWTPERNRIVSASQDGLIVWNALTSCKTHAIKLPCA  WVMTCAFSPNGQSVAC
          .*::::* : . :*****:**::: *:* * * * . : *****:*. : * *
          22          22

H_beta_4  GGLDNICSIYNLKT---REGNVRVSRELPGHTGYLSCCRFLD--DSQIVTSSGDITCAL
H_beta_1  GGLDNICSIYNLKT---REGNVRVSRELPGHTGYLSCCRFLD--DNQIVTSSGDITCAL
H_beta_2  GGLDNICSIYSLKT---REGNVRVSRELPGHTGYLSCCRFLD--DNQIITSSGDITCAL
H_beta_3  GGLDNMCSIYNLKS---REGNVKVSRELSAHTGYLSCCRFLD--DNNIVTSSGDITCAL
AGB1      GGLDSVCSIFSLSTADKDGTVPSRMLTGHRGYVSCCQYVPNEDAHLITSSGDQTCIL
          ****:****:..: :*. * * * * . * * * :*****: : * :***** * * *

                                2
H_beta_4  WDIETAQQTTF-----TGHSGDVMSLSLS-PDMRTFVSGACDASSKLWDIRDG-MCRQSF
H_beta_1  WDIETGQQTTF-----TGHTGDVMSLSLA-PDTRLFVSGACDASAKLWDVREG-MCRQTF
H_beta_2  WDIETGQQTIVGF-----AGHSGDVMSLSLA-PDGRTFVSGACDASIKLWDVDRS-MCRQTF
H_beta_3  WDIETGQQKIVF-----VGHTGDCMSLAVS-PDFNLFISGACDASAKLWDVREG-TCRQTF
AGB1      WDVITGLKTSVFGGFEFQSGHTADVLSVSISSGNPNWFISGSCDSTARLWDTRAASRAVRTF
          *: * . . *   **:* * :***** :. :*:*:*:*: :*** * . . ::*

                                2                                1
H_beta_4  TGHVSDINAVSFFPNGYAFATGSDDATCRLFDLRADQELLLYS-HDNIICG-ITSVAFSK
H_beta_1  TGHESDINAICFFPNGNAFATGSDDATCRLFDLRADQELMTYS-HDNIICG-ITSVSFSK
H_beta_2  IGHESDINAVAFFPNGYAFTTGSDDATCRLFDLRADQELLMYS-HDNIICG-ITSVAFSR
H_beta_3  TGHESDINAICFFPNGEAICTGSDDASCRLFDLRADQELICFS-HESIICG-ITSVAFSL
AGB1      HGHEGDVNTVKFFPDGYRFTGSDDGTCRLYDIRTGHQLQVYQPHGDGENGPVSIAFSV
          ** .*:::: :***:* : *****:***:*:*:*:* :. * . * :***:*

                                111
H_beta_4  SGRLLLAGYDDFN-CNVWDILKGDRAGVLAG----HDNRVSCLGVIDDGMAVATGSWDSF
H_beta_1  SGRLLLAGYDDFN-CNVWDALKADRAGVLAG----HDNRVSCLGVIDDGMAVATGSWDSF
H_beta_2  SGRLLLAGYDDFN-CNIWDAMKGDRAGVLAG----HDNRVSCLGVIDDGMAVATGSWDSF
H_beta_3  SGRLLFAGYDDFN-CNVWDSMKSERVGILSG----HDNRVSCLGVIADGMAVATGSWDSF
AGB1      SGRLLFAGYASNNTCYVWDTLLGEVVLDLGLQQDSHRNRISCLGLSADGSALCTGSWDSN
          *****:*** . * * :***: . . . * . * * * :*****: * * :*****

H_beta_4  LRIWN-----
H_beta_1  LKIWN-----
H_beta_2  LKIWN-----
H_beta_3  LKIWN-----
AGB1      LKIWAFGGHRRVI
          *:*

```

Figure 2.6: CLUSTALW alignment of human and arabidopsis Gβ protein sequences. Completely conserved (blue), identical (green) and WD repeats (bold face) are shown. Residues numbered are involved in contacts with Gγ (1), Gα switch regions (2) and Gα N-terminus; highlighted residues are similar but not identical to human residues.

palmitoylation; as both mutating this residue and incubating with a palmitoylation inhibitor resulted in cytosolic localization of YFP fusions in tobacco leaves [96].

Both AGG1 and AGG2 were identified from yeast two hybrid screens using AGB1 as bait. *In vitro* interaction was confirmed between AGB1 (*in vitro* translated and radioactively labeled) and AGG1/AGG2 (GST fused) by the presence of radioactivity after purification from glutathione beads. However in these papers analysis of GST fusion proteins neither by SDS-PAGE nor western blots is shown [5, 6].

The tobacco G β was shown to be localized on PM and was also detected in purified nucleus fractions [97], AGB1-CFP fusion was detected in both intracellular membrane and plasma membrane fractions of Arabidopsis leaves [98]. YFP-AGG1 was localized to PM in Arabidopsis protoplasts in both the presence and absence (agb1 null mutant line) of AGB1, whereas YFP-AGB1 was localized to both PM and cytosol. AGB1 was completely localized to PM when AGG1 was coexpressed on the same expression vector. FRET results show that AGB1 and AGG1 interact on PM [99]. In another study YFP-AGG1 was localized on both PM and Golgi, whereas YFP-AGG2 was completely localized to PM in cowpea protoplasts. The number of CFP-AGB1 expressing cells was higher when either G γ was coexpressed and C95S mutant YFP-AGG2 was shown to interact with CFP-AGB1 by FRET [95]. All these results support that G β and G γ can interact, before lipid modification and the dimer is translocated to PM.

Promoter::GUS analysis was done for AGB1, which exhibited ubiquitous expression in vegetative organs, and expression in stamens, stigma and the abscission zone of the floral organs. AGG1 expression was in apical meristem, leaves, mature roots, the abscission zone of the floral organs and stamens; and AGG2 was detected in vegetative organs, including meristematic tissues, leaves and the roots [100]. Quantitative PCR analysis showed that both GPA1 and AGB1 has higher levels of expression in roots as compared to shoots in *A. thaliana* seedlings[79].

2.3.3 Signaling Components

Although mammalian heterotrimeric G proteins are well characterized, studies on plant systems are limited. Recently two important heterotrimeric G protein signaling components were identified. The search for 7 TM domain proteins in *A. thaliana* genome resulted in only two proteins, a putative plant GPCR protein, G-Coupled Receptor1 (GCR1) and an unusual Regulator of G-protein Signaling protein (AtRGS1). The function of GCR1 as a G protein coupled receptor was suggested based on the evidence of *in vitro* interaction of the G protein α subunit with the receptor [101]. Studies with mutant plants reveal that GCR may have both heterotrimer dependent and independent functions [102]. A ligand for GCR1 could not be identified yet. The unique regulator of G protein signaling protein, AtRGS1, was shown to interact with Arabidopsis GPA1, to accelerate its intrinsic GTPase activity, and thereby modulate cell proliferation [83]. Furthermore AtRGS1 was shown to be involved in sugar and ABA signaling in seed germination [103] whereas GCR1 was shown to be involved in cell cycle [104, 105], brassinosteroids and gibberellins [102] and ABA signaling in seed germination [106].

AtRGS1 was shown to physically interact with GPA1 by *in vitro* GST pull down assay, with higher affinity to AlF_4^- bound form than both GDP and $GTP\gamma S$ bound forms. For this the C-terminal RGS box of AtRGS1 was produced as an N-terminal GST fusion in *E.coli*, and low amount of protein was reported to be soluble [107]. The presence of GST-RGS increased the GTPase activity of GPA1. AtRGS1 was also shown to interact with both GPA1 and Q222L GPA1 in yeast complementation assays. The full length AtRGS1 fused with GFP was shown to be localized on PM of Arabidopsis protoplasts [83] and the interaction was also shown with FRET in Arabidopsis root PM [77].

Two interesting Arabidopsis proteins were recently identified, which were named as GTG1 and GTG2. These proteins are localized in plasma membrane, have predicted 8-10 transmembrane domains and have GTP binding / hydrolysis activity, with a higher preference to GDP than GTP. The involvements of GTG1 and GTG2 in ABA signaling was shown with mutant studies and *in vitro* binding assays and thus are proposed to be

ABA receptors. Furthermore constitutively active (GTPase deficient) GPA1 was shown to interact and reduce GTPase activity of these proteins [92].

Although RGS and GTG1/2 have predicted transmembrane domains, these proteins are not directly verified to be receptors. The presence of receptor and regulator proteins raises the possibility that the mechanism of action of the heterotrimer in plants is similar to that observed in mammalian system, but it is obvious that there are additional mechanisms significantly different from the mammalian systems, which may be heterotrimer independent.

There are a limited number of possible effectors identified in plants. One of them is phospholipase D (PLD) and was shown to be activated during ABA inhibition of stomatal inwardly rectifying K^+ channels in *Vicia faba* guard cells and barley aleurone [108, 109]. PLD in membrane preparations from barley aleurone is stimulated by ABA also *in vitro*, and GTP γ S, an activator of G protein α subunit, was shown to mimic the effect of ABA on PLD. Thus PLD activation by ABA probably involves the active G protein as an essential component in barley aleurones [110]. This raises the possibility that PLD α 1 can be a GAP and this was supported by the increased GTPase activity of GPA1 in the presence of PLD [111]. The other putative effectors are Atpirin1, prephenate dehydratase (a cytosolic enzyme involved in regulation of the shikimate pathway), and THF1 (a protein located in plastid membranes) [112].

2.4 The plant heterotrimer

The *A. thaliana* heterotrimer structure was modeled by Ullah et al., [113] using the high resolution structure 1GOT as template for homology modeling. A similar structure at the $G\alpha/G\beta$ interface and the $G\beta\gamma$ dimer structure of the model and the crystal structure (Figure 2.8) suggest that plant heterotrimeric G protein exists and activation by nucleotide exchange may follow the mammalian pattern by means of subunit binding/dissociation.

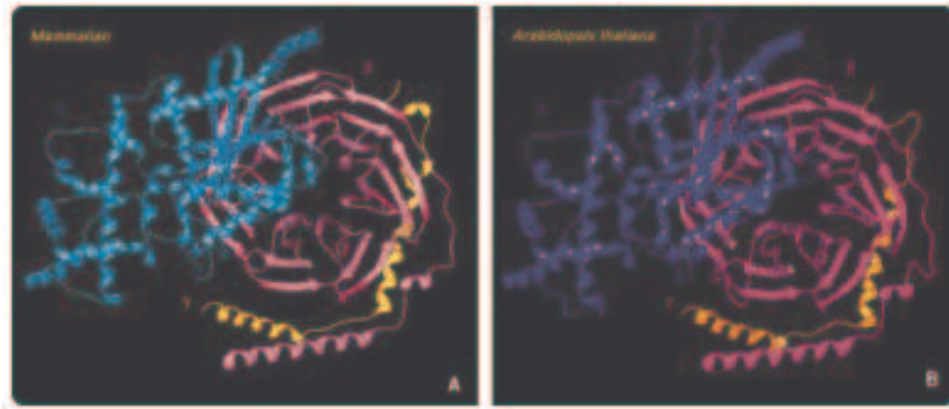


Figure 2.8: 1GOT (A) and the homology modeled Arabidopsis complex (B) [113]. The α , β and γ subunits colored blue, purple and gold, respectively.

There are various reports that suggest interaction of subunits both *in vivo* and *in vitro*. GPA1 and AGB1 was shown to interact by yeast complementation assay [114], GPA1 was shown to interact with dimer, but not with individual subunits in FRET assays and GPA1 did not co-immuno-precipitate with AGG1 in the absence of AGB1 [99]. The heterotrimer and subunits were found to be in large complexes with a molecular mass higher than that of estimated for heterotrimer in Arabidopsis PM fractions using a native –SDS-PAGE-western detection approach. GPA1 antibody reacted with complexes of variable size, but dominantly there were two bands, one with a very high molecular mass (HMM) and the smallest which could be representing the monomeric mass. The addition of GTP γ S to PM fractions resulted in a decrease in the amount of HMM but did not result in a complete dissociation into a monomeric form. Similarly AGB1 was found in HMM using a CFP antibody in CFP-AGB1 expressing leaves [99]. The exact mass of those HMM complexes and assumed monomers are not known since the first electrophoretic separation was done on Native-PAGE. A similar study was done with rice leaf plasma membranes, the solubilized PM proteins were applied to a gel filtration column and the fractions were analyzed with rice subunit specific antibodies. All these subunits were detected in fractions with mass 400-700 kDa, but RGB1, RGG1 and RGG2 were more in fractions with size 60-200 kDa. Addition of GTP γ S both during PM isolation and gel filtration resulted in elution of all subunits in complexes with mass with 100-200 kDa and RGB1, RGG1/2 isolated from null *rga* mutant rice had a similar pattern. When the GTPase deficient Q223L mutant RGA was introduced on null *rga* background, all subunits were again found in HMM

complexes although the amount was lower as compared to that of wild type rice. These results suggest that heterotrimer forms in plants together with yet unidentified proteins and subunit dissociation may not be the case for plant heterotrimeric G proteins. The observation of plant $G\alpha$ being localized with other proteins even in the constitutively active form may suggest that effector interactions also take place in plant membrane.

Plants have reduced numbers of each heterotrimeric G protein component identified until now. The number of $G\alpha$, $G\beta$ and $G\gamma$ will not be increased as rice and Arabidopsis genomes do not have any other putative isoforms. There may be other signaling proteins substituting the heterotrimer or the plants can manage with this low complexity of specificity. The heterotrimeric G proteins in mammalian systems function in several pathways and mainly these pathways lead to response to light (vision), odour and taste perception or are involved in neural transmission and muscle contraction. Mammalian systems have a diverse set of genes/proteins that work specifically in each tissue. Plant systems, on the other hand, have less overall complexity in terms of tissue types, cell communication and signaling. The diverse pathways that heterotrimeric G proteins are involved in mammalian systems can be converted to plants by two general mechanisms, hormone perception and regulation of ion channels. Although we may not yet have enough information about the complexity of plant signal transduction pathways, hormone sensing (ABA, auxin, GA, ethylene, JA) and ion channel regulation (stomatal regulation, pathogen response) can be regulated by a simpler repertoire of heterotrimeric G proteins, without the necessity of subunit specificity. The tissue specific behavior of GPA1 and AGB1 with response to same hormone/signal was shown especially in regulation of ion channels and cell division [81]. This may imply that the response of signaling is more dependent on the tissue specific effectors and not the heterotrimer subunits.

2.5 Biophysical Approach

2.5.1 Circular Dichroism Spectropolarimetry

Circular Dichroism measures the difference in absorbance of right and left circularly polarized light. The spectra are a combination of optical absorption (electric dipole moment) and asymmetry (magnetic dipole moment) and thus secondary structure elements have signature absorbances in CD spectra. CD is especially sensitive for α helical secondary structure. α helices have two distinct minima at 208 nm and 222 nm, and a maximum at 192 nm. Spectra of disordered structures have a minima \sim 200 nm and β -sheets have a minima at 217 nm which is very broad and a maxima at 193 nm (Figure 2.9). The far-UV region (180-230 nm) absorption is related to backbone conformational changes and the near-UV region is dominated by the absorption of aromatic amino acid side chains. The far-UV region is important for analysing secondary structure features, but below \sim 200 nm buffer components significantly contribute to signal which prevents a clear characterization [115]. The CD data is represented as ellipticity (θ) instead of absorbance. Protein concentration and cuvette path length are important parameters that affect ellipticity so these are also included in data processing and final data is represented as mean residue ellipticity, with units $\text{deg cm}^2 \text{dmol}^{-1}$. A polypeptide composed of only α helical secondary structure will give a mean residue ellipticity of \sim -30.000 $\text{deg cm}^2 \text{dmol}^{-1}$ at 222 nm, so a protein will have less ellipticity with a higher value [116]. A simple way of estimating the α helices is the ratio of intensities of two negative bands, $\theta_{208 \text{ nm}} / \theta_{222 \text{ nm}}$, which should be \sim 1 for mainly helical proteins. This ratio becomes < 1 for peptides with coiled-coil interactions and is > 1 if α -helical secondary structure formation occurs [117]. The near UV absorption gives information about the tertiary structure of the protein, as the conformations (asymmetry) of aromatic side chains depend on their local environment. Phenylalanine, tyrosine and tryptophan has absorption around 250-260 nm, 270-280 nm and 280-300 nm respectively (Figure 2.10), yet the signals from Tyr and Trp may overlap [116]. Unfolding results in disruption of the local environment and thus the asymmetry of these aromatic residues and CD signals are greatly reduced /lost. Molten globule or

partially folded structures display very weak / no signals at near-UV region, although the far-UV spectra is not generally affected. Thus, the presence of near UV signals is a good indicator that protein retained a well defined tertiary fold. The near-UV CD spectra is sensitive to small changes in overall structure resulting from solvent conditions or protein-protein interactions [115]. Near-UV CD mean residue ellipticities for the aromatic amino acid side chains should be generally lower than $200 \text{ deg cm}^2 \text{ dmol}^{-1}$ [116].

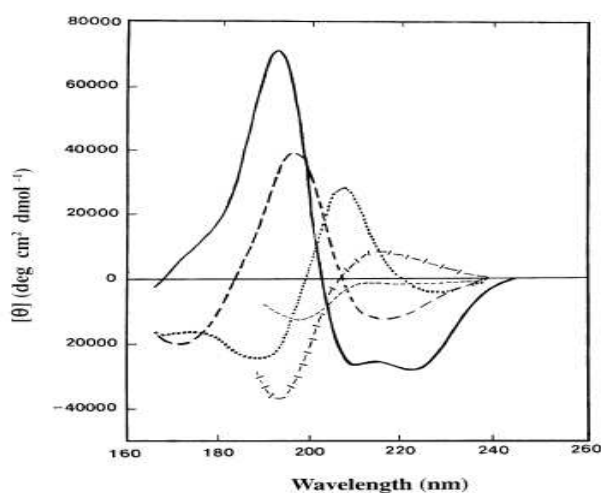


Figure 2.9: Far-UV CD spectral analysis of secondary structural elements. α -helix (—), anti-parallel β sheet (---), type 1 β turn (.....), extended 3_1 -helix (++) and irregular structure (- - - -), figure taken from [116].

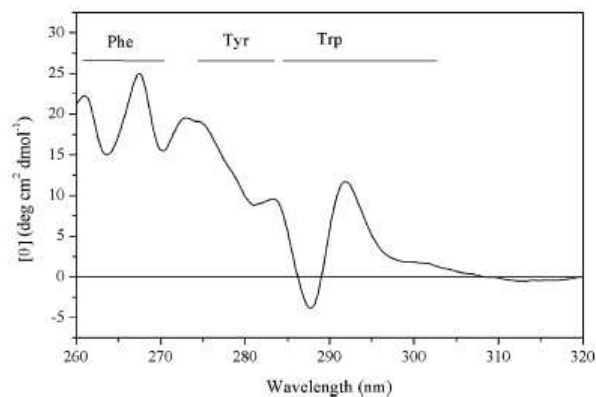


Figure 2.10: The near UV CD spectrum for type II dehydroquinase from *Streptomyces coelicolor*. Figure taken from [116].

2.5.2 The use and detection of detergents in membrane protein purification

The use of detergents is essential for solubilization integral membrane or transmembrane protein solubility and stability, but the presence of detergents generally lead to experimental difficulties. The main reason to use a detergent during a membrane attached/integrated protein is to try to mimic the physical properties of the membrane bilayer where protein structure is maintained [118]. It is important to verify the functional activity and structural integrity of proteins in the presence of detergents. Non-ionic detergents with medium / long alkyl chains are generally the choice, since zwitterionic detergents tend to denature proteins [119]. The detergent concentration used is an important parameter to be optimized, to ensure complete solubility of protein a concentration higher than critical micelle concentration (cmc) of the detergent should be used. Above cmc, the detergent will form micelles and in turn result in the formation of protein micelle complex (PMC). It is important to find the optimal concentration since use of very high amount of detergent can lead to removal of essential lipid moieties from the protein and protein aggregation. Addition of phospholipids was shown to improve the stability of PMC in some cases. Above cmc the micellar-monomeric form equilibrium will be reached and the amount of free monomer will be constant. The cmc of a detergent may be effected by temperature and ionic strength of the buffers used so requires careful inspection. Aggregation number refers to the number of detergent molecules in the detergent micelle and depends on the molecular mass of the monomeric form of the detergent. Detergents with high aggregation number will result in formation of high molecular mass PMC and thus will interfere with the experimental procedures that are used for protein size measurements [118]. The mode of detergent-protein binding depends on the nature of both components, detergents tend to form a prolate monolayer ring around the transmembrane region of TM proteins whereas a micellar binding mode is assumed for less hydrophobic proteins that are integrated into membrane with small regions [119].

The presence of detergent micelles in protein solution can be experimentally verified by different techniques, fourier transform infrared spectroscopy (FT-IR), thin layer chromatography and nuclear magnetic resonance (NMR). ¹H proton NMR was

shown to be a powerful tool to monitor the presence and the amount of detergent that remains after protein purification procedures [120].

2.5.3 Small Angle Solution X-ray Scattering

Small angle solution X-ray scattering (SAXS) results from the contrast of electron density of a macromolecular solution distributed isotropically in a solvent with uniform electron density. The macromolecules in solution scatter the incident beam at an angle 2θ (scattering angle) and the intensity of the scattered beam, $I(s)$ is proportional to the concentration of the molecules. In a monodisperse solution the intensity will reflect the scattering from a single particle averaged over all directions. The concentration of the molecule determines the magnitude of the signal. SAXS provides information about the molecular mass (MM), radius of gyration (R_g), hydrated volume and maximum intramolecular distance (D_{max}) [121].

Low resolution (1-2 nm) structural models can be built from SAXS data by fitting the electron density information into dummy residues *ab initio*. The availability of high resolution structural models (X ray crystallography atomic models) makes it possible to combine information about subunits of a multidomain protein or to determine the physiological oligomeric state of a protein in solution. For this the scattering from atomic models are calculated using a software (CRY SOL) and the resulting scattering is fitted on the experimental scattering (SAXS data) using a simulated annealing software (SASREF). SAXS data can also be used to model the missing portions of an atomic model [121].

CHAPTER 3

3 MATERIALS AND METHODS

3.1 Materials

3.1.1 Chemicals

Chemicals that are used are listed in Appendix A.

3.1.2 Molecular biology kits

Molecular biology kits that are used for DNA isolation, gel extraction, DNA cleanup/desalting, cloning /expression, protein purification, protein quantification and biophysical characterization are listed in Appendix B.

3.1.3 Other materials

Details of materials including, cells, plasmids, DNA markers, protein markers, purification media, enzymes and enzyme buffers are listed in Appendix C. Maps of plasmids are given in Appendix E.

3.1.4 Equipment

Equipment used for general laboratory procedures are listed in Appendix D.

3.1.5 Genes

The genes were amplified from plasmids purchased from TAIR. The details of plasmids are given in Table 3.1.

Table 3.1 Plasmids purchased from TAIR

Target gene	Vector	Resistance	Source	Accession	Vector size, bp	Gene size, bp	Total size, bp
AGB1	lambda ZipLox	amp	DH10B	162P20	4307	1134	5441
AGG1	pUNI51	kan	PIR1	U82042	2551	297	2848
AGG2	pUNI51	kan	PIR1	U84515	2551	303	2854

3.1.6 Buffers and solutions

Standard buffers and solutions used in cloning and molecular manipulations were prepared according to the protocols in Sambrook et al., 2000 [122].

3.1.7 Culture medium

a. *Escherichia coli*

LB Broth (Lenox L broth) containing tryptone, yeast extract and NaCl from Sigma (L-3022) was used for liquid culture of bacteria. 20 g of LB Broth was used for preparation of 1 L liquid medium. The liquid medium was autoclaved at 121° C for 15 min. before using. Ampicillin at a final concentration of 100 µg/ml was added to liquid medium for selection.

LB Agar (Luria Bertani, Miller) containing tryptone, yeast extract, NaCl and agar from Sigma (L-3147) were used for preparation of solid medium for the growth of bacteria. 40 g of LB Agar was used for preparation of 1 L of solid medium. The appropriate amount of LB Agar is dissolved in a corresponding amount of deionized water for autoclaving at 121° C for 15 min. Autoclaved medium was poured to Petri plates (~20 ml/plate) after cooling down to room temperature. Ampicillin at a final concentration of 100 µg/ml was added when antibiotic selection was required.

b. *Pichia pastoris*

YPD was used for liquid culture of yeast. The medium contains 1% yeast extract, 2% peptone and 2 % dextrose. Yeast extract and peptone were dissolved in water and autoclaved at 121° C for 15 min. Sterile dextrose was added before use. Zeocin, at a final concentration of 100 µg/ml was added when antibiotic selection was required.

BMGY, buffered complex glycerol medium, was used for biomass generation before induction of expression. This medium contains 1% yeast extract, 2% peptone, 100 mM potassium phosphate, pH 6.0, 1.34% YNB (yeast nitrogen base), 4 10⁻⁵ % biotin and 1% glycerol. Yeast extract and peptone were dissolved in water and autoclaved at 121° C for 15 min. Other components were separately either autoclaved or filter sterilized and added to the yeast extract and peptone mixture.

BMMY, buffered complex methanol medium, was used for induction of recombinant proteins. This medium is similar to BMGY, except that there is 1 % methanol instead of 1% glycerol.

YPD agar was used for growth of yeast on solid media. The medium contains 1% yeast extract, 2% peptone, 2% agar-agar and 2 % dextrose. Yeast extract and peptone was dissolved in water, agar was added and autoclaved at 121° C for 15 min. After cooling below 60° C sterile dextrose and zeocin at a final concentration of 100 µg/ml, when necessary, was added and medium was poured to Petri plates (~20 ml/plate).

3.1.8 Sequencing

Sequencing service was commercially provided by SEQLAB (Germany), TOPLAB (Germany), Iontek (Turkey) and an in-house sequencer was also used.

3.2 Methods

3.2.1 Culture growth

a. Escherichia coli

E. coli cells were grown overnight (12-16h) at 37 °C shaking at 300 rpm in LB Broth (Lenox L broth) prior to any application. LB Agar (Miller's LB agar) solid media was used as unselective and selective solid medium for bacterial growth at 37 °C. The protocols of Sambrook et al., [122] were used for liquid and solid culture growth as well as other applications including competent cell preparation and preparation of glycerol stocks.

b. Pichia pastoris

P. pastoris cells were grown overnight at 30 °C shaking at 250 rpm in YPD medium for general purposes. For biomass generation they were grown in BMGY medium for 48 hours before induction. Induction was performed in baffled flasks for 48 hours using BMMY medium, with 1 % methanol addition at the 6th and 24th hour.

3.2.2 PCR

Reaction volumes and final concentrations of PCR components were based on manufacturer's recommendations (Fermentas). Annealing temperatures of primers were estimated according to manufacturer instructions (Fermentas).

a. Template Isolation

Plasmids from TAIR were isolated with Qiaprep[®] Spin Miniprep Kit (250) according to the manufacturer's instructions (QIAGEN).

b. Amplification

PCR amplifications of *AGBI* and *AGGI* were carried out using the thermal cycle conditions given in Table 3.2.

Table 3.2: Thermal cycle conditions for *AGBI*, *AGGI* and *AGG2*.

Gene	Vector	Initial denat.	Cycle (30)			Final elongation
			denaturation	annealing	elongation	
		94 °C				72 °C
<i>AGBI</i>	pGEX-4T-2	3 min	94° C 1 min	65 °C 1min 5.5 °C gradient	72 °C 1min	10 min
<i>AGGI</i>	pGEX-4T-2	3 min	94° C 1 min	65 °C 1min 5.5 °C gradient	72 °C 1min	10 min
<i>AGBI</i>	pQE-80L	2 min	94° C 1 min	58 °C 1 min	72 °C 2 min	7 min
<i>AGG2</i>	pQE-80L	3 min	94° C 1 min	53 °C 1 min	72 °C 1min	10 min

PCR products were purified directly with Qiaquick® PCR Purification Kit (250) (QIAGEN).

3.2.3 Cloning

General molecular biology were done according to Sambrook et al., [122].

a. Cloning using pGEX-4T-2

10 µl of each PCR product and 400 ng of pGEX-4T-2 vector were double digested with the enzymes *EcoRI* and *XhoI* as recommended by the manufacturer (Fermentas). The digested PCR products and the vector were precipitated together with ethanol. The precipitated pellets were resuspended in water, T4 DNA ligase and ligation buffer as recommended by the manufacturer (Fermentas).

b. Cloning using pQE-80L

20 µl of *AGG2* and 5µl of *AGBI* PCR product and 2000 ng of pQE-80-L vector were double digested with the enzymes *BamHI* and *KpnI* as recommended by the manufacturer (Fermentas). The linearized vector was cleaned by phenol extraction and dephosphorylated using Shrimp Alkaline Phosphatase according to the manufacturer's

protocol (Fermentas). The digested PCR products and the vector were precipitated with ethanol and ligation was done as given in previous section.

3.2.4 Transformation

The ligation products were introduced into chemically competent *E.coli* TOP10F' cells. Briefly, 50 µl of competent cells were mixed with different volumes of the ligation products, the mixtures were incubated on ice for 30 minutes followed by heat shock, 2 minutes at 42 °C. Warm LB medium (800 µl) was added to the cells which were grown at 37 °C for 1 hour with shaking. Finally, cells were plated on selective LB agar containing 100 µg/ml ampicillin. The positive colonies appeared after overnight growth at 37 °C.

3.2.5 Agarose gel electrophoresis

1 X TAE (40 mM Tris-acetate and 1 mM EDTA pH 8.0) buffer was used for preparation of 1% agarose gels. Gels were run at constant voltage (100 mV) for 45 minutes. DNA was visualized by including 0.005% ethidium bromide in the gel during its preparation.

3.2.6 Verification and Sequencing

Colonies grown on selective medium were analyzed by colony PCR using gene specific primers. Plasmids were isolated from the PCR verified colonies and sent for sequencing.

3.2.7 Expression screen for GST-AGB1 and GST-AGG1

The verified constructs were isolated from TOP10F' cells and introduced into BL21(DE3) and BL21(DE3)RIPL expression cells. Cells were induced with different concentrations of IPTG at an optical density of ~0.6 and grown at different temperatures for optimization of expression. Samples of 1.5 ml volume were taken at different time points to monitor growth and analyzed by SDS-PAGE analyses as described below.

a. Cell lysis for cytoplasmic soluble protein

Cell pellets were resuspended in 25 μ l lysis buffer (1 mg/ml lysozyme, 25 mM Tris-HCl pH 8.5, 10 mM EDTA and 50 mM glucose). An equal volume of triton buffer I (25 mM DTT, 100 mM NaCl, 200 mM MgCl₂ and 0.8 % Triton X-100) was added to well-resuspended pellets. Solubilized cells were centrifuged for 10 minutes at 13,000 rpm in a microfuge at 4 °C. Supernatants were taken to a clean tube and mixed with SDS loading dye to be analyzed on SDS-polyacrylamide gels. Insoluble pellets were stored for inclusion body solubilization.

b. Solubilization of Inclusion Bodies

Insoluble pellets were resuspended in Triton Buffer II (50 mM Tris HCl, pH 8.0, 10 mM EDTA, 100 mM NaCl and 0.5 % Triton X-100) and incubated for 5 minutes at room temperature. The resuspended pellets were centrifuged at 4°C, 13,200 rpm for 15 minutes. Supernatants were stored in fresh tubes and are referred to as cell lysate 2. The pellet was resuspended in 100 μ l Inclusion-body Solubilization Buffer I (50 mM Tris HCl, pH 8.0, 1mM EDTA, 100 mM NaCl, 8 M urea and 0.1 mM PMSF). The solution was incubated at room temperature for 1 hour and 900 μ l of Inclusion-body Solubilization Buffer II (50mM KH₂PO₄, 1mM EDTA, 50mM NaCl) were added after

incubation. After 30 minutes of incubation at room temperature, the pH of the solution was decreased to 8 by addition of 12M HCl. After another 30 minutes of incubation at room temperature, the solution was pelleted at room temperature, 13200 rpm for 15 minutes. The supernatant, urea soluble inclusion body fraction was stored in fresh tubes. The pellet is the urea insoluble inclusion body fraction. Samples were analyzed on SDS-polyacrylamide gels.

3.2.8 Expression screen for RGS-his-AGB1 and RGS-his-AGG2

The verified constructs were isolated from TOP10F' cells and introduced into TOP10 and Rosetta 2 (DE3) cells. These were screened for recombinant protein expression at different temperatures and with different IPTG concentrations. Protein expression at different time points was monitored by SDS-PAGE with coomassie staining and western blot detection. Cell lysis for expression screening was carried out as described above under "Cell lysis for cytoplasmic soluble protein"

3.2.9 Large Scale Expression from *E.coli* cultures

Cells were grown in LB medium with 100 µg/ml ampicillin at 37 °C for 16-18 hours and inoculated into fresh medium with ampicillin to give a final OD600 of ~0.2. Fresh cultures were grown at the indicated temperature and IPTG was added at OD600 ~0.6. After harvesting, the pellets were stored at -80 °C until purification.

3.2.10 Purification of recombinant AGB1 and AGG2

The compositions of buffers are given in chapter 4.8 for ease of following the results. During all purification procedures Complete EDTA free protease inhibitor Cocktail tablets (EFPI) (Roche) were included in lysis buffers (1 tablet (50X)/50 ml).

a. Batch Affinity Purification

All steps were performed at +4 ° C. Cells were rapidly thawed and resuspended in lysis buffer, at a ratio of 5 ml buffer / 100 ml culture. Resuspended cells were lysed by sonication with a cycle of 8 seconds pulse and 9 seconds pause. Total sonication time was 4-10 minutes depending on the lysate volume. In order to solubilize the membranes, lysate was incubated with 1% Triton X-100 for 30 minutes with continuous rotation. Lysate was cleared from cell debris by high speed centrifugation, 30 minutes at 30,000g and supernatant was transferred to a fresh tube. Cleared lysate was equilibrated with purification buffer if necessary.

Ni-NTA- agarose was washed with water and equilibrated with purification buffer before binding. Briefly the resin slurry was loaded to a 15 ml conical tube and centrifuged at 900g for 5 minutes. Supernatant was discarded and resin was resuspended in an equal volume of water. After incubation for 5 minutes with continuous rotation, centrifugation was repeated. The same procedure was followed with purification buffer and the resin was resuspended in purification buffer after the final centrifugation step.

Cleared lysate was combined with resin in a 50 ml conical tube and incubated for 60 minutes with continuous rotation for binding. Solution was centrifuged at 900g for 5 minutes; the supernatant was saved as flow-through and resin was washed as described below. An equal volume of wash buffer was added to the resin and the slurry was loaded onto a 10 ml plastic column. Resin was washed 4 times with gravity using wash buffer. The wash buffer was made by addition of imidazole to purification buffer as indicated. An equal volume of elution buffer was loaded onto the column and proteins were eluted. The amount of imidazole in the elution buffers is indicated.

b. Column Affinity Purification

Cells were lysed as described in batch affinity purification. All column purifications were performed using an AKTA Prime system (GE Healthcare) and HisTrap HP, 5 ml column (GE Healthcare). The column was pre-equilibrated with binding buffer and clear lysate was loaded onto it at a flow rate of 3 ml/min. The

column was washed with wash buffer using 8 column volumes (CV) and a linear gradient elution was done in 6 CV. Flow rates for wash and elution steps are indicated for each experiment in the results section.

3.2.11 Large Scale Expression of GPA1-myc-his

The following procedure was adapted after several optimization trials, with details given in Chapter 4.1.

BMGY medium was inoculated with a single colony from a fresh YPD plate. Cells were grown until the culture reached an OD600 of 10 / ml. They were then inoculated into fresh BMGY medium and grown for 24 hours more. Harvested cells were resuspended in BMMY medium with a starting OD600 of ~10 / ml and 1% methanol was added at the 6th and 24th hour to maintain induction. Cells were harvested 48 hours after induction and the pellets were stored at -80 °C until purification.

3.2.12 Purification of recombinant GPA1

a. Affinity purification

Cells were lysed and cleared lysate was obtained at 4 °C as described below. According to our results *P. pastoris* was more efficiently lysed with zirconia beads (Bio Spec Products) than with glass beads but the efficiency of lysis was reduced after the beads were re-used 3 to 4 times (data not shown). Furthermore cell lysis in 250 ml chambers was less efficient than in 50 ml chambers in the Bead Beater (Bio Spec) cell breaker. Cell density was another parameter that affects lysis efficiency, the optimum ratio was found to be 72 for OD600 of cells/ lysis buffer volume.

- Column Affinity purification

The compositions of buffers are given in chapter 4.2.1 for ease of following the results. During all purification procedures Complete EDTA free protease inhibitor Cocktail tablets (EFPI) (Roche) were included in lysis buffers (1 tablet (50X)/ 50 ml).

Cells were rapidly thawed and resuspended in lysis buffer, at a ratio of 10 ml buffer / g pellet. All steps were performed at 4 ° C. Resuspended cells were lysed by beating with 0.5 mm diameter glass beads, with a cycle of 30 seconds beat and 30 seconds pause, for 3 times, followed by 30 seconds beat and 1 minute pause for 4 times. Beating was done using a Bio Spec Bead Beater keeping the cells on ice throughout the procedure. Lysate was cleared from cell debris by high speed centrifugation, 10 minutes at 22,000g and supernatant was transferred to a fresh tube.

All column purifications were performed using an AKTA Prime system (GE Healthcare) and HisTrap HP, 5 ml GE Healthcare), column; pre-equilibrated with binding buffer. Cleared lysate was loaded onto the column and the column was washed for 8 CV using a peristaltic pump at a flow rate of 1 ml/min in the cold room. Flowrate and volume of elution are indicated in results section for each experiment.

- Batch Affinity purification

Cells were rapidly thawed and resuspended in lysis buffer (50mM TrisHCl, pH 8.0, 10mM MgCl₂, 1mM EDTA, 5% glycerol, 2mM PMSF and EFPI), at a ratio of 10 ml buffer /g pellet. All steps were performed at +4 ° C. Resuspended cells were lysed by beating using the Bio Spec bead beater as described above. Lysate was cleared from cell debris by high speed centrifugation, 30 minutes at 22,000g and supernatant was transferred to a fresh tube. The cleared lysate was equilibrated with purification buffer by incubating 5 minutes with 10X purification buffer (500 mM Tris-HCl, pH 8.0, 3 M NaCl, 100 mM BME, 1 mM PMSF, 20 mM MgCl₂ and 200 μM GDP). The amounts of

imidazole were optimized throughout the experiments and the concentrations are given in Chapter 4.2.2.

Where necessary the membrane fraction was solubilized using a mixture of detergents. The pellet obtained after high speed centrifugation was resuspended in 10 ml lysis buffer, with fresh PMSF supplemented. The resuspension was centrifuged at 13,000 rpm for 30 minutes and supernatant was discarded. The pellet was resuspended in 5 ml of TBS-5 % Triton X-100 and allowed shaking to aid solubilization. Finally, 2.5 ml of TBS with 0.1% Lubrol PX, 0.1 % NP-40 and 1 mM DTT was added for complete solubilization of the membrane fraction.

Ni-NTA agarose was washed with water and equilibrated with purification buffer before binding as described in section 3.2.10. Cleared lysate was combined with resin in a 50 ml conical tube and incubated for 60 minutes under continuous rotation for binding. The solution was centrifuged at 900 g for 5 minutes; supernatant was saved as flow through and resin was washed as described below. An equal volume of wash buffer was added to the resin and the slurry was loaded to a 10 ml plastic column. The resin was washed with gravity for four times with two resin volume of wash buffer. Imidazole was added to purification buffer to make wash buffer, where indicated. Elution buffer was loaded onto the column and protein was eluted by gravity. The volume and imidazole amount of elution buffers and incubation time with elution buffer are indicated in Chapter 4.2.2.

- Batch Affinity purification with detergent

Detergent type and concentration for individual purifications are indicated in Chapter 4.2.3. Cells were rapidly thawed and resuspended in lysis buffer (50mM TrisHCl, pH 8.0, 10mM MgCl₂, 1mM EDTA, 5% glycerol, 2mM PMSF, EFPI, 50 μM GDP and detergent), at a ratio of 200 ml buffer per 20 g pellet. Resuspended cells were re-pelleted at 5086g for 15 minutes and the pellet was resuspended in 100 ml lysis buffer. All steps were performed at 4 ° C. Lysis was performed by beating as described

above, except with 0.5 mm diameter zirconia beads. Lysate was cleared from cell debris by high speed centrifugation for 30 minutes at 23,000g and the supernatant was transferred to a fresh tube. Cleared lysate was equilibrated by incubating 5 minutes with 10X purification buffer (500 mM Tris-HCl, pH 8.0, 3 M NaCl, 100 mM BME, 1 mM PMSF, 50 mM MgCl₂, 500 μM GDP, 200 mM imidazole and detergent). The wash buffer composition was 1X PB and elution buffer was composed of 1X PB with a final imidazole concentration of 300 mM.

Procedures for washing and equilibrating Ni-NTA agarose and binding were also carried as described above for the purification without detergent using 20 ml plastic column. Elution was repeated with 10 ml and 5 ml elution buffer respectively, making 10 ml of E1 and E2 and 5 ml of E3. Ni-affinity elutions were either directly concentrated and/or buffer exchanged or stored at -20 °C with 10 % glycerol until use.

b. Concentrators:

Initially an Ultracel YM-30 membrane (Millipore) was used to reduce the volume of the protein solution, but the presence of glycerol in the sample resulted in protein loss. Vivaspin 20 Polyethersulfone Membrane 30,000 MWCO (Sartorius) concentrators did not result in any protein loss. Briefly concentrators were pre-rinsed with water and washed with anion exchange start or gel filtration buffer by centrifugation for 10 minutes at 5000g. Ni-affinity purified GPA1 was concentrated by centrifugation at 5000g until the desired volume was reached. Proteins were concentrated at 4 °C using a Bioshield Windshielded Swinging Bucket Rotor (Thermo Scientific).

c. Desalting:

Desalting was done at room temperature using a HiPrep™ 26/10 Desalting column (GE Healthcare) following the manufacturer's instructions and the fractions were stored on ice until further use.

d. Dialysis:

Dialysis was done in cellulose ester dialysis tubing; MWCO: 12,000-14,000 (Cellu•Sep® T3 Membranes). Dialysis membranes were pre-equilibrated by boiling in distilled water and incubating in dialysis buffer at +4 °C for several hours. Dialysis was done against 250 ml of buffer for a total of 3 hours with a buffer change with 1 hour intervals. Fresh 1 mM PMSF and 1 mM DTT were added to each buffer; where indicated. Dialysis was done overnight against 1 L, when the buffer was changed from Tris HCl to HEPES.

e. Anion Exchange

Ni-affinity purified GPA1 samples were combined and centrifuged at 5000 rpm for 15 minutes at 4 °C. The elution pool was buffer exchanged to 50 mM TrisHCl, pH 8.0; using either a desalting column or dialysis before loading onto an anion exchange column. Samples were concentrated using a concentrator unit prior to buffer exchange where indicated.

A Q Trap HP, 5 ml, anion exchange column was washed with NaCl elution buffer (50 mM Tris HCl, pH 8.0, 700 mM NaCl) and equilibrated with start buffer (50 mM Tris HCl, pH 8.0). A 50 ml Super loop (GE Healthcare) was also washed with start buffer, before filling in the sample. After loading, the column was washed at a flow rate of 3 ml/min with start buffer until the absorbance stabilized (~40 ml + sample volume). A linear gradient (0-700 mM NaCl in 25 ml) was applied for elution.

f. Size Exclusion chromatography

Ni-affinity purified GPA1 samples were combined and centrifuged at 5000 rpm for 15 minutes at 4 °C. The elution pool was concentrated using a concentrator unit. The buffer was exchanged where indicated using a desalting column. The concentrated

sample was centrifuged at 14,000 g for 10 minutes at +4 °C and loaded onto a gel filtration column (Sephacryl -200 HR or Sephacryl-300 HR) through a 2 ml loop. The compositions of the gel filtration buffers and flow rates are indicated in chapter 4.4. Gel filtration column calibrations were done as described by the manufacturer (GE Healthcare).

3.2.13 SDS-PAGE

SDS-polyacrylamide gels (10%, 12% or 15%) were prepared according to Laemmli [123]. Samples of 20 µl, were prepared with SDS loading dye, boiled at 95 °C for 3 minutes and unless stated otherwise 10 µl were loaded into the wells. 2X, 3X or 6X SDS loading dye was used depending on sample concentration. Non-denatured samples were prepared with 6X native loading dye and heat treated if indicated. Gels were run at constant current, 20mA, for 45-90 minutes depending on the acrylamide concentration. 1X Tris-Glycine-SDS (sodium dodecyl sulfate) buffer was used for polyacrylamide gel electrophoresis. Buffer contains 1.51 g. Tris base, 9.4g. Glycine and 2.5 ml of 20% SDS in 500 ml.

3.2.14 Native-PAGE /TCA Stain

Native polyacrylamide gels (3% stacking-8% separating) were prepared without SDS and gels were run in 1X Tris-Glycine buffer at constant volt; 80mV for 2 hours. Samples for native-PAGE were prepared with loading dye without reducing agent and were directly loaded without heat treatment. Gels were run with 80 mV for 2 hours. Gel was fixed in 12.5% TCA (trichloroacetic acid) for overnight. Next day fresh TCA was put on the gel and gel was photographed against a dark background.

3.2.15 Western blotting

SDS-polyacrylamide gels (10%, 12% or 15%) were blotted on PVDF membranes at 25 mA constant current for 2 hours at room temperature in transfer buffer (14.41 g. Tris base, 3.028 g. Glycine and 200 ml methanol in 1 L.). Blotted membranes were blocked with Qiagen blocking solution on an orbital shaker for 1 hour and incubated with an appropriate HRP conjugated antibody for 1 hour at room temperature. The membranes were treated with Pierce ECL Western Blotting Substrates (Pierce, Thermo Scientific) after washing with TBS-Tween and resulting signals were analyzed on CL-XPosure Film (Pierce, Thermo Scientific).

3.2.16 Protein Concentration Determination

a. Bradford Assay

Bradford assay was performed with Bio-Rad Protein Assay Dye Reagent as described by the manufacturer (Bio-Rad). The measurements were done at 595 nm using a Microplate Reader (Bio-Rad). The BSA standards were prepared fresh in sample buffer and standard curves were plotted to determine the concentration as a linear function of absorbance.

b. Spectrophotometric Determination

The absorbance of the samples was measured in the range 200-310 nm using a Shimadzu, UV-3150 spectrophotometer. Unless otherwise stated in all measurements the reference buffer used was the same buffer that protein was eluted in or dialyzed against. Absorbance values at 260 and 280 nm were used to estimate protein concentration as described by Layne et al., [124] by the following equations;

$$\text{Eqn 4.1: mg/ml} = (1.55 \times A_{280}) - (0.76 \times A_{260})$$

$$\text{Eqn 4.2: mg/ml} = 0.92 \times A_{280}$$

Extinction coefficient was estimated as 0.92 from amino acid sequence of GPA1-myc-his using ExPASy Proteomics Server (<http://www.expasy.ch>).

The absorbance at 254 nm is used as an indirect estimate of GDP content of the protein samples [38]. The absorbance at 290 nm and the light scattering \geq 300 nm is monitored to detect aggregates [125]. Presence of aggregates may result in a non zero baseline due to the light scattering from those particles.

The molarity calculations were done assuming all protein is GPA1 with molecular mass 48 kDa. This overestimates the concentration for Ni-affinity purified GPA1.

3.2.17 GTP Binding Assay

The GTP binding of GPA1 was analyzed using $^{35}\text{GTP}\gamma\text{S}$ (GE Healthcare) binding experiments [126]. The buffers used are;

Protein Dilution Solution: 20 mM HEPES, 8.0, 1 mM EDTA, 1 mM DTT, 50 μM GDP, 0.1 % Lubrol.

GTP γ S Binding Solution (2X): 100 mM HEPES, 8.0, 120 mM MgCl_2 , 4 mM EDTA, 400 mM NaCl, 4 mM DTT, 4 μM GTP γ S, 2 μl $^{35}\text{GTP}\gamma\text{S}$ (250.000 cpm / μl).

$^{35}\text{SGTP}\gamma\text{S}$ Dilution Solution: 20 mM Na-HEPES, 8.0, 1 mM EDTA, 1 mM DTT, 0.1 % Lubrol.

Filtering Solution: 20 mM Tris-HCl, pH 8.0, 100 mM NaCl, 25 mM MgCl_2 .

Protein samples were prepared in protein dilution solution in 30 μ l. 30 μ l of GTP γ S Binding Solution (2X) was added. 100 μ M of nucleotides were added for competition assays. The reaction was incubated at 30 $^{\circ}$ C for 60 minutes. The reaction was stopped with the addition of 2 ml of ice-cold filtering solution. The solution was applied to nitrocellulose membranes and were washed using a vacuum filtration unit with 8 ml of filtering solution. Nitrocellulose membranes were left at 70 $^{\circ}$ C for 20 minutes and were resuspended in 2 ml scintillation liquid (Perkin Elmer). The radioactivity was measured as counts per minute (CPM) with a scintillation counter.

The specific activity (Ci/mol) of 35 GTP γ S was calculated from a decay table and the dilution factor. The amount of bound GTP γ S was calculated according to the formula:

$$\text{pmole GTP}\gamma\text{S} = (\text{CPM} \times 100) / (2,22 \times \% \text{counter efficiency} \times \text{specific activity})$$

3.2.18 GTPase activity Assay

The GTP hydrolysis activity of GPA1 was analyzed using 32 P-GTP (Izotop) by measuring the amount of released 32 P [35]. Protein samples were prepared in assay buffer at the appropriate dilution and equilibrated at room temperature. Assay buffer was composed of 50 mM HEPES, pH 8.0, 1 mM EDTA, 1 mM DTT, 10 mM MgCl₂ and 0.1% Lubrol-PX. The reaction started with the addition of indicated amount of 32 P-GTP at room temperature. Each reaction, 60 μ l, was stopped by the addition of 750 μ l ice-cold 5% activated charcoal solution at the indicated time points. The unbound 32 P-GTP precipitated by centrifugation at 2000g for 15 minutes. 400 μ l of supernatant was added to 2 ml of scintillation liquid (Perkin Elmer) and released radioactivity was measured as counts per minute (CPM) for 5 minutes using a scintillation counter. The CPM values were corrected by subtracting CPM of reaction without protein and with 32 P-GTP.

3.2.19 Biophysical characterization

a. Analysis of GDP Content

In order to analyze protein quality, GDP binding was measured [38]. Purified recombinant GPA1 samples (400 μ l) were boiled for 3 minutes and applied to micro concentrator units (Vivaspin 600), with MWCO of 10 or 30 kDa. The protein was separated from buffer and GDP by centrifugation at 12,000g for 15 minutes. The original sample tube was washed with 400 μ l of water and further applied to the micro concentrator unit. Centrifugation was repeated and the filtrate analyzed for GDP amount with a UV-vis spectrophotometer (Schimadzu, UV-3150).

b. Dynamic Light Scattering

Dynamic light scattering measurements were performed to monitor the homogeneity and the oligomeric state of the protein preparations. Protein samples were equilibrated to room temperature and measurements were recorded using a Nano-ZS (Malvern Ins.).

Scattering intensity is observed due to the Brownian motion of the molecules and particles in solution and fluctuations in the scattering intensity are dependent on the size of the particles. Heterogeneities in the size of proteins can be detected even at low concentrations. Results are obtained as intensity, volume fraction and number distribution. Among these the size distribution with respect to intensity is the most sensitive to presence of large particles in solution. Size distribution by intensity and number reveal the largest and the smallest particles in the solution, respectively. In the results section measurements are shown with alternative representations depending on the aim of the experiment.

c. Circular Dichroism

Circular Dichroism measurements were primarily conducted to analyze helical content and folding status of the recombinant proteins.

The CD measurements were done using JASCO J-810 CD Spectrometer with 300 μ l sample in 1 mm path length cuvette at room temperature. Measurements were done at standard sensitivity, with continuous scanning of speed 100 nm/min, 1 second response, 0.05 nm data pitch and 1 nm band width. Three accumulations were collected for each sample.

The effects of receptor mimetic compounds were also analyzed by comparing the helical content of the protein [40]. These measurements were done using 1 mm path length at standard sensitivity, with continuous scanning speed of 50 nm/min, 8 second response, 0.2 nm data pitch and 1 nm bandwidth.

Ellipticity was calculated from milidegrees using [127];

θ (deg cm² dmol⁻¹) = (milidegrees X mean residue weight) / (path length (mm) X protein concentration (mg/ml))

Mean residue weight of a protein is calculated by dividing the molecular mass by number of amino acids - 1. GPA1 mean residue weight is 116.573.

d. Mass spectrometry

Mass spectrometry analysis was commercially provided by TOPLAB (Germany). Buffer exchange was done using C18 ZipTip, C4 ZipTip or by dilution. Cysteines were modified with iodoacetamide. Samples were digested with trypsin and MALDI-TOF

MS was done in DHBS (2, 5 Dihydroxybenzoic acid: 2 Hydroxy-5 methoxy-benzoic acid 9:1) matrix.

e. **NMR**

NMR measurements were performed on Varian Unity Inova 500 MHz using a 500 MHz ^1H - ^{19}F (^{15}N - ^{31}P) 5 mm PFG Switchable Probe. The samples were labeled with 10% deuterium using D₂O. The ^1H NMR measurements were performed after solvent (H_2O) saturation. The NMR measurements were mainly conducted to characterize the detergent content of protein samples.

f. **SAXS**

SAXS measurements were performed at EMBL, DESY; X-33 beam line using a 2D Mar345 Image Plate detector. The X-33 beamline is located at DORIS III storage ring of the Deutsches Elektronen Synchrotron (DESY) in Hamburg. Scattering patterns were recorded in the range of momentum transfer $0.15 < s < 3.5 \text{ nm}^{-1}$ ($s = 4\pi\sin\theta / \lambda$, where 2θ is the scattering angle and λ the X-ray wavelength, 0.15 nm). All preliminary data analysis were done using ATSAS program package [128].

SAXS data can be used to obtain the overall shape and size of macromolecules. The data is represented as logarithm of the intensity of scattered radiation against the momentum transfer, s .

At small angles the logarithm of the intensity can be plotted as a function of the square of the scattering vector (Guinier approximation). For a monodisperse solution this yields a straight line with intercept proportional to the molecular mass and slope proportional to the radius of gyration.

$$\ln(I) = \ln(I(0)) - s^2 R_g^2 / 3$$

The Guinier plot is valid for globular particles for $sR_g < 1.3$

For protein solutions a known protein (e.g. BSA) can be used as molar mass reference in SAXS data collection and analysis. $I(0)$ values calculated from the Guinier plot of BSA are proportional to its molecular mass and the molar mass of sample with known concentration (c) can be calculated by:

$$\text{MM sample} = (I(0)_{\text{sample}}/c_{\text{sample}}) * (c_{\text{BSA}} * \text{MM}_{\text{BSA}} / I(0)_{\text{BSA}})$$

Intensity measurements are dependent on beam line conditions, so BSA measurements should be made for each set of samples. BSA is prepared in 20 mM HEPES, pH 8.0, 150 mM NaCl and 1 mM DTT with a concentration of ~5 mg/ml.

CHAPTER 4

4 RESULTS

4.1 Optimization of Expression of GPA1

The gene encoding GPA1 was cloned into the pPICZC vector in frame with the C-terminal myc epitope and a his-tag. The pPICZC-GPA1 construct was integrated into the genome of *Pichia pastoris* GS115 cells [7]. The expression is induced with methanol through the AOX promoter upstream of the GPA1 coding region. The recombinant protein has an estimated molecular mass of 48219 Da (amino acid sequence provided in Appendix I).

Expression of recombinant GPA1 was optimized by varying the medium composition, induction conditions and the time of induction. Cell growth was followed by measuring optical density of cells and the amount of protein was monitored with small scale purification trials. Results are summarized in Figure 4.1 to Figure 4.7.

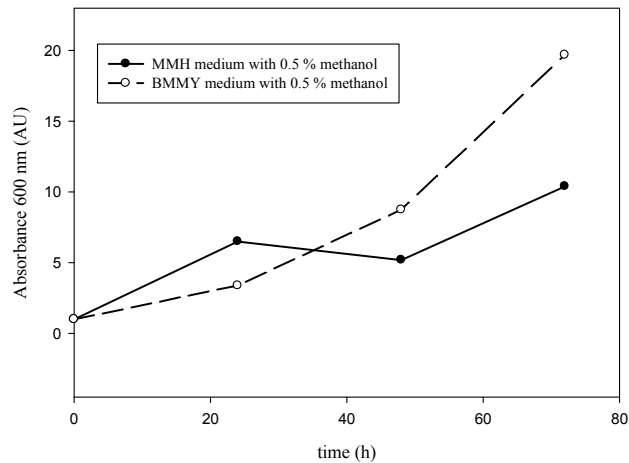


Figure 4.1 Growth of GS115 cells expressing GPA1 in MMH or BMMY. 0.5 % methanol was added to the medium at 24-hour intervals at the points shown above.

Cells grow to higher cell density in BMMY medium than in MMH, which does not contain yeast extract and peptone (Figure 4.1).

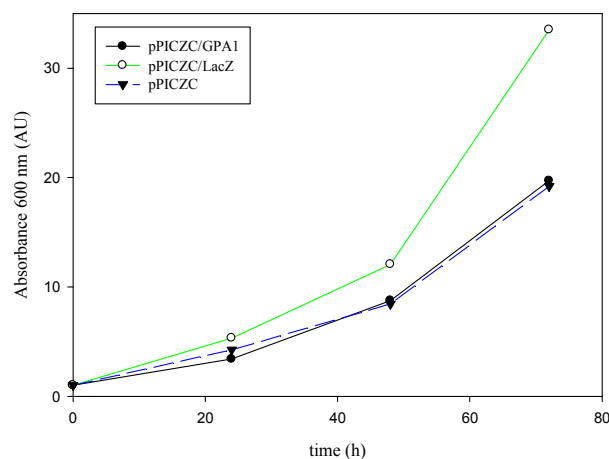


Figure 4.2: Comparison of growth of GS115 cells with the empty vector (pPICZC), the LacZ gene (pPICZC-LacZ) and the GPA1 gene (pPICZC-GPA1). BMMY medium contained 0.5 % methanol. Methanol (0.5 % final) was added to the medium at 24 hour intervals as in Figure 4.1.

Growth of *P. pastoris* was investigated under induction condition and as illustrated in Figure 4.2 expression of recombinant GPA1 did not have any negative effect on cell growth.

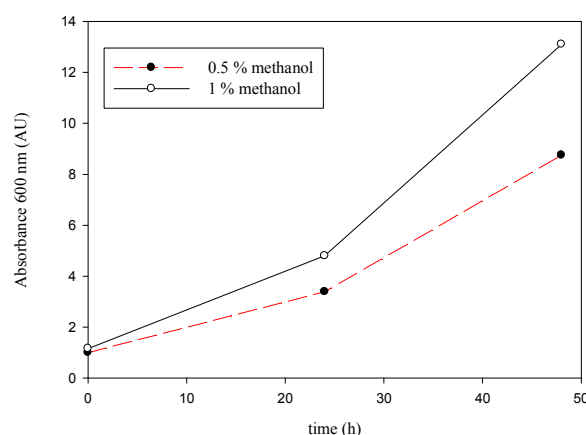


Figure 4.3: Comparison of growth of GS115 cells expressing GPA1 in BMMY medium after induction with 0.5 % (---) or 1 % (—) methanol. Methanol was added at 24th hour. Both cultures were 120 ml in 1L flasks.

Induction with 1% methanol yielded a higher cell density than 0.5% methanol (Figure 4.3), but protein expression was still very low (data not shown). The initial cell density before induction was increased from 1 to 10 which resulted in both higher cell density and amount of recombinant GPA1 synthesized after induction. In order to increase the starting cell density, cells were grown in BMGY medium for 48 hours with a change of fresh medium after 24 hours.

Following this, the time points at which 1% methanol was added to maintain induction were varied. In the initial trials cells were grown 24 hours in BMMY medium and methanol was given at different times of induction as summarized below.

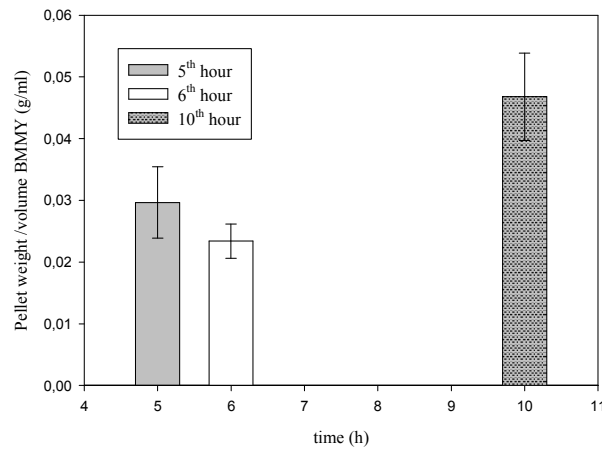


Figure 4.4: Pellet weight as function of methanol induction time. 1% methanol was supplemented at the indicated time of induction. Cultures were grown in baffled flasks for 24 hours.

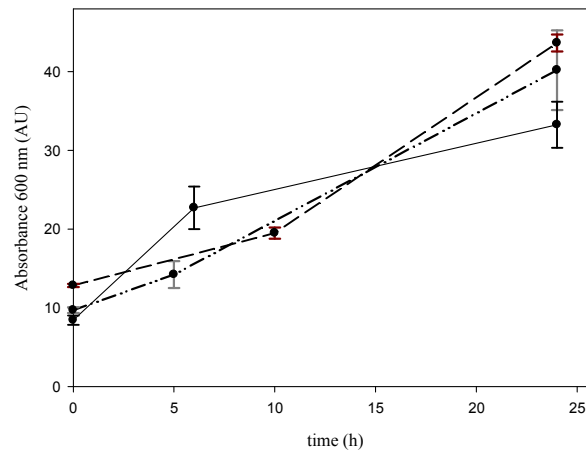


Figure 4.5: Optical densities of cell cultures as a function of methanol addition time. Methanol was given at 5th (····), 6th (—) or 10th (---) hour of induction. Cultures were grown in 100 ml BMMY in baffled flasks for 24 hours.

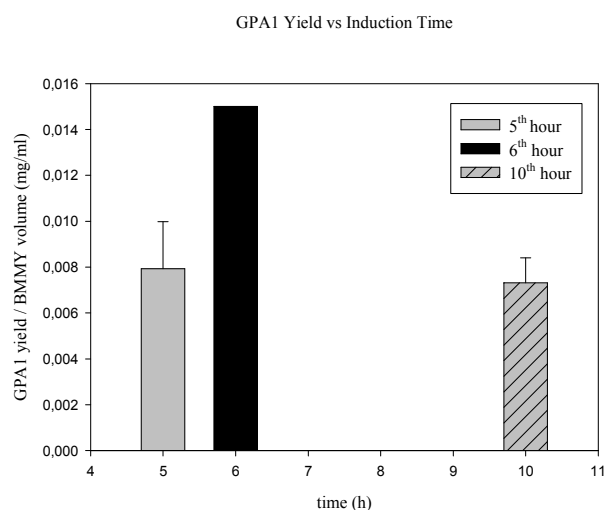


Figure 4.6: Affinity (HisTrap™ HP column) purified GPA1 amount as function of methanol addition time.

1% methanol was supplemented at the indicated time of induction. Cultures were grown in baffled flasks for 24 hours before induction.

Time points for methanol replenishment after induction affected cell growth as shown by pellet weight (Figure 4.4) and optical densities (Figure 4.5). Addition after 10 hours results in high cell growth but also reduces recombinant protein expression (Figure 4.6). Optimal time for methanol addition was selected at 6 hours after induction.

Under the conditions above the yield of recombinant GPA1 was still not sufficient to complete biophysical assays. To increase the yield, the total induction time and the volume were increased. The induction time was optimized for a total of 48 hours growth (Figure 4.7 and Figure 4.8).

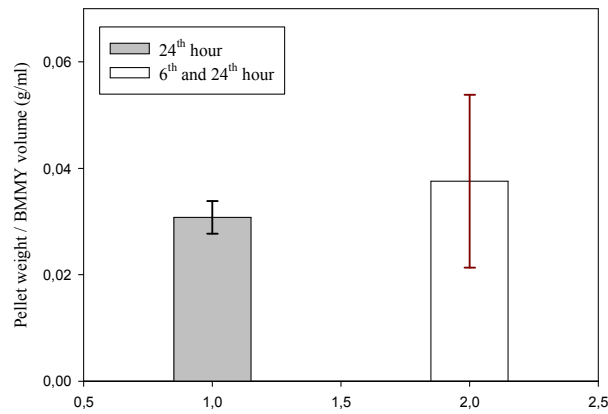


Figure 4.7: Comparison of pellet weight for cultures with methanol addition at 24 hours and at 6th and 24th hours after induction.

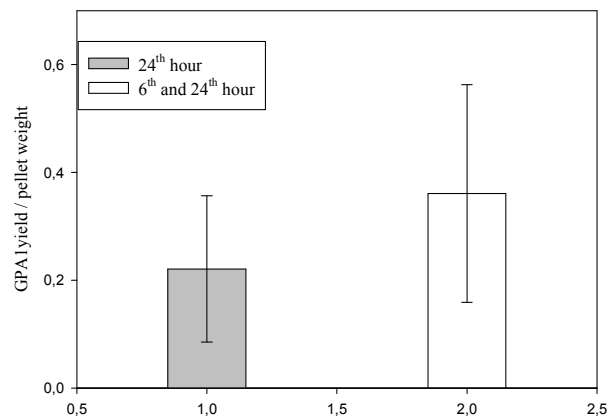


Figure 4.8: Amount of Ni-affinity purified GPA1 as function of the methanol addition time.

The optimized conditions correspond to addition of 1% methanol to induced cultures after 6 and 24 hours during the 48 hour induction period (Figure 4.9). After 48 hours of induction cells reached the stationary phase in the flask growth conditions (data not shown).

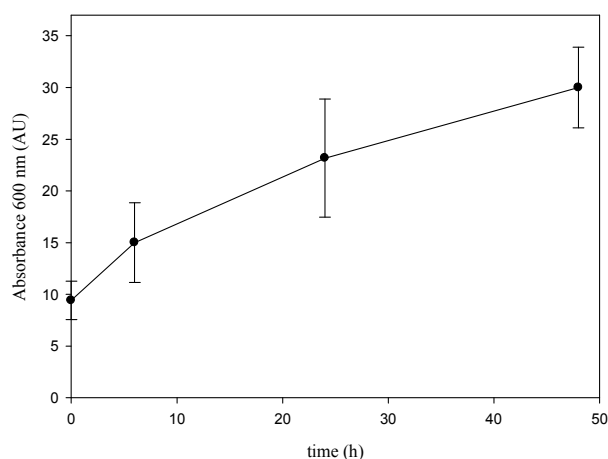


Figure 4.9: Growth of GPA1-GS115 cells in induction medium. Methanol was supplemented at 6 and 24 hours after induction.

4.2 Nickel-Affinity Purification of GPA1

4.2.1 Small scale purifications: HisTrap™ HP

Recombinant GPA1 was expressed with a histidine-tag to facilitate purification and labeling, and a nickel-affinity matrix was used as the first chromatography step. Lysis and purification procedures were optimized using small-scale (150-200 ml) cultures and a 5 ml HisTrap™ HP column (GE Healthcare). *P.pastoris* was induced for 24 hours, with methanol given after 6 hours. Buffers and some parameters for two procedures that gave best results are summarized in Table 4.1. Results of these procedures are given below for comparison with results of large-scale purifications that will be described separately.

Table 4.1: Purification Conditions for GPA1 HisTrap™ HP Affinity.

Prep	Buffers		Elution	
	Lysis	Purification Buffer (PB)	Gradient/Step	Flow rate
1. NaPO ₄ / 0.3 M NaCl (200 ml / 6 hour methanol)	50 mM Na-PO ₄ pH 7.4, 5% glycerol, 1 mM EDTA, 2 mM PMSF ,EFPI	20 mM Na-PO ₄ , pH 7.4 0.3 M NaCl	Gradient:0-500 mM imidazole in PB, 5 CV	1 ml/min
2. Tris HCl/0.3 M NaCl (175 ml / 6 hour methanol)	100 mM Tris HCl, pH 7.4, 5% glycerol, 1mM EDTA, 2 mM PMSF, EFPI	40 mM Tris-HCl, pH 7.4 0.3 M NaCl	Gradient:0-500 mM imidazole in PB, 5 CV	1 ml/min

1: Na-PO₄ / 0.3 M NaCl

Bound protein eluted from the column in 3 peaks with the 0-500 mM imidazole gradient (Figure 4.10). According to the result of SDS-PAGE analysis in Figure 4.11, the first two peaks contained the two major contaminants, one at 80 kDa and the other at 40 kDa, that bind to the Ni-affinity matrix. GPA1 eluted close to the end of the gradient and its separation from the contaminants was satisfactory.

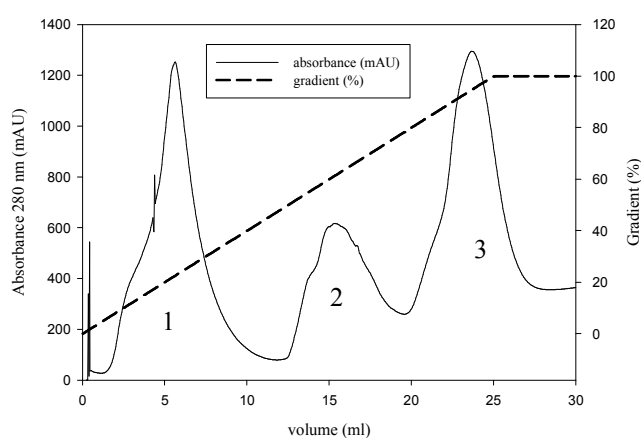


Figure 4.10: Elution of GPA1 from HisTrap™ HP column. Linear gradient of imidazole was from 0 to 500 mM (- - -) in NaPO₄ buffer. Flow rate was 1 ml/min for 5 CV (25 ml) and 1 ml fractions were collected.

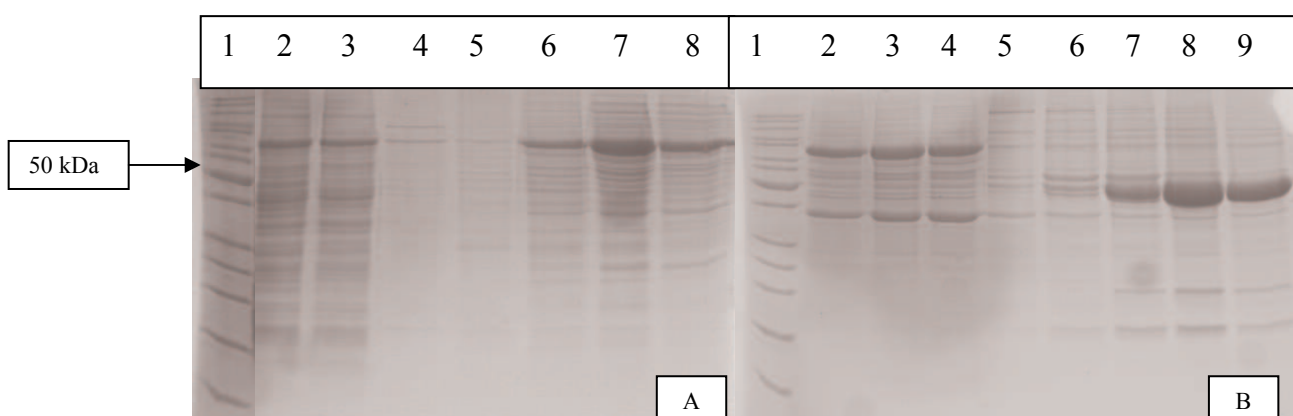


Figure 4.11: 12% SDS-PAGE analysis of HisTrap™ HP fractions. A: Lane 1: Protein ladder®, lane 2: cell lysate (CL), lane 3: flow through (FT), lane 4: wash, lanes 5-7: peak 1 fractions eluted at 4-7 ml. B: Lane 1: Protein ladder®, lanes 2-4: peak 2 fractions eluted at 16-18 ml, lanes 5-9: peak 3 fractions eluted at 21-25 ml. Samples were prepared with 2X SDS loading dye.

The GPA1 yield determined by Bradford assay was 3.2 mg from 200 ml culture.

2: Tris HCl /0.3 M NaCl

As the last parameter for optimization, the buffer was changed from Na-PO₄ to Tris-HCl in order to avoid interference in functional assays.

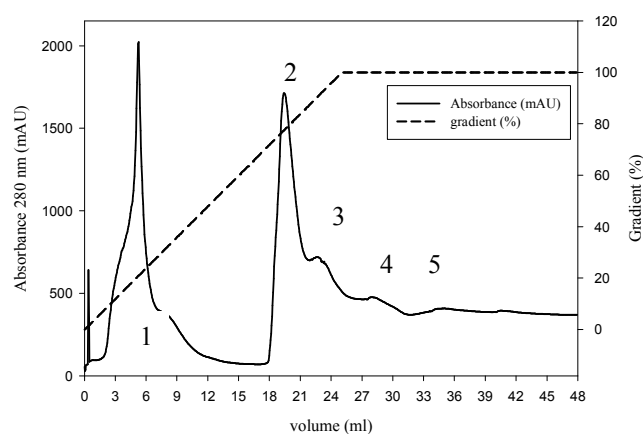


Figure 4.12: Elution of GPA1 from HisTrap™ HP column. Linear gradient of imidazole was from 0 to 500 mM (- - -) in Tris buffer. Flow rate was 1 ml/min for 5 CV (25 ml) and 1 ml fractions were collected.

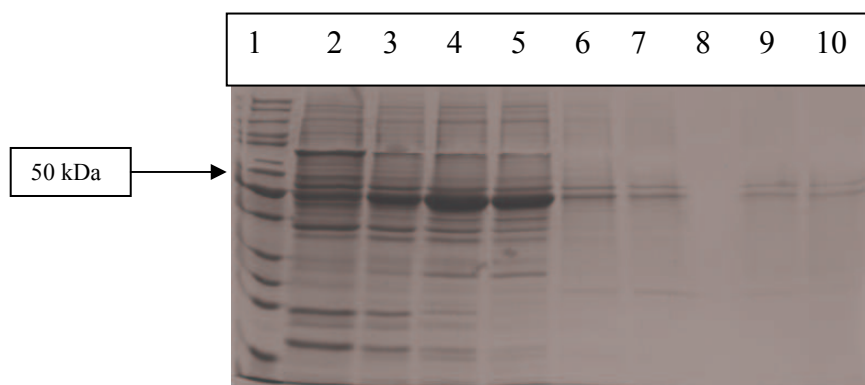


Figure 4.13: 12% SDS-PAGE analysis of HisTrap™ HP fractions. A: Lane 1: Protein ladder ®, lanes 2-5: peak 3 fractions eluted at 21-24 ml, lanes 6-7: peak 4 fractions eluted at 28-29 ml, lanes 9-10: peak 5 fractions eluted at 34-35 ml. Samples were prepared with 2X SDS loading dye.

Separation was better and GPA1 appeared to be more resistant to proteolytic attack in Na-PO₄ buffer but in large-scale purifications Tris- buffers were used to avoid interference with functional assays.

4.2.2 Large Scale GPA1 Purification

The large volume and viscosity of yeast cell lysate prevented the use of a HisTrap™ HP, 5ml, affinity column for large scale purification from 48 hour induced cultures. Purification with Probond™ Resin (Invitrogen) was investigated, but due to the low binding capacity yields were very low (data not shown) and Ni-NTA Agarose (Qiagen) was used in batch affinity purifications. As mentioned above Tris-buffers were used in purifications and some additives were included in buffers to improve storage and protein stability. The buffers used for GPA1 Ni-affinity purification are given in Chapter 3.2.

Based on the optimization results obtained from small scale purifications further conditions for *P. pastoris* induction and matrix-binding, wash and elution steps were investigated.

GPA1 was bound to the Ni-NTA agarose in the presence of 20 mM imidazole and remained bound through washes with the same buffer. Proteins bound to Ni-NTA agarose were eluted with step gradients at 100 mM, 150 mM, 200 mM, 250 mM and 300 mM imidazole in batch mode. GPA1 eluted in all fractions up to 300 mM imidazole from Ni-NTA agarose.

SDS-PAGE analysis shown in Figure 4.14 gives the results of elution with 200 mM and 300 mM imidazole. In both cases GPA1 eluted together with the contaminants at about 90 kDa, 80 kDa and another one just below 40 kDa.

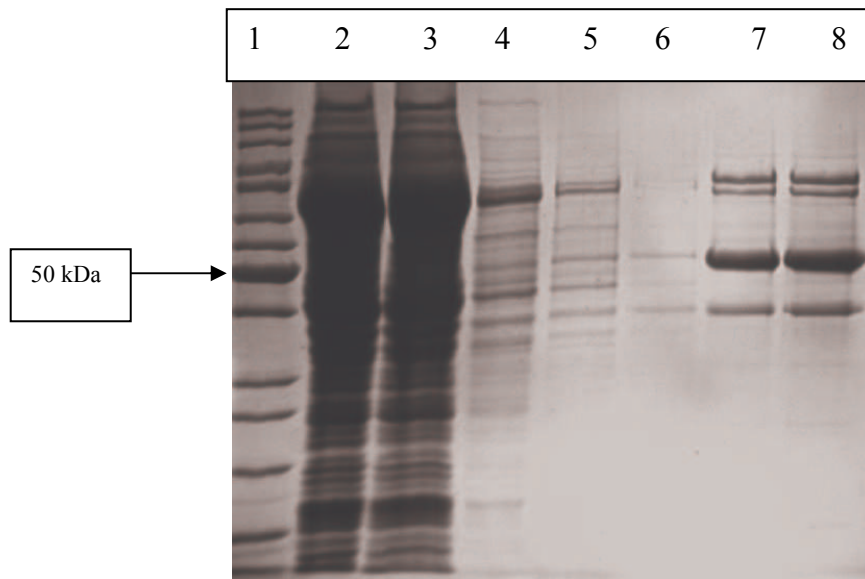


Figure 4.14: 12% SDS-PAGE analysis of Ni-affinity fractions. Lane 1: Protein ladder @, lane 2: CL, lane 3:FT, lanes 4-6: wash 2-4, lane 7: Elution with 200 mM imidazole, lane 8: Elution with 300 mM imidazole. Samples were prepared with 6X SDS loading dye.

Protein concentration in elution fractions was determined by Bradford assay based on standard curves obtained for BSA with 200 mM and 300 mM imidazole (data not shown). Results showed that similar amounts of protein, about 0.3 mg/ml, were eluted from the matrix for the two concentrations of imidazole. The total yield of protein was 3.6 mg GPA1 purified from a 300 ml culture, where 1% methanol was added after 24 hours during a of 48 hours induction.

For the standard procedure elution was carried out with 300 mM imidazole in three consecutive steps (E1: 5 ml, E2: 3 ml and E3:2 ml). For further analyses these eluates were pooled and although the total yield of protein was variable in general it was about 3-5 mg protein from 300 ml cultures.

UV spectrum of GPA1 eluted at 300 mM imidazole shown in Figure 4.15 displays a shoulder extending from about 250 nm to 280 due to the presence of bound nucleotide in the protein. This feature of the UV spectrum was investigated further by measurements against buffers containing different additives in the following sections.

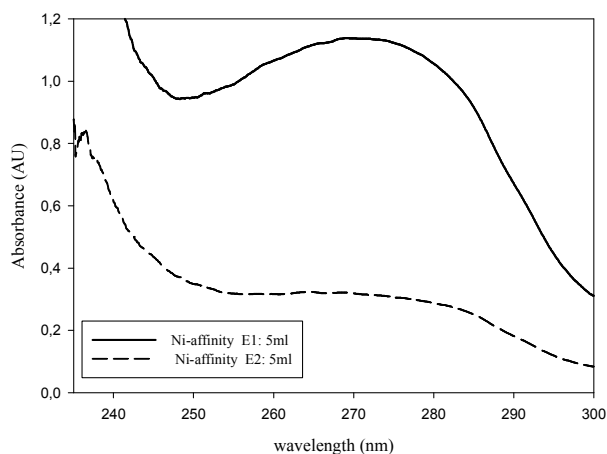


Figure 4.15: Comparison of UV spectra of Ni-affinity elutions; E1 and E2.

GPA1 samples precipitated when stored overnight at +4 °C in elution buffer. Storage at -20 °C did not result in any precipitation or protein degradation as shown in Figure 4.16.

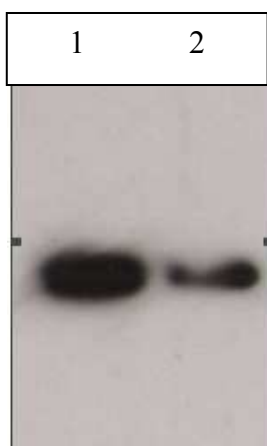


Figure 4.16: Western analysis of Ni-affinity elutions after storage at -20 °C. Lane 1 E1, lane 2:E3. Detection was done with 1:20,000 anti-myc-HRP.

Results of Dynamic Light Scattering (DLS) measurements shown in Figure 4.17 indicated that GPA1 was purified from Ni-affinity in oligomeric form. In DLS size distribution of particles in solution is determined according to the scattered intensity. This can also be converted to a volume and number distribution. Intensity distribution is

sensitive to the presence of large particles in solution whereas as volume and number distribution also detects the smaller particles. The dominating species in Ni-affinity eluted GPA1 solutions appears to have a diameter of about 85-100 nm according to DLS measurements. Larger particles in intensity plot correspond to elution buffer scattering (data not shown).

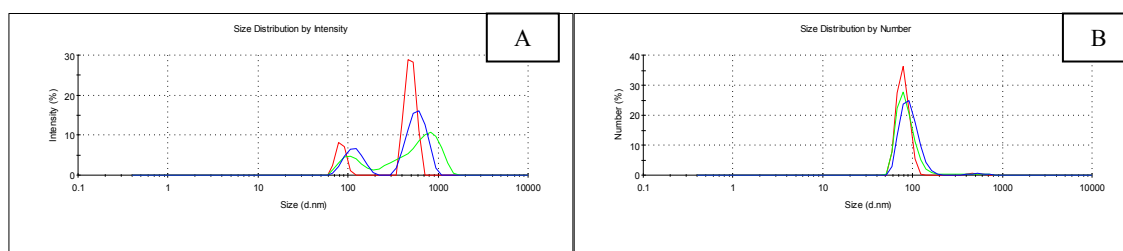


Figure 4.17: DLS, size distributions by intensity (A) and number (B) of Ni-affinity GPA1. Fraction was eluted with 300 mM imidazole.

- **Buffer Exchange**

Following partial purification of GPA1 fractions by Ni-affinity, optimum conditions for buffer exchange and for storage were investigated. Buffers were exchanged using either a HiPrep™ 26/10 Desalting column (GE Healthcare) or by dialysis against 50 mM TrisHCl, pH 8.0 buffer.

- **Dialysis**

In a preparation where the yield of the affinity step was 4.5 mg protein (in 9 ml) the elution pool was dialyzed against 50 mM Tris HCl, pH 8.0. Concentration estimations given in Table 4.2 showed that the dialysis procedure did not result in any protein loss.

Table 4.2: Absorbance values and concentration estimates after affinity and dialysis. The calculations were done either considering the presence of nucleotides (eqn 4.1) or using theoretical extinction coefficient (eqn 4.2).

Sample	Absorbance (AU)				Concentration (mg/ml)		Total Volume	Yield	A_{254}/A_{280}
	254 nm	260 nm	280 nm	310 nm	eqn 1	eqn 2	ml	mg	
Affinity pool	0.689	0.698	0.637	0.350	0.456	0.586	9.5	4.336	1.082
Dialyzed pool	0.726	0.718	0.645	0.329	0.454	0.593	9	4.086	1.125

Protein concentrations were estimated using equation 4.1, which takes into account the presence of bound nucleotide, since GPA1 was expected to be purified with bound GDP. Estimations of concentrations based on theoretical extinction coefficient from equation 4.2 were higher, due to the significant absorption of GDP at 280 nm. In routine calculations, protein concentrations were determined using eqn. 4.1. The ratio of A_{254}/A_{280} , also shown in Table 4.2 can be used as an indicator of the amount of GDP in protein solution, either bound or free. When the buffer exchange was carried out by dialysis after the affinity step this ratio did not change significantly.

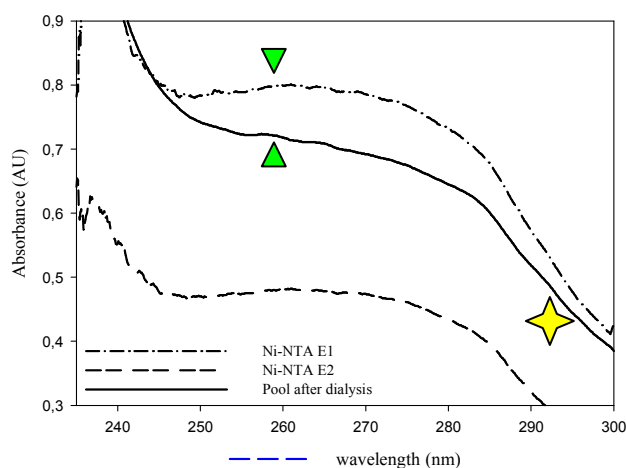


Figure 4.18: Comparison of UV spectra of Ni-affinity elutions; before and after dialysis. Absorbance of nucleotide (triangle) and aggregated protein (star) are shown.

A comparison of the UV spectra of the affinity elutions and the pool after dialysis shown in Figure 4.18 indicated that the sample contained aggregates after dialysis,

indicated by a shoulder starting at 290 nm and extending to the light scattering region [125].

Dialyzed samples were stored in the presence of different additives (Table 4.3) at -20 °C in order to investigate the optimum storage conditions.

Table 4.3: Absorbance values and concentration estimates of GPA1 with additives. The calculations were done considering either the presence of nucleotides (eqn 1) or using theoretical extinction coefficient (eqn 2).

Sample	Absorbance (AU)			Concentration (mg/ml)		A_{254}/A_{280}
	254 nm	260 nm	280 nm	eqn 1	eqn 2	
Dialyzed pool	0.726	0.718	0.645	0.454	0.593	1.125
S1	0.561	0.557	0.494	0.342	0.454	1.135
S2, 10 μ M GDP	0.408	0.416	0.388	0.285	0.356	1.051
S5, 10 μ M GDP and 10 % glycerol	0.541	0.545	0.505	0.368	0.464	1.071

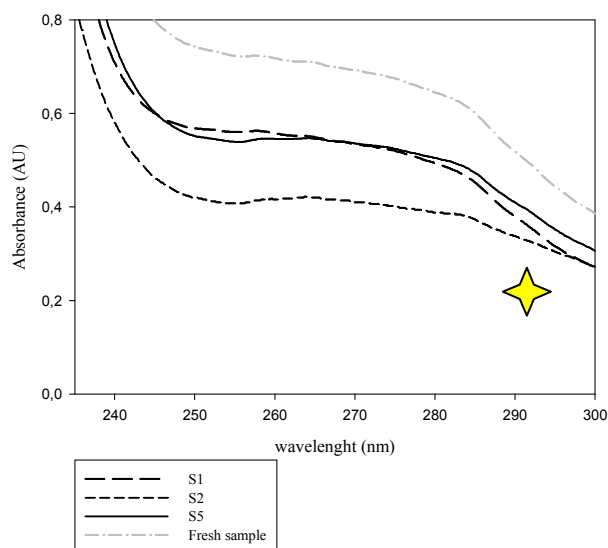


Figure 4.19: Comparison of fresh and -20 °C stored samples with different additives. Presence of aggregated protein (star) shown.

Samples stored without additive or with both GDP and glycerol had spectra similar to that of fresh protein and concentration values indicated that there was little protein loss. On the other hand storage with only GDP resulted in protein further aggregation (Figure 4.19).

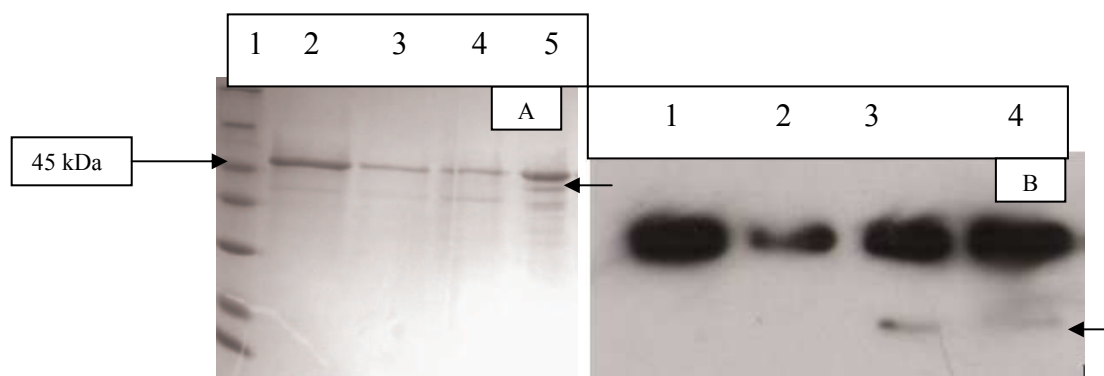


Figure 4.20: 12% SDS-PAGE (A) and Western (B) analysis of Ni-affinity elutions. A: Lane 1: Protein MW marker ®, lane 2: E1 (2 fold diluted), lane 3: E2, lane 4: E3 and lane 5: dialyzed pool. B: Lane 1: E1, lane 2: E3, lane 3: S1, lane 4: S5. Detection was done with 1:20,000 anti-myc-HRP. Gel samples were prepared immediately after dialysis and with 6X SDS loading dye.

Results of SDS-PAGE analysis shown in Figure 4.20 reveal that dialysed protein was prone to degradation (degradation product shown with arrows). Samples in the imidazole buffer did not show degradation although they were stored at -20 °C for 7 days. Furthermore, several freeze-thaw cycles did not result in protein degradation in imidazole elution buffer. DLS results obtained with dialyzed pool showed particle size distributions similar to those before the dialysis (data not shown).

- **Desalting**

The imidazole buffer of affinity purified GPA1 (total of 9 mg) was exchanged with 50 mM Tris-HCl pH 8.0 using a HiPrep™ 26/10 desalting column (Figure 4.21).

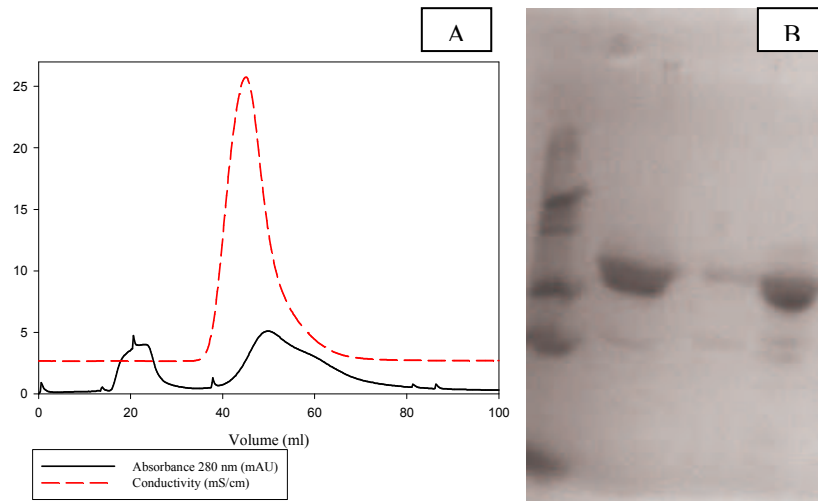


Figure 4.21: A: HiPrep™ 26/10 Desalting chromatogram. B: 12% SDS-PAGE analysis. A: The elution pool was desalted against 50 mM TrisHCl, pH 8.0 at 3 ml/min. B: Lane 1: PMW, lane 2: E1, lane 3: E3, lane 4:desalted pool. Samples were prepared with 6X SDS loading dye.

Table 4.4: The absorbance values after Ni-affinity and desalting.

sample	Absorbance (AU)			A_{254}/A_{280}
	254 nm	260 nm	280 nm	
E1	1.335	1.415	1.436	0.929
E2	0.663	0.687	0.634	1.045
E3	0.428	0.435	0.328	1.304
pool	0.983	1.022	0.934	1.052
desalted pool	0.767	0.733	0.63	1.217

The desalted pool was stored at -80 °C with 20 μ M GDP, 10% glycerol and 0.1 mM PMSF. Fresh and stored samples were analyzed to investigate the effect of storage on protein stability and preservation of the bound nucleotide.

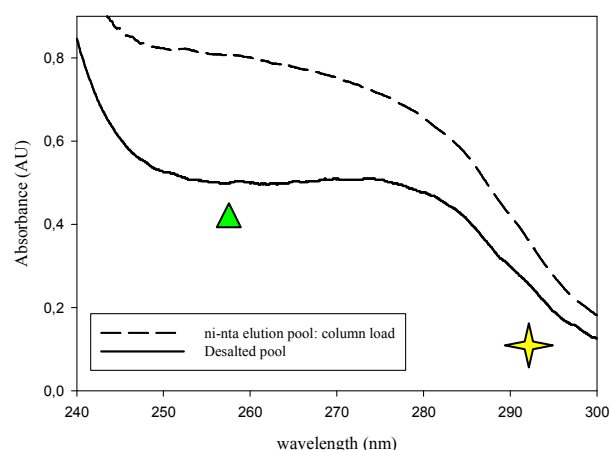


Figure 4.22: Comparison of UV-Vis spectra of desalting column load and desalted pool. Absorbance of nucleotide (triangle) and aggregated protein (star) are shown.

After desalting the GPA1 spectrum displayed a pronounced maximum at 280 nm accompanied by a second small peak at 254 nm (Figure 4.22). After desalting the total GDP amount in the samples was lower, but the amount of bound GDP did not decrease. Additional GDP that was in elution buffer was removed but the GDP bound to GPA1 was not affected. The affinity purified and desalted GPA1 samples bound GDP with a ratio of ~ 0.7 mole GDP / mole protein (Figure 4.81 and Table 4.14).

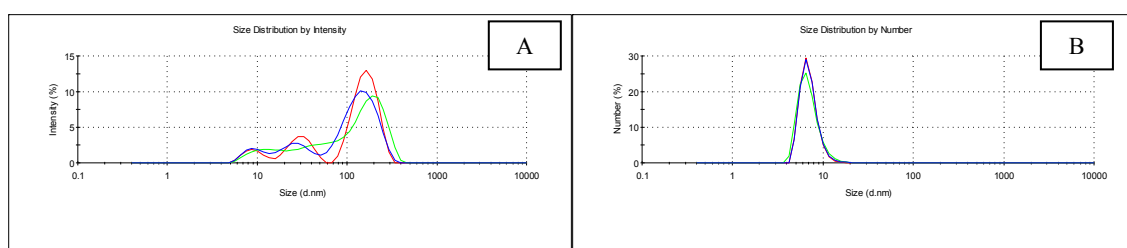


Figure 4.23: DLS size distributions by intensity (A) and number (B) of fresh desalted pool, without additives.

DLS results showed that use of HiPrep™ 26/10 Desalting column for buffer exchange yielded smaller oligomers (diameter 8 nm and 30 nm) of GPA1 which were detected in plots of the size distribution both by intensity and by number (Figure 4.23).

Aggregation and more heterogenous solutions started to form during - 80 °C storage (data not shown).

4.2.3 Affinity Purification with Detergents

Detergents were included in the lysis and purification buffers in order to increase the amount of solubilized GPA1 and to improve stability of the protein. The buffers used for GPA1 Ni-affinity purification are given in Chapter 3.2. Detergents used were Triton X-100 and Lubrol PX and characterization of detergent containing buffers by DLS measurements and UV spectra are given in APPENDIX K. The critical micelle concentration (cmc) for Triton X-100 is 0.25 mM, above this concentration detergent micelles form. Below the cmc, on the other hand, the detergent molecules cannot effectively dissolve membrane bound and/or lipid attached molecules. The cmc for Lubrol PX is 0.1 mM [119]. DLS analyses for both Triton X-100 and Lubrol PX showed that, below the cmc buffer solutions had heterogeneous particle size distributions but above cmc monodisperse solutions with particles of 8.5 nm diameter were observed (Figure K 2 - Figure K 9). One major drawback of using Triton X-100 in buffers is that the detergent absorbs at 280 nm, interfering with protein concentration estimations. This problem was not observed with Lubrol PX (Figure K 10 and Figure K 11). Lysis efficiency, on the other hand, was better with Triton X-100.

- Ni-Affinity with Triton X-100

Triton X-100 was added at a final concentration of 0.1 % (1.5 mM) and 0.02 % (0.3 mM) to lysis and purification buffers, respectively. Stepwise elution was done as described in previous section. This application resulted in the yield of the affinity step increasing to above 10 mg when compared with about 5 mg when no detergent was used from 300 ml *P. pastoris* cultures. It was also observed that the relative amount of the contaminating factors had decreased (Figure 4.24). The UV spectra of the Ni-affinity purified pools were similar to that without detergent and the A_{254}/A_{280} ratios were ~1.1.

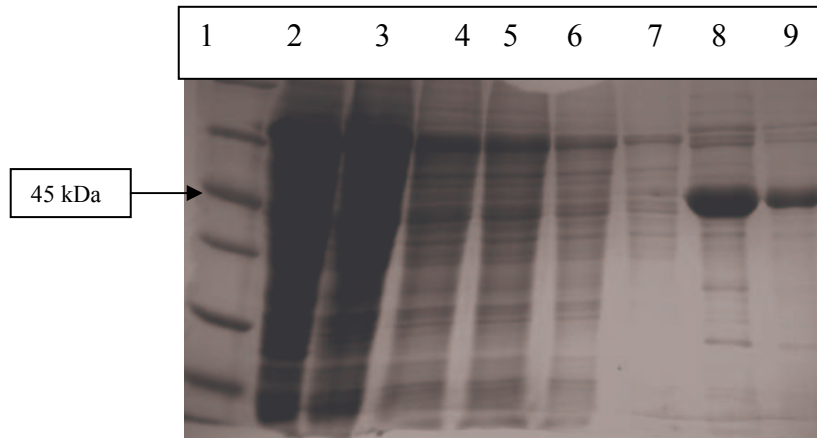


Figure 4.24: 12% SDS-PAGE analysis of Ni-affinity (Triton X-100) fractions. Lane 1: Protein MW marker®, lane 2: CL, lane 3: FT, lanes 4-7: wash 1-4, lanes 8-9: E1 and E2. Samples were prepared with 6X SDS loading dye.

The purification was repeated in the presence of AlF_4^- ($30 \mu\text{M Al}_2(\text{SO}_4)_3$ and 10 mM NaF), which in the presence of GDP, binds to GPA1 and mimics the GTPase transition state. Purity of the affinity pool was similar to that shown in Figure 4.24 (data not shown).

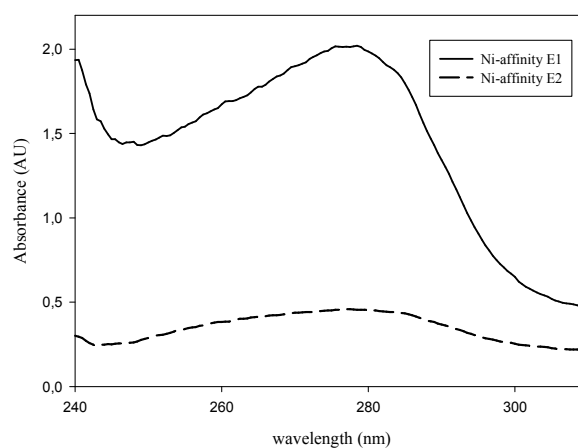


Figure 4.25: UV spectra of Ni-affinity pool (Triton X-100 and AlF_4^-). The A_{254}/A_{280} ratio for each elution was ~ 0.75 .

Table 4.5: Absorbance values and concentration estimation for Ni-affinity elutions

Sample	Absorbance (AU)			Concentration	Total Volume	Yield	A_{254}/A_{280}
	254 nm	260 nm	280 nm	mg/ml	ml	mg	
E1	1.52	1.67	1.98	1.80	10	18.06	0.76
E2	0.33	0.38	0.45	0.41	11	4.52	0.73

The Ni-affinity purified GPA1 had a A_{254}/A_{280} nm ratio <1 , and comparison of Figure 4.15 and Figure 4.25 (Table 4.2 and Table 4.5) show that in the presence of AlF_4^- , this ratio is lower. Since the GDP content of the purification buffer was constant, the increase in absorbance ~ 280 nm (higher yield) results in the reduction of the ratio.

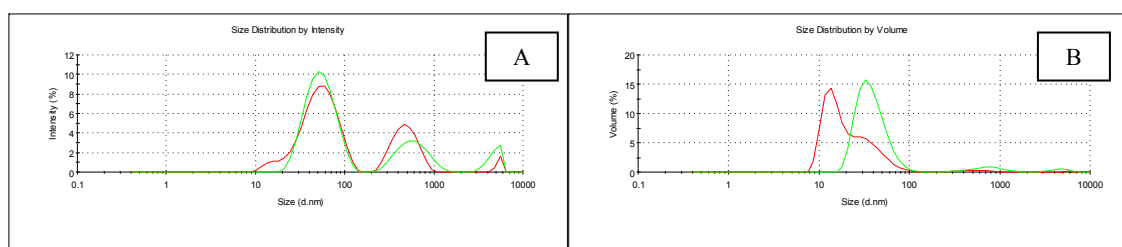


Figure 4.26: DLS size distributions by intensity (A) and volume (B) of Ni-affinity purified GPA1 (Triton X-100).

Two dominating types of particles with different sizes were observed in Ni-affinity purified GPA1 solutions with detergents. Although DLS pattern of Triton X-100 micelles show a peak corresponding to particles with 8.5 nm (APPENDIX K), the pattern observed in Figure 4.26 is likely to contain also the protein component with a diameter of 15 nm. Larger particles with a diameter 50 nm correspond to oligomeric forms of GPA1.

- Buffer Exchange

Buffer exchange was done either using HiPrep 26/10 Desalting Column or by dialysis as was described in section 4.2.2 for samples without detergent. Protein volume

was reduced using concentrator units before or after buffer exchange depending on the down stream process.

Desalting

A total of 12 mg GPA1 from the Ni-affinity pool was desalted against 50 mM Tris HCl, pH 8.0. Following desalting, the pool contained 5 mg GPA1 and was concentrated from 20 ml down to 2 ml.

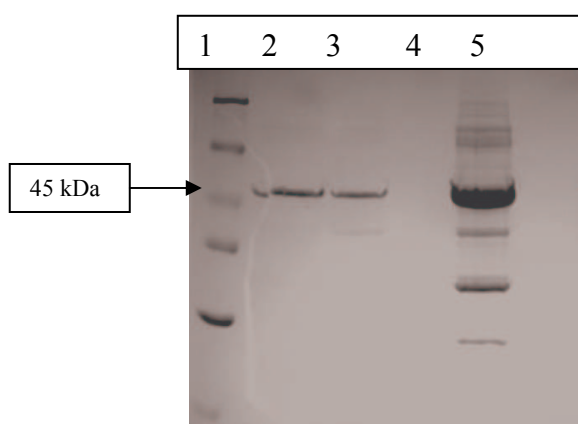


Figure 4.27: 12% SDS-PAGE analysis of Ni-affinity (Triton X-100) fractions. Lane 1: Protein MW marker®, lane 2: Ni-affinity pool, lane 3: desalted pool, lane 4: concentrator filtrate, lane 5: concentrated pool. Ni-affinity pool was loaded 2 fold diluted. Samples were prepared with 2X SDS loading dye.

Table 4.6: Absorbance values and concentration estimations for Ni-affinity fractions.
*calculated assuming all protein is GPA1.

Sample	Absorbance (AU)			Concentration mg/ml	Total Volume ml	Yield mg	Molarity* μM	A ₂₅₄ /A ₂₈₀
	254 nm	260 nm	280 nm					
Ni-affinity pool	1.16	1.22	1.03	0.67	17	11.45	14	1.12
Desalted pool	0.17	0.20	0.24	0.22	22	4.96	4.5	0.71

The recovery from the desalting column was only 50% (Figure 4.27 and Table 4.6). The concentration of bound GDP was 11.5 μM GDP for $\sim 4.5 \mu\text{M}$ GPA1, which corresponds to a ratio of 1 mole GDP /mole protein (calculations given in section 4.5.1).

Dialysis

As illustrated in Figure 4.28 after dialysis the particles ~ 20 nm were absent, which may imply formation of PMC (protein micelle complex) during dialysis. The dominating particles had a size ~ 55 nm and 85 nm. The larger particles correspond to components of the dialysis buffer (data not shown).

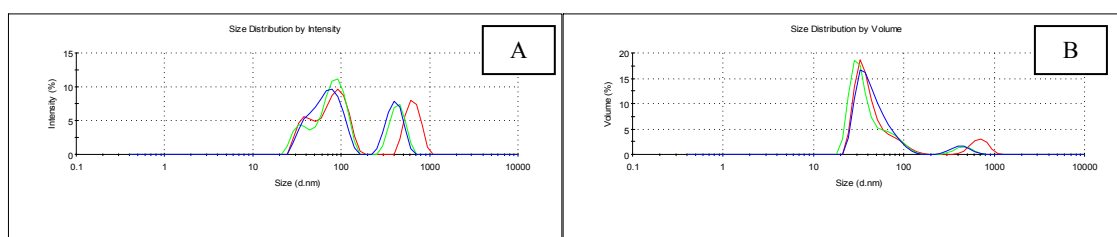


Figure 4.28: DLS size distributions by intensity (A) and volume of Ni-affinity pool after dialysis.

- Ni-Affinity with Lubrol PX

Lubrol PX was added at a final concentration of 1 % (17 mM) and 0.1 % (1.7 mM) to the lysis and purification buffers, respectively. Figure 4.29 shows that protein eluted with the high molecular mass contaminants from the affinity matrix in a fashion similar to that observed when Triton X-100 was used as the detergent (Figure 4.24).

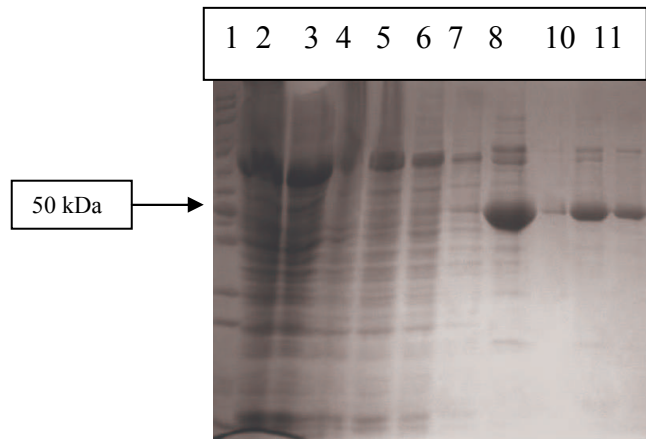


Figure 4.29: 12% SDS-PAGE analysis of Ni-affinity (Lubrol-PX) fractions. Lane 1: Protein ladder®, lane 2: CL, lane 3: FT, lanes 4-7: wash 1-4, lane 8: E1, lane 10: E2, lane 11: E3. Samples were prepared with 6X SDS loading dye.

The protein concentration in elution fractions was determined from UV spectra. The total yield of protein was ~15 mg GPA1 purified from 500-700 ml of culture and A_{254}/A_{280} ratios were about 0.9-1.0.

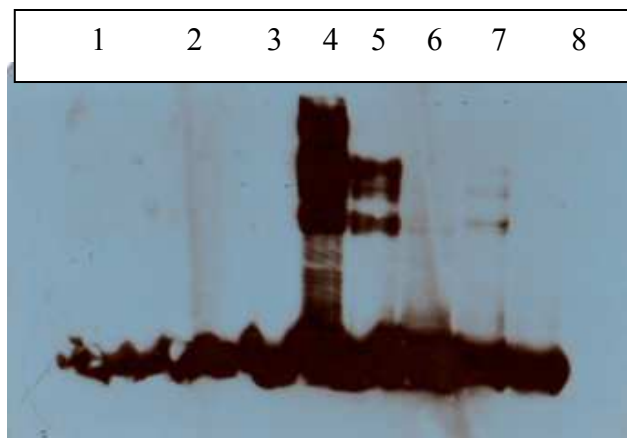


Figure 4.30: Western analysis of Ni-affinity (Lubrol-PX) elution E2. Lanes 1-2: with BME, boiled and not boiled, lanes 3-6: without BME, boiled, not boiled, heated to 60° C for 30 minutes, overflow, lanes 7-8: E2 stored at +4°C, prepared without BME not boiled and boiled. Samples were prepared with 6X SDS loading dye with or without BME. Membrane was incubated with 1:2500 tetra-his-HRP.

The Western blot analysis shown in Figure 4.30 revealed that the proteins with high molecular mass present in GPA1 elutions were actually oligomers of GPA1. These oligomers were absent in the samples prepared with BME but for samples prepared without BME and not exposed to high temperatures, the tetra-his antibody was bound to

oligomers. These results suggest that the oligomers were formed via intermolecular disulfide bridges.

Results of DLS measurements on the Ni-affinity preparations with Lubrol-PX were dominated by particles with 5.5 nm-8.5 nm diameter due to the detergent but also a small amount of particles with larger diameters (50 nm) were detected (Figure 4.31).

The Ni-affinity purified GPA1 was concentrated and the buffer was exchanged using either a concentrator unit or by dialysis. The DLS size distribution by intensity and volume for these samples indicated that besides particles of about 20 nm diameter the solutions also contained particles with 85 nm (Figure 4.32).

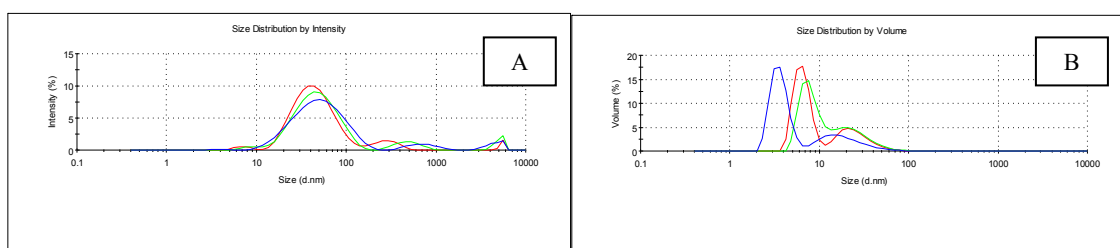


Figure 4.31: DLS size distributions by intensity (A) and volume (B) of concentrated Ni-NTA pool.

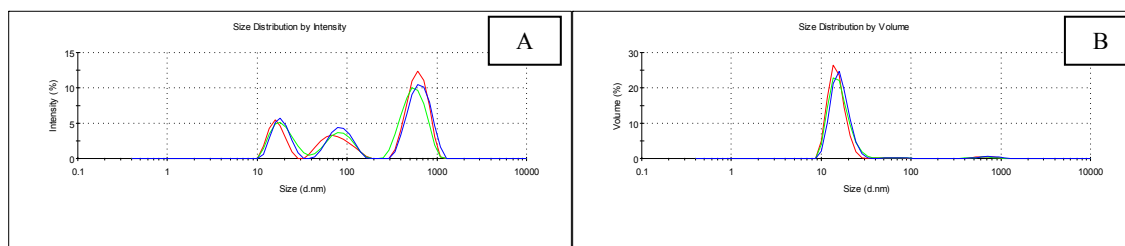


Figure 4.32: DLS size distributions by intensity (A) and volume (B) of N-affinity pool after dialysis.

The purification was also repeated in the presence of AlF_4^- and results were similar in terms of yields, protein homogeneity and the A_{254}/A_{280} ratio (data not shown).

4.3 Anion Exchange

Anion exchange chromatography was performed on Ni-affinity purified GPA1 using HiTrap QHP, 5 ml, columns (GE Healthcare). Purification was carried out using 0-700 mM NaCl gradient in 50 mM Tris HCl, pH 8.0. The presence of different additives in Ni-affinity and their effect in separation during anion exchange are summarized below. The NaCl concentrations and elution volumes are given in Table 4.7.

Table 4.7 Comparison of NaCl concentrations and elution volumes for anion exchange in the presence of different additives.
dns:data not shown

	NaCl, mM							
Additive /Figure	Peak 1		Peak 2		Peak 3		Peak 4	
	start	end	Start	end	start	end	start	end
None / 4.33	106.5 (6.8 ml)	145.4 (9.3 ml)	153 (9.8 ml)	192 (12.3 ml)	207.6 (13.3 ml)	285.3 (18.3 ml)	293 (18.8 ml)	370.7 (23.8 ml)
Triton /dns	114.1 (5.4 ml)	145.9 (6.8 ml)	167 (7.8 ml)	209.5 (9.8 ml)	230.7 (10.8 ml)	273.2 (12.8 ml)	294.4 (13.8 ml)	379.2 (17.8 ml)
Triton-AlF ₄ ⁻ / 4.39	103.7 (5.4 ml)	187.7 (9.8 ml)	206.7 (10.8 ml)	225.7 (11.8 ml)	235.2 (12.3 ml)	263.7 (13.8 ml)	301.7 (15.8 ml)	396.7 (20.8 ml)
Lubrol / 4.48	91.2 (4.3 ml)	123 (5.8 ml)	133.6 (6.3 ml)	165.4 (7.8 ml)	207.8 (9.8 ml)	250.3 (11.8 ml)	282 (13.3 ml)	366.9 (17.3 ml)
Lubrol AlF ₄ ⁻ / dns	57 (3 ml)	95 (5 ml)	152 (8 ml)	209 (11 ml)	228 (12 ml)	304 (16 ml)	323 (17 ml)	418 (22 ml)

4.3.1 Obtaining two biophysically different GPA1 pools

Separation of protein components after Ni-affinity preparations of GPA1 was investigated. The buffer of GPA1 was exchanged on a HiPrep™ 26/10 desalting column after affinity purification. The pool with a total of ~8 mg protein (in 31 ml), in buffer 50 mM Tris HCl, pH 8.0, 20 μ M GDP and 10 % glycerol, was loaded onto a 5 ml HiTrap Q HP column. The elution pattern of the Ni-affinity pool displayed four peaks as illustrated in Figure 4.33. SDS-PAGE analysis revealed that GPA1 eluted as the major component in peaks 3 and 4 (Figure 4.34) with about 95% homogeneity. The fractions of peak 3 and 4 were pooled separately (pool 3 and pool 4). Pools 3 and 4 were dialyzed against 20 mM HEPES, pH 8.0, 50 mM NaCl and 0.1 mM PMSF. After dialysis the samples were stored with 20 μ M GDP, 10% glycerol at -80 °C.

The absorbance values of peak 3 and peak 4 fractions were inconsistent with the SDS-PAGE results. On the chromatogram (Figure 4.33) the ratio of the area under the peak of pool 3 to pool 4 was about 4:1. Direct measurements made from the pools indicated the A_{280} to be about 2:1 (Table 4.8) and when equal sample volumes from peak 3 and peak 4 were loaded on the gel the proteins bands had similar intensity (Figure 4.34). This indicated that the absorbance of peak 3 at 280 nm could be mainly due to a component other than GPA1.

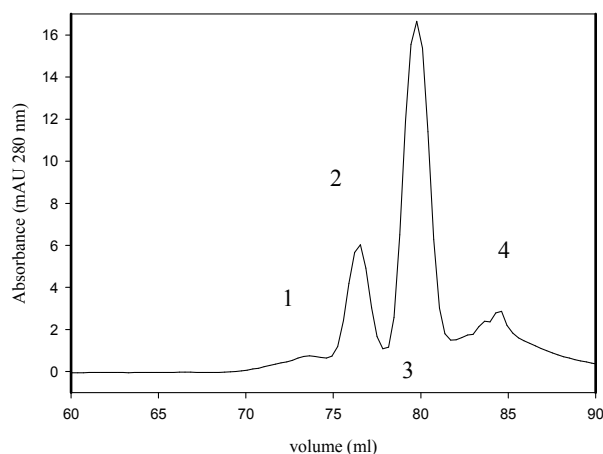


Figure 4.33: Elution of GPA1 from a HiTrap Q HP column with NaCl gradient. Linear gradient was applied with 0-700 mM NaCl in 50 mM Tris HCl, pH 8.0 over a volume of 25 ml with a flow rate of 5 ml/min. 0.5 ml fractions were collected.



Figure 4.34: 12% SDS-PAGE analysis of anion exchange fractions. Lane 1: Protein MW marker®, lanes 2-3: Ni-affinity elutions, E1-E2, lane 4: desalted pool, lanes 5-14: anion exchange fractions; lane 5: peak 1, lanes 6-7 peak 2, lanes 8-10: peak 3, lanes 11-14: peak 4.

Table 4.8: Absorbances and concentration estimates for pool 3 and 4. Measured immediately after dialysis and before addition of GDP and glycerol.

	Absorbance (AU)		Concentration mg/ml	Total Volume ml	Yield mg
	260nm	280nm			
sample					
pool 3	0.127	0.93	1.344	2	2.689
pool 4	0.38	0.41	0.346	5	1.733

The monodispersity of the two-anion exchange pools were monitored by DLS before and after dialysis.

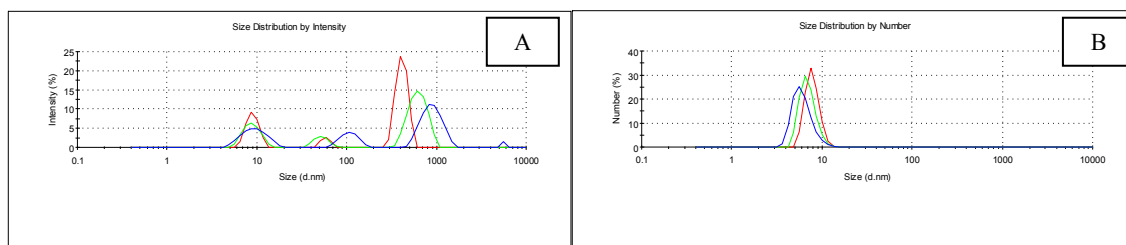


Figure 4.35: DLS size distributions by intensity (A) and number (B) of anion exchange pool 3 before dialysis.

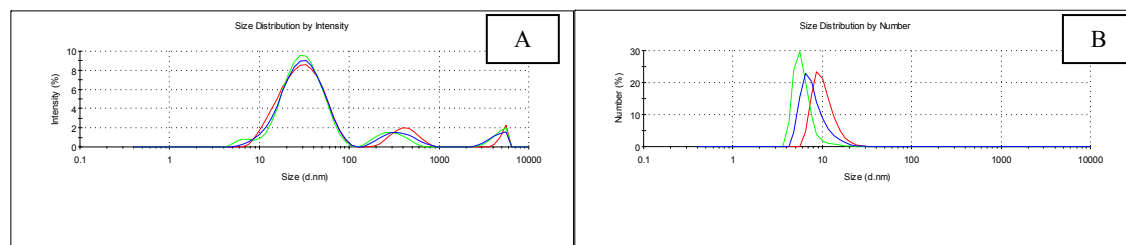


Figure 4.36: DLS size distributions by intensity (A) and number (B) of anion exchange pool 4 before dialysis.

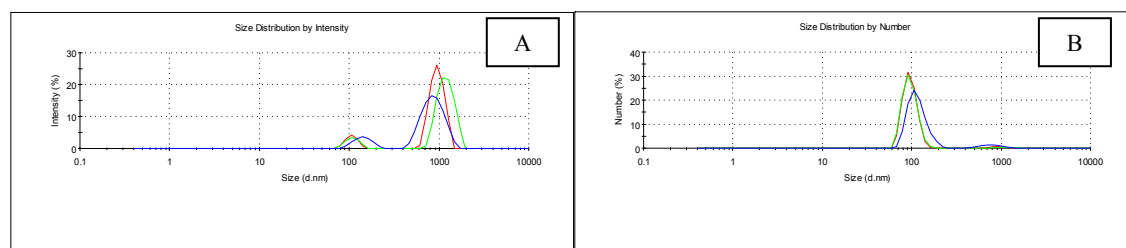


Figure 4.37: DLS size distribution by intensity (A) and number (B) for pool 3 after dialysis. Protein was stored at -80 °C in 20 mM HEPES 50 mM NaCl, 20 μ M GDP and 10% glycerol.

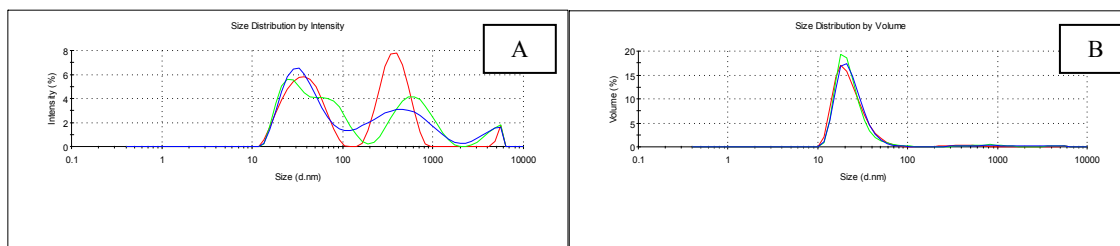


Figure 4.38: DLS size distribution by intensity (A) and number (B) for pool 4 after dialysis.

Protein was stored at $-80\text{ }^{\circ}\text{C}$ in 20 mM HEPES 50 mM NaCl, 20 μM GDP and 10% glycerol.

The particle size distributions of pool 3 and pool 4 indicate the presence of particles of different size (Figure 4.35 and Figure 4.36). Pool 3 contains larger oligomers with diameter 60 and 100 nm and yet the smallest particle size in the distribution is closer to that expected from monomers (10 nm). Pool 4 was composed of particles with sizes 30 nm and 10 nm. After dialysis and storage pool 3 molecules were in a homogenous but oligomeric form (100 nm) whereas the pool 4 molecules formed a more heterogeneous solution, with smaller sized oligomeric forms (40 and 70 nm) of GPA1 (Figure 4.37 and Figure 4.38).

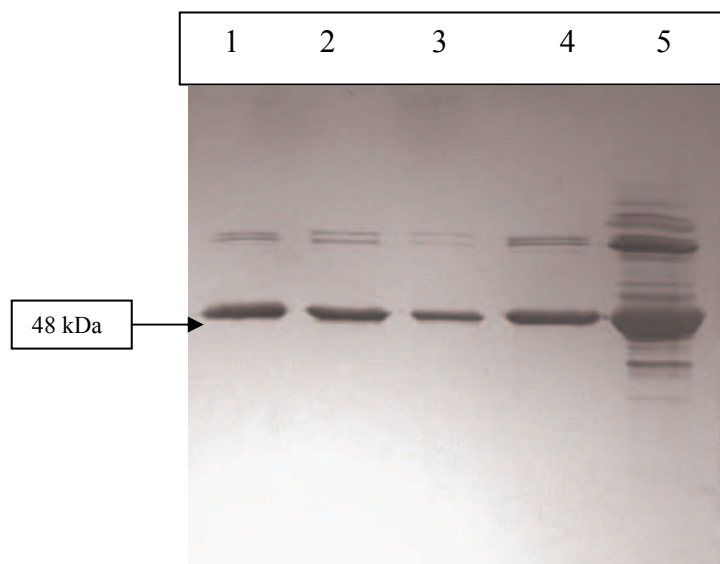


Figure 4.39: 12% SDS-PAGE and Silver stain analysis of anion exchange pools. Lane 1: Ni-affinity AD, lane 2: pool 3 BD, lane 3: pool 3 AD, lane 4: pool 4 BD, lane 5: pool 4 AD. Samples were prepared with 2X SDS loading dye. BD: before dialysis. AD: after dialysis.

The purity of pool 3 and pool 4 were compared by silver staining. Pool 3 was highly pure, there was low amount of HMM forms, whereas pool 4 contained significant amount of aggregation and degradation products as shown in Figure 4.39.

4.3.2 Anion Exchange, load with detergent

Anion exchange fractionation was carried out on GPA1, obtained from Ni-affinity purification in the presence of different detergents. Buffers used are given in Chapter 3.2.

1. Triton X-100 & AlF_4^-

In exploratory purifications, GPA1 purified from Ni-affinity matrix with Triton X-100 buffers was analyzed on the anion exchange column and results were similar to those obtained without detergent summarized above. As the last parameter to vary, AlF_4^- was added to the detergent buffers and concentration of GDP was raised to 50 μM as a stabilizing factor. GPA1 was purified from Ni-affinity matrix in the presence of 0.02% Triton X-100, 30 μM $\text{Al}_2(\text{SO}_4)_3$ and 10 mM NaF. Affinity purified protein was stored without buffer exchange at -20 °C after the addition of 10 % glycerol. Before separation by anion exchange, samples were thawed, concentrated and dialyzed against 50 mM Tris HCl pH 8.0, 1 mM DTT and 1 mM PMSF. GPA1 (20 mg in 11 ml) was loaded onto anion exchange column and protein eluted from the column with the profile in Figure 4.40. Fractions were pooled according to the result of SDS-PAGE analysis in Figure 4.41. Functional assays were done on GPA1 purified without AlF_4^- .

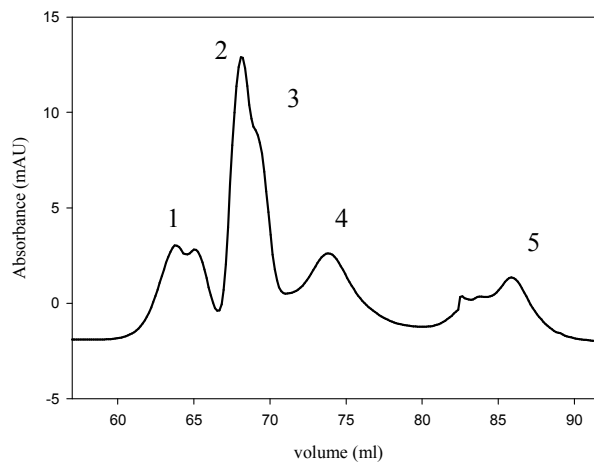


Figure 4.40: Elution of GPA1 from a HiTrap Q HP column with NaCl gradient. Linear gradient was applied with 0-700 mM NaCl in 50 mM Tris HCl, pH 8.0 over a volume of 30 ml with a flow rate of 3 ml/min and 0.5 ml fractions were collected.

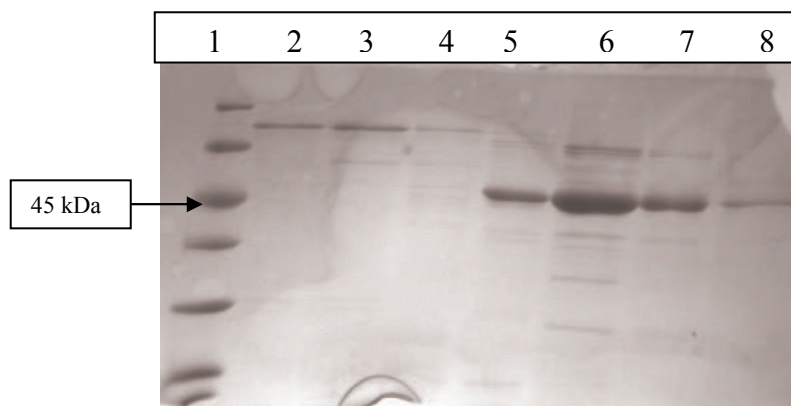


Figure 4.41: 12% SDS-PAGE analysis of anion exchange fractions. Lane 1: Protein MW marker®, lanes 2-3 : peak 1 top fractions and last fraction, lane 4: peak 2 first fraction, lane 5: peak 3 first fraction, lanes 6-7: peak 4 top and last fractions, lane 8: peak 5 top fraction. Samples were prepared with 6X SDS loading dye.

Fractions from peak 3 (NaCl from 235.2 to 263.7 mM, total of 2.6 ml) and peak 4 (NaCl from 301.7 to 396.7 mM, total of 7.5) were pooled and dialyzed against 5 mM Tris HCl, pH 8.0, 5 mM NaCl, 1 mM DTT and 1 mM PMSF. Following dialysis pools were lyophilized for 20 hours; after flash freezing in liquid nitrogen and stored at room temperature. Samples were taken before lyophilization for UV and DLS analysis.

Table 4.9 Comparison of absorbance values of dialyzed pools 3, 4 and 5

	Absorbance (AU)			Concentration mg/ml	A_{254}/A_{280}
	254 nm	260 nm	280 nm		
pool 3	0.867	0.814	0.701	0.468	1.236
pool 4	0.548	0.561	0.614	0.525	0.892
pool 5	0.321	0.312	0.188	0.054	1.707

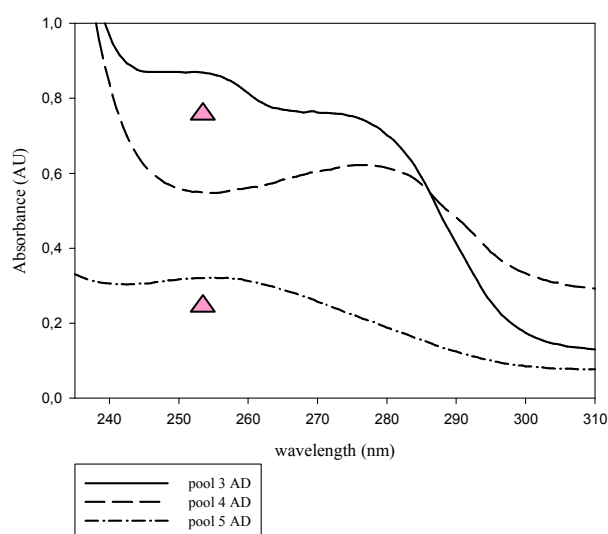


Figure 4.42: Comparison of UV spectra for pool 3, 4 and 5 (after dialysis). The absorbance at ~254 nm is indicated with triangles.

The discrepancy between the 280 nm absorbance values and protein content of pools 3 and 4 is clear from the values given in Table 4.9 and the SDS-PAGE analysis shown in Figure 4.41. Pool 3 GPA1 had excess GDP with a high A_{254}/A_{280} ratio, as compared to pool 4 GPA1. Pool 5 contained most unbound excess GDP and had very low protein content (Figure 4.42 and Table 4.9).

Pool 3 was highly aggregated after dialysis; there were no monomeric particles even in size distribution by number. Pool 4 contains particles with size ~15 nm (Figure 4.43 and Figure 4.44). The particle size did not change upon storage for neither of the

pools (data not shown). The particles with sizes above 300 nm in the distribution by intensity are also present in the buffer (data not shown).

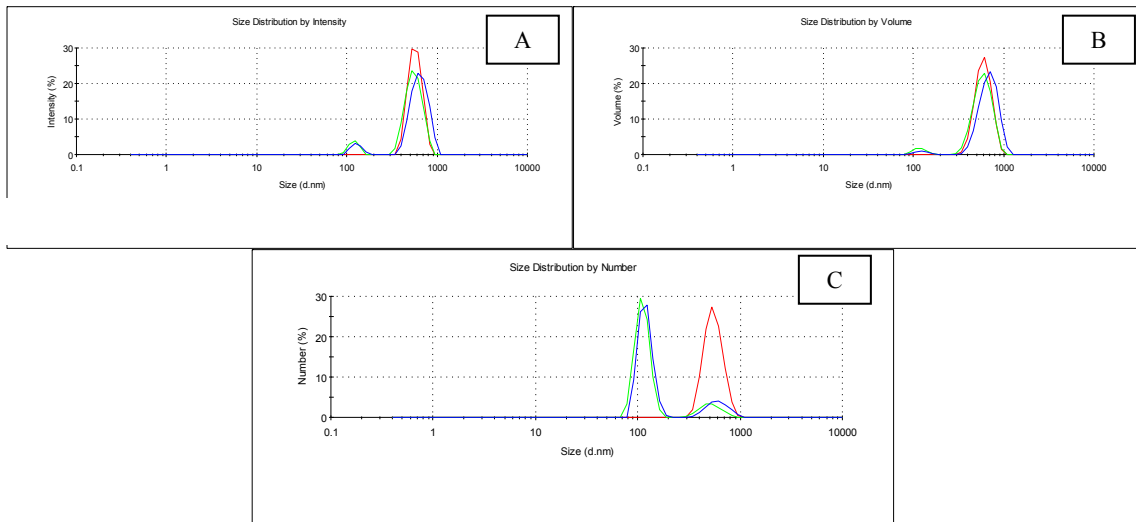


Figure 4.43: DLS size distributions by intensity (A), volume (B) and number (C) of fresh pool 3 in final dialysis buffer.

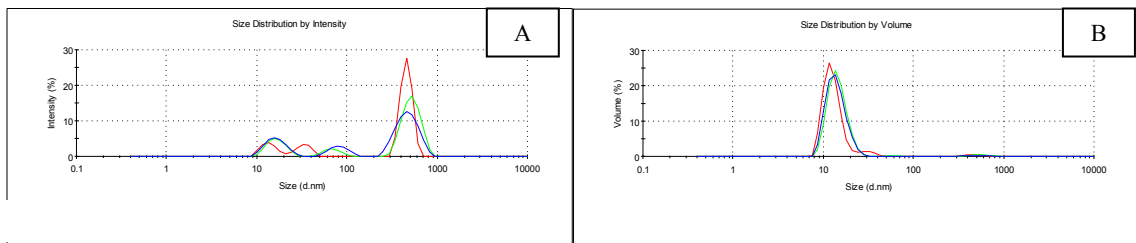


Figure 4.44: DLS size distributions by intensity (A) and volume (B) of fresh pool 4 in final dialysis buffer.

Lyophilized pool 3 and pool 4 proteins were resuspended in the final dialysis buffer in 10 fold-reduced volume compared to that before lyophilization. Samples were analyzed by SDS-PAGE /Silver stain, Figure 4.45, and western blotting, Figure 4.46, to investigate protein quality. DLS measurements were done on samples that were brought up to the original volume.

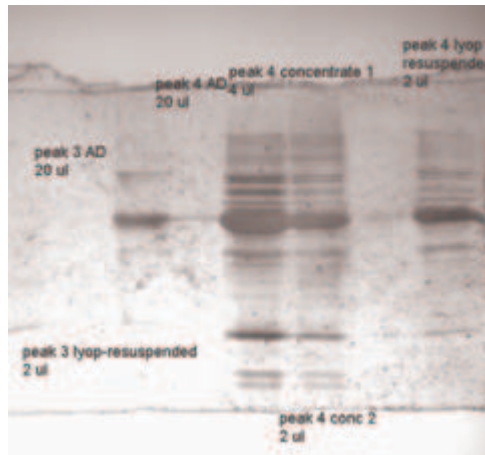


Figure 4.45: 12% SDS-PAGE analysis of anion exchange pools with Silver stain. Lane 1: Protein MW marker ®, lane 2: pool 3 AD, lane 3: pool 3 lyophilized, lane 4: pool 4 AD, lanes 5-6: pool 4 AD concentrated, lane 8: pool 4 lyophilized. Samples were prepared with 6X SDS loading dye with the indicated amount of protein.

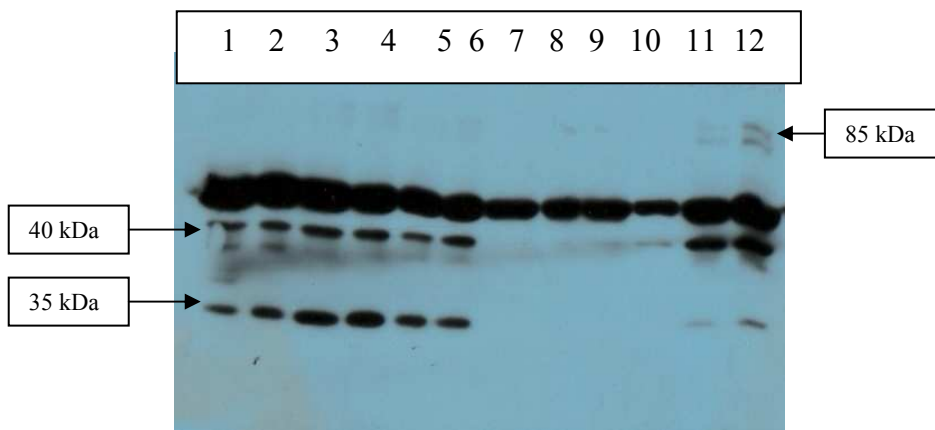


Figure 4.46: Western analysis of Ni-affinity and anion exchange fractions. Lanes 1-2: ni-nta pool 1 before and after concentrating, lanes 3-4: ni-nta pool 2, before and after concentrating lanes 5-6: pool BD and AD lanes 7-9: pool 3 BD, AD and lyophilized, lanes 10-12: pool 4 BD, AD and lyophilized. Samples in lanes 2,4, 5 and 6 were prepared with 6 μ l, in lane 9 with 2 μ l and in lane 10 with 10 μ l protein. Membrane was incubated with 1:2,000 tetra-his-HRP (Qiagen).

The Ni-affinity samples contained degradation products. In cases where GPA1 was partially degraded in the Ni-affinity step, the anion exchange selectively eliminated the degradation products from pool 3 but not from pool 4. HMM aggregation products were detected in both pools by silver and antibody staining (Figure 4.45 and 45), but the

amount was significantly higher in pool 4. Both degradation and aggregation were pronounced upon lyophilization for pool 4 but not pool 3 GPA1, also verified by DLS.

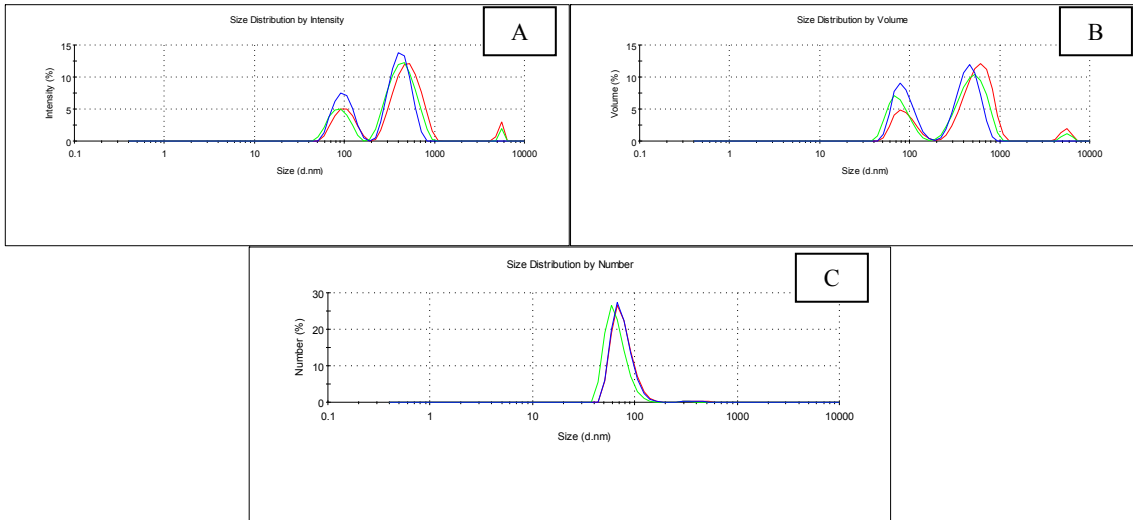


Figure 4.47: DLS size distributions by intensity (A), volume (B) and number (C) of lyophilized and resuspended pool 3 in final dialysis buffer.

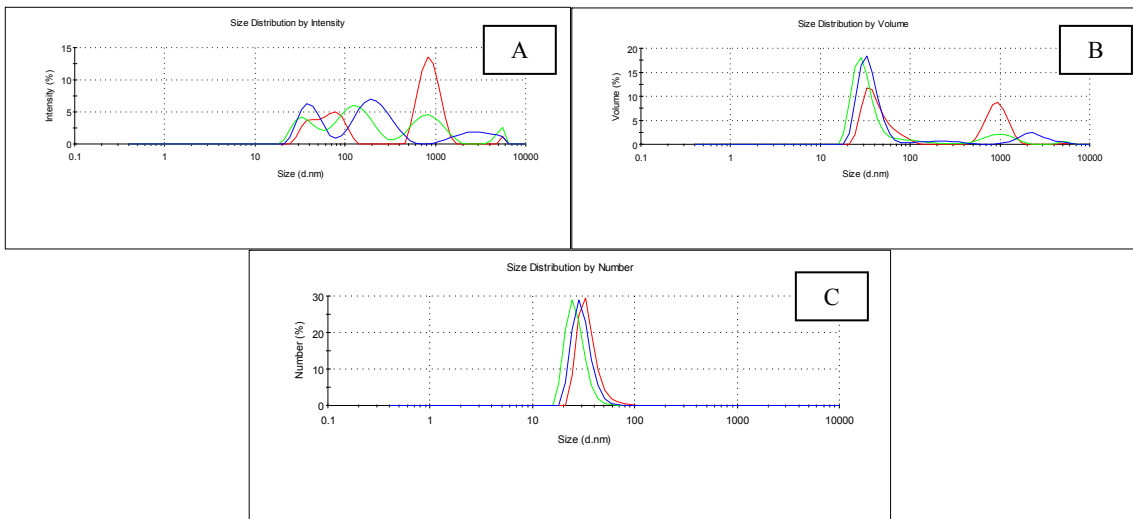


Figure 4.48: DLS size distributions by intensity (A), volume (B) and number (C) of lyophilized and resuspended pool 4 in final dialysis buffer.

Pool 3 samples were oligomeric, with the same particle size distribution as before lyophilization (Figure 4.47). Pool 4 was aggregated after lyophilization/resuspension with particle sizes shifted from ~15 nm to ~40 nm (Figure 4.48).

In conclusion western blot detection and silver staining revealed that the oligomeric form, pool 3 GPA1 contains more intact/pure protein. DLS results showed that pool 3 GPA1 was more stable to lyophilization than pool 4 GPA1.

2. Lubrol PX

The buffer of GPA1 purified by Ni-affinity in the presence of 0.02% Lubrol PX was exchanged by dialysis. About 6 mg GPA1 in 6 ml 50 mM Tris HCl, pH 8.0, 1 mM DTT and 1 mM PMSF buffer were loaded on the anion exchange column (Figure 4.49).

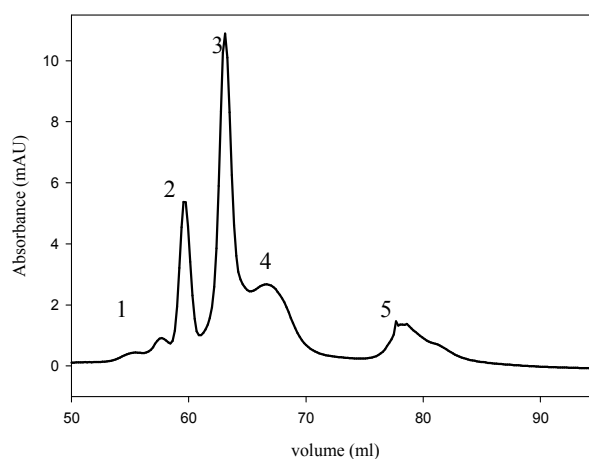


Figure 4.49: Elution of GPA1 from a HiTrap Q HP column with NaCl gradient. Linear gradient was applied with 0-700 mM NaCl in 50 mM Tris HCl, pH 8.0 over a volume of 25 ml with a flow rate of 3 ml/min. 0.5 ml fractions were collected.

Fractions from peaks 3 and 4 were pooled separately as described above and further analyzed by SDS-PAGE. Homogeneous GPA1 was eluted in both peaks 3 and 4 (Figure 4.50).

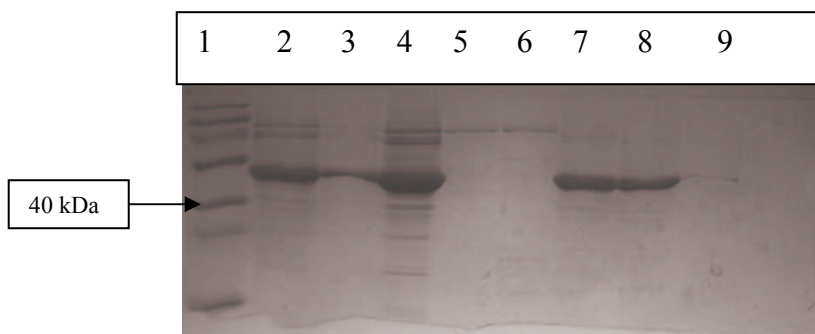


Figure 4.50: 12% SDS-PAGE analysis of anion exchange pools. Lane 1: Prestained protein ladder ®, lane 2: Ni-affinity pool, lane 3: concentrated pool (10 fold diluted), lane 4: dialyzed pool, lane 5: peak 1 top fraction, lane 6: peak 2 top fraction, lane 7: peak 3 top fraction, lane 8: peak 4 top fraction, lane 9: peak 5 top fraction. Samples were prepared with 6X SDS loading dye.

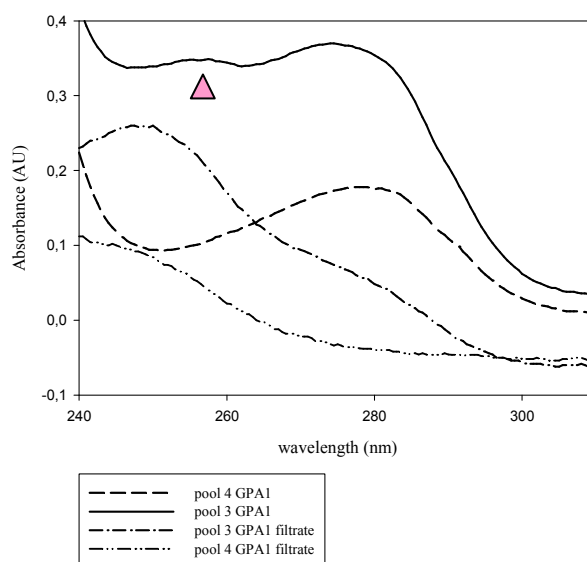


Figure 4.51: UV-vis spectra of pool 3 and pool 4 GPA1 and corresponding filtrates. The signal at ~253 nm (triangle) in pool 3 corresponds to free nucleotide.

UV-vis spectra of the pools (Figure 4.51) revealed that pool 3 GPA1 had an A_{254}/A_{280} ratio twice as high as pool 4 (0.98 and 0.56 respectively). The GDP content of GPA1 in the pools was determined as described in chapter 3.2 and the spectra of filtrates with GDP released from GPA1 are shown in Figure 4.51. Pool 3 contained high amounts of GDP, with a ratio of 1.4 mole GDP/ mole protein. Pool 4 was bound to 0.8 mole GDP / mole protein (Table 4.14).

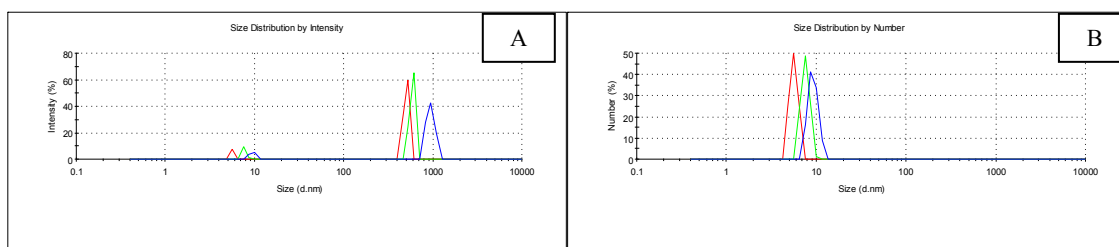


Figure 4.52: DLS size distributions by intensity (A) and number (B) of pool 3 GPA1.

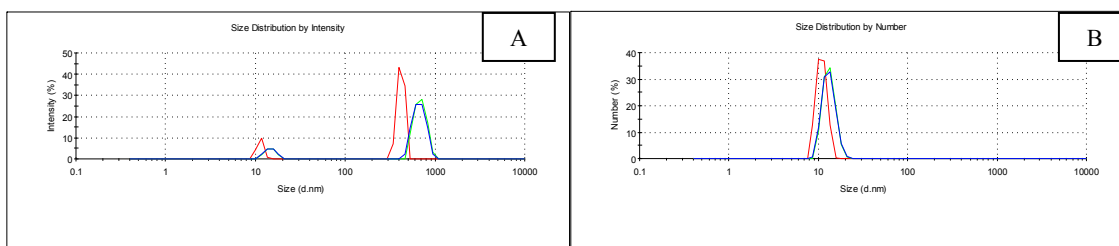


Figure 4.53: DLS size distributions by intensity (A) and number (B) of pool 4 GPA1.

DLS analysis showed that pool 3 was composed of particles with a diameter ~ 9 nm and pool 4 with ~ 15 nm (Figure 4.52 and Figure 4.53). These particles could be GPA1 with or without Lubrol micelles. The particles with size ~ 1000 nm are also present in the buffer (data not shown). The purification was repeated with GPA1 affinity purified in the presence of 0.1% Lubrol PX, $30 \mu\text{M Al}_2(\text{SO}_4)_3$ and 10 mM NaF and the separation was similar. The A_{254}/A_{280} ratios of pool 3 and pool 4 were 0.69 and 0.48 respectively; the value for pool 3 is lower than that obtained without AlF_4^- .

In summary, there were two distinguishable GPA1 molecules after Ni-affinity purification, which could be resolved by anion exchange. The NaCl concentrations at which peak 3 and peak 4 GPA1 eluted were similar for different affinity purification conditions (Table 4.7) but the separation from contaminants was worse when Triton X-100 was included in affinity step. These two forms were further analysed by CD, SAXS and nucleotide binding measurements and results are given in following sections.

4.4 Size Exclusion Chromatography

After establishing the oligomeric nature of GPA1 obtained by Ni-affinity chromatography, gel filtration columns with different resolution range were used to analyse the different oligomers. The first trial was carried out using a HiLoad 16/60 Superdex 75 pg column (GE Healthcare, 120 ml) which resolves proteins within the molecular masses between 3 kDa and 70 kDa. Here GPA1 purified from Ni-affinity was eluted in the void volume. Fractionation on Sephacryl S-300 (resolution range between 10 kDa to 1500 kDa) and Sephacryl S-200 columns (resolution range between 5 kDa to 250 kDa) were explored using different buffers (Table 4.10) as detailed below. Calibration curves for the columns with standard proteins are given in Appendix L.

Table 4.10: Purification Conditions for GPA1 Gel Filtration

	Lysis Buffer	Ni-Affinity, 10 X	Desalting	Gel filtration Buffer
1	50 mM Tris HCl, pH 8.0 10 mM MgCl ₂ , 1mM EDTA 5% glycerol, EFPI, 2 mM PMSF 0.1% Triton-X 100	500 mM Tris-HCl 8.0, 3 M NaCl 100 mM BME, 1 mM PMSF 200 μM GDP, 20 mM MgCl ₂ 200 mM imidazole, 0.2 % Triton-X 100	20 mM HEPES, pH 8.0, 100 mM NaCl	Buffer A: 20 mM HEPES, pH 8.0 100 mM NaCl
2	50 mM Tris HCl, 8.0 10 mM MgCl ₂ , 1 mM EDTA 5% glycerol, EFPI, 2 mM PMSF 0.1 % Triton-X 100 50 μM GDP	500 mM TrisHCl, 8.0, 3 M NaCl 100 mM BME, 2 mM PMSF 500 μM GDP, 50 mM MgCl ₂ 200 mM imidazole, 0.2% Triton-X 100	50 mM Tris HCl, 1mM DTT	Buffer B: 50 mM Tris HCl, pH 8.0 150 mM NaCl 1 mM DTT, 5% glycerol 50 μM GDP
3	50 mM Tris HCl, 8.0 10 mM MgCl ₂ , 1 mM EDTA 5% glycerol, EFPI, 2 mM PMSF 0.1 % Triton-X 100 50 μM GDP	500 mM TrisHCl, 8.0, 3 M NaCl 100 mM BME, 2mM PMSF 500 μM GDP, 50 mM MgCl ₂ 200 mM imidazole 0.2% Triton-X 100 300 μM Al ₂ (SO ₄) ₃ , 100 mM NaF	N.A.	Buffer C: 50 mM HEPES, pH 8.0 150 mM NaCl 1 mM DTT, 5% glycerol 50 μM GDP, 5 mM MgCl ₂
4	50 mM Tris HCl, 8.0 10 mM MgCl ₂ , 1 mM EDTA 5% glycerol, EFPI, 2 mM PMSF 1% Lubrol-PX 50 μM GDP	500 mM TrisHCl, 8.0, 3 M NaCl 100 mM BME, 2 mM PMSF 500 μM GDP, 50 mM MgCl ₂ 200 mM imidazole 1% Lubrol -PX 300 μM Al ₂ (SO ₄) ₃ , 100 mM NaF	N.A.	Buffer D: 20 mM HEPES, pH 8.0 150 mM NaCl 1 mM DTT, 5% glycerol 5 mM MgCl ₂

- Sephacryl S-300 HR 16/60, Buffer A

GPA1 affinity purified in the presence of Triton-X was desalted using a HiPrep™ 26/10 desalting column against 20 mM HEPES, pH 8.0 , 100 mM NaCl buffer and stored at -20 °C after addition of 20 μM GDP. A total of 5 mg protein was loaded onto the column after concentrating down to 2 ml. The DLS analysis (Figure 4.57) indicates that the protein loaded on the column was in oligomeric form with particles of diameter 20 and 100 nm.

Protein eluted from the column in a complex pattern (Figure 4.54) and the molecular masses corresponding to the elution positions of different peaks are shown in Table 4.11. Top fractions from the peaks were analyzed by SDS-PAGE for homogeneity. As illustrated in Figure 4.55 all peaks contained mainly GPA1 apparently in different oligomeric forms. The UV spectra (Figure 4.56) confirmed the presence of aggregates for fractions eluted at earlier volumes. The oligomers were monitored by DLS (Figure 4.58-Figure 4.61) and in accordance with the elution pattern from the gel filtration column the smallest size particles were observed in peak 4, with size ~10 nm. The smallest particles with 8.5 nm may correspond to Triton X-100 micelles (Table 4.11 and APPENDIX K)

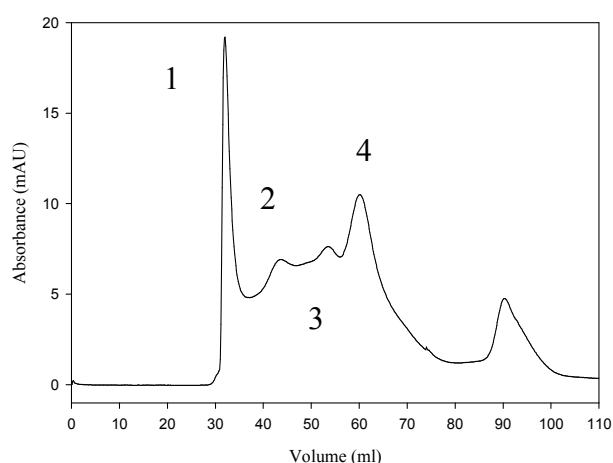


Figure 4.54: Elution pattern of GPA1 from S-300 HR 16/60 column with Buffer A. Flow rate was 0.3 ml/min and 0.5 ml fractions were collected.

Table 4.11 Molecular mass estimations for S-300 (Buffer A) peaks.
 Estimated from elution volumes and column calibration (Figure L 3).

	Ve ml	Range ml	Molecular Mass, Da			Diameter, nm (DLS)
			Top	Start	End	Top
peak 1	34.43	32-36	607506	755565	527364	50
peak 2	43.37	39-48	271600	4025430	179003	20
peak 3	53.44	50-56	109713	149504	87102	8.5, 15
peak 4	60	57-66	60799	79602	35398	8.5, 10

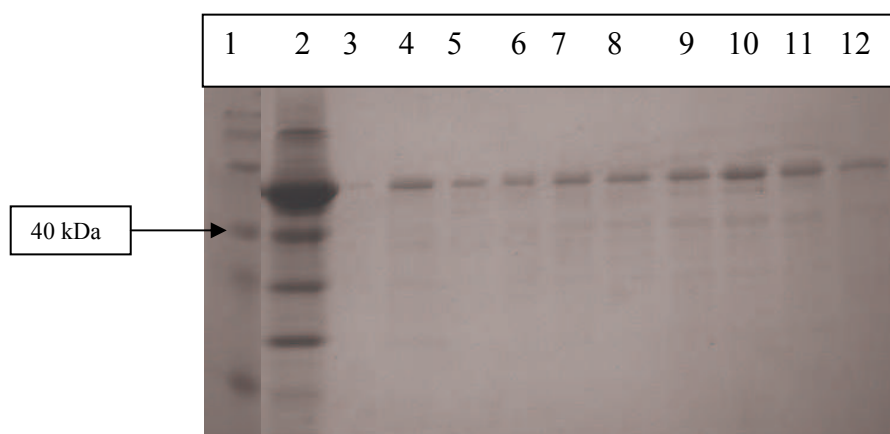


Figure 4.55: 12% SDS-PAGE analysis of S-300 (Buffer A) fractions.
 Lane 1: Prestained protein ladder®, lane 2: Ni-affinity concentrated pool, lane 3:
 concentrator filtrate, lanes 4-12 peak fractions at elution volumes. Lanes 4-5: peak 1
 fractions, 32 and 35 ml, lane 6: peak 2 fraction, 44 ml, lanes 7-8: peak 3 fractions, 51
 and 54 ml, lanes 9-12: Peak 4 fractions, 57, 60, 63 and 66 ml. Samples were prepared
 with 6X SDS loading dye.

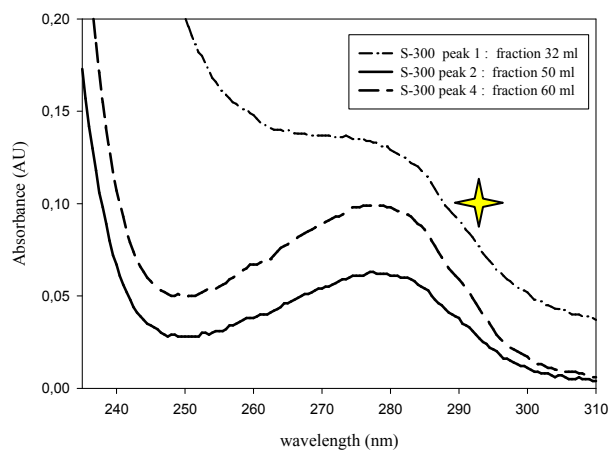


Figure 4.56: Comparison of UV spectra of GPA1 eluted in different elution volumes. Peak 1 fractions differ significantly from the others and there was more aggregation in peak 2 than in peak 4 (Absorbance above 290 nm, shown with star).

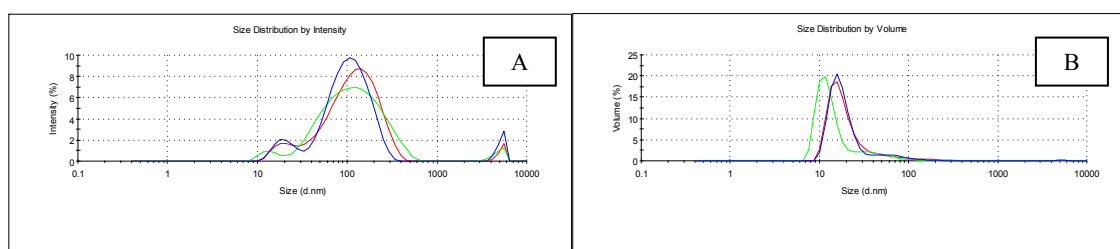


Figure 4.57: DLS size distributions by intensity (A) and volume (B) of concentrated GPA1 (column load).

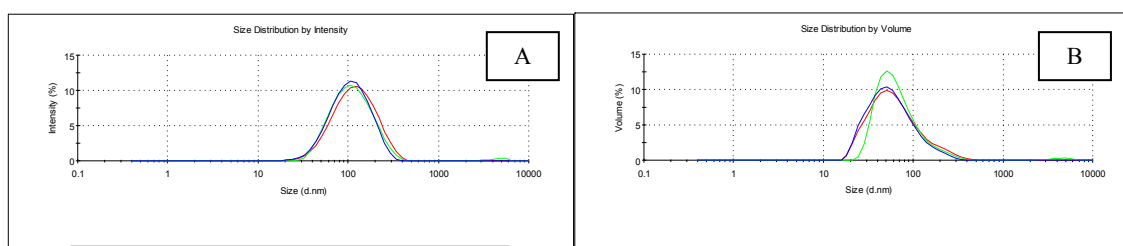


Figure 4.58: DLS size distributions by intensity (A) and volume (B) of peak 1 fraction 32 ml.

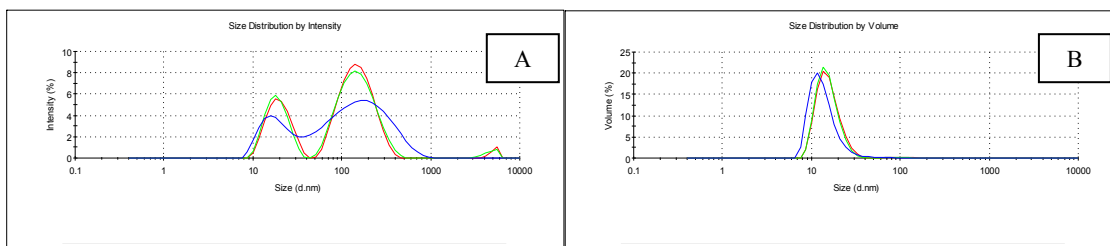


Figure 4.59: DLS size distributions by intensity (A) and volume (B) of peak 2 fraction 44 ml.

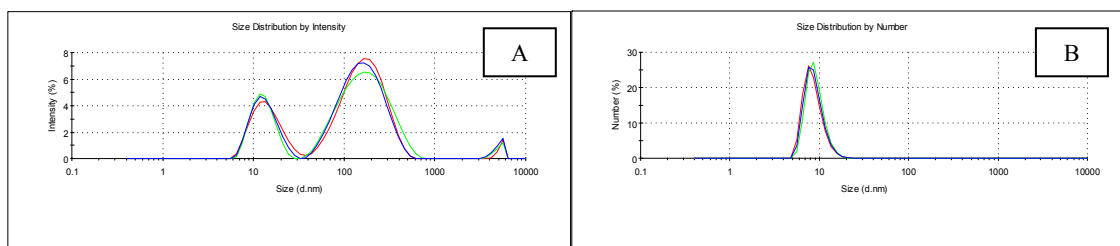


Figure 4.60: DLS size distributions by intensity (A) and number (B) of peak 3 fraction 54 ml.

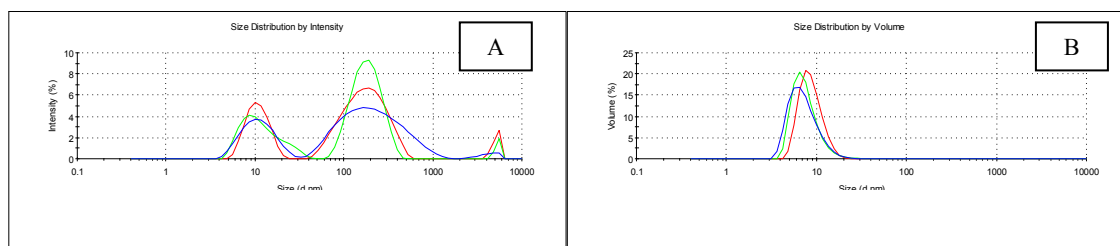


Figure 4.61: DLS size distributions by intensity (A) and volume (B) of peak 4 fraction 60 ml.

In peak 4 GPA1 could be obtained with a molecular mass of ~60 kDa. The protein solution was not monodisperse as revealed by DLS.

- Sephacryl S-300 HR 16/60, Buffer B

GPA1 affinity purified in the presence of Triton-X was desalted using a HiPrep™ 26/10 desalting column with 50 mM TrisHCl, pH 8.0 and 1 mM DTT buffer and 50 μM GDP was added to the desalted pool. A total of 4.5 mg protein was loaded onto a Sephacryl S-300 HR 16/60 column after concentrating down to 2 ml.

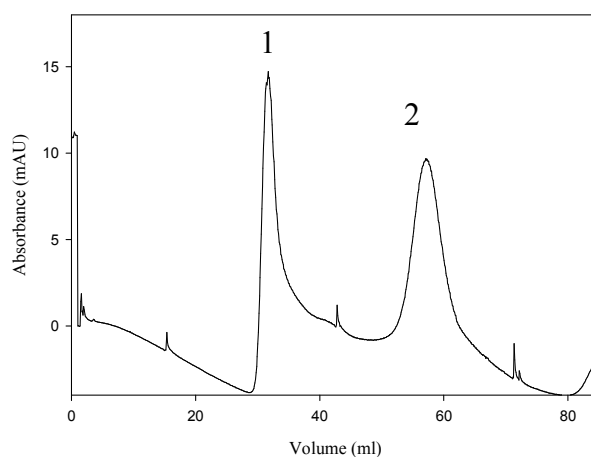


Figure 4.62: Elution pattern of GPA1 from S-300 HR 16/60 column with Buffer B. Flow rate was 0.5 ml/min and 0.5 ml fractions were collected.

Table 4.12 Molecular mass for S-300 (Buffer B) peak 2 fractions. Estimated from elution volumes and column calibration (Figure L 3).

	Ve ml	Range ml	Molecular Mass, Da			Diameter, nm
			Top	Start	End	Top
peak 2	58	53-62	72748	114114	50746	10, 15, 60

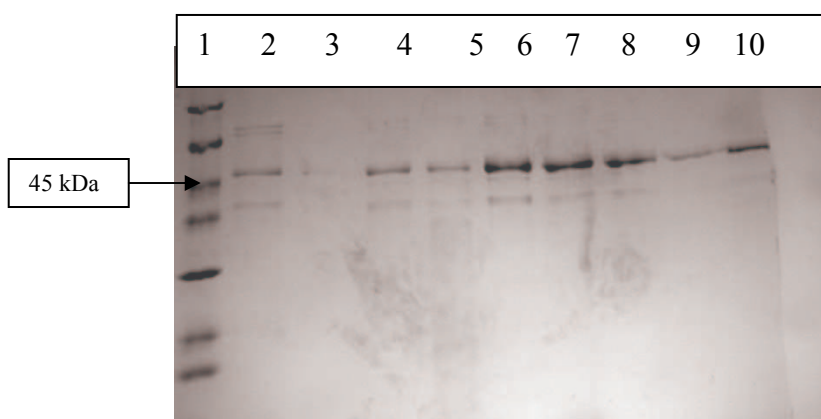


Figure 4.63: 12% SDS-PAGE analysis of S-300 HR 16/60 column peak 2 fractions. Lane 1: Protein MW marker®, lanes 2-10: fractions eluted at the 53, 54, 55, 56, 57, 58, 59 and 60 ml. Lane 9 is overflow of lane 8. Samples were prepared with 6X SDS loading dye.

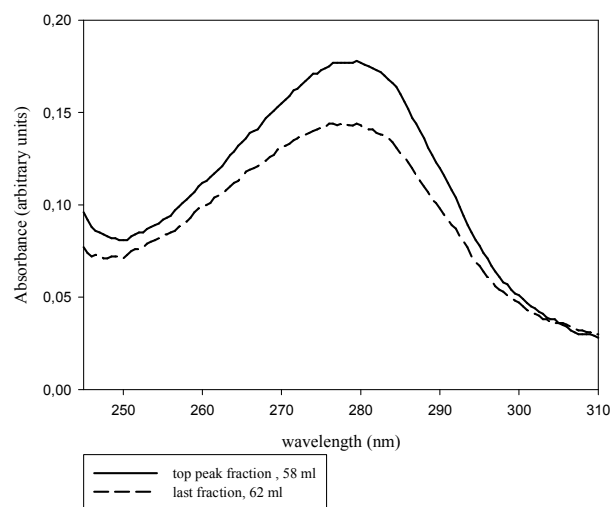


Figure 4.64: UV-vis spectra of S-300 peak 2 fractions.

In the elution pattern of GPA1 from the Sephacryl S-300 column, there were two main peaks at 32 ml and at 58 ml (from 53 to 62 ml). The latter corresponded to a molecular mass of about 70 kDa (Figure 4.62 and Table 4.12).

SDS-PAGE analysis of the fractions of peak 2 (Figure 4.63) indicated that the dominating species in this peak was GPA1 but the degradation product could also be observed. DLS measurements showed that although GPA1 existed possibly in monomeric form (10 nm), higher order oligomers were also present with diameter 15 nm and 60 nm (Figure 4.65 and Table 4.12).

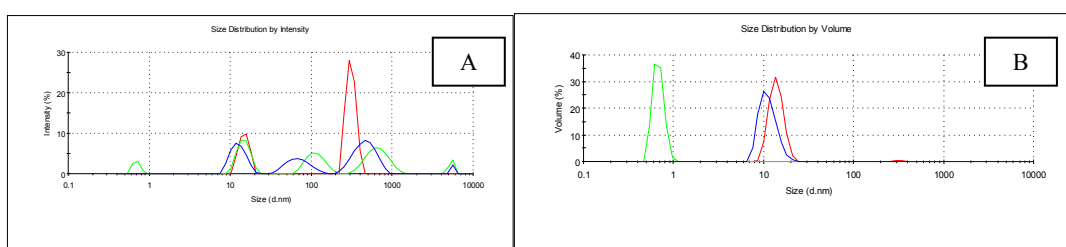


Figure 4.65: DLS size distributions by intensity (A) and volume (B) of a S-300 peak 2 pool. Samples was stored at -80 °C.

- Sephacryl S-300 HR 16/60, Buffer C

GPA1, purified by Ni-affinity in the presence of Triton-X and AlF_4^- was directly concentrated. The buffer exchange was done in the concentrator unit. A total of 23 mg GPA1 in 2 ml was loaded to the column.

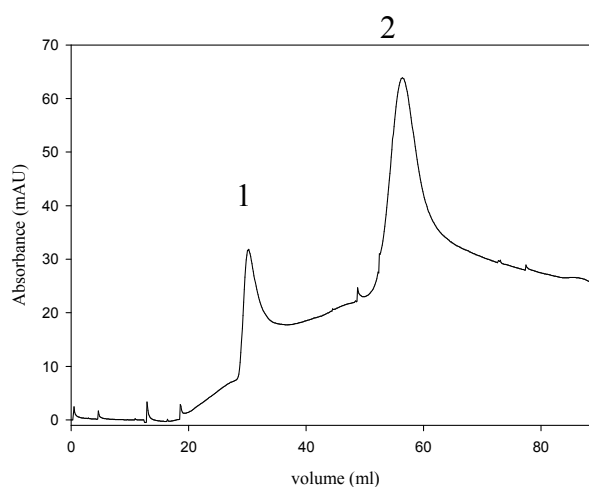


Figure 4.66: Elution pattern of GPA1 from S-300 HR 16/60 column with Buffer C. Flow rate was 0.3 ml/min and 0.5 ml fractions were collected.

Table 4.13 Molecular mass for S-300 peak 2 (Buffer C) fractions. Estimated from elution volumes and column calibration (Figure L 3).

	Ve ml	Range ml	Molecular Mass, Da			Diameter, nm
			Top	Start	End	
peak 2	57	53-61	79602	114114	55527	8.5, 10, 85

The elution volume of second peak was 57 ml, which corresponds to a molecular mass range of ~55 kDa to 114 kDa (Figure 4.66 and Table 4.13). Fractions of peak 2 (from 53 to 61 ml) were combined and the 10 ml protein pool was dialyzed against Buffer C. Free GDP and AlF_4^- were removed by dialysis. SDS-PAGE analysis of selected fractions (Figure 4.67) from peak 2 showed that GPA1 was purified to about 90% homogeneity. GPA1 yield was ~6 mg from 800 ml yeast culture.

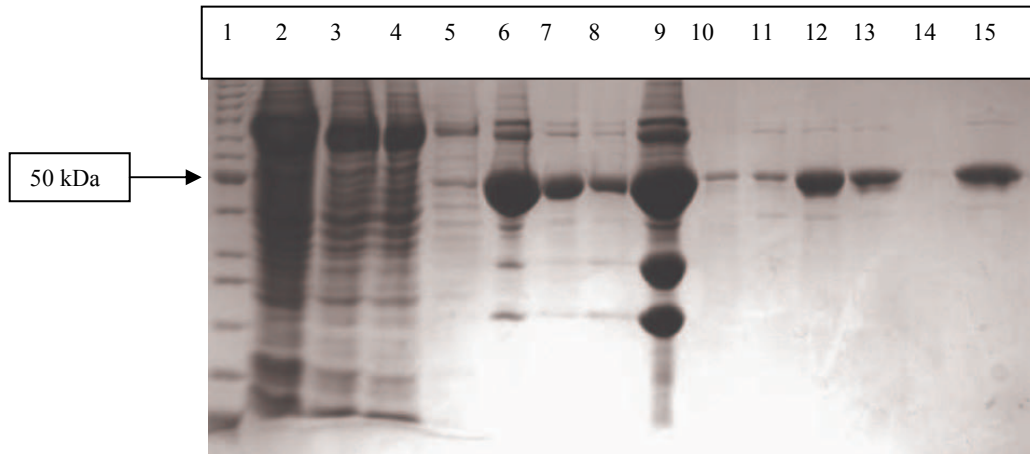


Figure 4.67: 12% SDS-PAGE analysis of Ni-affinity and S-300 (Buffer C) fractions. Lane 1: Protein ladder®, lane 2: FT, lanes 3-5: wash 1-3, lanes 6-8: Ni-affinity E1-E3, lane 9: Ni-affinity concentrated, lane 10: void fraction, lanes 11-13: peak 2 fractions, first, top and last, lane 15: S-300 pool BD. FT and wash samples were prepared with 2X SDS loading dye, others with 6X SDS-loading dye.

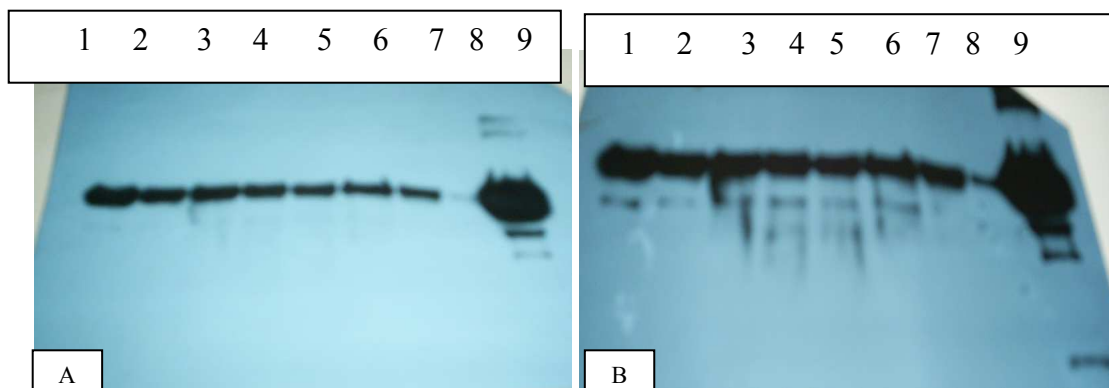


Figure 4.68: Western analysis of S-300 eluted GPA1 before and after dialysis. Lane 1: Ni-affinity pool, lanes 2-3: S-300 pool BD, stored at +4 °C and -80 °C, lanes 4 and 6: S-300 pool AD, at +4 °C and -80 °C, lane 5: 57 ml fraction, lane 7: 80 ml fraction, lane 8: S-300 FT, lane 9: S-300 load. Samples were prepared with 6X SDS loading dye, except S-300 load with 2X SDS loading dye. Membrane was incubated with 1:4000 anti-myc-HRP. A: Exposure time 1min, B: Exposure time 10 min.

Figure 4.68 obtained from western blot of the purified protein indicates that there was already a small amount of degradation at the affinity purification step which did not increase during dialysis. Depending on the assays in which the samples were used dialysis was employed to ensure removal of free additives.

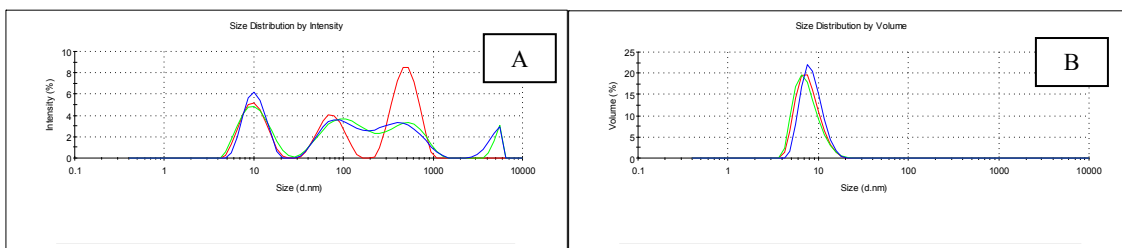


Figure 4.69: DLS size distribution by intensity (A) and volume (B) of 57 ml (top) fraction stored at +4 °C.

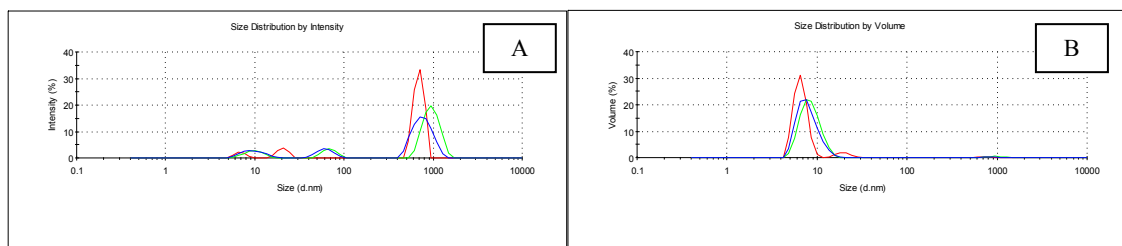


Figure 4.70: DLS size distribution by intensity (A) and volume (B) of 57.5 ml fraction stored at -80 °C.

DLS measurements showed that the purified protein was composed of particles with size 8.5, 10 and 85 nm and was not affected by storing at 4 °C or -80 °C (Figure 4.69 and Figure 4.70).

- Sephacryl S-200 HR 16/60, Buffer D

GPA1, purified by Ni-affinity in the presence of Lubrol-PX was loaded to a S-200 column but monomeric GPA1 did not elute from the column. In another trial AlF_4^- was included in Ni-affinity purification and affinity elutions were stored until use at -20 °C after addition of 20% glycerol. The pool was directly concentrated and the buffer was exchanged in the concentrator unit before loading 10 mg GPA1 in 2 ml onto a Sephacryl S-200 HR 16/60 column.

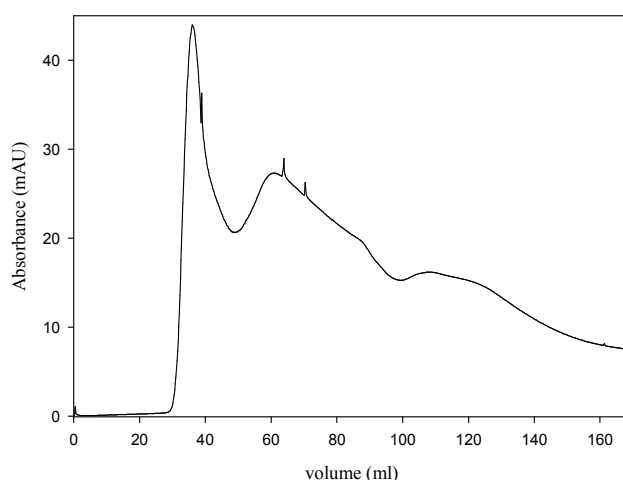


Figure 4.71: Elution pattern of GPA1 from S-200 HR 16/60 column with Buffer D. Flow rate was 0.5 ml/min and 0.5 ml fractions were collected.

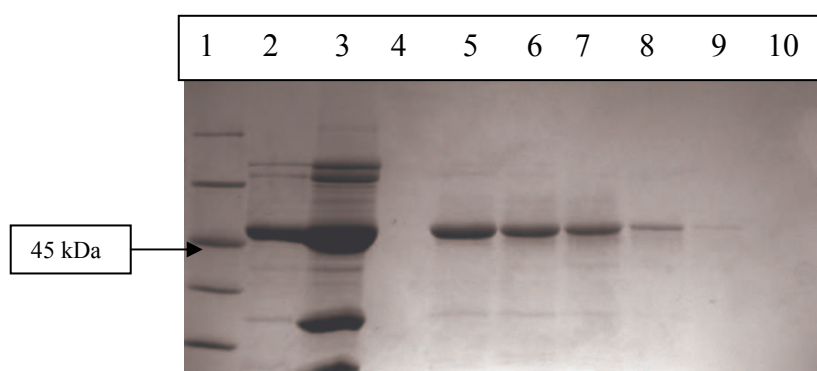


Figure 4.72: 12% SDS-PAGE analysis of S-200 (Buffer D) fractions. Lane 1: Protein MW marker®, lane 2: Ni-affinity pool, lane 3: concentrated pool, lane 5: void top fraction, lane 6: void middle fraction, lane 7: void last fraction, lane 8: fraction of 52 ml, lane 9: fraction of 60 ml, lane 10: fraction of 65 ml. Samples were prepared with 6X SDS loading dye.

Figure 4.71 illustrates that GPA1 was eluted in 2 different forms from S-200 column. The first pool with a molecular mass above 250 kDa; eluted before the void volume. The particle diameters for void pool were 10, 20 and 60 nm (Figure 4.74). The elution volume of the second peak was not directly determined from elution pattern. The peak was between 50 and 70 ml of elution, but only the fractions between 50 and 60 ml contained GPA1 (Figure 4.72) with a molecular mass range of 60-30 kDa (according to column calibration curve given in Figure L 6) and particle diameter of 10 nm and 20 nm (Figure 4.75). The later fractions did not contain any protein but excess (free) GDP and / or detergent micelles in the sample may be the reason for the increased

absorbance at 280 nm. The GPA1 eluted at the column void volume had excess/free GDP shown with an increased absorbance above 254 nm, which was absent for the fractions eluted after 50 ml (Figure 4.73).

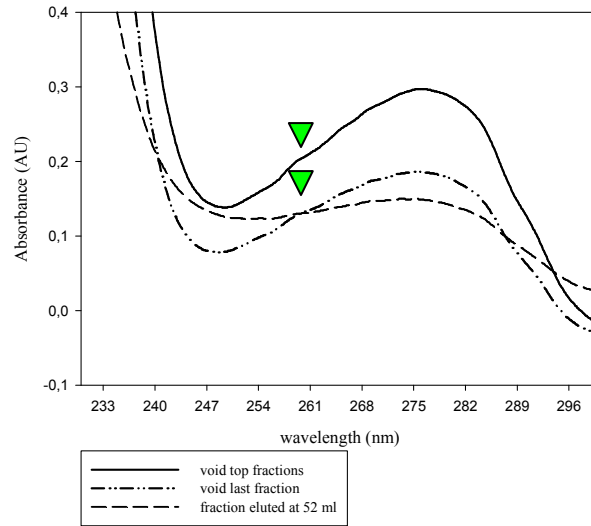


Figure 4.73: UV spectra of S 200 fractions.

GDP can be detected in void fractions by an increase above 254 nm (triangles).

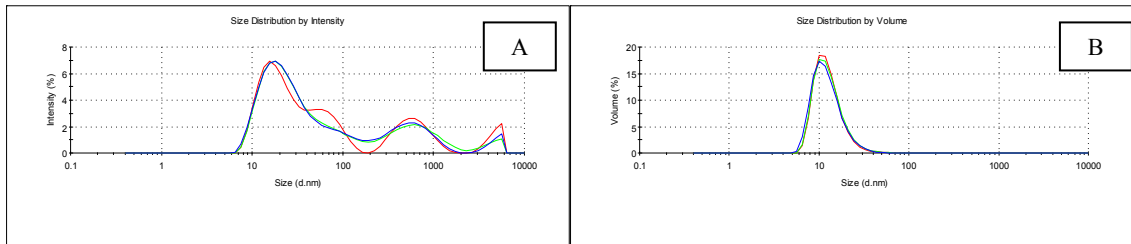


Figure 4.74: DLS size distributions by intensity (A) and volume (B) of void top fraction.

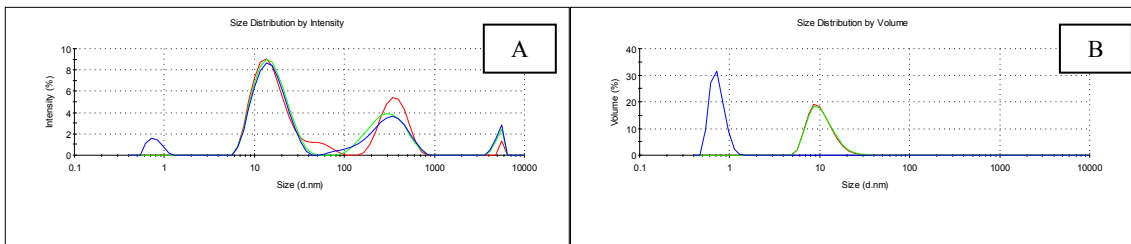
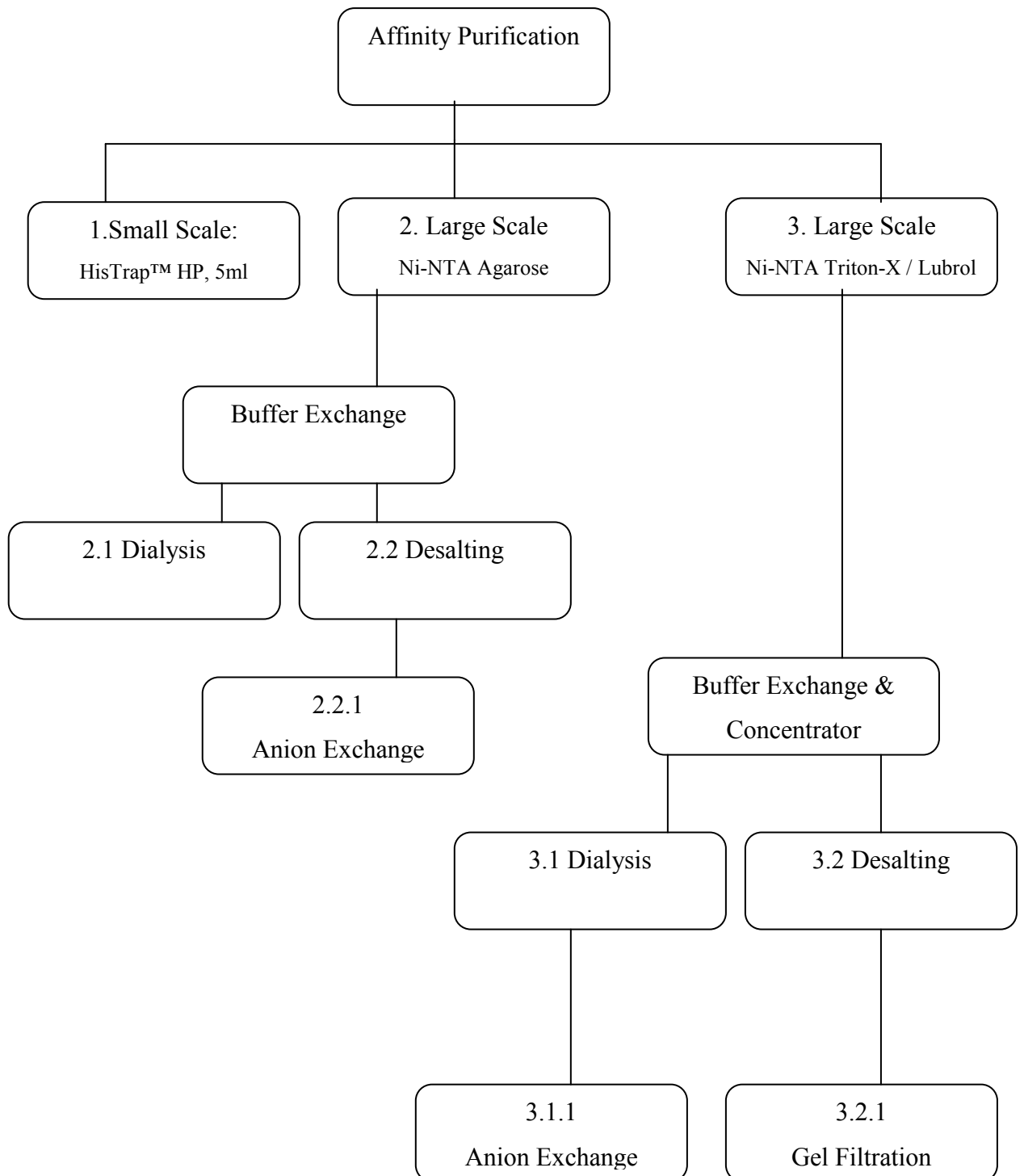


Figure 4.75: DLS size distributions by intensity (A) and volume (B) of 52 ml fraction.

In summary monomeric and homogenous GPA1 could not be obtained from Sephacryl columns, even the form with the smallest molecular mass and diameter contained oligomeric forms, albeit at lower amounts.

The purification scheme followed is given below. Protein obtained at different stages of purification step is numbered according to this scheme (e.g. stg. 3.2) for ease of following the functional/structural characterization results.



4.5 Functional Assays

4.5.1 GDP Binding

GDP bound form of GPA1 was stabilized by using a purification buffer that contained minimum of 20 μM GDP in the Ni-affinity step and further GDP was added according to the subsequent procedure. The GPA1-GDP solutions, therefore, also contained excess unbound GDP. Buffer exchange using a desalting column helped to separate unbound GDP from GPA1 as detected by changes in the shape of absorbance spectra at around 254 nm. As can be seen from Figure 4.76 the buffer exchanged samples display less absorbance around this position.

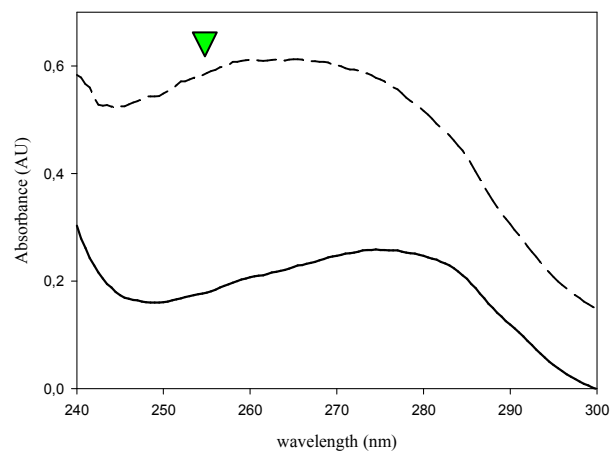


Figure 4.76: Comparison of UV spectra of GPA1 (stg. 3---) and desalted pool (stg. 3.2-).

Absorbance ~ 254 nm was further investigated by measuring the desalted pool against buffer with or without GDP. The effect of free and bound GDP on the UV spectra of Ni-affinity purified –desalted GPA1 samples can be seen in Figure 4.77 (stg 2.2) and Figure 4.78 (stg 3.2) for samples that were purified in the absence and presence of detergents respectively. The GDP peak at 254 nm can be readily seen when the measurement is carried out against the buffer without GDP, and is still visible when the measurement was against the GDP containing buffer. The bound GDP can thus be detected in samples coming from the affinity purification step.

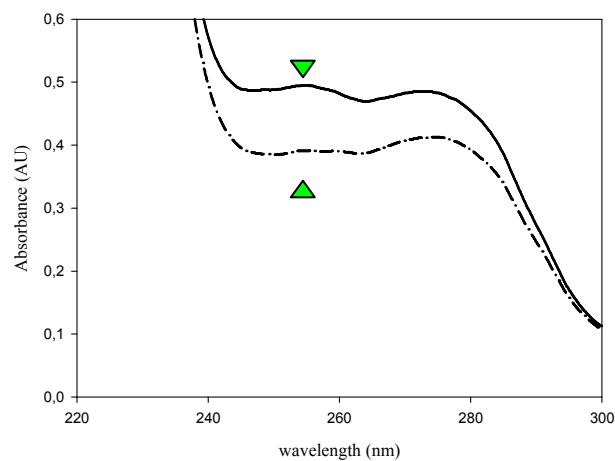


Figure 4.77: Comparison of UV spectra of GPA1 (stg 2.2) measured against different buffers.

GPA1 was stored in 20 μ M GDP, 10 % glycerol in 50 mM TrisHCl, pH 8.0 and measured against buffer with (- -) and without (—) additives.

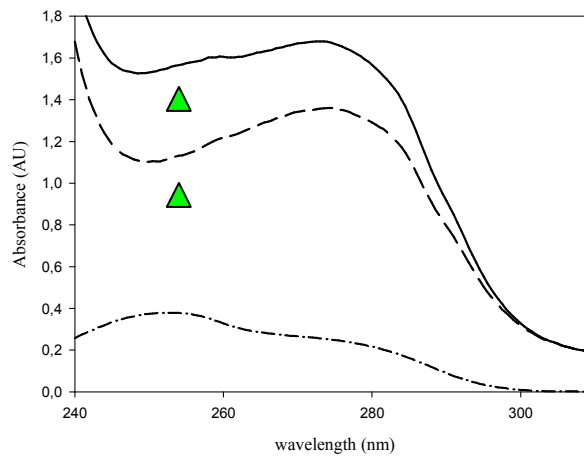


Figure 4.78: Comparison of UV spectra of GPA1 (stg. 3.2) measured against different buffers. Measured against buffer with (---) and without GDP (-). The spectrum of 30 μ M GDP is also shown (-·-·-·).

Estimation of GDP amount bound to GPA1 was carried out by boiling GPA1 and measuring the GDP content of the filtrate as described in chapter 3.2. The calibration curve was obtained by measuring A_{254} values of solutions of GDP at different concentrations (Figure 4.79).

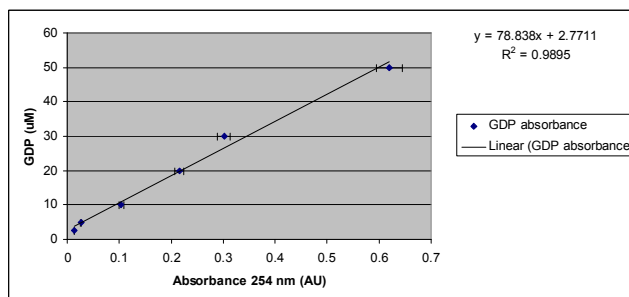


Figure 4.79: Dependence of absorbance at 254 nm on GDP concentration in 50 mM Tris HCl, pH 8.0.

Table 4.14: Estimation of GDP content of GPA1 at different stages of the purification.
 * the protein was not boiled so the amount of remaining GDP is calculated.

GPA1 stage	Absorbance 254 nm (AU)	GDP $y = 78.838x + 2.7711$	GDP Content		Protein concentration	GDP /Protein Mole/mole
			Added GDP	Bound GDP		
2.2	0.304	26.73 μ M	20 μ M	6.73 μ M / 2.7 nmole	0.18 mg/ml; 3.74 nmole	0.72
3.2 *	0.452	38.4 μ M	50 μ M	11.59 μ M / 4.63 nmole	0.22 mg/ml 4.57 nmole	0.98
3.1.1 pool 3	0.236	21.37 μ M	-	21.37 μ M / 8.55 nmole	0.287 mg/ml 5.96 nmole	1.42
3.1.1 pool 4	0.064	7.81 μ M	-	7.81 μ M / 3.12 nmole	0.183 mg/ml 3.8 nmole	0.82

Filtrates containing the released GDP (Figure 4.81) displayed spectral features that were similar to that of GDP solutions (Figure 4.80). The GDP content of GPA1 obtained in pool 3 of the anion exchange column was different from that of pool 4 indicating that these two pools contain different forms of GPA1. The average value of bound GDP for pool 3 and for pool 4 is ~equal to that of affinity purified GPA1 (Table 4.14).

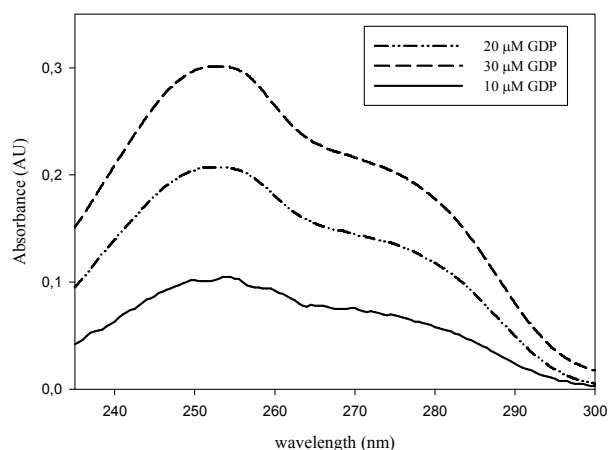


Figure 4.80: The UV spectra of different concentrations of GDP in Tris buffer.

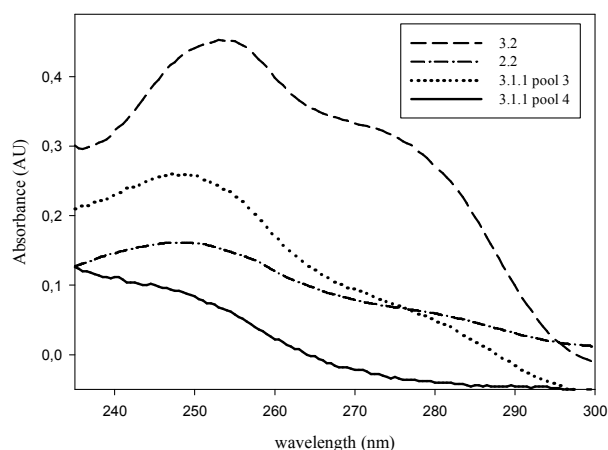


Figure 4.81: UV-Vis Spectra of GDP filtrates of GPA1 from stg. 2.2 and 3.2.

4.5.2 GTP Binding

GTP-binding activity of GPA1 obtained at different stages of the purification procedure was investigated using [^{35}S]GTP γ S. GPA1 purified from Ni-affinity column without detergents (stg. 2.2) binds ~ 0.3 mole GTP γ S / mole protein (± 0.067) and in the presence of $100 \mu\text{M}$ cold GTP this ratio is lowered to 0.06 (± 0.035) (Figure 4.82).

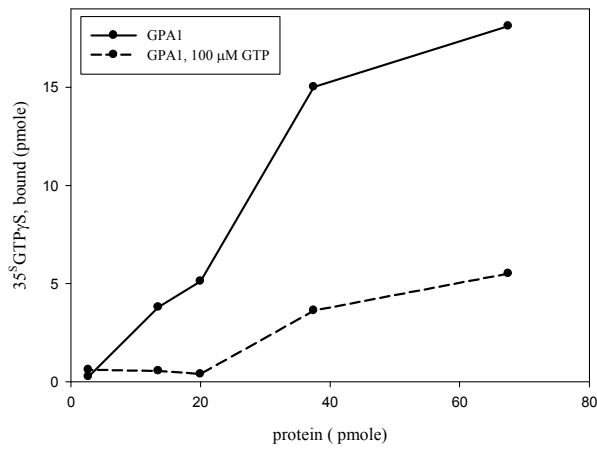


Figure 4.82: Dependence of [³⁵S]GTP γ S binding to GPA1 (stg. 2.2) concentration.

Pool 3 GPA1 (stg. 3.1.1, Triton X-100) binds ~0.3 mole GTP γ S / mole protein, the presence of GTP was less competitive as compared to affinity purified GPA1 (Figure 4.83).

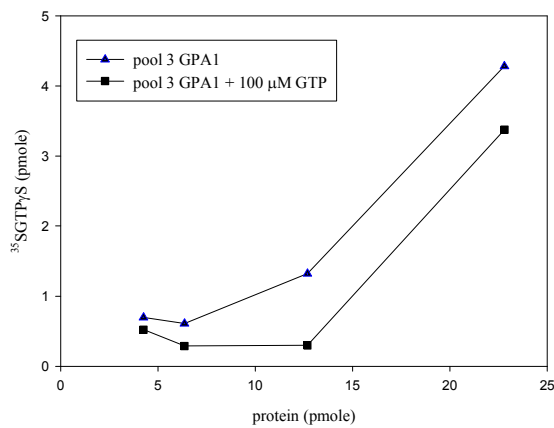


Figure 4.83: Dependence of [³⁵S]GTP γ S binding to pool 3 (stg. 3.1.1) concentration.

4.5.3 GTP Hydrolysis

GTP hydrolysis activity of GPA1 from different stages of the purification procedure was investigated using ^{32}P -GTP and by measuring released ^{32}P in the reaction mixture. The background level of radioactivity measured for buffers and protein samples was around 20-60 CPM. Data represent CPM data that was integrated for 5 minutes. All experiments were performed with protein initially affinity purified in the presence of Triton X-100 (stg.3).

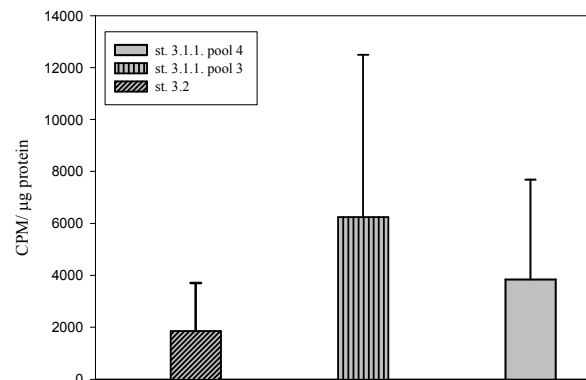


Figure 4.84: Dependence of released ^{32}P on protein purity. 0.14 nM ^{32}P -GTP / assay was used. ^{32}P release was measured after 30 minutes.

Figure 4.84 shows the specific activity of GPA1 which increases as the purity of GPA1 increased during purification.

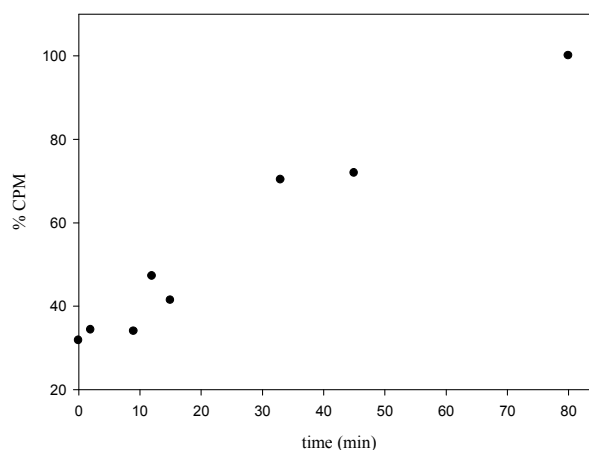


Figure 4.85: Time course of GTPase activity of 290 nM pool 3 GPA1 (stg 3.1.1). 0.167 nM ^{32}P GTP / assay was used. The CPM value of last data was assumed 100 %.

Table 4.15: CPM values of 290 nM pool 3 GPA1 (stg 3.1.1). 0.167 nM ^{32}P GTP / assay was used

time(min)	0	2	9	12	15	33	45	80
CPM	5042	5443	5392	7489	6569	11153	11407	15866

Figure 4.85 (and Table 4.15) shows that pool 3 GPA1 has GTPase activity and the hydrolyzed amount of Pi was increased as the incubation time of GPA1 with ^{32}P GTP was increased.

Figure 4.86 (Table 4.16) and Figure 4.87 (Table 4.17) show that in the absence of Lubrol PX, pool 3 and pool 4 GPA1 had comparable GTPase activity.

Table 4.16: CPM values of pool 3 GPA1 (stg. 3.1.1) as a function of concentration. 1.67 nM ^{32}P -GTP /assay were used. ^{32}P release was measured after 60 minutes.

GPA1 (mM)	1.2	2.4	3.6
CPM	295846.5	317417	326717.5
stdev	4296.381	1303.198	7881.412

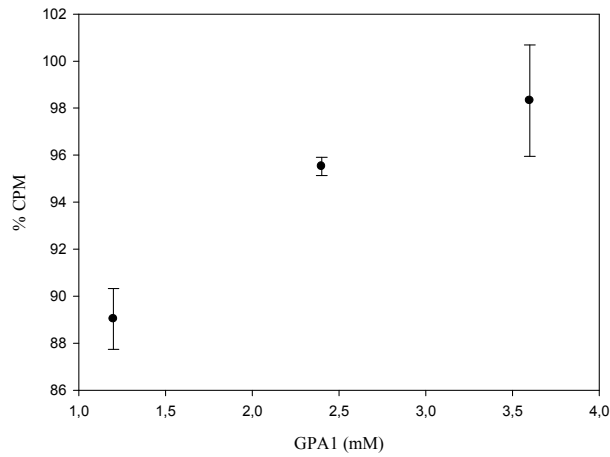


Figure 4.86: Concentration dependence of GTPase activity of pool 3 GPA1 (stg. 3.1.1). Assay buffer was prepared without Lubrol. 1.67 nM ^{32}P -GTP /assay were used. ^{32}P release was measured after 60 minutes. The higher CPM value of highest concentration was assumed 100 %.

Table 4.17: CPM values of pool 4 GPA1 (stg. 3.1.1) as a function of concentration. 1.67 nM ^{32}P -GTP /assay were used. ^{32}P release was measured after 60 minutes.

GPA1 (mM)	0.19	0.385	0.555	1.111	1.667
CPM	177882.5	184775.5	250053	317030	311293.5

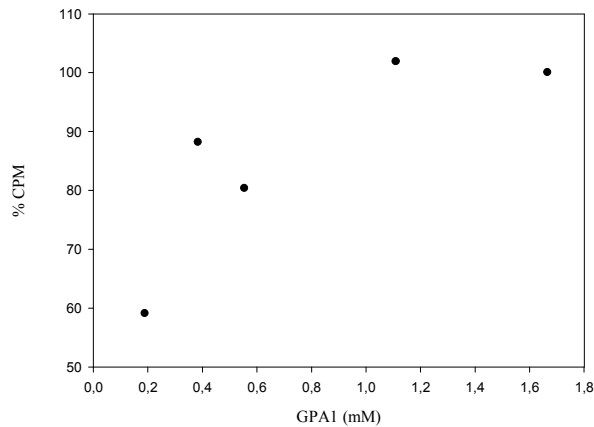


Figure 4.87: Concentration dependence of GTPase activity of pool 4 GPA1 (stg. 3.1.1). Assay buffer was prepared without Lubrol. 1.67 nM ^{32}P -GTP /assay were used. ^{32}P release was measured after 60 minutes. The CPM value of highest concentration was assumed to be 100 %.

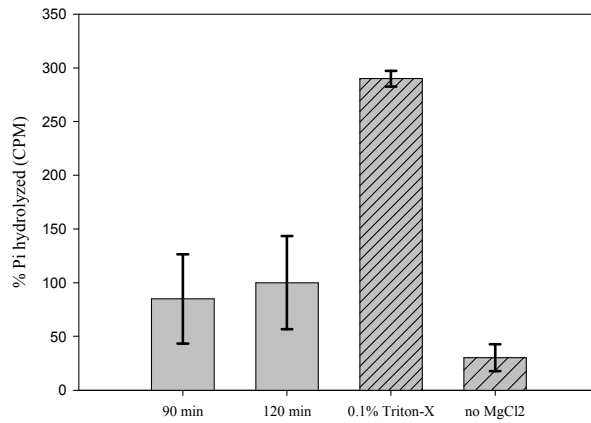


Figure 4.88: Effect of detergent and $MgCl_2$ on GTPase activity of pool 4 (stg. 3.1.1). The CPM value of 120 minutes was assumed to be 100 %. 400 nM GPA1 and 1.6 nM ^{32}P -GTP was used for each assay. Lubrol PX was not added to assays.

Figure 4.88 shows the $MgCl_2$ dependency of GTPase activity of GPA1, in the absence of Mg^{+2} the released Pi amount is reduced 3 fold. The released Pi amount was increased ~3 fold when detergent (Triton X-100) was included in assay buffer.

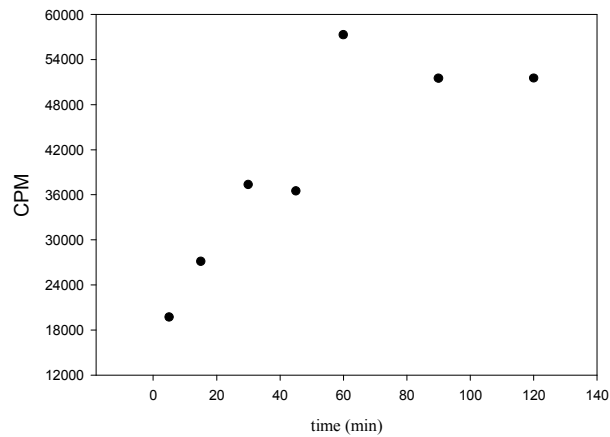


Figure 4.89: Time course of GTPase activity of 70 nM GPA1 (stg 3.2.1). 1.67 nM ^{32}P GTP / assay was used.

Figure 4.89 shows that S-300 purified GPA1 has GTPase activity and the hydrolyzed amount of Pi was increased as the incubation time of GPA1 with ^{32}P GTP was increased.

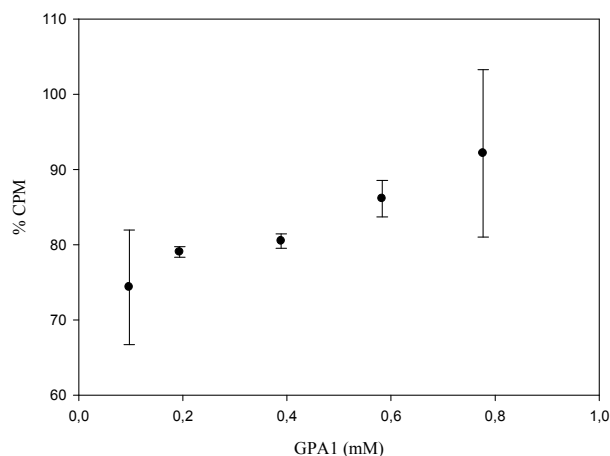


Figure 4.90: Concentration dependence of GTPase activity of GPA1 (stg. 3.2.1). 1.6 nM of ^{32}P -GTP was used per assay. ^{32}P release was measured after 30 minutes. The CPM value of highest concentration was assumed 100 %.

Table 4.18: CPM values of GPA1 (stg. 3.2.1) as a function of concentration. 1.6 nM of ^{32}P -GTP was used per assay. ^{32}P release was measured after 30 minutes.

GPA1 (mM)	0.097	0.194	0.389	0.583	0.777
CPM, average	286916.5	304968	310612	332313	355577
st. dev.	29419.88	2706.098	3646.55	9359.972	42917.85

The GTPase activity of GPA1 purified from S-300 gel filtration column was slightly higher than those of anion exchange purified proteins (Figure 4.90 and Table 4.18).

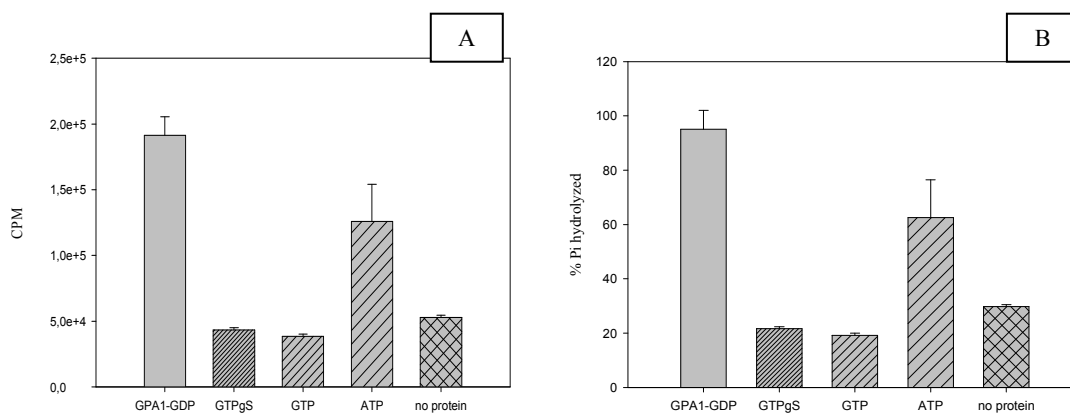


Figure 4.91 Effect of nucleotide competition on GTPase activity of GPA1 (stg.3.2.1). Nucleotides were added at a final concentration of 50 μ M. A: percent B: CPM values. 100 nM GPA1 and 3.3 nM 32 P-GTP was used for each assay. 32 P release was measured after 60 minutes.

As shown in Figure 4.91, in the presence of GTP γ S and GTP the hydrolyzed 32 P amount was the same as that from the control sample with no protein. The raw data was used for analysis, since blank (total count) subtraction resulted in negative values in the presence of competitor nucleotides. The hydrolyzed Pi amount was reduced ~30 % in the presence of ATP, which was not expected.

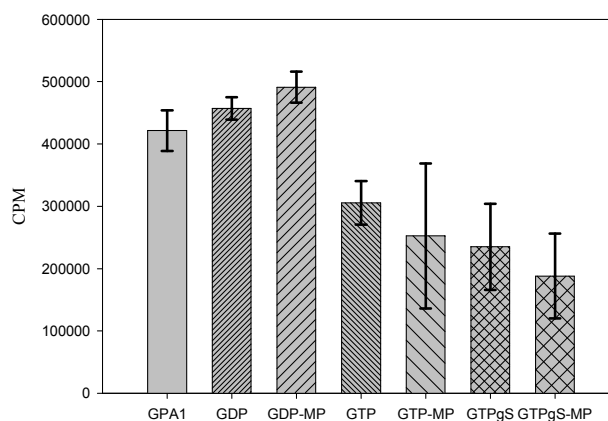


Figure 4.92: Effects of receptor mimetics compound (MP) on GTPase activity of GPA1 (stg. 3.2.1.). Assay was started 15 minutes after the addition of MP. 1.67 nM 32 P-GTP and 200 nM (0.56 μ g) GPA1 was added per assay. 32 P release was measured after 60 minutes.

The raw data was used for analysis, since blank (total count) subtraction resulted in negative values in the presence of competitor nucleotides. The addition of receptor mimetic compound, MP (100 μ M) resulted in a slight increase in the amount of hydrolyzed Pi when the protein is bound to GDP or GTP. In the presence of GTP γ S the receptor mimetic compound caused a slight decrease in GTPase activity of GPA1 (Figure 4.92).

4.6 Biophysical Characterization

4.6.1 Membrane Localization

Membrane fractions of *P.pastoris* cells were solubilized in order to investigate localization of GPA1. Figure 4.93 shows that GPA1 was detected in both soluble cytosolic and insoluble membrane fractions. The membrane fraction in lane 2 was from lysis without detergent and the smear pattern may indicate improper solubilization of the membrane bound proteins. The sample in lane 3 was from lysis in the presence of Triton-X 100.

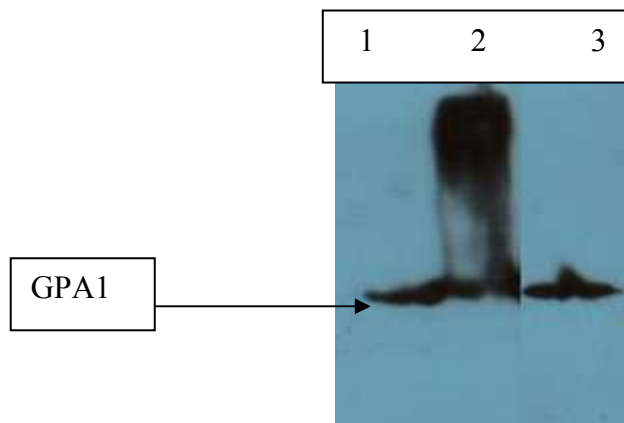


Figure 4.93: Western detection of GPA1 in membrane fractions of *P.pastoris*. Lane 1: Soluble lysate without detergent, lane 2: Membrane fraction after lysis without detergent, lane 3: membrane fraction after lysis with Triton X-100. Samples were prepared with 6X SDS loading dye. Membrane was incubated with 1:2000 tetra-his-HRP Exposure time was 10 min.

4.6.2 Interaction with AGB1/AGG2 Dimer

The effect of AGB1/AGG2 interaction on GPA1 was analyzed with SDS-PAGE followed by Western blot (Figure 4.94). GPA1 eluted in the void volume of S-200 (stg. 3.2.1) was incubated with GTP γ S or dimer before loading on SDS-polyacrylamide gel. Degradation occurred during room temperature incubation and presence of the dimer prevented this. GPA1 was aggregated and aggregates were visible even the sample was boiled before loading. Addition of dimer reversed the aggregation unlike addition of GTP γ S.

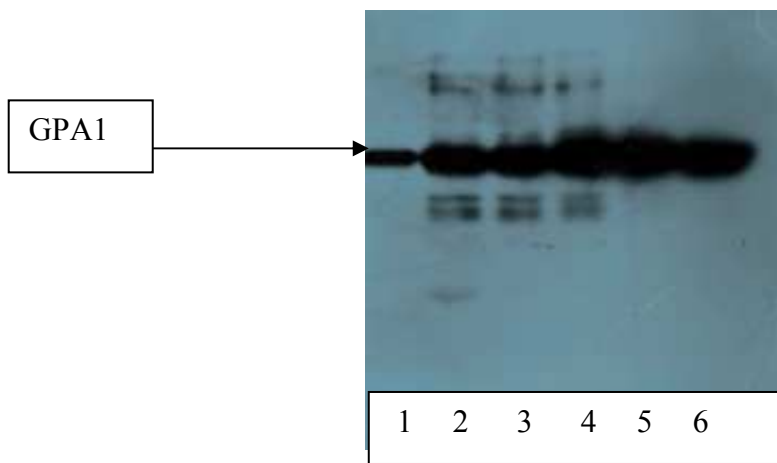


Figure 4.94: Western blot analysis of S-200 GPA1 (stg. 3.2.1, Lubrol-PX) fractions. Lane 1 GPA1 60 kDa, lanes 2-6: void fraction; Samples were incubated at room temperature for 30 minutes with lane 4: 5 μ M GTP γ S, lanes 5 and 6, equal volume of G $\beta\gamma$. Samples were prepared with 6X SDS loading dye. Samples in lanes 3 to 6 were not boiled before loading. Membrane was incubated with 1:2000 tetra-his-HRP.

4.6.3 Analysis for presence of detergents

- **NMR**

GPA1 was purified in the presence of detergents at affinity step followed by either size exclusion or anion exchange chromatography. Proton NMR shifts of detergent and GPA1 solutions were compared in order to detect if the detergent co-purified.

The spectra of samples labeled with deuterium were recorded after solvent (H_2O) saturation. The shift at 4.8 ppm corresponds to the solvent (Figure 4.95) and the peaks before 4.8 ppm were not used for analysis. The chemical structures of buffer components and detergents are given in APPENDIX N.

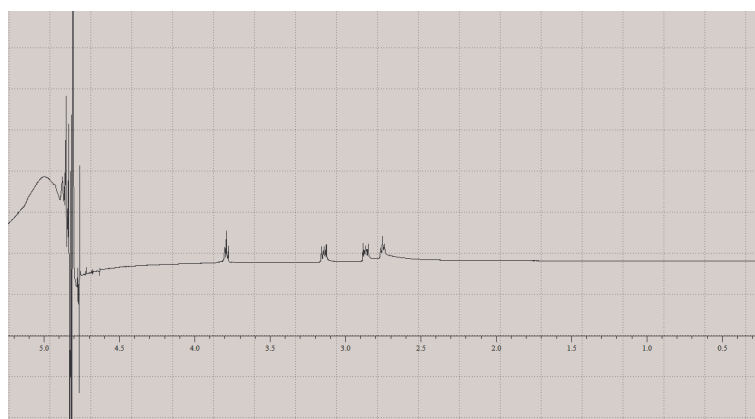


Figure 4.95: NMR spectrum for HND buffer (ppm values are given).

The proton shifts of Lubrol-PX hydrocarbon chain (CH_3 (CH_2)₁₁) can be seen around 1.6 ppm (CH_2), 1.3 ppm ($(\text{CH}_2)_n$) and 0.9 ppm (CH_2CH_3) (Figure 4.96).

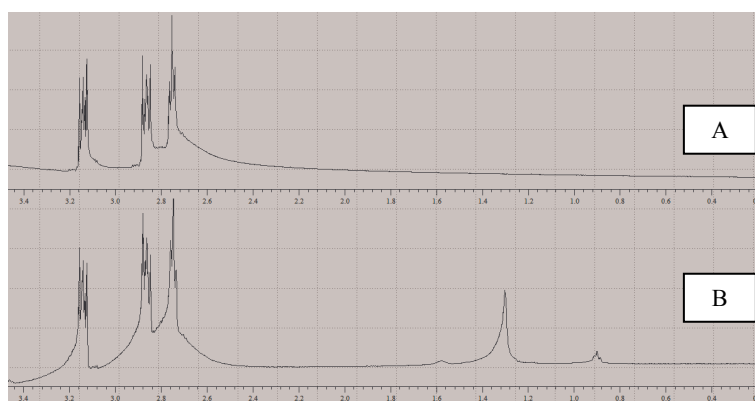


Figure 4.96: NMR spectrum of HND buffer (A) and 0.1% Lubrol-PX in HND (B). Signals below 3.4 ppm are shown.

The polyethylene glycol chain ((CH₂CH₂O)_n) of Lubrol-PX was seen at ~3.7 ppm (Figure 4.97). The hydroxyl group shift is invisible due to solvent (water) saturation.

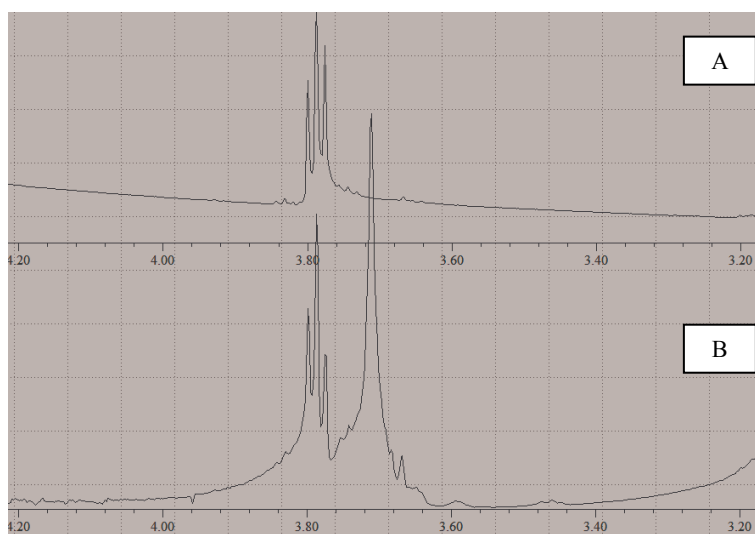


Figure 4.97: NMR spectrum of HND buffer (A) and 0.1% Lubrol-PX in HND (B). Signals above 3 ppm are shown.

In order to see if Lubrol-PX can be detected in the presence of a protein, BSA was prepared in HND with Lubrol-PX. The signature peaks verified the presence of Lubrol-PX (Figure 4.98).

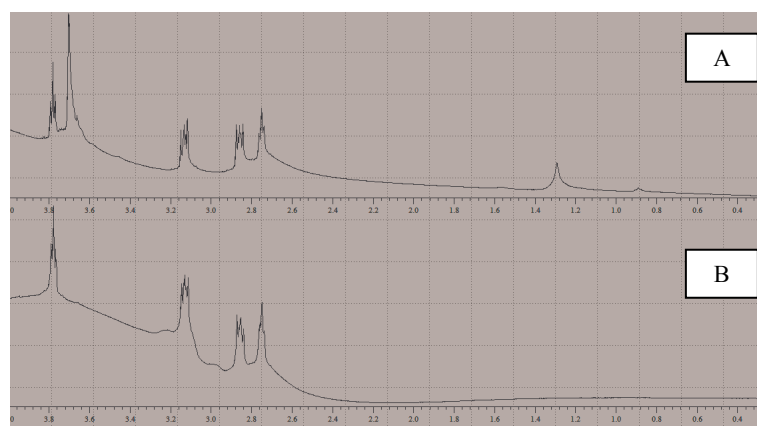


Figure 4.98: NMR spectrum of BSA in HND, with (A) or without (B) 0.1 % Lubrol. BSA concentration 1.6 mg/ml.

The presence of Lubrol was shown for GPA1 (stg. 3.2.1, Lubrol-PX) purified from S-200 column in buffer HND (Figure 4.99).

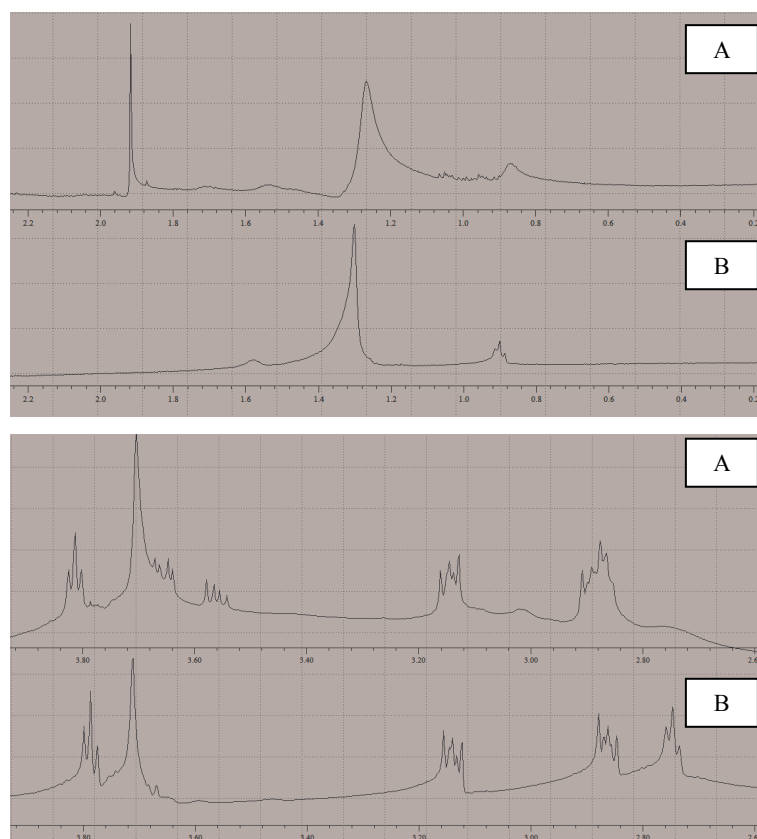


Figure 4.99: NMR spectrum of GPA1 (stg. 3.2.1) (A) and 0.1% Lubrol (B) in HND. Upper panel shows ppm between 0.5 to 2.2, lower panel shows 2.4 to 3.8 ppm. GPA1 concentration was 1.4 mg/ml.

The amount of Lubrol-PX was calculated by using HEPES (4-(2-hydroxyethyl)-1 piperazine-ethane sulfonic acid) ethyl proton shift as reference. The buffer concentration was constant (20 mM), so the integration value of the shift will be of equivalent value in either GPA1 or 0.1% Lubrol-PX solution. The proton shift of CH₃ (alkyl chain) of Lubrol-PX was selected for comparison and the amount in known concentration solution was calculated as a control (Figure 4.100). The ratio of integrations of two peaks (HEPES/Lubrol) is equal to their proton number X concentration ratio; 2 (CH₂) X 20 mM/ 3 (CH₃) X unknown and Lubrol concentration was found 1.67 mM.

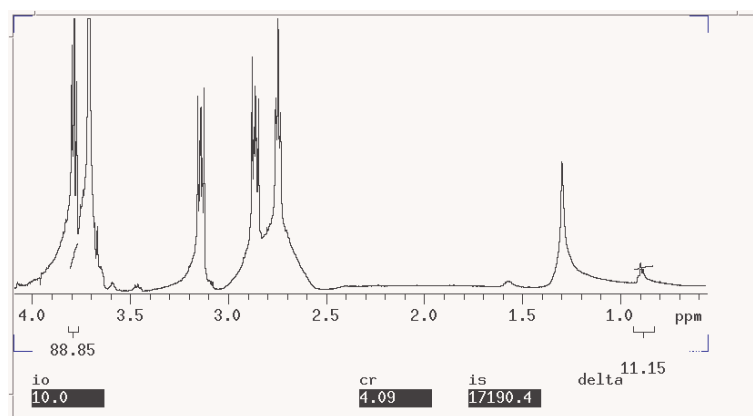


Figure 4.100: Calculation of Lubrol-PX concentration from NMR spectrum of 0.1% Lubrol-PX in HND.

Peak integration at 3.8 ppm (2 protons) was used as a reference to calculate the concentration of Lubrol-PX from the integration value at 0.9 ppm (3 protons). HEPES concentration was 20 mM.

The Lubrol concentration in GPA1 (stg. 3.2.1) was estimated as described above and was found 1.87 mM (Figure 4.101). All of the Lubrol added to affinity purification buffer was co-eluted with GPA1 from gel filtration column.

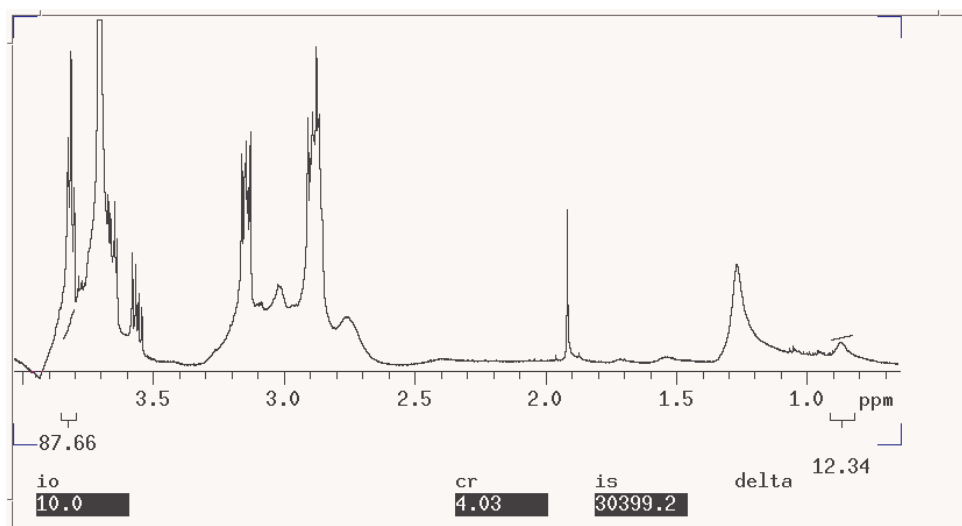


Figure 4.101: Calculation of Lubrol-PX concentration from NMR spectrum of GPA1 in HND. Calculations were done as described in Figure 4.100.

All of the proton shifts of Triton X-100 could not be identified in HND-GGM buffer, due to the presence of buffer signals. The significantly different protons shifts were at ~ 0.65 ppm (tert-butyl) and 1.65 ppm (CH_2) from the alkyl chain of Triton X-100 as shown in Figure 4.102 for 0.02 % Triton X-100.

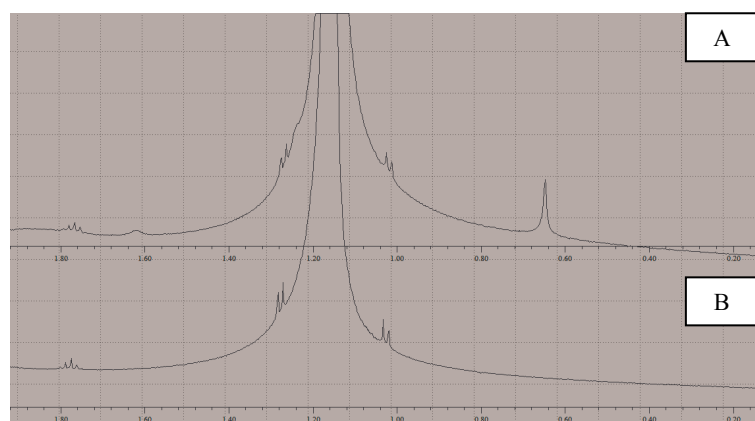


Figure 4.102 NMR spectrum of 0.02 % Triton X-100 (A) and HND-GGM (B).

Triton X-100 added at the affinity purification step did not co-purify with GPA1 from anion exchange column as can be seen from the NMR spectra of pool 3 and Triton X-100 (Figure 4.103).

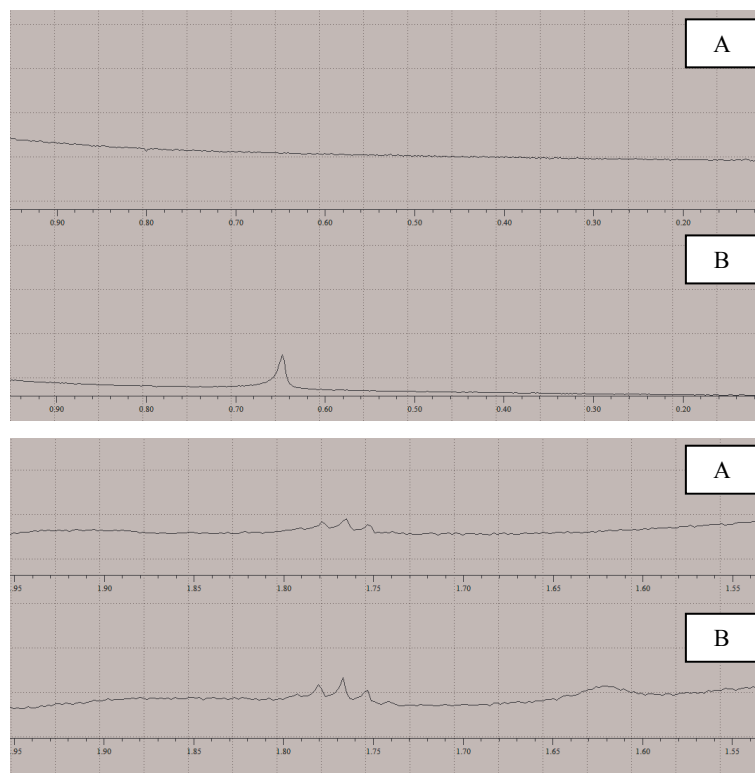


Figure 4.103: NMR spectrum of GPA1 (stg. 3.1.1) (A) and 0.02% Triton X-100 (B) in HND-GGM (B). Upper panel shows 0 to 1 ppm, lower panel shows 1.55 to 1.95 ppm. GPA1 concentration was 0.1 mg/ml.

- **TCA stain**

GPA1 purified from different stages were compared for the presence of detergent. Samples that were either purified in the presence of detergent or those that were incubated with detergents were run on 8% native polyacrylamide gel, followed by TCA staining [129].



Figure 4.104: TCA stained 8% Native-PAGE analysis for detergents and GPA1. Lane 1: GPA1 stg.3.2 (Lubrol), lanes 2-4: pool 4 (stg.2.2.1) with Triton, with Lubrol and no detergent, lane 5: pool 3 (stg.3.1.1, Triton), lane 6: pool 3 (stg. 3.1.1, Lubrol), lanes 7-9: pool 3 (stg. 2.2.1) with triton, lubrol and no detergent, lane 10: Triton, lane 11: Lubrol, lanes 12-14: GSTdmt with triton, lubrol and no detergent. Samples were prepared with 6X native loading dye.

Result in Figure 4.104 show that detergents Lubrol, 1.7 mM and Triton, 0.3 mM can be detected with TCA staining and GPA1 after affinity purification contained detergent if this was included in purification buffers. After anion exchange detergent was separated from GPA1, Lubrol or Triton did not co-elute from anion exchange column with GPA1.

The gel was washed in water overnight after TCA staining and stained with coomassie blue. The result (Figure 4.105) show that only lane 1 (affinity purified , stg. 3.2) and lane 7 (pool 3, stg 3.1.1 Lubrol) samples can be seen with a smear pattern on the gel. The control (GSTdmt) samples, each 0.5 mg/ml, are in lanes 12-14. The samples were also analyzed on SDS-PAGE for protein quality and quantity (Figure 4.106).

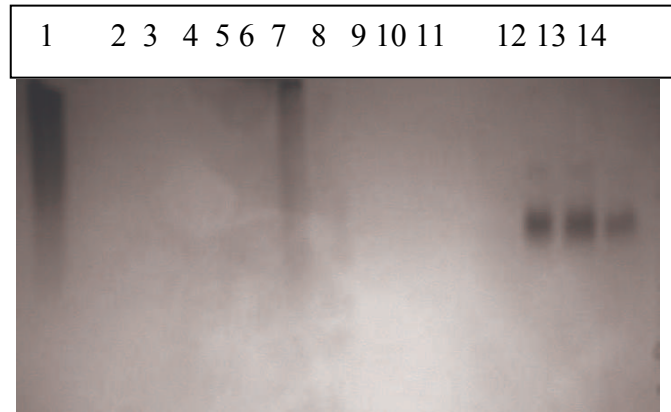


Figure 4.105: 8% Native-PAGE analysis of GPA1 from different stages. Lane numbering is identical to Figure 4.104. Samples were prepared with 6X native loading dye.

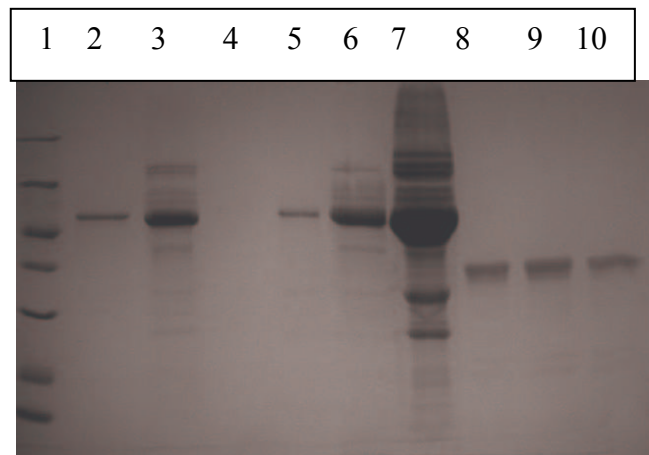


Figure 4.106: 12% SDS-PAGE analysis of samples used in native gel (Figure 4.105). Lane 1: Protein MW marker ®, lane 2: pool 3 (stg. 2.2.1), lane 3: pool 3 (stg.3.1.1, Lubrol), lane 4: pool 3 (stg. 3.1.1, Triton), lane 5: pool 4 (stg.2.2.1), lane 6: GPA1 stg.3. (Lubrol), lane 7: GPA1 stg.3.2 (Lubrol), lanes 8-10: GSTdmt, no detergent, with Lubrol and with Triton. Samples were prepared with 6X SDS loading dye.

4.6.4 MALDI-TOF MS

Matrix Assisted Laser Desorption (MALDI) Time of Flight (TOF) mass spectrometry (MS) was done on pool 3 and pool 4 (stg. 2.2.1).

Pool 3 MALDI-TOF MS resulted in fragments covering 86.72 % of GPA1 amino acid sequence (Figure 4.107). The resulting sequence is given in APPENDIX I. Some peptide fragments were not visible, including the 6 amino acid N-terminal region. According to the amino acid sequence of GPA1, the N-terminal peptide containing the C as Carbamidomethyl-cystein (GLLC*SR) should appear at 705.4 Da. This peptide was visible in pool 4, however not in pool 3.

Some of the peptides missing correspond to $G\alpha$ conserved residues; a long 23 amino acid region which contain the P-loop and GoLoco binding residues (GAGESGK), two amino acids in switch I (VR) and in switch II (RK) and six residues of putative receptor binding site (VFKIYR). Two plant $G\alpha$ specific insertion regions were also not detected; LDYPR and SGEVYR. There were five undigested arginine and eleven lysine residues, including one in GDP/GTP binding site and three in putative receptor binding site.

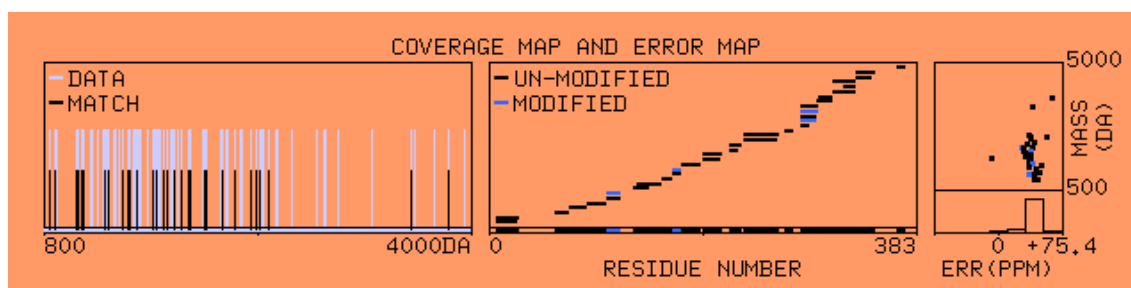


Figure 4.107: MALDI-TOF result and data analysis for pool 3 (stg. 2.2.1).

Pool 4 MALDI-TOF MS resulted in fragments covering 86.72 % of GPA1 amino acid sequence (Figure 4.108). The resulting sequence is given in APPENDIX I. The m/z for N-terminal peptide containing the C as Carbamidomethyl-cystein (GLLC*SR) was present at 705.4 Da, but was assigned manually.

For pool 4 again the missing fragments correspond to $G\alpha$ conserved residues; but did not completely overlap to the missing fragments in pool 3. The long missing region

was 32 amino acids long (as compared to 23 for pool 3). The P-loop and GoLoco binding residues (GAGESGK), two amino acids in switch I (VR) and in switch II (RK) were missing as in pool 3. Only three residues of putative receptor binding site (VFK) were absent and unlike pool 3 all the lysines in this site were digested by trypsin. The two plant G α specific insertion regions were also not detected SGEVYR and LDYPR, but following 3 residues were also absent (LTK) in pool 4. There were six undigested arginine and seven lysine residues. Lysine in GDP/GTP binding site besides all three in putative receptor binding site and another at position 329 were all accessible to tryptic digestion, unlike in pool 3 where they were all undigested.

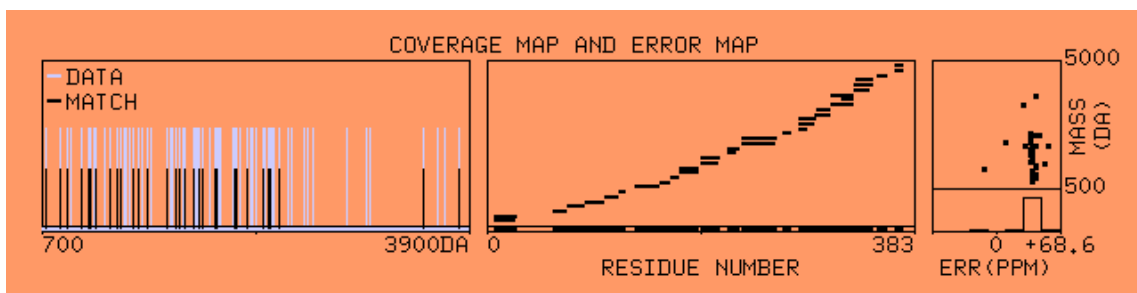


Figure 4.108: MALDI-TOF result and data analysis for pool 4 (stg. 2.2.1).

The peptide containing a palmitoylation at C4 should appear at 886.4 Da. This mass was not present in any of the two samples. The peptide containing a palmitoylation at C4 and a myristoylation at the N-terminus should appear at 1096.5 Da. This mass is also not visible in any of the two samples. According to these results, pool 4 does not contain any lipid modifications attached to its N-terminus. Since pool 3 N-terminal 6 amino acid fragment was invisible in MS, the absence / presence of lipid modifications can not be deduced.

4.7 Structural Characterization of GPA1

4.7.1 Secondary Structure Analysis

- **Secondary Structure Comparison of GPA1 from different purification procedures**

CD measurements were done mainly to investigate the quality of the purified protein. GPA1 is expected to have high helical content, hence the presence of α helical CD signature was followed throughout the purifications. Furthermore, the folding of proteins was also analyzed by inspecting the presence of ellipticity in the near-UV region of the CD spectrum. The CD spectra of buffers are given in APPENDIX M.

- Affinity Purified GPA1:

The protein storage conditions were optimized depending on near-UV spectrum signals.

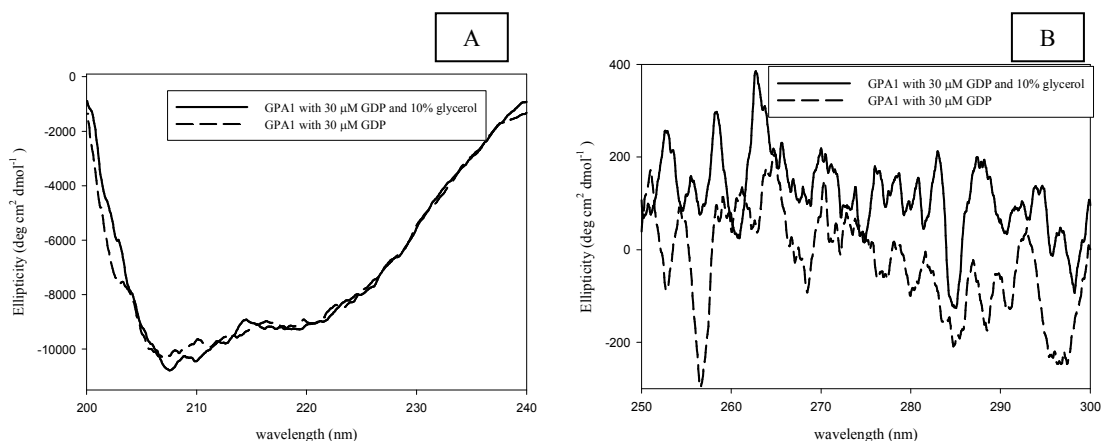


Figure 4.109: Far (A) and Near-UV (B) spectra of GPA1 (stg.2.1). GPA1 was stored with different additives in 50 mM TrisHCl, pH 8.0 buffer as given.

GPA1 stored with GDP and glycerol has more signal in near-UV region, which may indicate all (more) aromatic amino acid residues are correctly folded giving rise to optical rotation (Figure 4.109). This may indicate that storage without glycerol damages the tertiary structure of the protein. $\theta_{208 \text{ nm}} / \theta_{222 \text{ nm}}$ are similar, 1.2 for GPA1 stored with GDP and glycerol, 1.17 stored with only GDP; and $\theta_{222 \text{ nm}}$ value was -8857 and -8594 respectively. The corresponding western blot results are given in Figure 4.20.

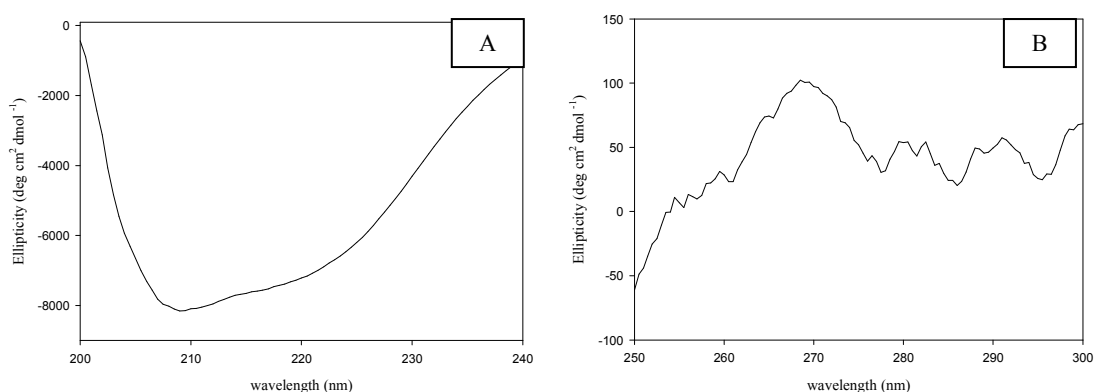


Figure 4.110: Far (A) and near-UV (B) spectra for GPA1 (stg.3.1, Triton X-100). Sample was in buffer with 50 mM TrisHCl, 1mM DTT, 1mM PMSF.

GPA1 Ni-affinity purified in the presence of Triton X-100 and dialyzed had an $\theta_{208 \text{ nm}} / \theta_{222 \text{ nm}}$ ratio of 1.16, similar to protein purified without detergent, but $\theta_{222 \text{ nm}}$ value was -6788. In contrast, the near-UV spectral region is quite different, which may indicate that tertiary structure of GPA1 is different in the presence and absence of Triton X-100 (Figure 4.110).

- Anion Exchange:

Anion exchange separated two biophysically different GPA1, pool 3 was more stable as shown by SDS-PAGE, Western and DLS analysis. CD measurements also support the view that pool 3 and pool 4 has different properties (Figure 4.111).

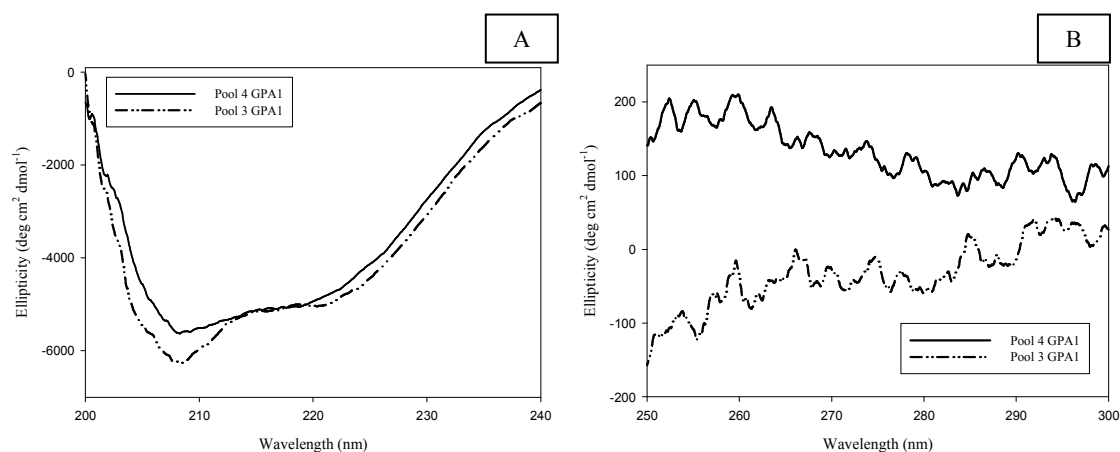


Figure 4.111: Far-UV (A) and Near-UV (B) CD spectra of pool 3 and pool 4 (stg.2.2.1).

The two different GPA1 pools (stg. 2.2.1) had different helical content as shown (Figure 4.111) by far-UV CD spectra and pool 3 showed more pronounced minima with $\theta_{208 \text{ nm}} / \theta_{222 \text{ nm}}$ of 1.27 as compared to 1.19 for pool 4. The values for $\theta_{222 \text{ nm}}$ was -4906 for pool 3 and -4710 for pool 4. Furthermore the two proteins had different near-UV spectra which may imply that the environment of aromatic residues were different in

pool 3 and pool 4; the two proteins have different tertiary structures, but the signals are too weak to do more conclusions.

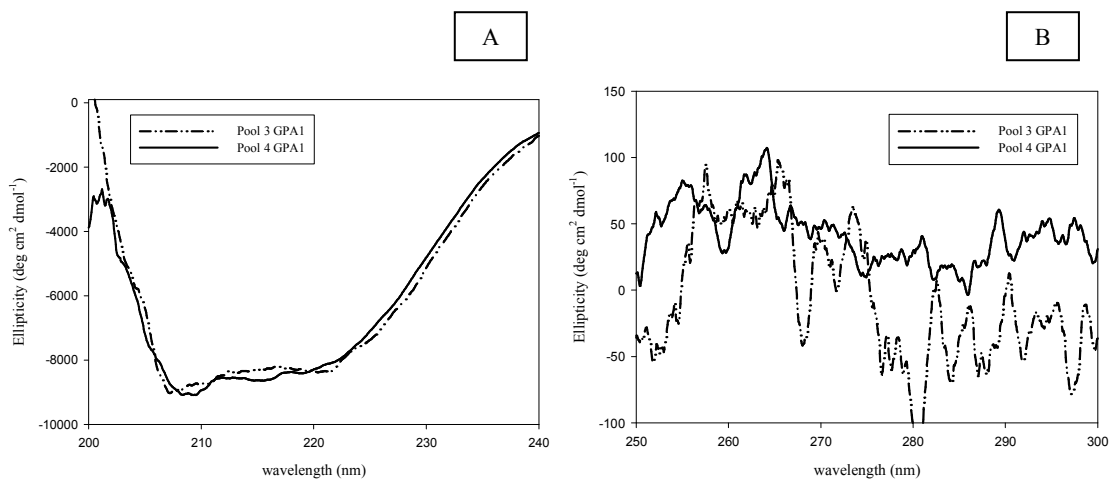


Figure 4.112: Far-UV (A) and Near-UV (B) CD spectra of pool 3 and pool 4 (stg.3.1.1, Triton X-100).

The two different GPA1 pools (stg. 3.1.1 with Triton-X) had similar $\theta_{208 \text{ nm}} / \theta_{222 \text{ nm}}$ ratio, 1.0 for pool 3 and 1.1 for pool 4. $\theta_{222 \text{ nm}}$ was -8211 for pool 3 and -8036 for pool 4. In contrast, the near-UV regions are different, pool 3 has more distinct bands (Figure 4.112).

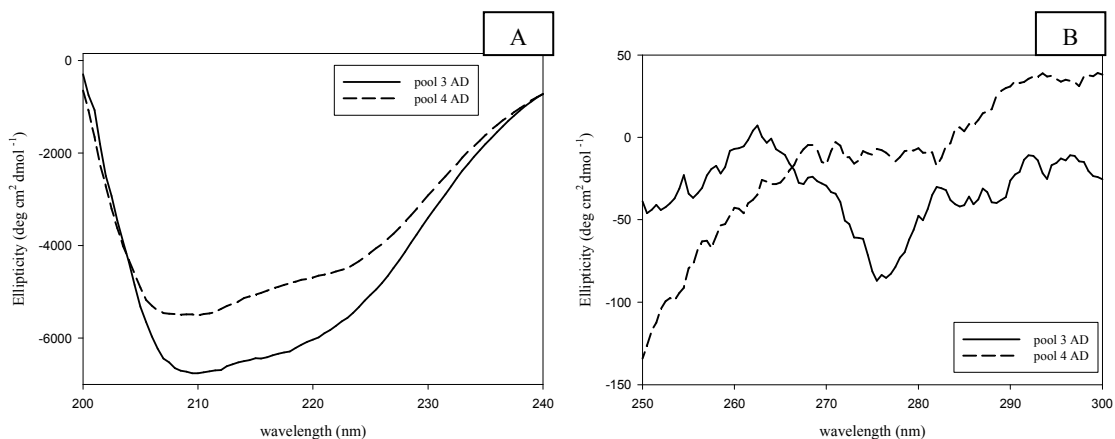


Figure 4.113: Far-UV (A) and Near-UV (B) CD spectra of pool 3 and pool 4 (stg.3.1.1, Triton X-100 and AlF_4^-). Samples were in buffer with 5 mM Tris HCl, pH 8.0, 5 mM NaCl, 1 mM DTT and 1 mM PMSF.

The two different GPA1 pools (stg. 3.1.1 with Triton X-100 / AlF_4^-) had similar $\theta_{208 \text{ nm}} / \theta_{222 \text{ nm}}$ ratios, 1.15 for pool 3 and 1.16 for pool 4 but the $\theta_{222 \text{ nm}}$ values were different; -6892 for pool 3 and -4563 for pool 4. The near-UV regions are different. Pool 4 has a band around 265 nm, which is shifted to 260 nm in pool 3 (Figure 4.113).

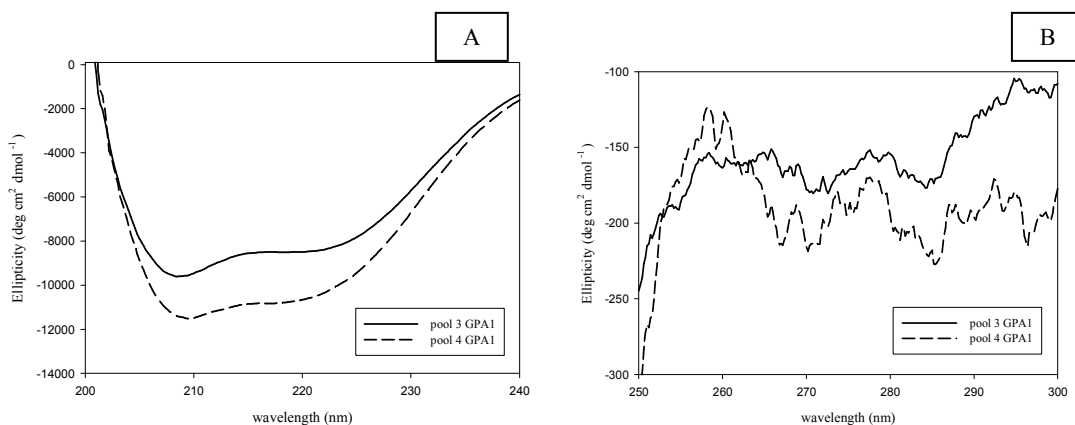


Figure 4.114: Far-UV (A) and Near-UV (B) CD spectra of pool 3 and pool 4 (stg. 3.1.1, Lubrol-PX).

The two different GPA1 pools (stg. 3.1.1 with Lubrol PX) had different $\theta_{208 \text{ nm}}/\theta_{222 \text{ nm}}$ ratios, 1.13 for pool 3 and 1.0 for pool 4. Pool 4 showed a more pronounced minimum with $\theta_{222 \text{ nm}}$ of -10350 as compared to $\theta_{222 \text{ nm}}$ of -8389 for pool 3. The ellipticity wavelengths are similar for pool 3 and pool 4 in the near-UV region of the spectra, with small difference in the intensity of bands (Figure 4.114).

The near-UV region in CD spectrum is a good indicator of tertiary structure of a protein and the presence of signals can be attributed to a folded protein. Near -UV region is sensitive to small conformational/ structural changes arising from protein environment. In summary the folding of aromatic residues/ intermolecular disulfides appear to be different in pool 3 and pool 4 GPA1, considering the observation that, independently of purification procedure, they had different near-UV spectra.

- **Change in helical content upon Receptor interaction**

Secondary and tertiary structural changes that may occur upon addition of GTP γ S to pool 3 GPA1 (stg. 3.1.1) were analyzed (Figure 4.115). The $\theta_{208 \text{ nm}}/\theta_{222 \text{ nm}}$ ratio was changed from 1.13 to 1.232 and $\theta_{222 \text{ nm}}$ was changed from -6867 to -8630 with the presence of GTP γ S. In the near-UV CD region the 270 nm band was shifted to 265 nm and 285 nm band was shifted to 290 nm, which can be caused by the different environments of Tyr and Trp in the presence of GTP γ S. It was shown that pool 3 GPA1 can bind GTP γ S (Figure 4.83), these results suggest that the structure of GPA1 is altered in the presence of different nucleotides.

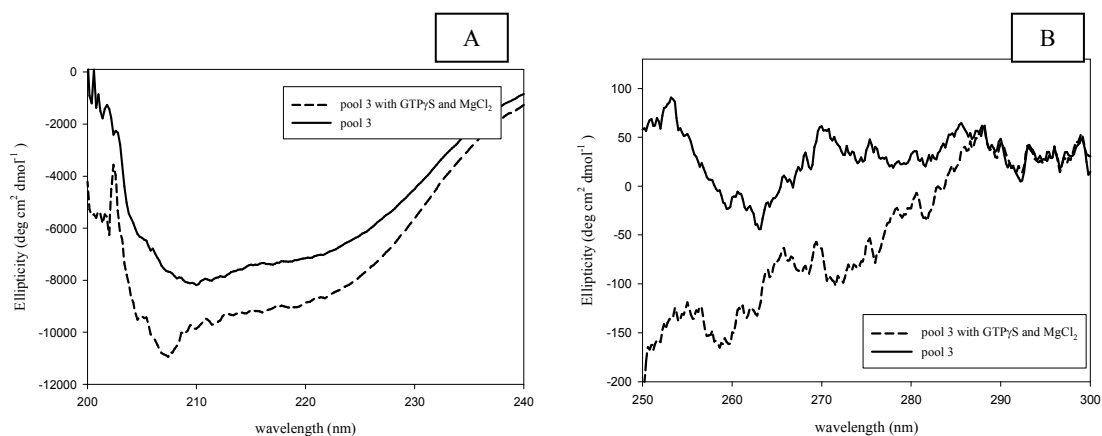


Figure 4.115: Far-UV (A) and Near-UV (B) CD spectra for pool 3 with and without GTP γ S and MgCl₂.

One of the receptor interaction site on heterotrimeric G protein alpha subunits is their C-terminal helical region and this interaction results in a structural change. This was investigated by using receptor mimetic compounds, compound 48/80 (C48/80), mastoparan (MP) and Mas7 (highly active mastoparan analog). These compounds are known to interact with and activate mammalian G protein alpha subunits. Receptor mimetic compounds were added to GPA1 and CD spectra were recorded in order to see if any structural change occurred. MP and Mas7 are unstructured peptides and fold into a helical structure upon interaction with mammalian G α [40].

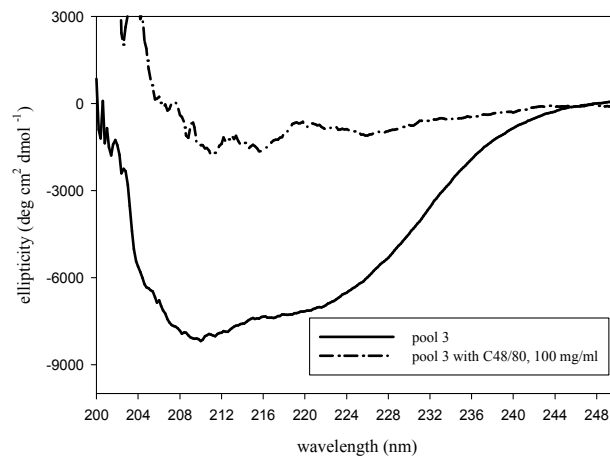


Figure 4.116: Ellipticity of pool 3 with and without C48/80.

In the presence of C48/80 the α helical signature bands at 208 nm and 222 nm were lost and $\theta_{208 \text{ nm}} / \theta_{222 \text{ nm}}$ ratio was reduced to 0.45 from a value of 1.13 and $\theta_{222 \text{ nm}}$ was increased to -5200 from -6867 (Figure 4.116).

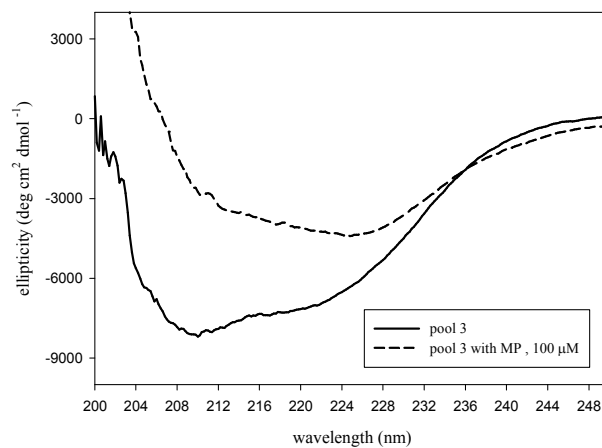


Figure 4.117: Ellipticity of pool 3 with and without 100 μM of MP.

In the presence of MP the intensity of α helical signature bands at 208 nm and 222 nm decreased and $\theta_{208 \text{ nm}}/\theta_{222 \text{ nm}}$ ratio was reduced to 0.33 from a value of 1.13 and $\theta_{222 \text{ nm}}$ was increased to -4242 (Figure 4.117).

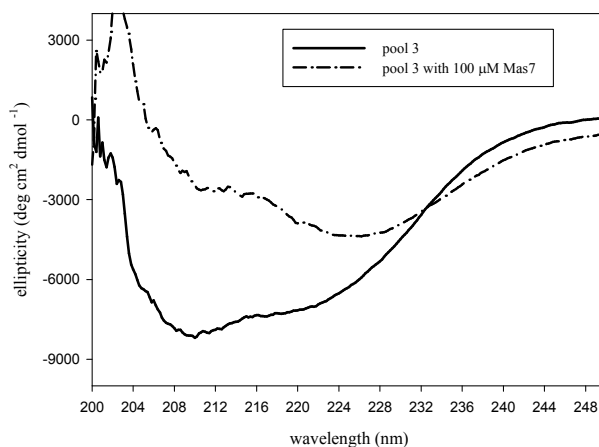


Figure 4.118: Ellipticity for pool 3 with and without 100 μM Mas 7.

In the presence of Mas 7 the intensity of α helical signature bands at 208 nm and 222 nm decreased and $\theta_{208 \text{ nm}}/\theta_{222 \text{ nm}}$ ratio was reduced to 0.38 from a value of 1.13 and $\theta_{222 \text{ nm}}$ was increased to -4148 (Figure 4.118).

The ellipticity increased upon addition of all three compounds, which may indicate that the α -helical content was decreased upon interaction with these receptor mimetic compounds. MP and Mas7 fold into a helical structure when interacting with GPA1. The subtracted curves show the change in pool 3 GPA1.

4.7.2 SAXS data analysis

SAXS data measurements were carried out on different GPA1 samples; affinity, anion exchange or gel filtration purified. Results are summarized below.

1: Affinity purified GPA1

The protein was desalted and final buffer was 50 mM Tris HCl, pH 7.4, 0.3 M NaCl, 40 μ M GDP and 2 mM MgCl₂. Protein concentration was measured before SAXS data collection and was 1.22 mg/ml.

Affinity purification did not suffice to obtain pure and monodisperse recombinant GPA1. The intensity plot showed that the protein was aggregated and it was not possible to find a linear region for the Guinier estimation (data not shown).

The intensity and Guinier plot for 4.36 mg/ml BSA are given in Figure 4.119.

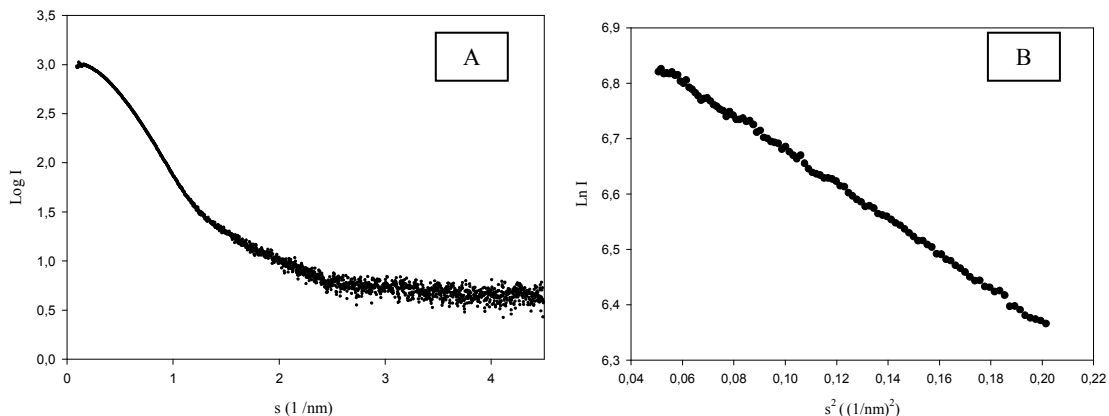


Figure 4.119: Intensity plot (A) and Guinier plot (B) of BSA. The Guinier region was estimated with the AutoRg software [128].

The R_g of BSA (3.05 nm) was calculated with sR_g limits 0.71 - 1.295. The R_g can be converted to radius by multiplying with a factor of 1.29 for spherical particles. The radius of BSA estimated in this manner is 3.9 nm, but BSA (proteins) is (are) not an ideal sphere. Therefore, radius calculations should be done according to distance distribution function.

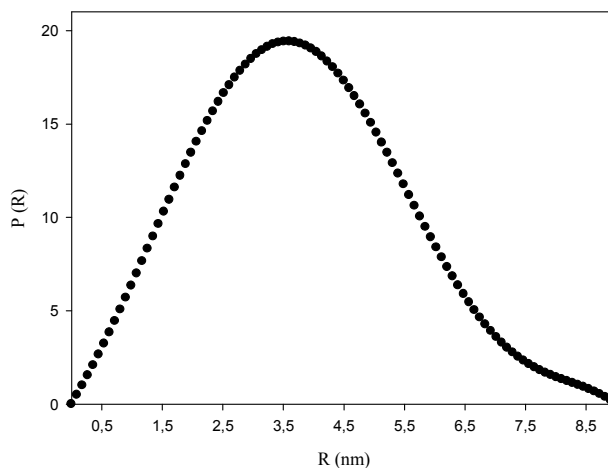


Figure 4.120: The distance distribution function of BSA. The R_{max} was set to 9.0 nm and the R_g was 3.05 nm.

The distance distribution function for a homogeneous particle gives the probability of finding two volume elements of the particle separated by a distance R . The radius of BSA was estimated ~ 3.5 nm from $P(R)$ plot (Figure 4.120).

2: Anion Exchange Purified GPA1 (stg.2.2.1)

Pool 3 and pool 4 GPA1 were stored in 20 mM HEPES, pH 8.0 50 mM NaCl, 20 μ M GDP and 10% glycerol at -80 °C and were transported to EMBL, Hamburg on dry ice. Since both samples contained 10% glycerol, dialysis was done against 50 mM HEPES pH 8.0 and 50 mM NaCl. Following dialysis samples were centrifuged using an airfuge (Beckman) and concentrations (Table 4.19) were measured using a nanodrop spectrometer (Thermo Scientific). Pool 4 GPA1 was significantly aggregated as judged from intensity plot and it was not possible to find a linear region for the Guinier estimation (data not shown).

Table 4.19: Concentration estimations for pool 3 (stg.2.2.1).

sample	Absorbance (AU)		Concentration
	260 nm	280 nm	mg/ml
pool 3	0.675	0.561	0.356
pool 3 air	0.618	0.507	0.316

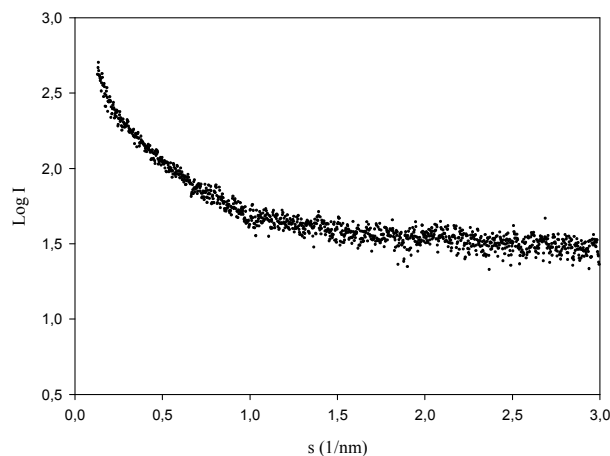


Figure 4.121: Intensity plot for anion exchange GPA1 pool 3. Data collected from the supernatant after airfuge centrifugation.

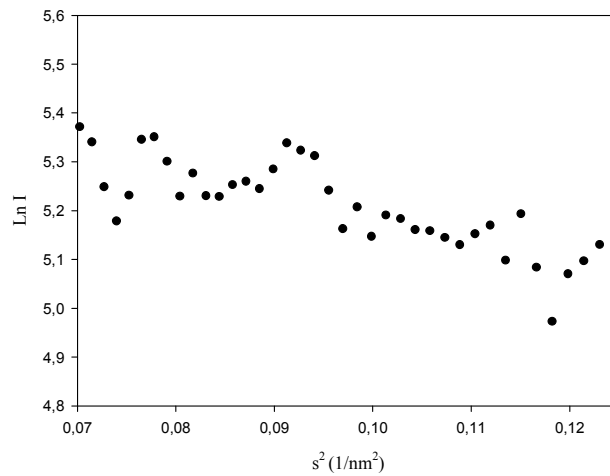


Figure 4.122: Guinier plot for anion exchange GPA1 pool 3. Data collected from the supernatant after airfuge centrifugation. The Guinier region was estimated with the AutoRg software.

Table 4.20: Summary of SAXS measurements and MM estimations.

		Auto RG				MM,kDa	
sample	concentration	I(0)/c	Rg	points	quality, %	Expected	calculated
BSA	4.5	313.13	2.98	72	77	67	
pool 3 air	0.3	282.12	3.66	40	58	48	60

Pool 3 sample was expected to have a higher molecular mass than that of GPA1 and SAXS measurements verified this (Table 4.20 and Figure 4.121). Still the data was not sufficient for building a low resolution structural model. The DLS measurements before airfuge centrifugation showed a radius of 100 nm for pool 3 (Figure 4.37).

3: Size exclusion purified GPA1 (stg. 3.2.1, Lubrol-PX)

GPA1 was purified from Sephacryl S-200 HR 16/60 (Buffer D) and samples were stored in 20 mM HEPES, pH 8.0, 150 mM NaCl, 1 mM DTT, 5% glycerol and 5 mM MgCl₂ at 4 °C and were transported to EMBL, Hamburg on ice. The S-200 fractions were pooled according to their elution volumes from column and 4 pools were obtained with the estimated MM (Table 4.21). Samples were stored at +4 °C until measurement (3 days).

Table 4.21: Molecular mass estimations from column calibration curve.

	Ve	MM, kDa
pool 1	35.88	247.6
pool 2	40.87	143.3
pool 3	43.62	108.1
pool 4	47.37	75.1

The buffer was exchanged to remove the glycerol in the samples using Vivaspin 500, 30,000 MWCO (Sartorius) to 20 mM HEPES, pH 8.0, 150 mM NaCl and 1 mM DTT prior to SAXS data collection. Protein concentrations were measured using a Nanodrop spectrometer (Table 4.22).

Table 4.22: Concentration estimations for GPA1 pools (stg. 3.2.1).

Sample	Absorbance (AU)			A_{254}/A_{280}	Concentration	
	254 nm	260 nm	280 nm		(Eqn 1) mg/ml	(Eqn2) mg/ml
pool 1	0.773	0.873	1.56	0.49	1.754	1.4
pool 2	1.147	N.A	2.721	0.42	-	2.44
pool 3	1.452	1.816	3.131	0.46	3.473	2.82
pool 4	0.622	0.725	1.25	0.49	1.386	1.12

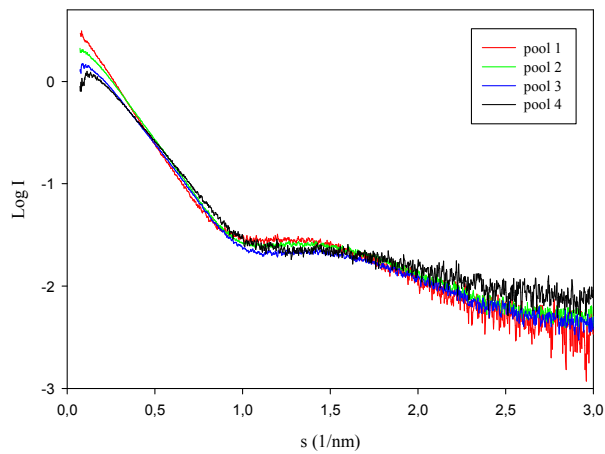


Figure 4.123: Comparison of scattering plots of GPA1 with different molecular masses.

The scattering plots verify the expected molecular mass difference within different pools of GPA1, pool 1 with the highest and pool 4 with the lowest $I(0)$ value (Figure 4.123).

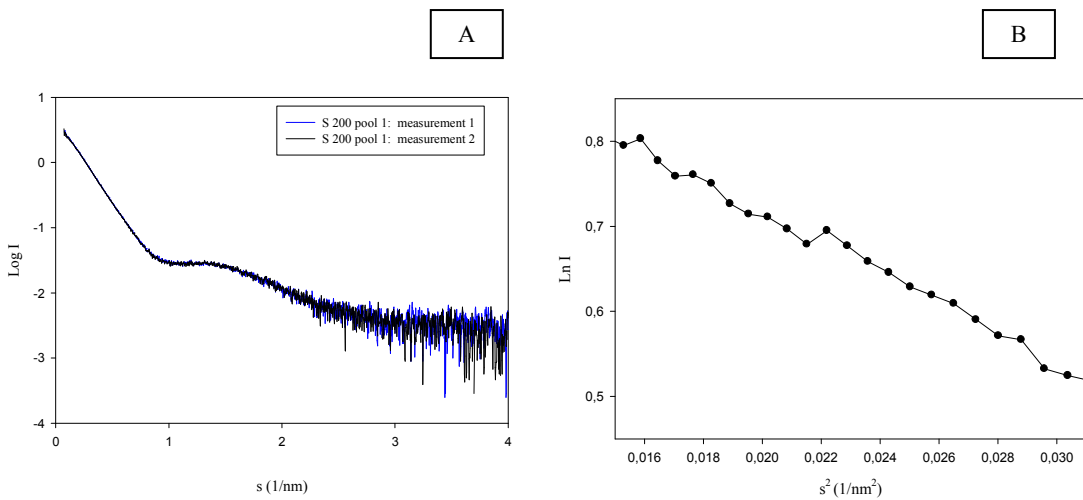


Figure 4.124: A: Scattering pattern of S-200 pool 1 GPA1 (two consecutive measurements). B: Guinier plot for pool 1 GPA1, sR_g limits 0.732-1.297.

Figure 4.124 shows that there is no detectable radiation damage in the small angle region, since the scattering profiles overlay in the small angle region.

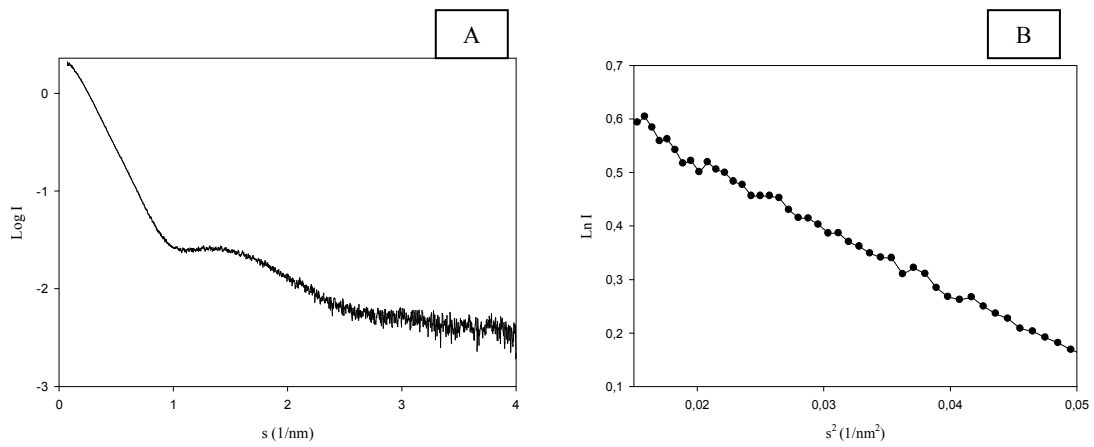


Figure 4.125: Scattering plot (A) and Guinier plot (B) for S-200 pool 2. sR_g limits: 0.808 to 1.202.

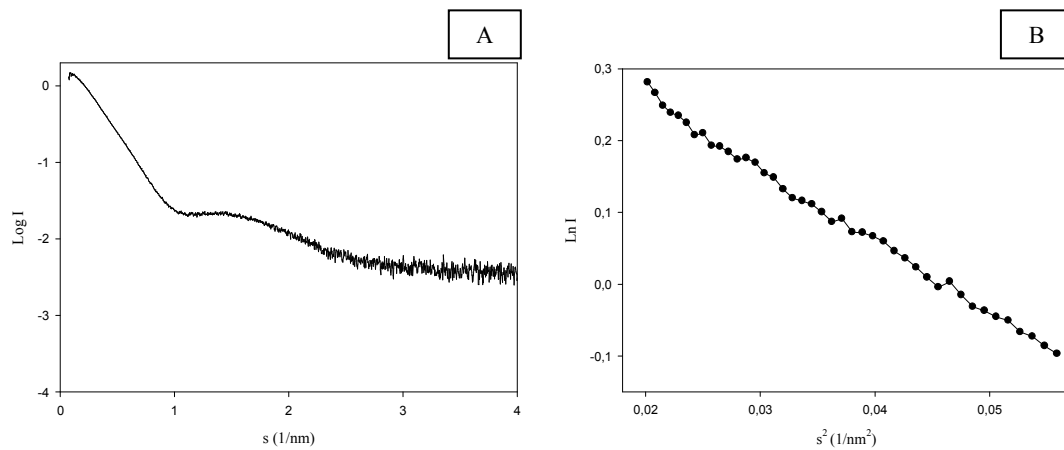


Figure 4.126: Scattering plot (A) and Guinier plot (B) for S-200 pool 3. sR_g limits: 0.81-1.297.

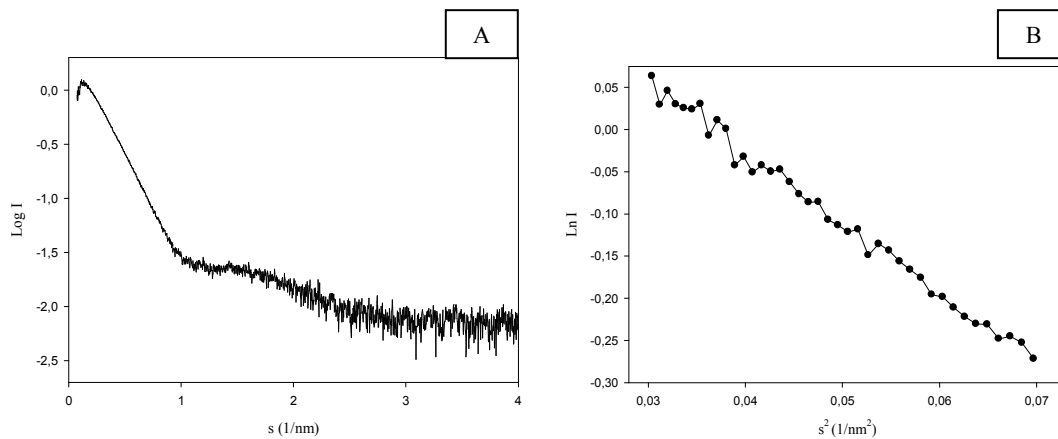


Figure 4.127: Scattering plot (A) and Guinier plot (B) for S-200 pool 4. sR_g limits: 0.867-1.302.

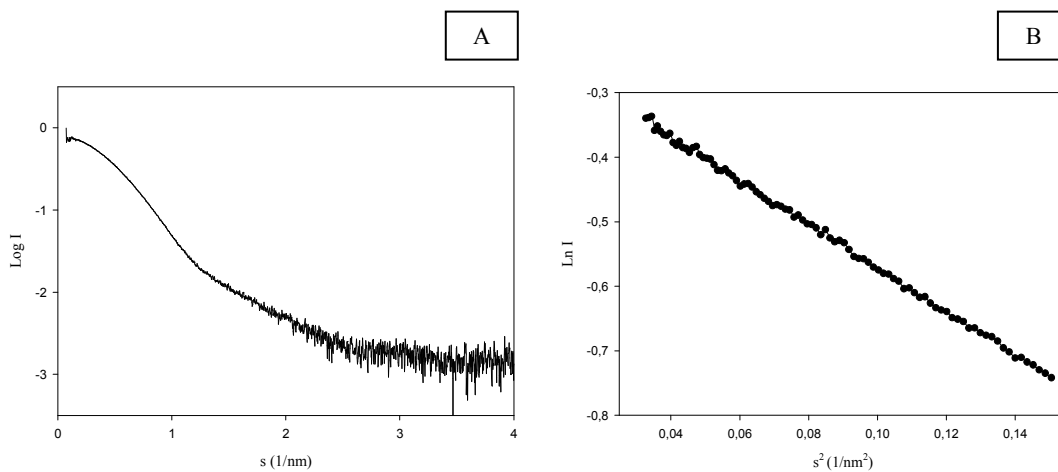


Figure 4.128: Scattering plot (A) and Guinier plot (B) of BSA (3.91 mg/ml). sR_g limits 0.597-1.255.

Table 4.23: MM estimations from SAXS data of BSA and S-200 pools.

sample	mg/ml	Auto RG				MM, kDa	Calculated		Ratio MM
		$I(0)/c$	R_g (nm)	points	quality, %		SAXS	Column	
BSA	3.91	0.79	3.18 ± 0	91	87	67	-	-	
pool 1	1.14	2.97	7.44 ± 0.02	34	94	48	252	247.6	5.247
pool 2	2.44	2.13	5.98 ± 0.03	37	88	48	181	143.3	3.763
pool 3	2.82	1.57	5.43 ± 0	40	87	48	133	108.1	2.774
pool 4	1.12	1.35	4.98 ± 0	39	83	48	114	75.1	2.385

Table 4.24: Comparison of Rg (Guinier), volume (Porod) and diameter (DLS).

Sample	Guinier		Porod			DLS
	I(0)/c	Rg (nm)	I(0)/c	Rg (nm)	Ex.volume (nm)	d (nm)
pool 1	2.97	7.44	2.89	7.21	808.8	25
pool 2	2.13	5.98	2.12	5.98	501.94	20
pool 3	1.57	5.43	1.566	5.44	420	N.A.
pool 4	1.35	4.98	1.36	4.98	342.35	15

The molecular mass estimations from SAXS data are given in Table 4.23. The intensity plots for all S-200 GPA1 samples (Figure 4.125 - Figure 4.127) were different from intensity plot of BSA (Figure 4.128). The plots were similar to those of protein-micelle complex and/or multi domain protein complexes [130-132]. The molecular mass estimations support the presence dimers in case of pools 2, 3 and 4 and tetramers for pool 1 and possibly another component that increases the mass in solution. This may be Lubrol-PX in the purified protein as shown by NMR (Figure 4.99).

The average particles size estimations are given in Table 4.24, Rg values calculated from Guinier and Porod plot match. The Porod volume is the excluded volume of the hydrated particle which equals to four time of the volume for a hard sphere [133]. The estimated particle diameter using the values of the radius of gyration were in agreement with DLS measurements. The DLS measurements verify the presence of a nearly monodisperse solution with decreasing particle size according to elution volume (Figure 4.129-Figure 4.131).

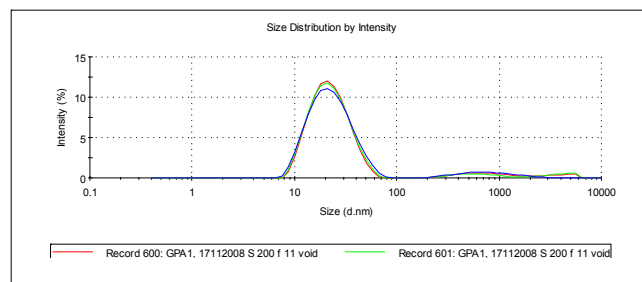


Figure 4.129: DLS size distributions by intensity of GPA1 pool 1 (stg.3.2.1).

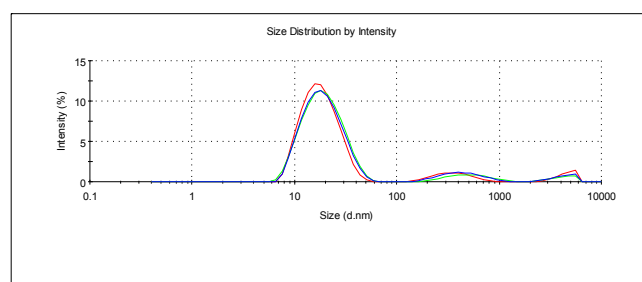


Figure 4.130: DLS size distributions by intensity of GPA1 pool 2 (stg.3.2.1).

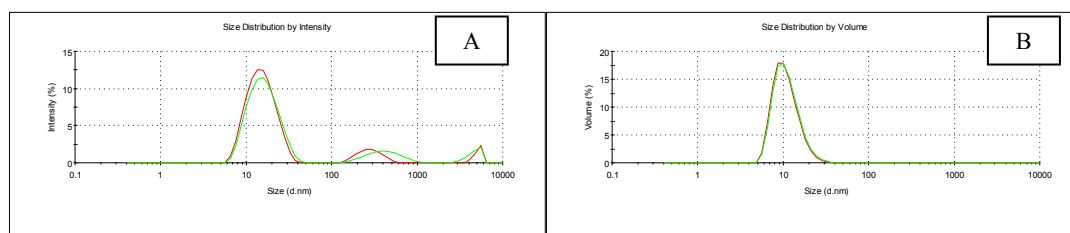


Figure 4.131: DLS size distributions by intensity (A) and volume (B) GPA1 pool 4 (stg.3.2.1).

Model calculations to determine structures that would give rise to the observed SAXS patterns were carried out using rigid body modelling. The scattering expected from the crystal structure for mammalian $G\alpha$ on GPA1 was fitted to the experimental scattering profile using SASREF and GPA1 was modeled as an oligomeric protein [132]. The crystal structure 1GFI [134] monomer was used as template with different subunit numbers. Data points from 35-1300 corresponding a S range to 0.1513-3.0630 nm^{-1} portion of the pool 4 scattering curve was selected in analyses. P1 overall

symmetry was chosen with angular units for momentum transfer (S) given by $4\pi\sin(\theta)/\lambda$ (nm⁻¹). Results of several are given in Table 4.25.

Table 4.25: SASREF Parameters and error values.

Model	monomers	fraction to fit	Penalty of shift	best chi values	Shift from the origin		
					X	Y	Z
g111e	5	1	0.00192	1.73	-0.09	0	0.01
g111f	5	0.5	2.8477	1.28	79.28	-79.5	81.57
g111g	4	0.5	3.97213	1.37	138.68	132.67	-13.92
g111h	6	0.5	0.00047	1.25	0	0.02	-0.01

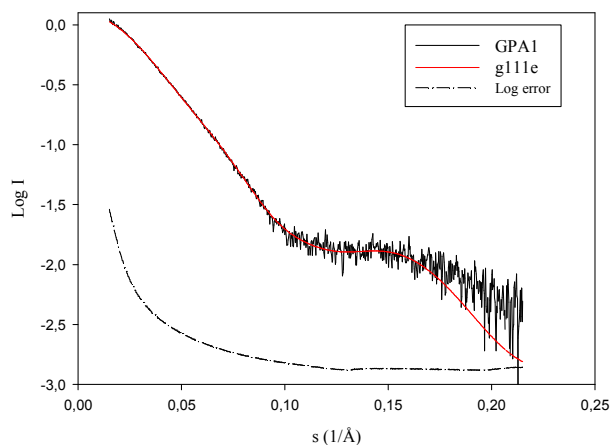


Figure 4.132: SASREF fit (g111e) to scattering curve.

5 monomers of GFI were used to fit on the total scattering curve (fraction to fit selected 1.0). Best chi value was 1.738 at the end of simulated annealing.

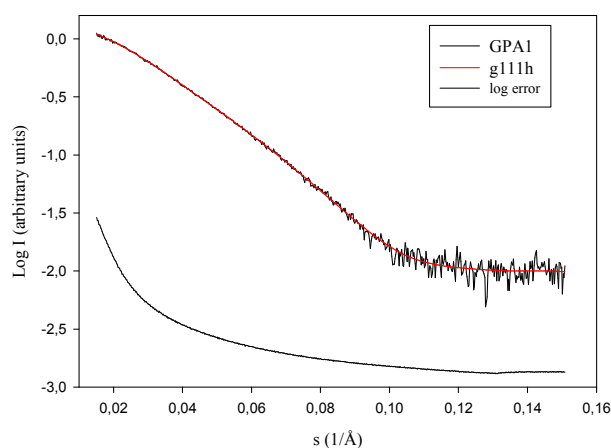


Figure 4.133: SASREF fit (g111h) to scattering curve. 6 monomers of GFI were used to fit with fraction to fit 0.5. Best chi value was 1.256 at the end of simulated annealing.

As a result the models g111e (5 subunits, Figure 4.132) and g111h (6 subunits, Figure 4.133) are selected as the most reliable models (Figure 4.134). The two models were superimposed by using SUPCOMB (Automatic Superposition of High- and Low-Resolution Structural Models) [135]. The resultant model (g111er) from the superimposition of g111e and g111h is given in Figure 4.135 and overlay with individuals models is given in Figure 4.136. The crystal structure of 1GFI and the corresponding unit cell is given in Figure 4.137 and Figure 4.138 respectively.

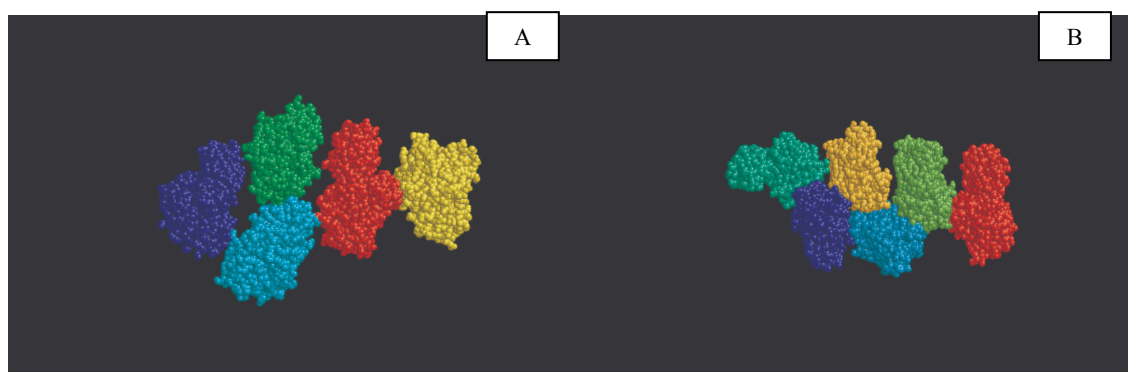


Figure 4.134: SASREF models.g111e (A) and g111h (B).

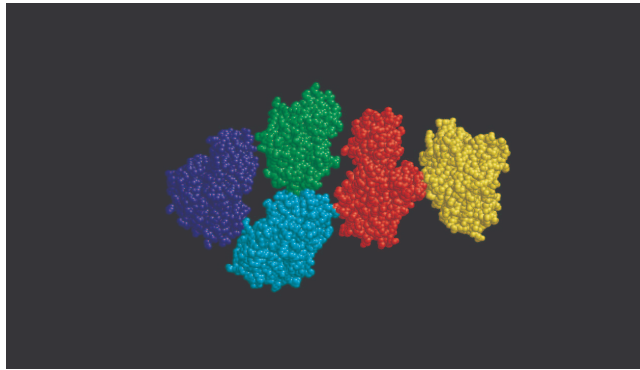


Figure 4.135: SUPCOMB superimposed model, g11er

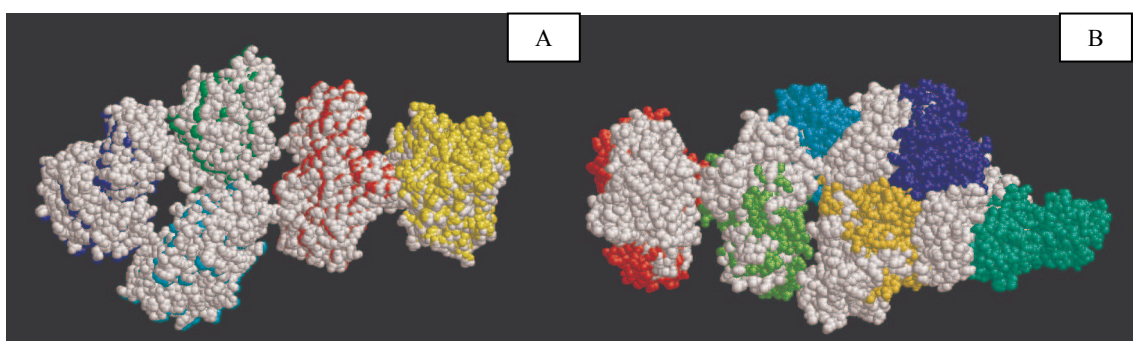


Figure 4.136: Overlay of g11er (gray) with g111e (A) and g111h (B).

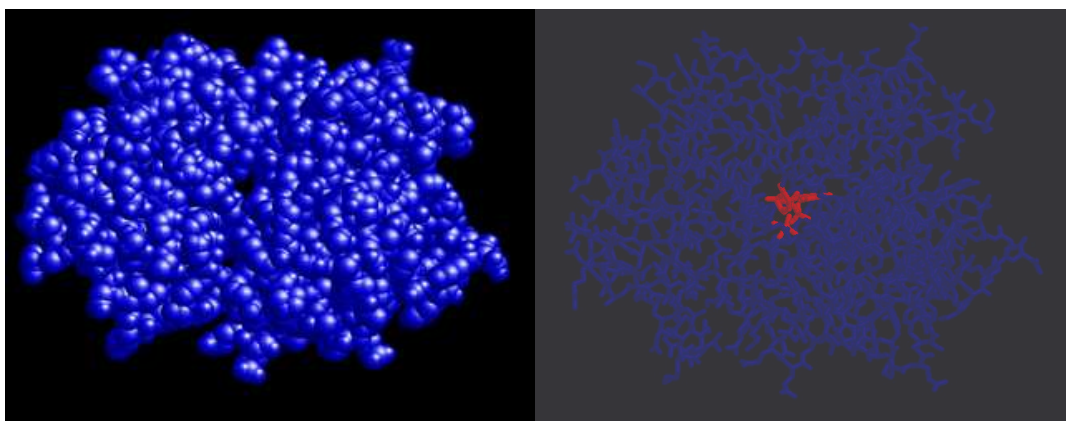


Figure 4.137: Crystal structure of 1GFI (Galphai bound to GDP and AlF₄⁻).
A: space fill model, B: stick model, GDP- AlF₄⁻ is shown.

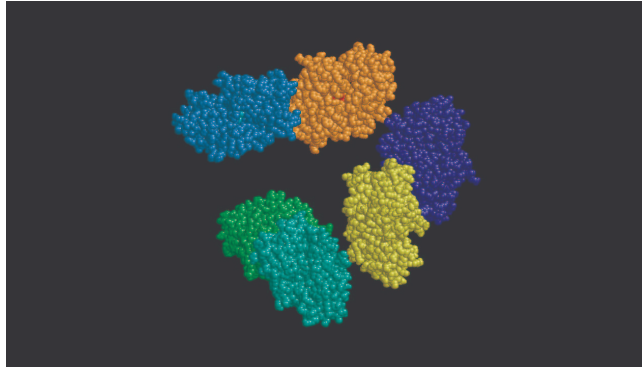


Figure 4.138: Unit cell structure of 1GFI (Gi with GDP and AlF_4^-).

In summary according to SAXS data, the molecular mass of GPA1 is more than the expected MM of a dimer. SASREF analyses with known structures, on the other hand, suggest the presence of a molecule with shape resembling a pentameric $\text{G}\alpha$ protein. The presence of detergent micelles increases the size of the molecule.

4.8 Expression of AGB1 and AGG1 / 2 subunits

In order to establish the *A. thaliana* heterotrimer, AGB1 and AGG1/2 proteins were cloned and expressed in *E. coli* using pGEX-4T-2 (GE Healthcare) and pQE-80L (Qiagen) vectors. pGEX-4T-2 results in GST fusion form of the recombinant proteins, whereas pQE-80L introduces an N terminal his tag with additional RGS residues. GST-AGB1, GST-AGG1, RGS-his-AGB1 and RGS-his-AGG2 sequences were verified and the results are given in APPENDIX F. There was one silent mutation in GST-AGB1 sequence.

4.8.1 Cloning into pGEX-4T-2 vector

The TAIR plasmids (Table 3.1) harboring the genes encoding *AGB1* and *AGG1* were isolated from host *E. coli* DH10B and PIR1 cells respectively and used as templates in PCR amplification. *AGB1* and *AGG1* were PCR amplified using primers designed according to the PUBMED sequences (Gene ID: 829597 and 825517 respectively) with *EcoRI* and *XhoI* restriction enzyme sites (Table 4.26).

Table 4.26: Primers designed for cloning into pGEX-4T-2.
Restriction enzyme sites are underlined.

Primers for <i>AGB1</i>		
Forward Primer	BF2	5'-AAACCC <u>GAATTC</u> CCCATGTCTGTCTCCGAGCTCA-3'
Reverse Primer	BR2	5'-TTTGGGCTCGAGTCAAATCACTCTCCTGTGTCC-3'
Primers for <i>AGG1</i>		
Forward Primer	FG1E	5' AAACCC <u>GAATTC</u> CCCATGCGAGAGGAAACTGTGG-3'
Reverse Primer	RG1X	5'-TTTGGGCTCGAGTCAAAGTATTAAGCATCTGCA-3'

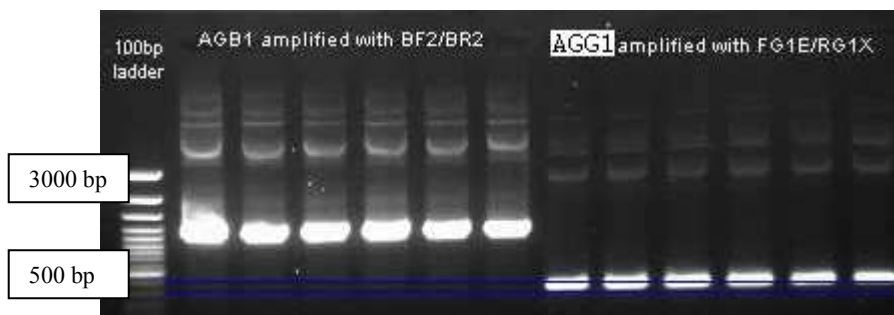


Figure 4.139: 1% Agarose gel electrophoresis analysis of PCR amplification of *AGBI* and *AGGI* fragments.

Lane 1: 100bp DNA ladder Plus®, lanes 2-7: *AGBI* fragments, lanes 8-13: *AGGI* fragments. Lanes 2 & 8: 61.3 °C, lanes 3 & 9: 62.6 °C lanes 4 & 10: 64°C, lanes 5 & 11: 65.6 °C, lanes 6 & 12: 67°C, lanes 7 & 13: 68.4 °C.

As can be seen from Figure 4.139, *AGBI* of size 1200 bp (lanes 2-7) and *AGGI* of size 300 bp (lanes 8-13) fragments were amplified at all annealing temperatures tested. *AGBI* fragment amplified at 65.5°C and *AGGI* fragment amplified at 65°C were used for cloning. Purified PCR products and pGEX-4T-2 vector were digested with restriction enzymes EcoRI and XhoI.

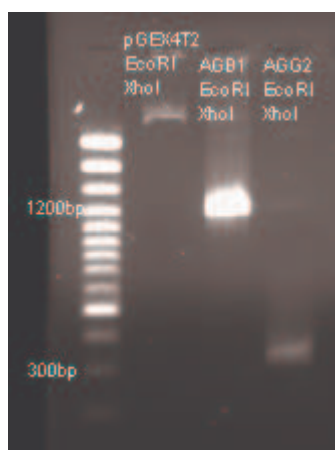


Figure 4.140: 1% Agarose gel electrophoresis analysis of restriction enzyme digestion for insertion into pGEX-4T-2. Lane 1: 100 bp. DNA Ladder Plus ®.

Restriction enzyme digested PCR products and the linear vector (Figure 4.140) were ligated and *E.coli* TOP10F' cells were transformed with different amounts of the ligation mixtures as described in chapter 3.2. Positive clones were chosen from the colonies that grew on LB-amp plates and the presence of inserts was verified by colony

PCR and restriction enzyme digestion. The constructs chosen for expression were labeled GST-AGB1 and GST-AGG1.

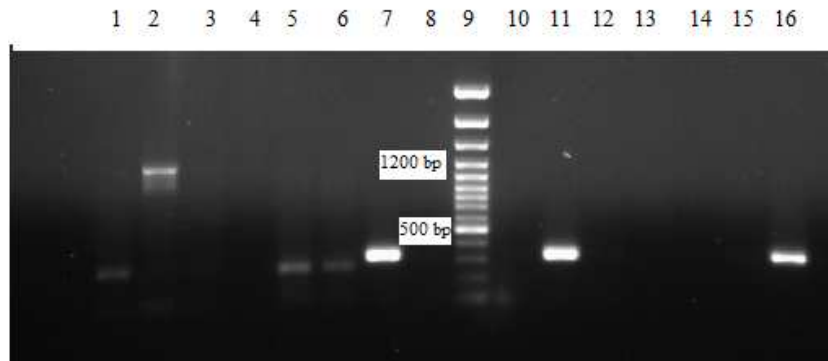


Figure 4.141: 1% Agarose gel electrophoresis analysis of colony PCR for pGEX-4T-2 constructs. Lanes 1-6: AGB1, lanes 7, 8, 10-16: AGG1, lane 9: 100 bp.DNA Ladder Plus ®.

Colony PCR results shown in Figure 4.141 display strong bands around 1200 bp for *AGBI* (lane 2) and around 300 bp for *AGGI* (lanes 7,11 and 16).

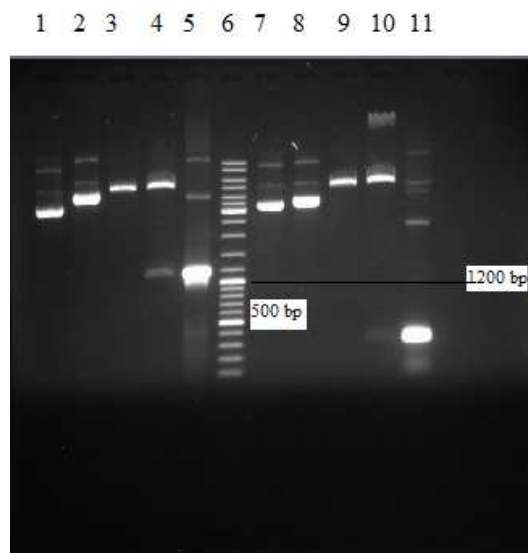


Figure 4.142: 1% Agarose gel electrophoresis analysis of restriction enzyme digestion. Lanes 1 and 7: pGEX-4T-2, lane 2: pGEX-4T-2-*AGBI*, lanes 3 and 9: pGEX-4T-2 *EcoRI* / *XhoI*, lane 4: pGEX-4T-2-*AGBI-EcoRI* / *XhoI*, lane 5: *AGBI* control lane 6: O'GeneRuler Mix ®, lane 8: pGEX-4T-2-*AGGI*, lane 10: pGEX-4T-2-*AGGI-EcoRI* / *XhoI*, lane 11: *AGGI* control.

The selected clones were verified by restriction enzyme digestion (Figure 4.142). These plasmids, GST-AGB1 and GST-AGG1 were selected for sequencing and after verification they were used for expression studies.

4.8.2 Cloning into pQE-80L vector

The TAIR plasmids (Table 3.1) harboring the genes encoding *AGB1* and *AGG2* were isolated from host *E. coli* DH10B and PIR1 cells to be used as template in PCR. *AGB1* and *AGG2* were PCR amplified using primers designed according to the PUBMED sequences (Gene ID: 829597 and 825532 respectively) with *Bam*HI and *Kpn*I restriction enzyme sites (Table 4.27). In the forward primers start codon was not included in order to fuse the coding sequence with the RGS-His tag.

Table 4.27: Primers designed for cloning into pQE-80L.
Restriction enzyme sites are underlined.

Primers for <i>AGB1</i>		
Forward Primer	AGB1F	5'-AAA <u>AGGATCCT</u> CTGTCTCCGAGCT-3'
Reverse Primer	AGB1R	5'-:TCT <u>GGTACCAATCA</u> CTCTCCTGTG-3'
Primers for <i>AGG2</i>		
Forward Primer	AGG2F	5'-AA <u>AGGATCCG</u> AAGCGGGTAGCT-3''
Reverse Primer	AGG2R	5'-AA <u>AGGTACCA</u> AAGAATGGAGCAG-3'

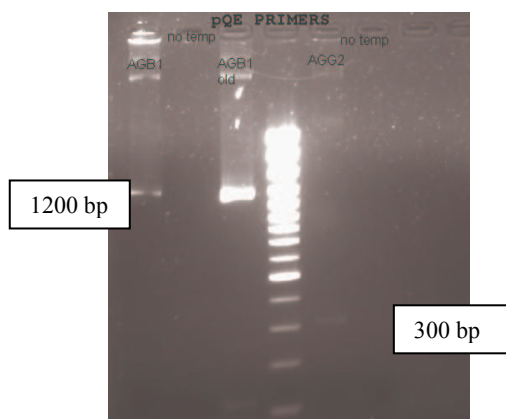


Figure 4.143: 1% Agarose gel electrophoresis analysis of PCR amplification of *AGB1* and *AGG2* with primers designed for pQE-80L.

Results of PCR, shown in Figure 4.143, indicate amplification of fragments AGB1, 1200 bp and AGG2, 300 bp long.

Restriction enzyme digested PCR products and the linear vector were ligated and *E.coli* TOP10F' cells were transformed with different amounts of the ligation mixtures. Positive clones were chosen from the colonies that grew on LB-amp plates and the presence of inserts was verified by colony PCR and restriction enzyme digestion.

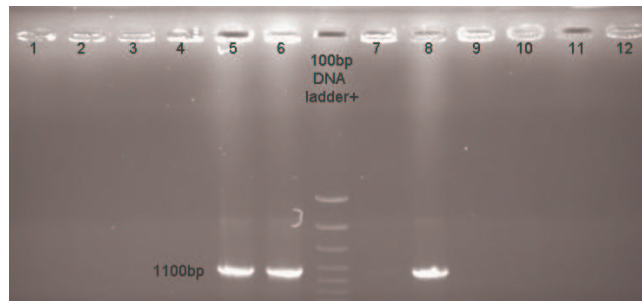


Figure 4.144: 1% Agarose gel electrophoresis analysis of colony PCR with *AGB1* primers.

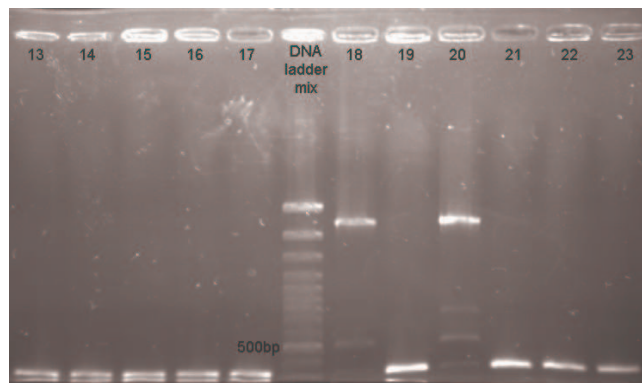


Figure 4.145: 1% Agarose gel electrophoresis analysis of colony PCR with *AGG2* primers.

The colonies 5, 6 and 8 contain the *AGB1* gene (Figure 4.144) and all colonies except 18 and 20 contain the *AGG2* gene (Figure 4.145). Plasmids were isolated from

the selected colonies harboring the inserted genes. Plasmids were double digested with the restriction enzymes *Bam*HI and *Kpn*I to verify the presence of the inserts.

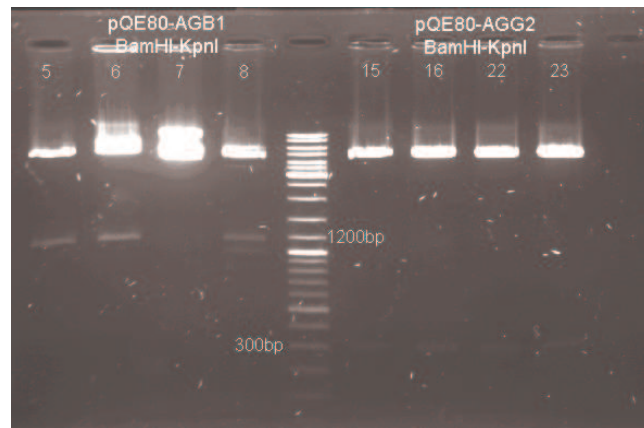


Figure 4.146: 1% Agarose gel electrophoresis analysis of restriction enzyme digestion of selected plasmids. Lane 5: O'GeneRuler Mix ®.

Colonies 5 and 6 contain the *AGB1* gene. All colonies tested for *AGG2* contained the gene. Plasmids from colony 6 and colony 16 (Figure 4.146) were sequenced and after verification they were used for expression studies. The constructs were named RGS-his-AGB1 and RGS-his-AGG2.

4.8.3 Expression and Purification of AGB1

a. GST-AGB1

GST-AGB1 was obtained in inclusion body fractions and different host strains (BL21 (DE3) and BL21 (DE3) RIPL) and induction parameters (Table 4.28) were investigated to solubilize the protein. The molecular mass of GST is 27 kDa and that of AGB1 is 41 kDa, so that the recombinant fusion protein is expected to have a molecular mass of 69 kDa.

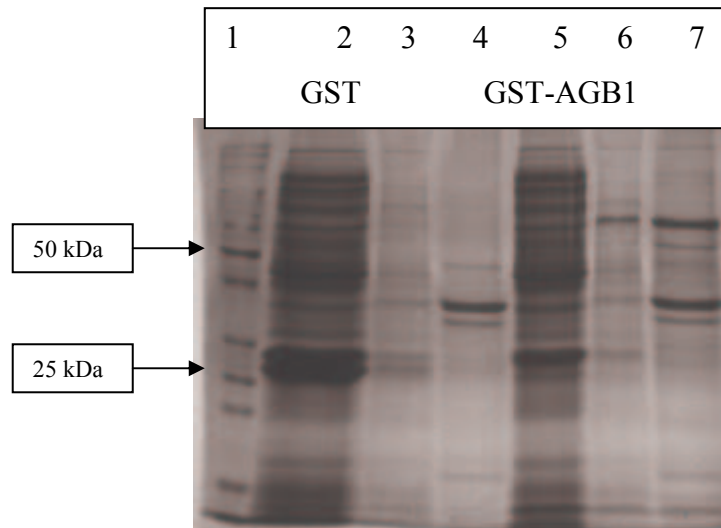


Figure 4.147: 12% SDS-PAGE analysis of GST-AGB1 expression at 18 ° C. Induction was with 0.3 mM IPTG for 4 hours. Lane 1: Protein ladder @, lanes 2 and 5: lysate, lanes 3 and 6: supernatant (UP), lanes 4 and 7: pellet (IP). Samples were prepared with 6X loading dye.

Table 4.28 Expression of GST-AGB1 in inclusion body fractions at different induction parameters. UP: urea soluble, IP: urea insoluble.

Host	Temperature	IPTG, mM	Fraction
BL21(DE3)	37 °C	0.6	IP
BL21(DE3)	37 °C	0.5	IP
BL21(DE3)	28 °C	0.5	IP
BL21(DE3)	18 °C	0.5	UP and IP
BL21(DE3)	18 °C	0.3	UP and IP
BL21(DE3)RIPL	29 °C	0.5	UP/IP

GST-AGB1 was not in soluble fractions even under low temperature and low IPTG conditions (Figure 4.147). In order to obtain soluble protein pQE-80L expression system was investigated.

b. RGS-his-AGB1

RGS-his-AGB1 construct was introduced into TOP10 and Rosetta 2 (DE3) cells. TOP10 cells harboring the RGS-his-AGB1 construct were induced with 0.5 mM IPTG at 25 °C. The expected size of the recombinant protein is ~ 44 kDa. The expression was screened by RGS-his–HRP antibody binding after transfer to PVDF membranes.

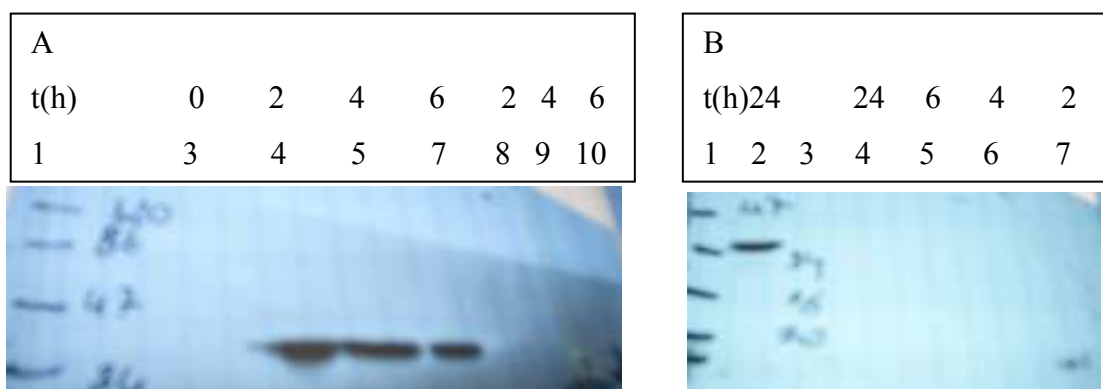


Figure 4.148: Western analysis of RGS-his-AGB1 expression.

A: Lane 1: Prestained protein MW marker ®, lanes 3-6: samples induced with 0.5 mM IPTG, lanes 7-9: non-induced samples. B: Lane 1: Prestained protein MW marker ®, lane 2: RGS-his-AGB1, lanes 4-7: pQE-80 empty vector induced with 0.5 mM IPTG. Membranes were incubated with 1:2400 antibody in Qiagen reagent.

The Western blots in Figure 4.148 indicated that the recombinant protein was expressed in the soluble cytosolic fraction 2 hours after induction at 25 °C.

Several different purification conditions, given in Table 4.29, were investigated to improve the yield and homogeneity of purified recombinant proteins. The results show that RGS-his-AGB1 was co-eluted with a 60 kDa contaminant protein at ~200 mM imidazole. There was another co-purifying protein with a molecular mass ~43 kDa, this protein was separated from RGS-his-AGB1 when NaPO₄ buffers were used. The yield of RGS-his-AGB1 was very low for all the expression and purification conditions investigated.

Table 4.29: Purification Conditions for RGS-his-AGB1

Prep /Culture	Buffers		Affinity Media	Gradient	Result
	Lysis	Purification			
1: Tris pH 8.0 / 100 ml -5 h	50 mM Tris HCl, pH 8.0, 5 % glycerol, 10 mM MgCl ₂ , 2 mM PMSF , EFPI	50 mM Tris HCl pH 8.0, 300 mM NaCl, 10 mM BME, 0.1 mM PMSF and 10 mM imidazole	Ni-NTA Agarose	N.A	Eluted in flowthrough
2: PBS pH 7.5 / 100 ml -20 h	1X PBS pH 7.5, 0.5 mM MgCl ₂ , 5 % glycerol, 1 mM DTT , EFPI	Binding:Lysis Buffer, Wash: 5 mM imidazole in Lysis Buffer	Ni-NTA Agarose	N.A	150 and 200 mM imidazole, very low amount.
3: NaPO ₄ pH 7.0 / 170 ml -5 h	50 mM NaPO ₄ , pH 7.0, 150 mM NaCl, 10 mM MgCl ₂ , 5% glycerol, 2 mM PMSF, EFPI	Binding:Lysis Buffer Wash: 10 mM imidazole in Lysis Buffer	HisTrap HP, 5 ml	10-400 mM imidazole, 6 CV	200 mM imidazole,very low amount.
4: NaPO ₄ , pH elution / 500 ml - 5 h	50 mM NaPO ₄ , pH 7.0, 150 mM NaCl, 10 mM MgCl ₂ , 2 mM PMSF, EFPI	Binding:Lysis Buffer Wash: 30 mM imidazole in Lysis Buffer, pH 7.2	HisTrap HP, 5 ml	30-400 mM imidazole (pH 7.2 to 7.5), 6 CV	200 mM imidazole with 60 kDa protein. 43 kDa protein separated.
5: NaPO ₄ pH 7.0, Lubrol / 500 ml - 5 h	50 mM NaPO ₄ , pH 7.0, 150 mM NaCl, 10 mM MgCl ₂ , 2 mM PMSF, 1 mM EDTA, 0.1 % Lubrol, EFPI	Binding:Lysis Buffer Wash: 30 mM imidazole in Lysis Buffer,with 0.05% Lubrol, 1mM DTT and no EDTA	HisTrap HP, 5 ml	30-400 mM imidazole, 6 CV	200 mM imidazole with 60 kDa protein. 43 kDa protein separated
6: Tris pH 8.9 / 600 ml - 5 h	50 mM Tris HCl, pH 8.9, 150 mM NaCl, 10 mM MgCl ₂ , 5% glycerol, 2 mM PMSF, EFPI	Binding:Lysis Buffer Wash: 10 mM imidazole in Lysis Buffer	HisTrap HP, 5 ml	10-400 mM imidazole, 6 CV	200 mM imidazole with 60 kDa and 43 kDa protein

- **Purification with NaPO₄ Buffer , pH elution**

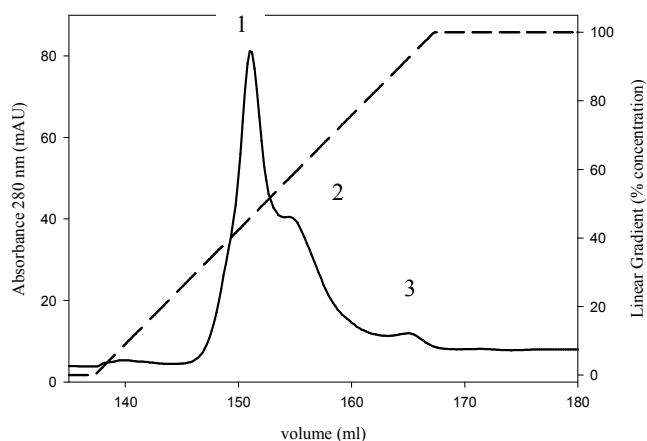


Figure 4.149: HisTrap HP column chromatogram of elution of RGS-his-AGB1 with linear imidazole and pH gradient. Imidazole gradient (- -) and absorbance at 280 nm (-) are shown.

The linear gradient resulted in the separation of 3 main peaks (Figure 4.149), fractions of which were pooled and buffer exchanged either by dialysis or by desalting on a HiTrap desalting column using 50 mM NaPO₄, pH 7.0, and 150 mM NaCl buffer.

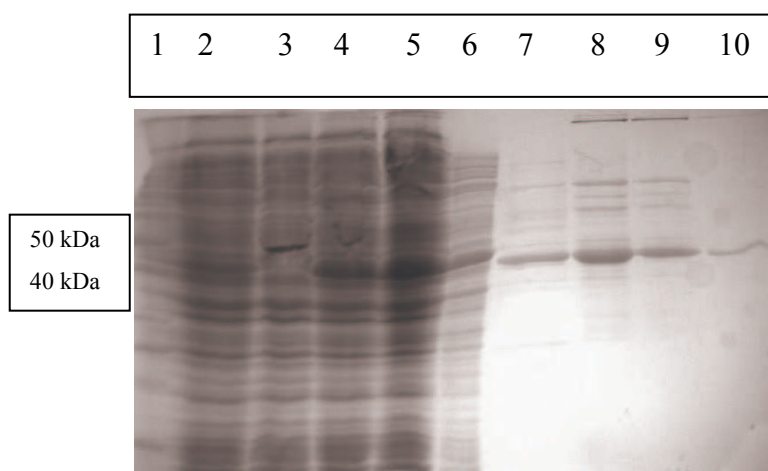


Figure 4.150: 12% SDS-PAGE analysis of HisTrap HP column fractions. Lane 1: Protein ladder ®, lane 2: CL, lanes 3-5: FT, lane 6: wash, lane 7: peak 1 first fraction, lane 8: pool 1, lane 9: pool 1 desalted, lane 10: pool 1 dialyzed. Proteins in lanes 2-6 were prepared with 3X, others were prepared with 6X loading dye.

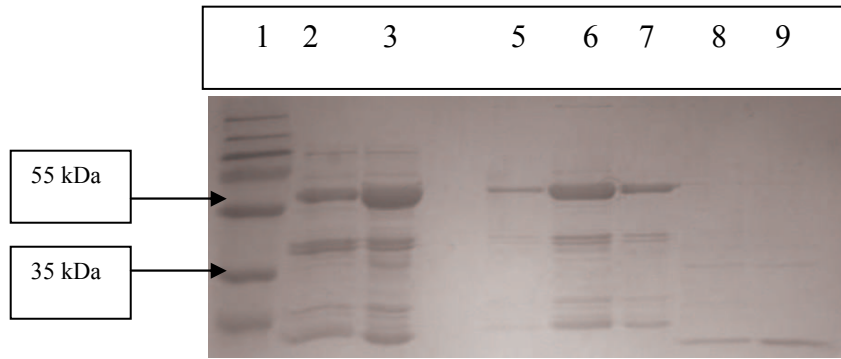


Figure 4.151: 12% SDS-PAGE analysis of HisTrap HP column fractions. Lane 1: Prestained Protein ladder Plus ®, lane 2: peak 2 first fraction, lane 3: peak 2 pool, lane 5: peak 2 last fraction, lane 6: desalted pool, lane 7: dialysed pool, lanes 8-9: peak 3 fractions. Samples were prepared with 6X loading dye.

The dominating protein in pool 1 had a molecular mass between 40-50 kDa (Figure 4.150) whereas the major component in pool 2 was in the range 55-70 kDa (Figure 4.151). There were two proteins with molecular masses ~43 kDa in pool 2. RGS-his-AGB1 was identified by Western blot with RGS-his-HRP antibody.

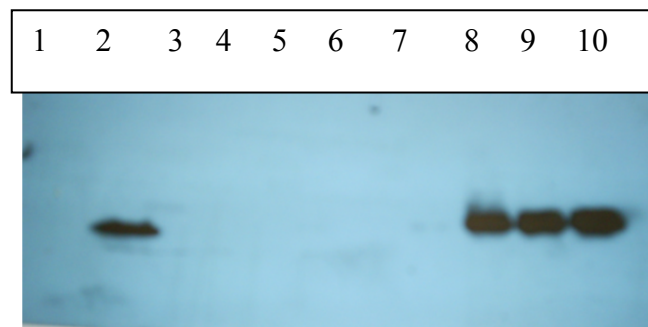


Figure 4.152: Western analysis of HisTrap HP column fractions. Lane 1: Prestained protein ladder ®, lane 2: CL, lane 3: FT, lane 4: wash, lane 5: pool 1, lane 7: pool 1 dialyzed, lane 8: pool 2, lane 9: pool 2 desalted, lane 10: pool 2 dialyzed. Membrane was incubated with 1:3000 RGS-his -HRP and film was exposed for 1 minute.

The signal from antibody was seen only for pool 2 fractions after 1 min (Figure 4.152) or 30 min exposure (data not shown). The dominant protein in pool 1 was probably another protein of similar molecular mass.

- **Purification with Tris Buffer pH 8.9**

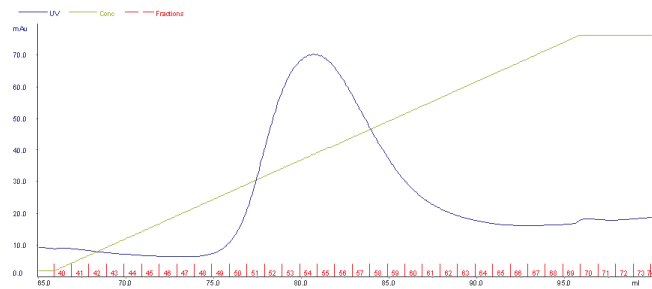


Figure 4.153 HisTrap HP column chromatogram of elution of RGS-his-AGB1 with a linear imidazole gradient. Imidazole gradient (green), absorbance at 280 nm (blue) and fraction numbers (red) are shown.

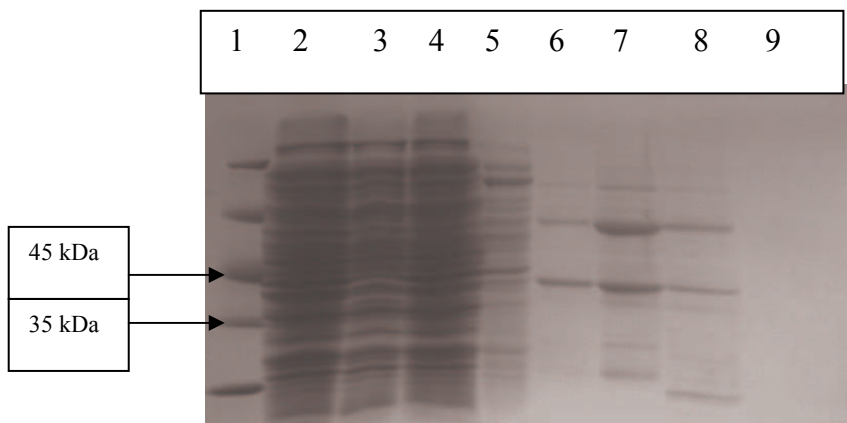


Figure 4.154: 12% SDS-PAGE analysis of HisTrap HP column fractions. Lane 1: Protein MW marker ®, lane 2: CL, lanes 3-4: FT, lane 5: wash, lane 6: f51, lane 7: f54, lane 8: f61, lane 9: f72. Samples were prepared with 6X loading dye.

60 kDa and ~43 kDa proteins co-eluted from HisTrap HP column (Figure 4.153 and Figure 4.154). RGS-his-AGB1 was identified by Western blot with RGS-his-HRP antibody.

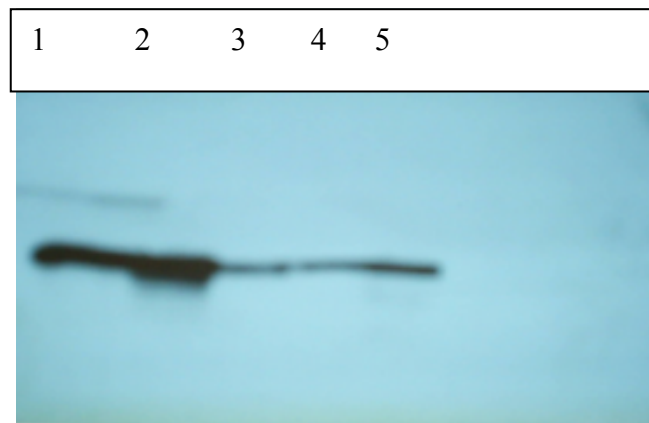


Figure 4.155: Western analysis of HisTrap HP column fractions. Lane 1: CL, lanes 2-3: FT, lane 4: f55, lane5: f66. Membrane was incubated with 1:2000 RGS-his-HRP and film was exposed for 1 min.

The RGS-his-AGB1 protein was purified from cells with Tris pH 8.9 buffer, but most of the protein was lost in flow-through fractions (Figure 4.155). The proteins with molecular masses of 60 and 43 kDa were blotted onto PVDF membranes for Edman degradation. The results are given in Appendix I. The 60 kDa protein is similar to GRoEL, a chaperone protein. The 43 kDa band contains two proteins; the dominant one is *E.coli* lac repressor protein. The ratio of RGS-his-AGB1 in the sample was not enough to assign amino acids.

As a final approach the RGS-his-AGB1 construct was introduced into Rosetta 2 (DE3) cells which contain an extra plasmid that supply the tRNA for the rare codons in *E.coli* for Arg (AGG, AGA,CGG), Ile (AUA), Leu (CUA), Pro (CCC) and Gly (GGA). The transformed cells were grown at 29 °C until OD reached 0.8 and were induced with 0.5 mM IPTG. The results in Figure 4.156 show that the expression of RGS-his-AGB1 was still very low and decreased after prolonged induction. As a control the expression of RGS-his-AGG2 was also screened to compare the expression levels.

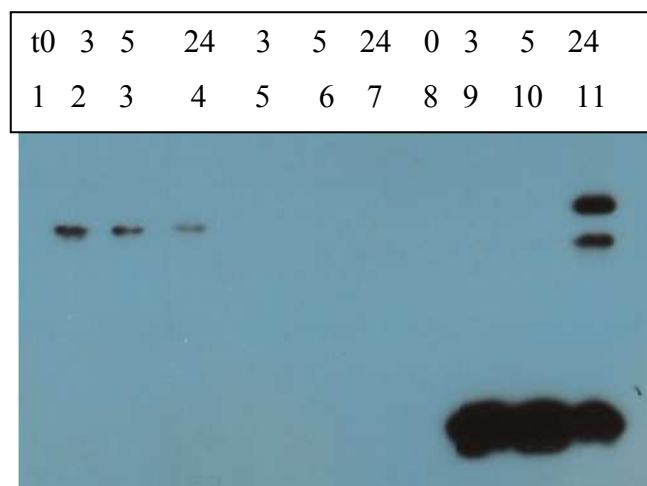


Figure 4.156: Western analysis RGS-his-AGB1 expression from Rosetta 2 (DE3) cells. Lanes 1-7: RGS-his-AGB1 screen, lanes 1-4: samples induced with 0.5 mM IPTG, lanes 5-7: non-induced samples. Lanes 8-11: RGS-his-AGG2 screen, samples induced with 0.5 mM IPTG. Membranes were incubated with 1:2000 antibody in Qiagen reagent. Exposure time was 10 minutes.

4.8.4 Expression and Purification of GST-AGG1

GST-AGG1 was obtained in inclusion body fractions of BL21 (DE3) cells and different induction parameters (Table 4.30) were investigated to solubilize the protein. The molecular mass of GST is 27 kDa and that of AGG1 is 12 kDa, so that the recombinant fusion protein is expected to have a molecular mass of 39 kDa. GST-AGG1 was found in urea insoluble inclusion body fractions (pellet) for all conditions screened, including induction at 18 °C with 0.3 mM IPTG (Figure 4.157).

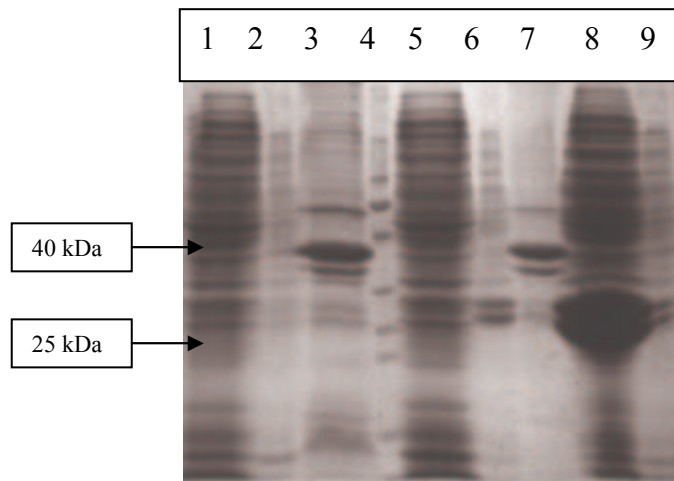


Figure 4.157: 12% SDS-PAGE analysis of GST-AGG1 expression at 18 °C. Induction was done with 0.5 mM (lanes 1-3) or 0.3 mM (lanes 5-7) for 24 hours. Lanes 1 and 5: GST-AGG1 lysate, lanes 2 and 6: GST-AGG1 supernatant (UP), lanes 3 and 7: GST-AGG1 pellet (IP), lane 4: Protein ladder®, 8: GST lysate. Samples were prepared with 6X loading dye.

Table 4.30: Expression of GST-AGG1 in inclusion body fractions at different induction parameters. UP: urea soluble, IP: urea insoluble.

Host	Temperature	IPTG, mM	Fraction
BL21(DE3)	37 °C	0.6	IP
BL21(DE3)	37 °C	0.5	IP
BL21(DE3)	28 °C	0.5	IP
BL21(DE3)	18 °C	0.5	IP
BL21(DE3)	18 °C	0.3	IP

4.8.5 Expression and Purification of RGS-his-AGG2

TOP10 cells harboring the RGS-his-AGG2 construct were induced with 0.5 mM IPTG 25 °C. The expected molecular mass of the recombinant protein is ~ 14 kDa. The expression was screened by RGS-his-HRP antibody binding after transfer to PVDF membranes. The recombinant protein was expressed in the soluble cytosolic fraction after 4 hours of induction at 25 °C (Figure 4.158).



Figure 4.158: Western analysis of RGS-his-AGG2 expression at 25 °C. Lane 1: Prestained protein MW marker @, lanes 2-5: samples induced with 0.5 mM IPTG, Lanes 6-8: non-induced samples. The membrane was incubated with 1:2400 RGS-his-HRP.

Several different purification conditions, as indicated in Table 4.31 were investigated to improve the yield and homogeneity of purified recombinant proteins.

Table 4.31: Purification conditions for RGS-his-AGG2

Prep/Culture	Buffers		Affinity Media	Gradient	Flowrate	Result
	Lysis	Purification				
1: PBS pH 7.5 / 100 ml - 20h	PBS pH 7.5, 0.5 mM MgCl ₂ , 5 % glycerol, 1 mM DTT , EFPI	Binding:Lysis Buffer Wash: 5 mM imidazole in Lysis Buffer	Ni-NTA Agarose	N.A	N.A	Eluted pure at 250 mM, 150 and 200 mM imidazole; low purity.
2: PBS pH 7.5 / 100 ml - 5 h	PBS pH 7.5, 0.5 mM MgCl ₂ , 5 % glycerol, 1 mM DTT , EFPI	Binding:Lysis Buffer Wash: 10 mM imidazole in Lysis Buffer	HisTrap HP, 5 ml	10-1000 mM imidazole, 6 CV	3 ml/min binding and wash, 1 ml/min elution	Eluted at the end of gradient; 1M imidazole with high purity.
3: NaPO ₄ , pH 7.0 / 200 ml - 5 h	50 mM NaPO ₄ , pH 7.0, 150 mM NaCl, 2 mM MgCl ₂ , EFPI	Binding:Lysis Buffer Wash: 100 mM imidazole in Lysis Buffer	Ni-NTA Agarose	N.A	N.A	Eluted with 400 mM imidazole, purity lower.
4: Tris pH 7.5, / 150 ml /-5 h	50 mM Tris HCl pH 7.5, 150 mM NaCl, 0.5 mM MgCl ₂ , 5 % glycerol, 1 mM DTT, 2 mM PMSF, EFPI	Binding: Lysis Buffer Wash: 10 mM imidazole in Lysis Buffer	HisTrap HP, 5 ml	10-1000 mM imidazole, 6 CV	3 ml/min binding and wash, 1 ml/min elution	Eluted with ~500 mM imidazole, high purity.

- **Purification with PBS Buffer pH 7.5**

Cell lysate, flow-through, wash and elution fractions were analyzed both by coomassie staining and RGS-his-HRP antibody binding.

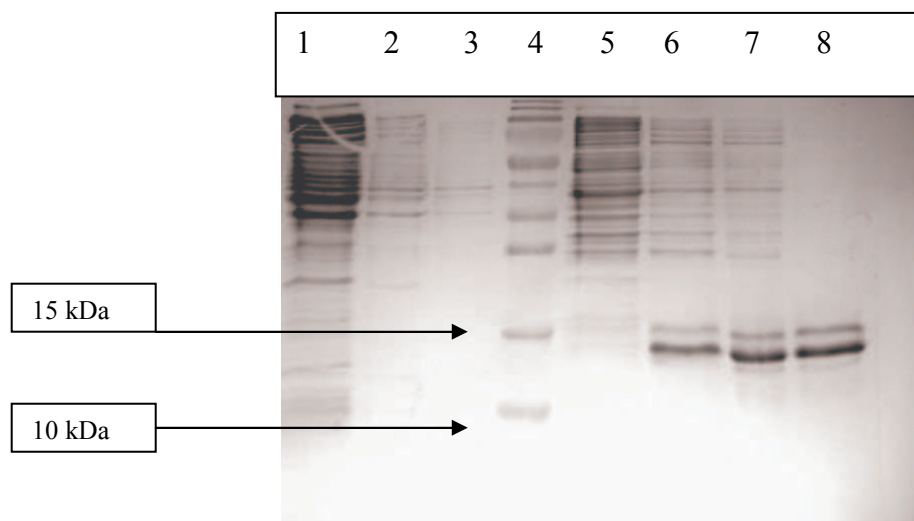


Figure 4.159: 15% SDS-PAGE analysis of Ni-NTA RGS-his-AGG2 fractions. Lane 1: FT, lane 2-3: wash 1-2, lane 4: Prestained protein ladder®, lane 5-8: 1 ml elutions with 100, 150, 200 and 250 mM imidazole respectively. Samples were prepared with 6X loading dye.

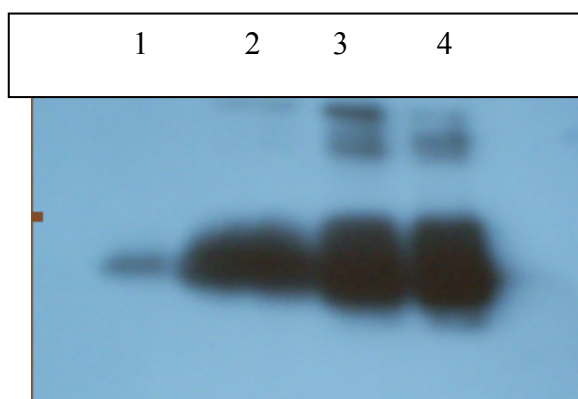


Figure 4.160: Western analysis of Ni-NTA RGS-his-AGG2 fractions. Lanes 1-4: elution fractions; 1: 100 mM, 2: 150 mM, 3: 200 mM and 4: 250 mM respectively. Membrane was incubated with 1:3000 RGS-his-HRP.

High purity protein was obtained with 250 mM imidazole (Figure 4.159). In the western blot there are high molecular mass proteins/complexes that give a significant signal (Figure 4.160).

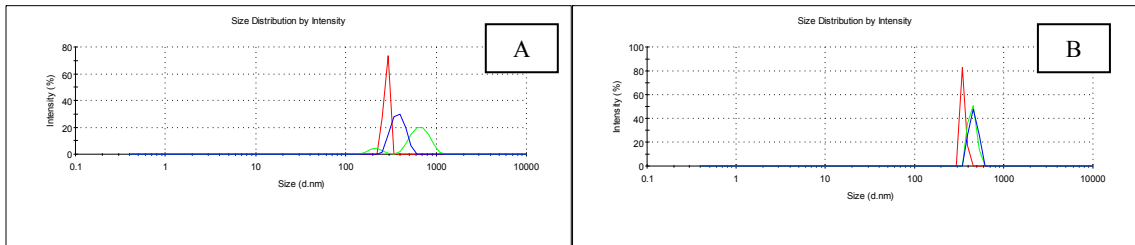


Figure 4.161: DLS size distributions by intensity of RGS-his-AGG2 (A) and (B) PBS buffer.

The DLS measurements (Figure 4.161) were not conclusive since the buffer itself contains particles with similar size to those observed in the protein solution.

- **Purification with NaPO₄ Buffer pH 7.0**

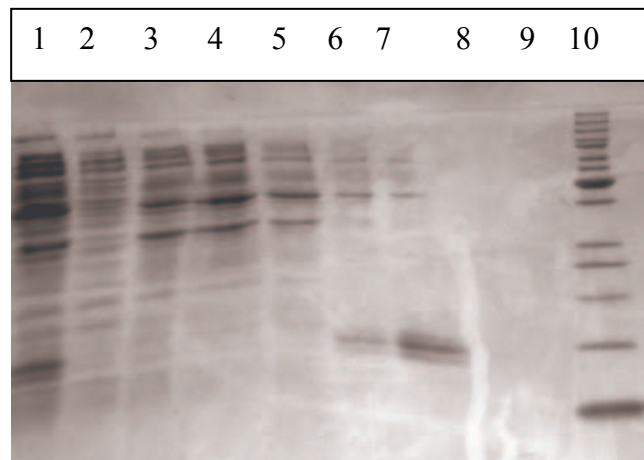


Figure 4.162: 15% SDS-PAGE analysis of batch purification RGS-his-AGG2 fractions. Lane 1: CL, lane 2: FT, lanes 3-5: wash, lanes 6-7:400 mM imidazole elutions 1 and 2, lane 10: protein ladder ®. Samples in lanes 1-5 were prepared with 2X; others were prepared with 6X loading dye.

Table 4.32: Absorbance values and concentration estimations for RGS-his-AGG2

Sample	Absorbance (AU)		concentration mg/ml
	260 nm	280 nm	
RGS-his-AGG2 E1	1.02	0.63	0.5355
RGS-his-AGG2 E2	0.54	0.35	0.2975

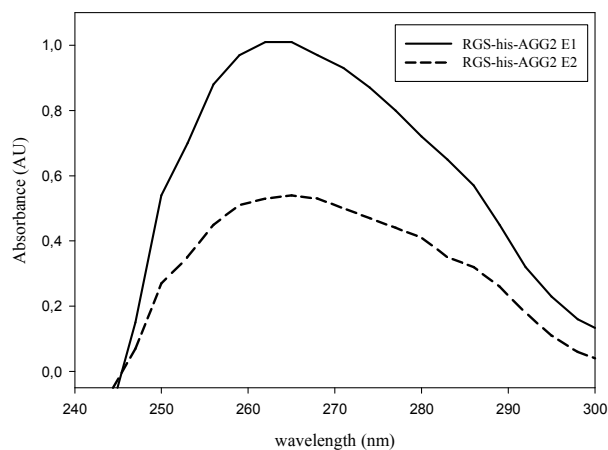


Figure 4.163: UV spectra of RGS-his-AGG2.

The samples were eluted with 5 ml imidazole buffer. The absorbance of proteins at 280 nm was measured (Figure 4.163 and Table 4.32) and concentrations were calculated with a theoretical extinction coefficient of 0.85. The total protein in E1 was 2.6 mg and 1.5 mg in E2. The total yield was ~4 mg protein / 200 ml culture. The protein purity was lower in NaPO₄ buffer than with PBS. The particle diameter was found ~10 nm by DLS measurements (Figure 4.164).

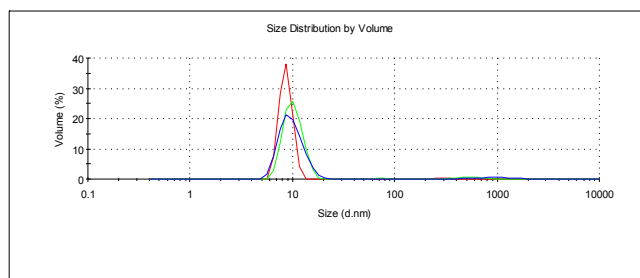


Figure 4.164: DLS size distributions by volume of RGS-his-AGG2 (elution 2).

- **Purification with Tris Buffer pH 7.5; Column Purification**

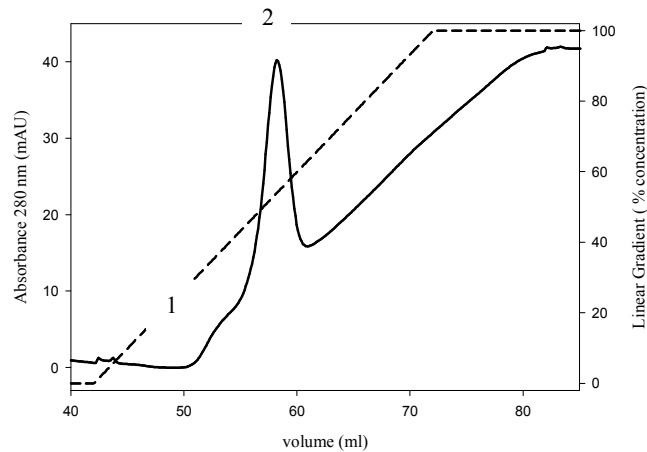


Figure 4.165: HisTrap HP chromatogram of RGS-his-AGG2 elution with a linear imidazole gradient. Imidazole gradient (- - -) and absorbance at 280 nm (-) are shown.

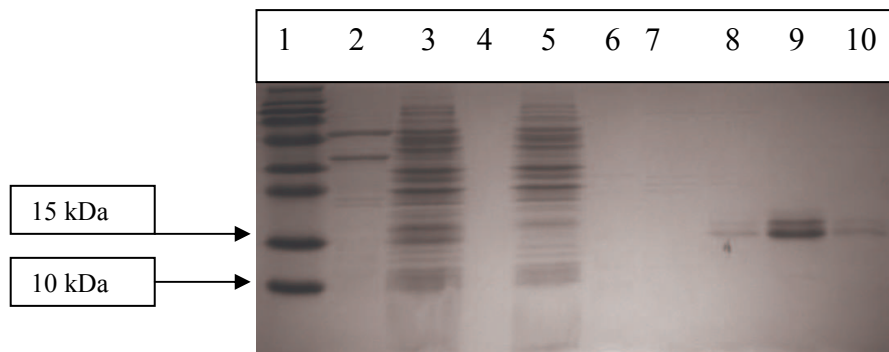


Figure 4.166: 15% SDS-PAGE analysis of RGS-his-AGG2 fractions. Lane 1: Prestained protein ladder Plus ®, lane 2: RGS-his-AGB1 sample, lane 3: CL, lane 5: FT, lane 6: wash, lane 7: peak 1 fraction lanes 8-10: peak 2 fractions, first, top and last. Samples in lanes 3, 5 and 6 were prepared with 2X; others were prepared with 6X loading dye.

Pure RGS-his-AGG2 was eluted with ~500 mM imidazole (Figure 4.165 and Figure 4.166) and fractions were pooled and dialyzed against 50 mM Tris HCl, pH 8.9, 150 mM NaCl, 1 mM PMSF. After dialysis the absorbance value at 280 nm was 0.261

(Figure 4.167) and concentration was 0.22 mg/ml. The total yield was 1.33 mg /150 ml culture.

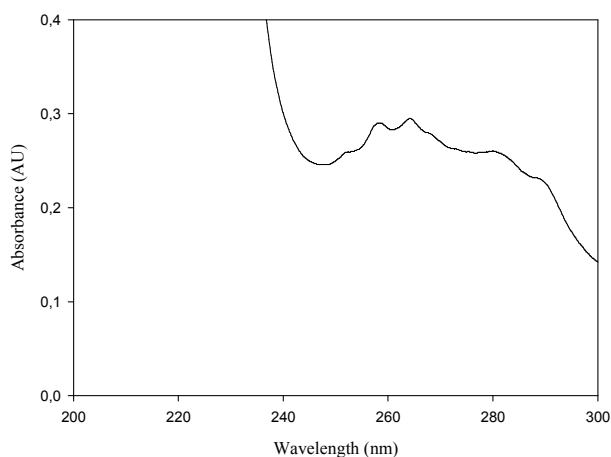


Figure 4.167: UV spectra of RGS-his-AGG2.

The pool was further characterized by DLS, and the size distribution was similar to that in PBS. Unlike PBS there was no contribution from the buffer to the size distribution (Figure 4.168).

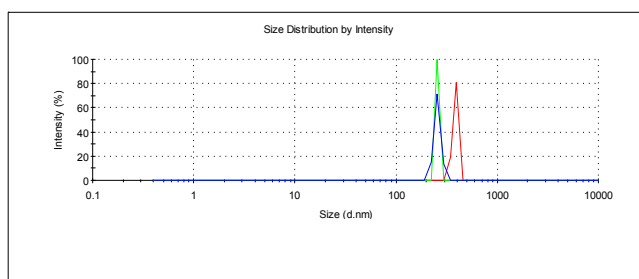


Figure 4.168: DLS size distributions by intensity of RGS-his-AGG2 after dialysis.

4.8.6 Dimerization

Attempts to produce AGB1 and AGG1/2 dimers *in vitro* were carried out on purified proteins in buffer NaPO₄, pH 7.0 purified from prep number 3 (Table 4.29) and prep 2 (Table 4.31) respectively. The proteins were concentrated and the buffer was exchanged to NaPO₄, pH 7.0 using an Amicon YM-3 kDa Centricon unit.

Equal volumes of each protein (without taking into account concentration differences) were combined and equilibrated at room temperature for 2 hours before storing at -20 °C. The presence of dimers was monitored by loading a non-denatured sample onto SDS-polyacrylamide gels together with boiled samples in denaturing loading dye. The non-denatured sample was prepared with 6X native loading dye and was not boiled.

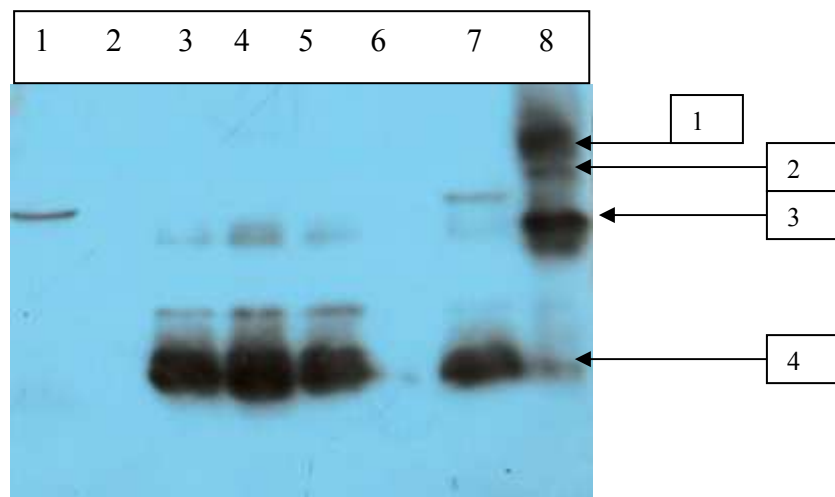


Figure 4.169: Western analysis of complexes of RGS-his-AGB1 and RGS-his-AGG2. Lane 1:RGS-his-AGB1, desalted Ni-NTA fraction, lanes 3-5: RGS-his-AGG2, Ni-NTA elution, concentrated and desalted, lane 8: dimer with 6X SDS loading dye, lane 9: dimer with 6X native loading dye. Membrane incubated with 1:2000 RGS-his HRP.

A comparison of the bands in western blot analysis shown in Figure 4.169 lanes 8 and 9 reveals the presence of large molecular mass components in the non-denatured sample (lane 9). This experiment was repeated with RGS-his-AGB1 and RGS-his-AGG2 samples from different purifications and the same result was obtained (data not

shown). The large molecular mass components seen only in non-denatured protein mixtures show that the two subunits can form complexes.

The intensity of RGS-his-AGB1 and RGS-his-AGG2 bands are lower in non-denatured sample as compared to denatured sample. In the denatured sample (lane 8) the discrepancy between the concentrations of the beta and the gamma subunits is clearly seen.

In the non denatured samples 4 bands are observed. Band 4 corresponds to monomeric form of RGS-his-AGG2 and band 3 is observed also in the gamma subunit samples in lanes 3-5. Band 2 migrates to a position that is slightly above that observed for RGS-his-AGB1 and is likely to represent the dimer. Band 1 may represent complexes with varying gamma subunit content. Note that a band corresponding to RGS-his-AGB1 is missing and band 4 is significantly weaker than the corresponding band in lane 8.

CHAPTER 5

5 DISCUSSION

The structures of the plant G-protein heterotrimer or the individual subunits are not yet known, unlike the mammalian heterotrimer, which is both biochemically and structurally well characterized.

Sequence homologies show that plant heterotrimeric G proteins contain the functional domains present in mammalian counterparts and models generated based on sequence alignments point to a very similar structure.

Mammalian G α was mainly produced using *E.coli* or insect cells, or was directly isolated from native tissue. Chimeric or N-terminus truncated proteins were produced in some cases to increase expression levels and solubility [14]. The general purification procedure for *E.coli* produced mammalian G α involved DEAE ion exchange, phenyl sepharose hydrophobic interaction chromatography, followed by Q Sepharose anion exchange and/or gel filtration [136]. His-tagged recombinant G α was purified using a nickel affinity purification followed by a anion exchange chromatography procedure [56]. Our initial plan for purification of GPA1 from *P.pastoris* followed a similar line.

G β and G γ subunits were either isolated from tissue or recombinantly produced from insect cells [26] or by in vitro translation [25]. G β was shown to be unstable in the

absence of $G\gamma$. Separately produced proteins were shown to dimerize, co-expression/translation is not necessary for dimerization [25]

We have been working on recombinant protein production mainly for structural analysis which requires highly purified and monodisperse protein at high concentration.

Protein quality is affected by main factors, including ionic strength and pH of the environment, the stability of the buffer system used, storage conditions and freeze-thaw cycles, and presence of ligands or other proteins. The stability of the recombinant proteins can be modified by changing any of these parameters. Well-defined and reproducible methods must be developed to analyse these changes.

There are several possible outcomes if the correct parameters are not applied; the most important ones are degradation and aggregation. Western transfer can detect degradation if there are available antibodies against different sites of the protein. Aggregation can be detected by native polyacrylamide gels and also with uv-vis spectrophotometry and dynamic light scattering measurements.

Following initial purification trials, it was shown that the purification results differ from those of mammalian $G\alpha$ expressed in *E.coli* with the above mentioned parameters. The purification procedure was optimized in detail as discussed below.

5.1 Purification of GPA1

The present study is, to our knowledge, the first report in the literature on expression of GPA1 in a eukaryotic expression system for purification and biophysical characterization of the recombinant protein. The GPA1 gene was introduced into the genome of *P.pastoris* with a C-terminal his tag and recombinant protein expression was optimized with respect to cell viability and protein amount. In order to improve the amount of protein methanol addition time was optimized and cells were harvested at the 48th hour of induction, methanol was supplemented at 6th and 24th hours during induction. GPA1 could be synthesized satisfactorily in the *P. pastoris* system, however, the level of protein expression was not reproducible which is an observation made also by others for other proteins [137, 138]. Similarly, the effect of proteolytic enzymes was also variable despite the use of protease inhibitors.

The initial step of purification involved isolation of the recombinant GPA1 from the cell lysate by nickel affinity chromatography. The best results were obtained using a Ni-NTA agarose matrix for batch purification. GPA1 was eluted with 300 mM imidazole in elution buffers. GPA1 co-purified with contaminating proteins of mass ~90, ~80 and ~40 kDa. (Figure 4.14) The 40 kDa protein appears to be a common contaminant of nickel affinity purification from *P.pastoris* [139]. The 90 kDa protein was later shown to be an oligomeric form of GPA1 that formed via intermolecular disulfide bridges (Figure 4.30).

The heterogeneity in affinity purified GPA1 preparations was also shown by DLS measurements (Figure 4.17). Removal of imidazole by desalting increased the sample homogeneity but resulted in protein loss (Table 4.6). Therefore dialysis was performed routinely. Following buffer exchange, GPA1 was found to be stable when stored with GDP and glycerol. The affinity elution buffer supplemented with glycerol was the optimum condition for storage (Figure 4.20). Affinity purified GPA1 was stored at -20

°C with 10 % glycerol and buffer exchange was done immediately before further purification steps.

The initial protein characterization was done by monitoring the UV spectrum, which indicated the presence of GDP in the protein solutions. For protein concentration calculations an equation which took into account the presence of nucleotides was therefore used [124]. Excess GDP was added to affinity purification buffers to stabilize GDP - GPA1. Excess nucleotide resulted in a broad peak extending between 250 and 290 nm (Figure 4.15). After desalting, the excess nucleotide was removed, and the spectrum was dominated by a peak at 280 nm (Figure 4.22). The measurements of GPA1 desalted pool against a buffer without GDP still displayed a hump at 254 nm, which verified the presence of bound GDP (Figure 4.77).

Detergents were included in lysis and purification buffers in order to increase the amount of solubilized GPA1 and to improve protein stability. The effect of Triton X-100 and Lubrol-PX were screened. These two detergents have high aggregation numbers and therefore result in micelles with high molecular mass. Both detergents were shown to effectively solubilize and stabilize membrane integrated proteins without severely affecting protein activity [119]. Furthermore, Lubrol-PX is a routinely used detergent in G α activity assays in order to mimic the physiological environment of the protein [126]. In the presence of Triton X-100 lysis efficiency was better, but the phenyl group of the detergent molecule interfered with the UV measurements (Figure K 10). Further addition of AlF_4^- increased the amount and purity of GPA1 at the nickel affinity step. A similar observation was made by Willard and Siderovski in their work on purification of 6his-GPA1 from *E.coli* [107].

Both detergents formed micelles with diameter ~8.5 nm as shown by DLS (Figure K 5 and Figure K 8). GPA1 purified in the presence of Triton X-100 showed 2 different distributions of particles with diameters 15 and 50 nm (Figure 4.26), which may correspond to protein detergent complexes and/or their higher oligomeric forms. Dialysis resulted in further oligomerization of smaller particles (Figure 4.28). GPA1 affinity purified with Lubrol-PX formed relatively smaller particles, again with diameters increasing after dialysis (Figure 4.32).

Affinity purified GPA1 was found to bind ~0.72 mole GDP/mole protein and 1 mole GDP/mole protein, respectively in the absence and presence of Lubrol-PX (Table 4.14). GTP binding was analyzed with radioactive GTP γ S and was found to be 0.3 mole GTP γ S/ mole protein (Figure 4.82).

The helical content of affinity purified GPA1 was verified by far-UV CD spectra. The near-UV region in CD spectrum of Triton X-100 (\pm AlF $_4^-$) purified GPA1 had more distinct signals (Figure 4.110) compared to those purified with Lubrol-PX, where the signal/noise ratio was lower. This may be attributed to the stronger stabilizing effect of Triton X-100. CD was previously used by McCusker and Robinson to determine the quality of refolded G α from inclusion bodies from *E.coli* [140]. These authors show that the features observed in the near-UV CD spectrum can serve as indicators of proper folding. Comparison of the signals between 260-280 nm with the control G α i [140] indicated that GPA1 produced from *P.pastoris* was folded correctly (Figure 4.109 and Figure 4.110). Similarly Mannelli et. al. [41] also used CD to verify quality of secondary structure of nickel affinity purified G α o/i

Anion exchange chromatography resulted in separation of two different forms of GPA1, designated as pool 3 and pool 4 (Figure 4.33). Anion exchange pool 3 GPA1 was pure and free of degradation products that were formed during lysis/ affinity purification (Figure 4.39). Pool 3 GPA1 was composed of large molecules with diameter ~100 nm (Figure 4.37.) and this oligomeric form was stable upon storage or lyophilization (Figure 4.47 and Figure 4.45). It was also resistant to degradation or further aggregation (Figure 4.46).

Pool 3 was shown by CD measurements to possess both secondary α helical and tertiary structure. In the presence of GTP γ S the $\theta_{222\text{nm}}$ and $\theta_{208\text{nm}}$ values were lower as compared to those of the GDP bound form (Figure 4.115). This may indicate a structure similar to G α i. G α i has a random coil N-terminus in GDP form and upon GTP binding this becomes buried in the protein, resulting in a better defined structure with a higher α -helical content [20].

Interaction with receptor mimetic compounds was also shown by CD measurements. Previously, Tanaka et.al. had used N-terminal histag fusion G α i from *E.coli* and reported that the interaction with receptor mimetic compounds is dependent on C-terminus by using N-terminus truncated forms [40]. Upon interaction with the receptor the C-terminal helical region may form a coiled-coil loosing its α -helical structure. This in turn will lead to a decrease in helical content and an increase in ellipticity values, as observed for pool 3 GPA1 in the presence of C48/80, MP and Mas7 (Figure 4.116 to Figure 4.118).

In contrast, pool 4 GPA1 was a heterogenous solution containing the degradation products mentioned above (Figure 4.39) and was prone to both degradation and aggregation (Figure 4.46). Pool 4 GPA1 had GTP hydrolysis activity (Figure 4.87) in experiments done on fresh protein preparations but the functional stability was not determined.

The two forms of the protein had different GDP content as analysed by spectrophotometric measurements of both protein and filtrate. UV spectra showed that pool 3 GPA1 had higher amount of GDP as compared to pool 4 GPA1; 1.4 mole GDP/mole protein and 0.8 mole GDP/mole protein, respectively (Table 4.14). Pool 3 GPA1 had slightly higher GTPase activity than pool 4, when Lubrol-PX was used in assay buffers (Figure 4.84). In contrast, both pools had comparable activity when detergent was not included in assay buffers (Table 4.16 and Table 4.17).

The environment of aromatic residues, as deduced from near-UV CD spectra, of pool 4 GPA1 was different from those in pool 3, indicating a difference in their conformation (Figure 4.111-Figure 4.114).

MALDI-TOF-MS results further supported different conformations because the trypsin digestion patterns of pool 3 and pool 4 GPA1 were different (Figure 4.107 and Figure 4.108). The lysine residues in GDP/GTP binding and putative receptor interaction sites were protected in pool 3 but were digested in pool 4 (APPENDIX I). Pool 4 did not contain any lipid modifications as deduced from the detected mass of the N-terminal fragments. On the other hand, pool 3 GPA1 N-terminal 6 amino acid

fragment (GLLCSR) was not detected at all. This can be due to its absence in the original sample or the high hydrophobicity of this region (with the lipid modifications both present) which may prevent this fragment from flying.

The MYR predictor (a server for myristoylation site detection) and CSS Palm 2.0 (a server that detects palmitoylation targets) both predicted GLLCSR peptide as a potential myristoylation (Glycine) and palmitoylation (Cysteine) target (APPENDIX J).

In the case of mammalian $G\alpha$, a myristoylation deficient form of $G\alpha_i$ was shown to be localized in the cytosol [42], a palmitoylation mutant form of myristoylated $G\alpha_o$ was found in cytosol in high amounts [45] and dual lipidated $G\alpha_o$ forms GTP γ S non-reversible oligomers [46]. In plants *in vivo* studies with fluorescent labeled proteins indicate that GPA1 is localized to PM [99] and mutations in the G2, C5 and G2C5 residues resulted in distribution of GPA1 to both cytosol and PM [95]. Following these, our data indirectly supports the presence of the lipid modifications. The evidence are; membrane affinity of GPA1 (Figure 4.93), increased yield upon addition of detergents during affinity purification and a more stable GPA1 oligomer in pool 3.

Size exclusion chromatography was performed in order to separate the monomeric form of GPA1 from oligomers and to determine the molecular mass of the oligomers. According to our results purified GPA1 appeared in different oligomeric forms with masses between 50 kDa and 600 kDa. DLS measurements showed particles with a diameter of 10 nm for the lowest molecular mass fractions (Figure 4.131).

Results of size exclusion chromatography may be interpreted in terms of separation of monomer-oligomer mixtures with different equilibrium constants. Separation of the lowest molecular mass form was only achieved if the protein was purified with GDP- AlF_4^- in the affinity purification step. Thus the presence of AlF_4^- which is commonly used during $G\alpha$ purifications [21], appears to shift the equilibrium in favor of monomers.

Anion exchange pools (pool 3 and pool 4) and the low molecular mass GPA1 obtained by gel filtration had GTP hydrolysis activity as shown by the release of

radioactive phosphate from ^{32}P -GTP. The specific activity was shown to increase with higher protein purity (Figure 4.84). The presence of MgCl_2 was essential for hydrolysis and additionally the presence of detergent resulted in a further increase in the amount of hydrolyzed Pi (Figure 4.88). S-300 purified GPA1 had a slightly higher GTP hydrolysis activity than pool 4 GPA1 (Figure 4.90). The presence of GTP or $\text{GTP}\gamma\text{S}$ inhibited radioactive Pi release, indicating competition (Figure 4.91). In the GDP or GTP bound state the presence of receptor mimetic compound MP resulted in an enhanced GTPase activity, whereas the activity decreased for the $\text{GTP}\gamma\text{S}$ bound form (Figure 4.92).

Recombinant expression of GPA1 from *E.coli* was investigated previously. Wise et al., produced protein by co-transforming a plasmid carrying the *E.coli* rare arginine codons. The protein was purified from an anion exchange column with yields of 1-2 mg/L culture [76]. Willard and Siderovski cloned GPA1 in fusion with an N-terminal his tag and purified it by Ni-affinity followed by gel filtration using a 26/60 S-200 HR column. The yield of protein expression and purification as well as the elution volume from the column indicating the apparent mass of the purified protein was not reported [107]. Wang et al., also report purification of his tagged GPA1 using Ni-NTA agarose [99]. In GTP binding studies of recombinant GPA1, Wise et al., [76] found a ratio of 0.3 mole GTP/mole protein. In another study, Johnston et al. [77] reports a significantly different ratio of 0.9 mole GTP/mole protein using the purification procedure of Willard and Siderovski [107]. In this last study, the recombinant GPA1 was suggested to be GTP bound most of the time and to have a very low hydrolysis rate, suggesting that in contrast to the mammalian $\text{G}\alpha$, GTP form of GPA1 is more abundant in the cell. The rate determining step in GTP hydrolysis was shown to be GDP release for mammalian $\text{G}\alpha$ [38]. Wang et. al. report GTP binding activity but refrain from quantifying of the binding ratio.

Results of Wise et. al. and Johnston et al., should be interpreted cautiously due to complete lack of protein characterization. Our work shows that recombinantly expressed GPA1 is likely to be a heterogenous mixture containing different forms of the protein. These forms differ in stability, oligomeric state and GDP content. Lack of quantification of GTP/GDP binding activity by Wang et al., may also be due to the heterogeneity of the protein produced in *E.coli*.

Our results show that, during gel filtration GPA1 co-purified with detergents, when these were used in the affinity step. Proton NMR data analysis verified the presence of Lubrol-PX (Figure 4.99), and the molarity was found to be nearly equal to the added amount during affinity (Figure 4.101). Detergents added during affinity purification of other membrane integrated/TM proteins were shown to co-elute and were not separated even after extensive dialysis [131]. After anion exchange separation, neither of the GPA1 pools contained detergent, as shown by TCA stain (Figure 4.104). The absence of Triton X-100 was also verified by proton NMR spectra (Figure 4.103).

Small angle solution X-ray scattering experiments performed on affinity purified GPA1 showed the presence of a heterogeneous and aggregated protein pool, verifying the particle size distribution found in DLS measurements. Pool 3 GPA1 scattering data was better but it was still low quality, the molecular mass of the protein after airfuge centrifugation was estimated as 60 kDa, with a radius of gyration of 3.66 nm (Table 4.20). Data collected from S-200 column purified GPA1 pools, each with different molecular mass, resulted in intensity plots similar to those protein-micelle solutions (Figure 4.123). The lowest molecular mass fraction from gel filtration eluted at a mass corresponding to ~75 kDa and SAXS measurements gave a molecular mass of ~100 kDa for the same sample. This corresponds to ~2.5 fold of the theoretical molecular mass of GPA1 (Table 4.23). The calculated particle diameter using the Guinier approximation were in agreement with DLS measurements (Table 4.24). Attempts were made to model this oligomeric form of GPA1-Lubrol using a rigid body approach [132]. The high-resolution crystal structure for G α i-GDPAlF₄ [19] was used to estimate GPA1 oligomeric state. A pentameric form that protein would fit the low angle region of GPA1 scattering plot within acceptable limits (Figure 4.132 and Figure 4.133).

5.2 Expression and Purification of AGB1, AGG1 and AGG2

AGB1 and AGG1 were expressed from pGEX-4T-2 vector as N-terminus GST fusions from BL21(DE)3 cells. Both proteins were produced in inclusion body fractions and attempts to solubilize the proteins failed even at very low temperature and IPTG concentrations (Figure 4.147 and Figure 4.157).

GST-AGB1 was found in the urea soluble pellet only when cells were grown at 18 °C and induced with 0.3 mM IPTG. GST-AGG1 was always produced in the urea insoluble fractions.

A low copy and cis-repressed expression vector, pQE-80L was chosen to obtain soluble protein. Recombinant AGB1 and AGG2 were expressed as an N-terminal fusion with RGSHHHHHH amino acids. Cloning of AGG1 using pQE-80L expression system was not investigated.

RGS-his-AGB1 was produced in very low amounts from both TOP10 and Rosetta 2 (DE) 3 cells. Affinity purification trials resulted in co-purification together with a contaminant protein of similar molecular mass (Figure 4.150 and Figure 4.152). This protein was identified as Lac repressor expressed from the vector itself (APPENDIX I). Cells expressing RGS-his-AGB1 were producing high levels of a 60 kDa protein (Figure 4.151), which was identified as *E. coli* chaperone GRoEL ((APPENDIX I). Both contaminants were expressed predominantly from cells carrying pQE-80L-AGB1 and not from pQE-80L-AGG2. Considering the high numbers of rare *E.coli* codons in the AGB1 gene sequence, expression from Rosetta 2 (DE3) cells was investigated, but the amount of recombinant protein obtained from these cells was still very low (Figure 4.156). The folding process/rate of AGB1 may be energetically unfavorable and slow; resulting in co-expression of the chaperone. Furthermore the co-expression of lac repressor may indicate that the AGB1 which is produced is toxic.

Solubilization of GST-AGB1 from inclusion bodies and renaturation of the protein was not investigated, since we do not have a direct assay to control refolding into the native structure.

Cells harboring GST-AGG1 or RGS-his-AGG2 constructs grew to lower plateau levels than cell expressing AGB1 under all conditions tested (Appendix H). This can be due to the high expression levels of both $G\gamma$ subunits or leaky expression that may lead to toxicity.

RGS-his-AGG2 was produced from TOP10 cells in soluble fractions in moderate amount. The yield after affinity purification was approximately 1-4 mg per 150 ml culture. The highest purity protein was obtained with, Tris pH 7.5 buffer (Figure 4.166), but Na-PO₄ buffer pH 7.0 and PBS pH 7.5 also resulted in separation from contaminants. According to UV spectrophotometry and DLS measurements (Figure 4.163 and Figure 4.164), the affinity purification was optimized with Na-PO₄ buffer. The particle diameter of RGS-his-AGG2 in solution obtained by DLS is approximately 10 nm ie, much larger than expected for a 14 kDa protein. This can be due to the presence of contaminants in the affinity purified protein (Figure 4.162), but the amounts were very low as compared to AGG2. As the mammalian $G\gamma$ are unstructured and very elongated when not in complex with $G\beta$, our results suggests that this is also the case for plant $G\gamma$.

Further optimization of RGS-his-AGG2 purification was not pursued considering the experimental difficulties of both purifying and characterizing this small molecular mass and probably unstructured protein. Furthermore the structural and functional effect of plant $G\gamma$ will be interesting when it is complexed with $G\beta$.

5.2.1 Dimerization

The formation of G $\beta\gamma$ dimer was analyzed by Western detection using RGS-his-AGB1 and RGS-his-AGG2. Large molecular mass components, that do not match to size of either protein alone, were detected only for the non-denatured protein mixtures and were absent from samples loaded in SDS-sample buffer. Furthermore bands corresponding to individual proteins were weaker in the non denatured sample (Figure 4.169). These results show that the two subunits can form complexes.

5.3 Heterotrimer Formation

The interaction of GPA1 with AGB1/AGG2 dimer was shown by Western detection. The presence of dimer reversed the aggregation that was already present in higher molecular mass form (stg. 3.2.1) and furthermore protected GPA1 from degradation (Figure 4.94).

CHAPTER 6

6 CONCLUSIONS

The general aim of the work presented in this thesis was to investigate the structure of Arabidopsis heterotrimeric G proteins. To achieve this goal the Arabidopsis subunits were heterologously expressed. Purification schemes were developed, purified proteins were characterized and the structure of the alpha subunit was investigated by SAXS.

Recombinant GPA1 expression in *P.pastoris* and recombinant expression of AGB1, AGG1 and AGG2 in *E.coli* was achieved. His-tagged recombinant proteins could be purified from host organisms with variable yields. GPA1 was affinity purified with yields of 10-20 mg/L from *P.pastoris*. This is to our knowledge the first report of production of a plant G α from an eukaryotic expression system. GPA1 was shown to bind GTP with a ratio of 0.3 mole GTP/ mole protein.

AGG2 was purified from small scale cultures with yields of about 1-4 mg per 150 ml from *E.coli*. AGB1 yield was very low for all the conditions explored. This is to our knowledge the first study in the literature where plant G β subunit recombinant expression was shown. This work can provide a basis for future studies where co-expression of AGB1 with AGG1/2 will be investigated to increase the yield. Dimerization of AGB1 and AGG2 and heterotrimer formation was detected by western blots.

This is to our knowledge the first study in the literature where protein quality, homogeneity and oligomerization state have been systematically addressed for plant $G\alpha$ proteins. Affinity purified GPA1 was shown to be heterogeneous and two biophysically distinct forms (pool 3 and pool 4) were separated by anion exchange chromatography. Pool 3 appeared to be an oligomeric (as determined by DLS) stable form, whose folding was confirmed by CD measurements and had higher GDP content as shown by UV-spectrophotometry. Pool 3 was bound to 1.4 mole GDP/ mole protein, whereas this ratio was 0.8 mole GDP/mole protein in pool 4. Pool 3 showed higher GTP hydrolysis activity in comparison to pool 4. Patterns of near-UV CD and trypsin digestion for mass spectrometry analysis indicated different conformations in the two pools. In future work kinetic parameters for GTPase activity should be determined to provide insight into activation of the heterotrimer and signaling mechanism in plants.

Membrane localization, higher yield in the presence of detergents and a stable oligomeric form of purified GPA1 point to the presence of lipid modifications. Further work is required to clarify the presence/absence of lipid modifications and in order to perform structural comparisons with mammalian $G\alpha$.

Gel filtration in the presence of detergent resulted in the separation of different oligomeric forms of GPA1. The lowest molecular mass form was stabilized by AlF_4^- . GPA1 was co-purified with the added amount of detergent as determined by proton NMR.

SAXS data of the lowest molecular mass and monodisperse form indicated protein-micelle structures in the solution. Rigid body models were compatible with oligomers of GPA1 resembling pentameric $G\alpha_i$. Solution neutron scattering should be performed in order to gain more information about GPA1 conformation in the protein-micelle complex.

REFERENCES

1. Milligan, G. and E. Kostenis, *Heterotrimeric G-proteins: a short history*. Br J Pharmacol, 2006. **147 Suppl 1**: p. S46-55.
2. Assmann, S.M., *Heterotrimeric and unconventional GTP binding proteins in plant cell signaling*. Plant Cell, 2002. **14 Suppl**: p. S355-73.
3. Ma, H., M.F. Yanofsky, and E.M. Meyerowitz, *Molecular cloning and characterization of GPA1, a G protein alpha subunit gene from Arabidopsis thaliana*. Proc Natl Acad Sci U S A, 1990. **87**(10): p. 3821-5.
4. Weiss, C.A., et al., *Isolation of cDNAs encoding guanine nucleotide-binding protein beta-subunit homologues from maize (ZGB1) and Arabidopsis (AGB1)*. Proc Natl Acad Sci U S A, 1994. **91**(20): p. 9554-8.
5. Mason, M.G. and J.R. Botella, *Completing the heterotrimer: isolation and characterization of an Arabidopsis thaliana G protein gamma-subunit cDNA*. Proc Natl Acad Sci U S A, 2000. **97**(26): p. 14784-8.
6. Mason, M.G. and J.R. Botella, *Isolation of a novel G-protein gamma-subunit from Arabidopsis thaliana and its interaction with Gbeta*. Biochim Biophys Acta, 2001. **1520**(2): p. 147-53.
7. Kaplan, B., *Investigation of cloning strategies for A. thaliana G Protein [alpha]-subunit gene in Pichia Pastoris*, in *Biological Sciences and Bioengineering*. 2004, M.Sc. Thesis, Sabanci University: Istanbul.
8. Hoffman, C.S., *Except in every detail: comparing and contrasting G-protein signaling in Saccharomyces cerevisiae and Schizosaccharomyces pombe*. Eukaryot Cell, 2005. **4**(3): p. 495-503.
9. Fry, M.R., et al., *Early and late molecular events of glucose-induced pexophagy in Pichia pastoris require Vac8*. Autophagy, 2006. **2**(4): p. 280-8.
10. Luttrell, L.M., *Transmembrane signaling by G protein-coupled receptors*. Methods Mol Biol, 2006. **332**: p. 3-49.
11. McCudden, C.R., et al., *G-protein signaling: back to the future*. Cell Mol Life Sci, 2005. **62**(5): p. 551-77.
12. Siderovski, D.P. and F.S. Willard, *The GAPs, GEFs, and GDIs of heterotrimeric G-protein alpha subunits*. Int J Biol Sci, 2005. **1**(2): p. 51-66.
13. Cabrera-Vera, T.M., et al., *Insights into G protein structure, function, and regulation*. Endocr Rev, 2003. **24**(6): p. 765-81.
14. Lambright, D.G., et al., *The 2.0 A crystal structure of a heterotrimeric G protein*. Nature, 1996. **379**(6563): p. 311-9.
15. Wall, M.A., et al., *The structure of the G protein heterotrimer Gi alpha 1 beta 1 gamma 2*. Cell, 1995. **83**(6): p. 1047-58.
16. Hamm, H.E., *The many faces of G protein signaling*. J Biol Chem, 1998. **273**(2): p. 669-72.
17. Noel, J.P., H.E. Hamm, and P.B. Sigler, *The 2.2 A crystal structure of transducin-alpha complexed with GTP gamma S*. Nature, 1993. **366**(6456): p. 654-63.

18. Oldham, W.M. and E.H. H, *Structural basis of function in heterotrimeric G proteins*. Q Rev Biophys, 2006. **39**(2): p. 117-66.
19. Coleman, D.E., et al., *Structures of active conformations of Gi alpha 1 and the mechanism of GTP hydrolysis*. Science, 1994. **265**(5177): p. 1405-12.
20. Mixon, M.B., et al., *Tertiary and quaternary structural changes in Gi alpha 1 induced by GTP hydrolysis*. Science, 1995. **270**(5238): p. 954-60.
21. Tesmer, J.J., et al., *Structure of RGS4 bound to AIF4--activated G(i alpha1): stabilization of the transition state for GTP hydrolysis*. Cell, 1997. **89**(2): p. 251-61.
22. Schmidt, C.J., et al., *Specificity of G protein beta and gamma subunit interactions*. J Biol Chem, 1992. **267**(20): p. 13807-10.
23. Sondek, J., et al., *Crystal structure of a G-protein beta gamma dimer at 2.1A resolution*. Nature, 1996. **379**(6563): p. 369-74.
24. Downes, G.B. and N. Gautam, *The G protein subunit gene families*. Genomics, 1999. **62**(3): p. 544-52.
25. Schmidt, C.J. and E.J. Neer, *In vitro synthesis of G protein beta gamma dimers*. J Biol Chem, 1991. **266**(7): p. 4538-44.
26. Robishaw, J.D., V.K. Kalman, and K.L. Proulx, *Production, processing and partial purification of functional G protein beta gamma subunits in baculovirus-infected insect cells*. Biochem J, 1992. **286** (Pt 3): p. 677-80.
27. Fung, B.K. and C.R. Nash, *Characterization of transducin from bovine retinal rod outer segments. II. Evidence for distinct binding sites and conformational changes revealed by limited proteolysis with trypsin*. J Biol Chem, 1983. **258**(17): p. 10503-10.
28. Winslow, J.W., J.R. Van Amsterdam, and E.J. Neer, *Conformations of the alpha 39, alpha 41, and beta.gamma components of brain guanine nucleotide-binding proteins. Analysis by limited proteolysis*. J Biol Chem, 1986. **261**(16): p. 7571-9.
29. Sondek, J., et al., *GTPase mechanism of Gproteins from the 1.7-A crystal structure of transducin alpha-GDP-AIF-4*. Nature, 1994. **372**(6503): p. 276-9.
30. Li, Q. and R.A. Cerione, *Communication between switch II and switch III of the transducin alpha subunit is essential for target activation*. J Biol Chem, 1997. **272**(35): p. 21673-6.
31. Frank, M., et al., *G Protein activation without subunit dissociation depends on a G{alpha}(i)-specific region*. J Biol Chem, 2005. **280**(26): p. 24584-90.
32. Levitzki, A. and S. Klein, *G-protein subunit dissociation is not an integral part of G-protein action*. Chembiochem, 2002. **3**(9): p. 815-8.
33. Vogler, O., et al., *Membrane interactions of G proteins and other related proteins*. Biochim Biophys Acta, 2008. **1778**(7-8): p. 1640-52.
34. Northup, J.K., M.D. Smigel, and A.G. Gilman, *The guanine nucleotide activating site of the regulatory component of adenylate cyclase. Identification by ligand binding*. J Biol Chem, 1982. **257**(19): p. 11416-23.
35. Higashijima, T., et al., *The effect of GTP and Mg2+ on the GTPase activity and the fluorescent properties of Go*. J Biol Chem, 1987. **262**(2): p. 757-61.
36. Higashijima, T., et al., *The effect of activating ligands on the intrinsic fluorescence of guanine nucleotide-binding regulatory proteins*. J Biol Chem, 1987. **262**(2): p. 752-6.
37. Higashijima, T., et al., *Effects of Mg2+ and the beta gamma-subunit complex on the interactions of guanine nucleotides with G proteins*. J Biol Chem, 1987. **262**(2): p. 762-6.

38. Ferguson, K.M., et al., *The influence of bound GDP on the kinetics of guanine nucleotide binding to G proteins*. J Biol Chem, 1986. **261**(16): p. 7393-9.
39. Shichi, H., K. Yamamoto, and R.L. Somers, *GTP binding protein: properties and lack of activation by phosphorylated rhodopsin*. Vision Res, 1984. **24**(11): p. 1523-31.
40. Tanaka, T., et al., *Alpha helix content of G protein alpha subunit is decreased upon activation by receptor mimetics*. J Biol Chem, 1998. **273**(6): p. 3247-52.
41. Di Cesare Mannelli, L., et al., *Gi/o proteins: expression for direct activation enquiry*. Protein Expr Purif, 2006. **47**(1): p. 303-10.
42. Wedegaertner, P.B., P.T. Wilson, and H.R. Bourne, *Lipid modifications of trimeric G proteins*. J Biol Chem, 1995. **270**(2): p. 503-6.
43. Kleuss, C. and E. Krause, *Galpha(s) is palmitoylated at the N-terminal glycine*. Embo J, 2003. **22**(4): p. 826-32.
44. Dunphy, J.T., et al., *G-protein palmitoyltransferase activity is enriched in plasma membranes*. J Biol Chem, 1996. **271**(12): p. 7154-9.
45. Grassie, M.A., et al., *The palmitoylation status of the G-protein G(o)1 alpha regulates its activity of interaction with the plasma membrane*. Biochem J, 1994. **302 (Pt 3)**: p. 913-20.
46. Yang, H., et al., *Palmitoylation participates in G protein coupled signal transduction by affecting its oligomerization*. Mol Membr Biol, 2008. **25**(1): p. 58-71.
47. Barclay, E., M. O'Reilly, and G. Milligan, *Activation of an alpha2A-adrenoceptor-Galphao1 fusion protein dynamically regulates the palmitoylation status of the G protein but not of the receptor*. Biochem J, 2005. **385**(Pt 1): p. 197-206.
48. Loisel, T.P., et al., *Activation of the beta(2)-adrenergic receptor-Galpha(s) complex leads to rapid depalmitoylation and inhibition of repalmitoylation of both the receptor and Galpha(s)*. J Biol Chem, 1999. **274**(43): p. 31014-9.
49. Wedegaertner, P.B. and H.R. Bourne, *Activation and depalmitoylation of Gs alpha*. Cell, 1994. **77**(7): p. 1063-70.
50. Iiri, T., et al., *Reciprocal regulation of Gs alpha by palmitate and the beta gamma subunit*. Proc Natl Acad Sci U S A, 1996. **93**(25): p. 14592-7.
51. Tu, Y., J. Wang, and E.M. Ross, *Inhibition of brain Gz GAP and other RGS proteins by palmitoylation of G protein alpha subunits*. Science, 1997. **278**(5340): p. 1132-5.
52. Higgins, J.B. and P.J. Casey, *In vitro processing of recombinant G protein gamma subunits. Requirements for assembly of an active beta gamma complex*. J Biol Chem, 1994. **269**(12): p. 9067-73.
53. Takida, S. and P.B. Wedegaertner, *Heterotrimer formation, together with isoprenylation, is required for plasma membrane targeting of Gbetagamma*. J Biol Chem, 2003. **278**(19): p. 17284-90.
54. Saini, D.K., et al., *A family of G protein betagamma subunits translocate reversibly from the plasma membrane to endomembranes on receptor activation*. J Biol Chem, 2007. **282**(33): p. 24099-108.
55. Kerov, V., et al., *N-terminal fatty acylation of transducin profoundly influences its localization and the kinetics of photoresponse in rods*. J Neurosci, 2007. **27**(38): p. 10270-7.
56. Medkova, M., et al., *Conformational changes in the amino-terminal helix of the G protein alpha(i1) following dissociation from Gbetagamma subunit and activation*. Biochemistry, 2002. **41**(31): p. 9962-72.

57. Preininger, A.M., et al., *The myristoylated amino terminus of Galpha(i)(1) plays a critical role in the structure and function of Galpha(i)(1) subunits in solution.* Biochemistry, 2003. **42**(26): p. 7931-41.
58. Vogler, O., et al., *The Gbetagamma dimer drives the interaction of heterotrimeric Gi proteins with nonlamellar membrane structures.* J Biol Chem, 2004. **279**(35): p. 36540-5.
59. Zhang, Z., et al., *How a G protein binds a membrane.* J Biol Chem, 2004. **279**(32): p. 33937-45.
60. Palczewski, K., et al., *Crystal structure of rhodopsin: A G protein-coupled receptor.* Science, 2000. **289**(5480): p. 739-45.
61. Mustafi, D. and K. Palczewski, *Topology of class A G protein-coupled receptors: insights gained from crystal structures of rhodopsins, adrenergic and adenosine receptors.* Mol Pharmacol, 2009. **75**(1): p. 1-12.
62. Fotiadis, D., et al., *The G protein-coupled receptor rhodopsin in the native membrane.* FEBS Lett, 2004. **564**(3): p. 281-8.
63. Oldham, W.M. and H.E. Hamm, *Heterotrimeric G protein activation by G-protein-coupled receptors.* Nat Rev Mol Cell Biol, 2008. **9**(1): p. 60-71.
64. Oldham, W.M., et al., *Mechanism of the receptor-catalyzed activation of heterotrimeric G proteins.* Nat Struct Mol Biol, 2006. **13**(9): p. 772-7.
65. Milligan, G., *G protein-coupled receptor dimerization: function and ligand pharmacology.* Mol Pharmacol, 2004. **66**(1): p. 1-7.
66. Chabre, M. and M. le Maire, *Monomeric G-protein-coupled receptor as a functional unit.* Biochemistry, 2005. **44**(27): p. 9395-403.
67. Martin, E.L., et al., *Potent peptide analogues of a G protein receptor-binding region obtained with a combinatorial library.* J Biol Chem, 1996. **271**(1): p. 361-6.
68. Afshar, K., et al., *RIC-8 is required for GPR-1/2-dependent Galpha function during asymmetric division of C. elegans embryos.* Cell, 2004. **119**(2): p. 219-30.
69. Kimple, R.J., et al., *Structural determinants for GoLoco-induced inhibition of nucleotide release by Galpha subunits.* Nature, 2002. **416**(6883): p. 878-81.
70. Ishikawa, A., et al., *Molecular cloning and characterization of a cDNA for the alpha subunit of a G protein from rice.* Plant Cell Physiol, 1995. **36**(2): p. 353-9.
71. Ishikawa, A., Y. Iwasaki, and T. Asahi, *Molecular cloning and characterization of a cDNA for the beta subunit of a G protein from rice.* Plant Cell Physiol, 1996. **37**(2): p. 223-8.
72. Kato, C., et al., *Characterization of heterotrimeric G protein complexes in rice plasma membrane.* Plant J, 2004. **38**(2): p. 320-31.
73. Hossain, M.S., T. Koba, and K. Harada, *Cloning and characterization of two full-length cDNAs, TaGAI and TaGA2, encoding G-protein alpha subunits expressed differentially in wheat genome.* Genes Genet Syst, 2003. **78**(2): p. 127-38.
74. Seo, H.S., et al., *Biochemical characteristics of a rice (Oryza sativa L., IR36) G-protein alpha-subunit expressed in Escherichia coli.* Biochem J, 1997. **324** (Pt 1): p. 273-81.
75. Iwasaki, Y., et al., *Characterization of the putative alpha subunit of a heterotrimeric G protein in rice.* Plant Mol Biol, 1997. **34**(4): p. 563-72.
76. Wise, A., et al., *Expression of the Arabidopsis G-protein GP alpha1: purification and characterisation of the recombinant protein.* Plant Mol Biol, 1997. **33**(4): p. 723-8.

77. Johnston, C.A., et al., *GTPase acceleration as the rate-limiting step in Arabidopsis G protein-coupled sugar signaling*. Proc Natl Acad Sci U S A, 2007.
78. Perfus-Barbeoch, L., A.M. Jones, and S.M. Assmann, *Plant heterotrimeric G protein function: insights from Arabidopsis and rice mutants*. Curr Opin Plant Biol, 2004. **7**(6): p. 719-31.
79. Chen, J.G., Y. Gao, and A.M. Jones, *Differential Roles of Arabidopsis Heterotrimeric G-Protein Subunits in Modulating Cell Division in Roots*. Plant Physiol, 2006.
80. Assmann, S.M., *Plant G proteins, phytohormones, and plasticity: three questions and a speculation*. Sci STKE, 2004. **2004**(264): p. re20.
81. Jones, A.M. and S.M. Assmann, *Plants: the latest model system for G-protein research*. EMBO Rep, 2004. **5**(6): p. 572-8.
82. Trusov, Y., et al., *Heterotrimeric G proteins-mediated resistance to necrotrophic pathogens includes mechanisms independent of salicylic acid-, jasmonic acid/ethylene- and abscisic acid-mediated defense signaling*. Plant J, 2008.
83. Chen, J.G., et al., *A seven-transmembrane RGS protein that modulates plant cell proliferation*. Science, 2003. **301**(5640): p. 1728-31.
84. Coursol, S., et al., *Sphingolipid signalling in Arabidopsis guard cells involves heterotrimeric G proteins*. Nature, 2003. **423**(6940): p. 651-4.
85. Joo, J.H., et al., *Different signaling and cell death roles of heterotrimeric G protein alpha and beta subunits in the Arabidopsis oxidative stress response to ozone*. Plant Cell, 2005. **17**(3): p. 957-70.
86. Navari-Izzo, F., et al., *Copper excess triggers phospholipase D activity in wheat roots*. Phytochemistry, 2006. **67**(12): p. 1232-42.
87. Ma, H., *Plant G proteins: the different faces of GPA1*. Curr Biol, 2001. **11**(21): p. R869-71.
88. Weiss, C.A., et al., *The G protein alpha subunit (GP alpha1) is associated with the ER and the plasma membrane in meristematic cells of Arabidopsis and cauliflower*. FEBS Lett, 1997. **407**(3): p. 361-7.
89. Jones, A.M., *G-protein-coupled signaling in Arabidopsis*. Curr Opin Plant Biol, 2002. **5**(5): p. 402-7.
90. Temple, B.R. and A.M. Jones, *The Plant Heterotrimeric G-Protein Complex*. Annu Rev Plant Biol, 2007.
91. Oki, K., et al., *Study of the constitutively active form of the alpha subunit of rice heterotrimeric G proteins*. Plant Cell Physiol, 2005. **46**(2): p. 381-6.
92. Pandey, S., D.C. Nelson, and S.M. Assmann, *Two novel GPCR-type G proteins are abscisic acid receptors in Arabidopsis*. Cell, 2009. **136**(1): p. 136-48.
93. Okamoto, H., M. Matsui, and X.W. Deng, *Overexpression of the heterotrimeric G-protein alpha-subunit enhances phytochrome-mediated inhibition of hypocotyl elongation in Arabidopsis*. Plant Cell, 2001. **13**(7): p. 1639-52.
94. Boisson, B., C. Giglione, and T. Meinnel, *Unexpected protein families including cell defense components feature in the N-myristoylome of a higher eukaryote*. J Biol Chem, 2003. **278**(44): p. 43418-29.
95. Adjobo-Hermans, M.J., J. Goedhart, and T.W. Gadella, Jr., *Plant G protein heterotrimers require dual lipidation motifs of G{alpha} and G{gamma} and do not dissociate upon activation*. J Cell Sci, 2006. **119**(Pt 24): p. 5087-97.
96. Zeng, Q., X. Wang, and M.P. Running, *Dual Lipid Modification of Arabidopsis Gamma Subunits Is Required for Efficient Plasma Membrane Targeting*. Plant Physiol, 2007.

97. Peskan, T. and R. Oelmüller, *Heterotrimeric G-protein beta-subunit is localized in the plasma membrane and nuclei of tobacco leaves*. *Plant Mol Biol*, 2000. **42**(6): p. 915-22.
98. Wang, S., S. Narendra, and N. Fedoroff, *Heterotrimeric G protein signaling in the Arabidopsis unfolded protein response*. *Proc Natl Acad Sci U S A*, 2007. **104**(10): p. 3817-22.
99. Wang, S., S.M. Assmann, and N.V. Fedoroff, *Characterization of the Arabidopsis heterotrimeric g protein*. *J Biol Chem*, 2008. **283**(20): p. 13913-22.
100. Chen, Z., et al., *Expression analysis of the AtMLO Gene Family Encoding Plant-Specific Seven-Transmembrane Domain Proteins*. *Plant Mol Biol*, 2006. **60**(4): p. 583-97.
101. Pandey, S. and S.M. Assmann, *The Arabidopsis putative G protein-coupled receptor GCRI interacts with the G protein alpha subunit GPA1 and regulates abscisic acid signaling*. *Plant Cell*, 2004. **16**(6): p. 1616-32.
102. Chen, J.G., et al., *GCRI can act independently of heterotrimeric G-protein in response to brassinosteroids and gibberellins in Arabidopsis seed germination*. *Plant Physiol*, 2004. **135**(2): p. 907-15.
103. Chen, Y., et al., *The regulator of G-protein signaling proteins involved in sugar and abscisic acid signaling in Arabidopsis seed germination*. *Plant Physiol*, 2006. **140**(1): p. 302-10.
104. Colucci, G., et al., *GCRI, the putative Arabidopsis G protein-coupled receptor gene is cell cycle-regulated, and its overexpression abolishes seed dormancy and shortens time to flowering*. *Proc Natl Acad Sci U S A*, 2002. **99**(7): p. 4736-41.
105. Apone, F., et al., *The G-protein-coupled receptor GCRI regulates DNA synthesis through activation of phosphatidylinositol-specific phospholipase C*. *Plant Physiol*, 2003. **133**(2): p. 571-9.
106. Pandey, S., et al., *G-protein complex mutants are hypersensitive to ABA-regulation of germination and post-germination development*. *Plant Physiol*, 2006.
107. Willard, F.S. and D.P. Siderovski, *Purification and in vitro functional analysis of the Arabidopsis thaliana regulator of G-protein signaling-1*. *Methods Enzymol*, 2004. **389**: p. 320-38.
108. Jacob, T., et al., *Abscisic acid signal transduction in guard cells is mediated by phospholipase D activity*. *Proc Natl Acad Sci U S A*, 1999. **96**(21): p. 12192-7.
109. Ritchie, S. and S. Gilroy, *Abscisic acid signal transduction in the barley aleurone is mediated by phospholipase D activity*. *Proc Natl Acad Sci U S A*, 1998. **95**(5): p. 2697-702.
110. Ritchie, S. and S. Gilroy, *Abscisic acid stimulation of phospholipase D in the barley aleurone is G-protein-mediated and localized to the plasma membrane*. *Plant Physiol*, 2000. **124**(2): p. 693-702.
111. Zhao, J. and X. Wang, *Arabidopsis phospholipase Dalpha1 interacts with the heterotrimeric G-protein alpha-subunit through a motif analogous to the DRY motif in G-protein-coupled receptors*. *J Biol Chem*, 2004. **279**(3): p. 1794-800.
112. Chen, J.G., *Heterotrimeric G-proteins in plant development*. *Front Biosci*, 2008. **13**: p. 3321-33.
113. Ullah, H., et al., *The beta-subunit of the Arabidopsis G protein negatively regulates auxin-induced cell division and affects multiple developmental processes*. *Plant Cell*, 2003. **15**(2): p. 393-409.

114. Chen, J.G., et al., *RACK1 mediates multiple hormone responsiveness and developmental processes in Arabidopsis*. J Exp Bot, 2006. **57**(11): p. 2697-708.
115. Volkin, D.B., et al., *Preformulation studies as an essential guide to formulation development and manufacture of protein pharmaceuticals*. Pharm Biotechnol, 2002. **14**: p. 1-46.
116. Kelly, S.M., T.J. Jess, and N.C. Price, *How to study proteins by circular dichroism*. Biochim Biophys Acta, 2005. **1751**(2): p. 119-39.
117. Lazo, N.D. and D.T. Downing, *Circular dichroism of model peptides emulating the amphipathic alpha-helical regions of intermediate filaments*. Biochemistry, 1997. **36**(9): p. 2559-65.
118. Prive, G.G., *Detergents for the stabilization and crystallization of membrane proteins*. Methods, 2007. **41**(4): p. 388-97.
119. le Maire, M., P. Champeil, and J.V. Moller, *Interaction of membrane proteins and lipids with solubilizing detergents*. Biochim Biophys Acta, 2000. **1508**(1-2): p. 86-111.
120. Maslennikov, I., et al., *NMR spectroscopic and analytical ultracentrifuge analysis of membrane protein detergent complexes*. BMC Struct Biol, 2007. **7**: p. 74.
121. Petoukhov, M.V. and D.I. Svergun, *Analysis of X-ray and neutron scattering from biomacromolecular solutions*. Curr Opin Struct Biol, 2007. **17**(5): p. 562-71.
122. Sambrook, J.a.R., D.W., "*Molecular Cloning: A Laboratory Manual*", Cold Spring Harbor Laboratory Press, 3rd Edition. 2000.
123. Laemmli, U.K., *Cleavage of structural proteins during the assembly of the head of bacteriophage T4*. Nature, 1970. **227**(5259): p. 680-5.
124. Layne, E., *Spectrophotometric and Turbidimetric Methods for Measuring Proteins*. Methods in Enzymology, 1957. **3**: p. 447-455.
125. Mach, H., et al., *Ultraviolet absorption spectroscopy*. Methods Mol Biol, 1995. **40**: p. 91-114.
126. Carty, D.J. and R. Iyengar, *Guanosine 5'-(gamma-thio)triphosphate binding assay for solubilized G proteins*. Methods Enzymol, 1994. **237**: p. 38-44.
127. Greenfield, N.J., *Using circular dichroism spectra to estimate protein secondary structure*. Nat Protoc, 2006. **1**(6): p. 2876-90.
128. Petoukhov, M.V., et al., *ATSAS 2.1 - towards automated and web-supported small-angle scattering data analysis*. J. Appl. Cryst. , 2007. **40** (Supplement): p. s223-s228.
129. Newby, A.C. and A. Chrambach, *Disaggregation of adenylate cyclase during polyacrylamide-gel electrophoresis in mixtures of ionic and non-ionic detergents*. Biochem J, 1979. **177**(2): p. 623-30.
130. Lipfert, J. and S. Doniach, *Small-angle X-ray scattering from RNA, proteins, and protein complexes*. Annu Rev Biophys Biomol Struct, 2007. **36**: p. 307-27.
131. Columbus, L., et al., *Expression, purification, and characterization of Thermotoga maritima membrane proteins for structure determination*. Protein Sci, 2006. **15**(5): p. 961-75.
132. Petoukhov, M.V. and D.I. Svergun, *Global rigid body modeling of macromolecular complexes against small-angle scattering data*. Biophys J, 2005. **89**(2): p. 1237-50.
133. Porod, G., *General Theory*, in *Small-angle X-ray Scattering*, O. Glatter and O. Kratky, Editors. 1982, Academic Press, London

134. Coleman, D.E., et al., *Crystallization and preliminary crystallographic studies of Gi alpha 1 and mutants of Gi alpha 1 in the GTP and GDP-bound states*. J Mol Biol, 1994. **238**(4): p. 630-4.
135. Kozin, M.B. and D. Svergun, *Automated matching of high- and-low resolution structural models*. J. Appl. Cryst., 2001. **34**: p. 33-41.
136. Lee, E., M.E. Linder, and A.G. Gilman, *Expression of G-protein alpha subunits in Escherichia coli*. Methods Enzymol, 1994. **237**: p. 146-64.
137. Carrier, D.J., et al., *Heterologous Expression of a Membrane-Spanning Auxin Importer: Implications for Functional Analyses of Auxin Transporters*. Int J Plant Genomics, 2009. **2009**: p. 848145.
138. Macauley-Patrick, S., et al., *Heterologous protein production using the Pichia pastoris expression system*. Yeast, 2005. **22**(4): p. 249-70.
139. Swiatek, W., et al., *Biochemical characterization of recombinant subunits of type 2A protein phosphatase overexpressed in Pichia pastoris*. Eur J Biochem, 2000. **267**(16): p. 5209-16.
140. McCusker, E. and A.S. Robinson, *Refolding of G protein alpha subunits from inclusion bodies expressed in Escherichia coli*. Protein Expr Purif, 2007.

APPENDIX A

CHEMICALS

(in alphabetical order)

Name of Chemical	Supplier Company	Catalog Number
Acetic Acid	Riedel-de Haén, Germany	27225
Acrylamide/Bis-acrylamide	Sigma, Germany	A3699
	Biorad Inc., USA	161-0158
Agar-agar	Merck, Germany	101614
Agarose low EO	Applichem, Germany	A2114
Aluminum Sulfate	Fluka, Switzerland	60060
Ammonium persulfate	Carlo-Erba, Italy	420627
Ampicillin	Sigma, Germany	A9518
Biotin	CALBIOCHEM, Germany	2031
β -galactosidase	Sigma, Germany	G-2531
Bromophenol blue sodium salt	Applichem, Germany	A3640
Chloroform	Merck, Germany	102431
Complete EDTA-free	Roche, Germany	11 873 580 001
Protease Inhibitor Cocktail Tablets		
Coomassie Brilliant Blue	Merck, Germany	115444
Deuterium Oxide	Cambirdge Isotope Laboratories Inc., USA	DLM-4-25
Distilled water, sterile, MilliQ Filtered	Millipore, France	
DTT	Fluka, Switzerland	43815
EDTA	Riedel-de Haén, Germany	27248
Ethanol	Riedel-de Haén, Germany	32221
Ethidium Bromide	Merck, Germany	OCO28942
D-(+) Glucose	Sigma, Germany	G-7021
GDP	Sigma, Germany	G7127
Glycerol	Riedel-de Haén, Germany	15523
Glycine	Amresco, USA	0167
GTP	Sigma, Germany	G8877
GTP γ S	Sigma, Germany	G8634
HCl	Merck, Germany	100314
HEPES	Fluka, Switzerland	54461

L-Histidine	Applichem, Germany	A3719
Imidazole	Sigma, Germany	I0250
IPTG	Promega, Germany	V39517
Isopropanol	Riedel-de Haén, Germany	24137
Kanamycin	Sigma, Germany	K4000.102
KCl	Fluka, Switzerland	60129
KH ₂ PO ₄	Riedel-de Haén, Germany	04243
KOH	Riedel-de Haén, Germany	06005
Liquid nitrogen	Karbogaz, Turkey	
Lithium chloride (anhydrous)	Fluka, Switzerland	62478
Lubrol PX	MP Biomedicals, France	195299
Luria Agar (Miller's LB Agar)	Sigma, Germany	L-3147
Luria Broth (Lennox L Broth)	Sigma, Germany	L-3022
2-Mercaptoethanol	Sigma, Germany	M370-1
Methanol	Riedel-de Haén, Germany	24229
NaCl	Riedel-de Haén, Germany	13423
NaF	Sigma, USA	201154
Na ₂ O ₂ C ₂ H ₃ .3H ₂ O	Riedel-de Haén, Germany	25022
NaOH	Merck, Germany	106462
NaPO ₄ H ₂	Riedel-de Haén, Germany	04269
Peptone	Applichem, Germany	A2208
Phenol	Applichem, Germany	A1153
Phenol/chloroform /isoamylalkohol	Applichem, Germany	A0889
PMSF	Amresco, USA	0754
Sodium Dodecyl Sulphate	Sigma, Germany	L-4390
D(-) Sorbitol	Applichem, Germany	A2222
TEMED	Sigma, Germany	T-7029
Triton [®] X-100	Applichem, Germany	A1388
Tris	Fluka, Switzerland	93349
Tween [®] 20	Merck, Germany	822184
Yeast Extract	Applichem, Germany	A1552
Yeast Nitrogen Base (with ammonium sulfate without amino acids)	Sigma, Germany	Y0626
Zeocin	Invitrogen, Germany	R250
³² P-GTP (3000 Ci/mmol)	Izotop, Hungary	SCP-302
³⁵ S-GTPγS (1000 Ci/mmol)	GE Healthcare, UK	SJ1320

APPENDIX B

MOLECULAR BIOLOGY KITS

(in alphabetical order)

Name of Kit	Supplier Company	Catalog Number
ECL Western Blotting Substrate	Pierce Protein Research Products Thermo Scientific, USA	32109
Quiaquick® PCR Purification Kit (250)	Qiagen, Germany	28106
Quiaquick® Gel extraction Kit (250)	Qiagen, Germany	28706
Quiaprep® Spin Miniprep Kit (250)	Qiagen, Germany	27106
QIAGEN® Plasmid Midi Kit (100)	Qiagen, Germany	12145
RGS-His HRP Conjugate Kit	Qiagen, Germany	34450
Silver Stain Kit	BIO-RAD, USA	161-046
Tetra-His HRP Conjugate Kit	Qiagen, Germany	34470

APPENDIX C

OTHERS

(in alphabetical order)

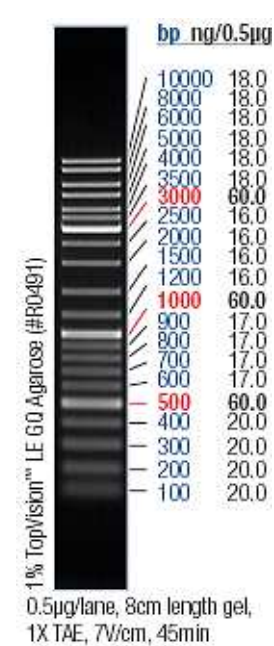
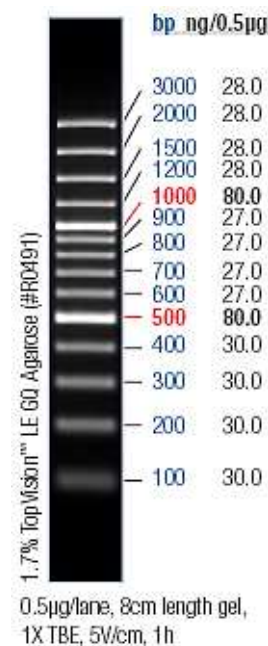
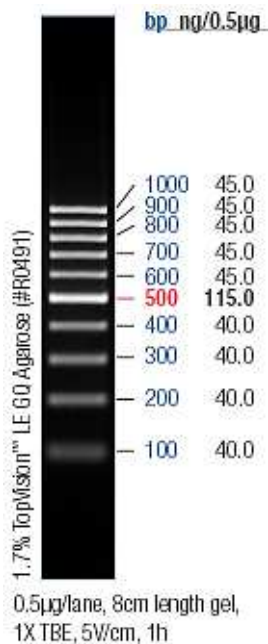
NAME	Supplier Company	Catalog Number
<i>Bam</i> HI	Fermentas, Germany	#ER0051
BL21(DE3)	Stratagene, USA	200131
CL-XPosure Film	Pierce Protein Research Products	34093
CYROBANK MIXED COLOURS	Thermo Scientific, USA	
<i>Eco</i> RI	MAST GROUP Ltd, UK	Cyro/M
Glass beads 0.5 mm d	Fermentas, Germany	#ER0271
HiPrep 16/60 Sephacryl S-200 HR	Biospec Products, Inc, USA.	11079105
HiPrep 16/60 Sephacryl S-300 HR	GE Healthcare, Sweden	17-1166-01
HiPrep 26/10 Desalting Column	GE Healthcare, Sweden	17-1167-01
HiTrap HP, 5 ml	GE Healthcare, Sweden	17-5087-01
HiTrap Desalting, 5 ml	GE Healthcare, Sweden	17-5248-02
HiTrap Q HP, 5 ml	GE Healthcare, Sweden	17-1408-01
Hybond-P membrane (PVDF)	GE Healthcare, Sweden	17-1154-01
<i>Kpn</i> I	GE Healthcare, Sweden	RPN2020F
Lamda DNA/HindIII	Fermentas, Germany	#ER0521
(Agarose gel photograph and MW values of bands are provided below)	Fermentas, Germany	#SM0123
Mass Ruler DNA Ladder, Mix	Fermentas, Germany	#SM0403
(Agarose gel photograph and MW values of bands are provided below)		
MF™ Nitrocellulose Membrane Filters	Millipore, Ireland	HAWPO2500
0.45 µM HA		
<i>Myc</i> tag antibody (HRP)	abcam, UK	ab1326
Ni-NTA Agarose	Qiagen, Germany	30230
O'GeneRuler™ 100 bp	Fermentas, Germany	#SM1143
O'GeneRuler™ 100 bp Plus	Fermentas, Germany	#SM1153
O'GeneRuler™ Mix	Fermentas, Germany	#SM1173
Protein MW Marker	Fermentas, Germany	#SM0431
(gel photograph and MW values of bands are provided below)		
Prestained Protein MW Marker	Fermentas, Germany	#SM0441
(gel photograph and MW values of bands are provided below)		
PageRuler™ Improved Prestained Protein Ladder	Fermentas, Germany	#SM0671

PageRuler™ Plus Prestained Protein Ladder	Fermentas, Germany	#SM1811
PageRuler™ Unstained Protein Ladder	Fermentas, Germany	#SM0661
Cellu•Sep T3; Nominal MWCO: 12,000-14,000	Bioron, Germany	O-1230-25
Regenerated Cellulose Tubular Membrane		
Shrimp Alkaline Phosphatase	Fermentas, Germany	#EF0511
Super loop, 50 ml, 4M Pa	GE Healthcare	18-1113-82
T4 DNA Ligase	Promega, Germany	M180B
Taq DNA polymerase	Fermentas, Germany	#EP0401
TOP10	Invitrogen, Germany	Supplied
		with TOPO® TA Cloning Kit
TOP10F'	Invitrogen, Germany	Supplied with
		EasySelect™ <i>Pichia</i> Expression Kit
Ultima Gold XR Scintillation Liquid	Packard, USA	6013119
Ultracel YM-30 membrane	Millipore, USA	4306
Vivaspin 20, 30,000 MWCO	Sartorius, Germany	VS2022
Vivaspin 500, 10,000 MWCO	Sartorius, Germany	VS0101
Vivaspin 500, 30,000 MWCO	Sartorius, Germany	VS0121
Zirconia/Silica beads, 0.5 mm	Biospec Products, Inc, USA	11079105z
<i>Xho</i> I	Fermentas, Germany	#ER0691

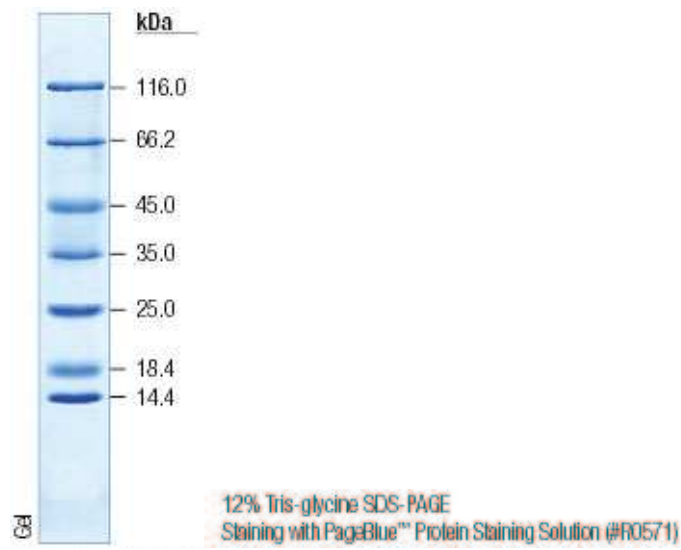
O'GeneRuler™ 100 bp

100 bp.DNA Ladder Plus

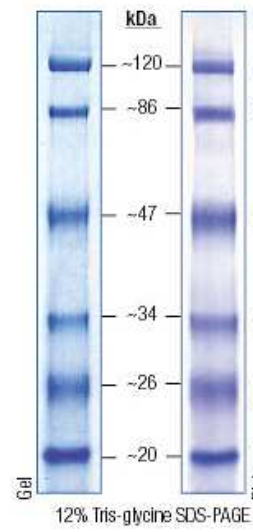
O'GeneRuler™ Mix



Protein MW Marker



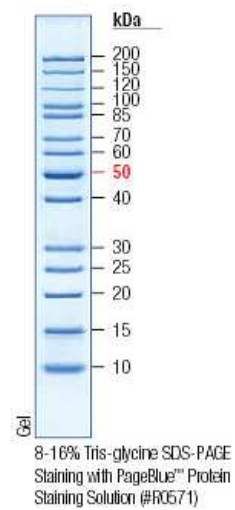
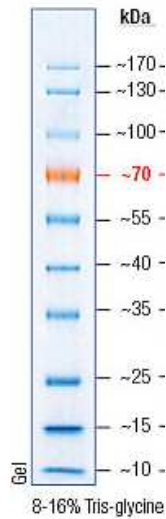
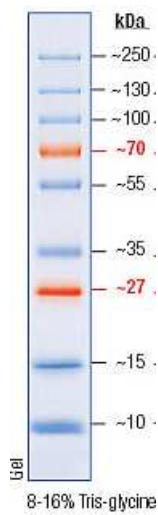
Prestained Protein Molecular Weight Marker



PageRuler™ Prestained Protein Ladder

PageRuler™ Unstained Protein Ladder

Plus



APPENDIX D

EQUIPMENT

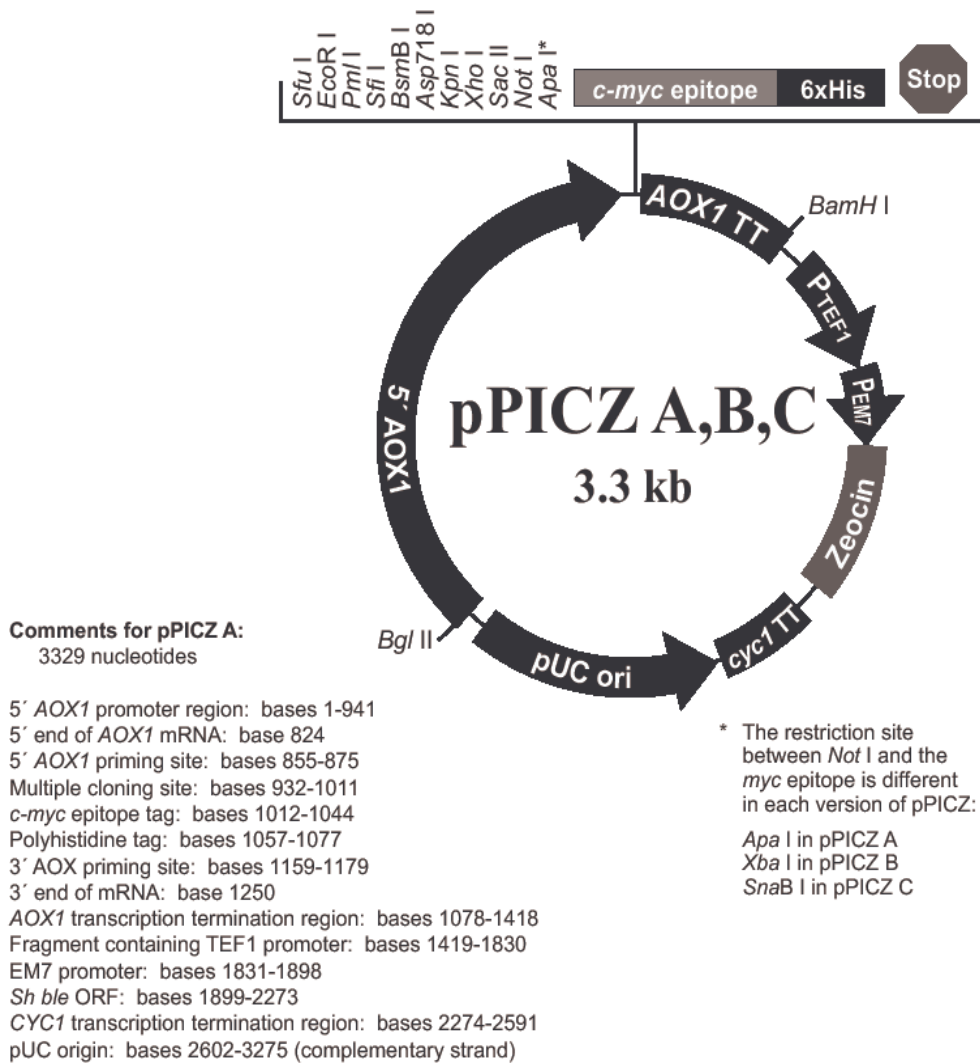
AKTA Prime	GE Healthcare, UK
Autoclave:	Hirayama, Hiclave HV-110, JAPAN
Balance:	Sartorius, BP211D, GERMANY Sartorius, BP221S, GERMANY Sartorius, BP610, GERMANY Schimadzu, Libror EB-3200 HU, JAPAN
Bead Beater	Biospec Products, Inc, USA
Blot Module	X Cell II™ Blot Module, Novex, USA
CD Spectropolarimeter	JASCO J-810, USA
Centrifuge:	Eppendorf, 5415C, GERMANY Eppendorf, 5415D, GERMANY Eppendorf, 5415R, GERMANY Kendro Lab. Prod., Heraeus Multifuge 3L, GERMANY Hitachi, Sorvall RC5C Plus, USA Hitachi, Sorvall Discovery 100 SE, USA
Deepfreeze:	-70° C, Kendro Lab. Prod., Heraeus Hfu486, GERMANY -20° C, Bosch, TÜRKİYE
Distilled Water:	Millipore, Elix-S, FRANCE Millipore, MilliQ Academic, FRANCE
Electrophoresis:	Biogen Inc., USA Biorad Inc., USA X Cell SureLock™ Electrophoresis Cell, Novex USA
680 Microplate Reader	BIO-RAD, Japan
Gel Documentation:	UVITEC, UVIdoc Gel Documentation System, UK Biorad, UV-Transilluminator 2000, USA
Ice Machine:	Scotsman Inc., AF20, USA
Incubator:	Memmert, Modell 300, GERMANY Memmert, Modell 600, GERMANY
Laminar Flow:	Kendro Lab. Prod., Heraeus, HeraSafe HS12, GERMANY
Magnetic Stirrer:	VELP Scientifica, ARE Heating Magnetic Stirrer, ITALY VELP Scientifica, Microstirrer, ITALY
Microliter Pipette:	Gilson, Pipetman, FRANCE Mettler Toledo, Volumate, USA
Microwave Oven:	Bosch, TÜRKİYE
Nano-ZS-DLS	Malvern Ins. UK
Unity Inova 500 MHz NMR	Varian, Inc. USA
pH meter:	WTW, pH540 GLP MultiCal®, GERMANY

Power Supply:	Biorad, PowerPac 300, USA Wealtec, Elite 300, USA
Refrigerator:	+4° C, Bosch, TÜRKİYE
TRI-CARB 2900 TR Liquid	Scintillation Analyzer Packard, USA
Shaker:	Forma Scientific, Orbital Shaker 4520, USA GFL, Shaker 3011, USA New Brunswick Sci., Innova™ 4330, USA
Sonicator	Vibracell 75043, Bioblock Scientific, FRANCE
Spectrophotometer:	Schimadzu, UV-1208, JAPAN Schimadzu, UV-3150, JAPAN
Speed Vacuum:	Savant, Speed Vac® Plus Sc100A, USA Savant, Refrigerated Vapor Trap RVT 400, USA
Thermocycler:	Eppendorf, Mastercycler Gradient, GERMANY
Vacuum:	Heto, MasterJet Sue 300Q, DENMARK
Water bath:	Huber, Polystat cc1, GERMANY

APPENDIX E

VECTOR MAPS

E.1 Vector map of pPICZC



Multiple cloning site of pPICZC

```

                    5' end of AOX1 mRNA
                    |
811 AACCTTTTTT TTTATCATCA TTATTAGCTT ACTTTCATAA TTGCGACTGG TTCCAATTGA
                    |
                    5' AOX1 priming site

871 CAAGCTTTTG ATTTTAACGA CTTTTAACGA CAACTTGAGA AGATCAAAAA ACAACTAATT

          Sfu I      EcoR I      Pml I      Sfi I      BsmB I Asp718 I Kpn I Xho I
931 ATT|CGAAACG AGGA|ATTCAC GTGG|CCCAGC CGGC|CGTCTC GGAT|CGGTAC CTCG|AGCCGC

          Sac II Not I      SnaB I      myc epitope
991 GGC|GGCCGCC AGCTT |ACGTA| GAA CAA AAA CTC ATC TCA GAA GAG GAT CTG
                    |
                    Glu Gln Lys Leu Ile Ser Glu Glu Asp Leu

1041 AAT AGC GCC GTC GAC CAT CAT CAT CAT CAT CAT TGA GTTTGTAGCC TTAGACATGA
      Asn Ser Ala Val Asp His His His His His His ***
                    Polyhistidine tag

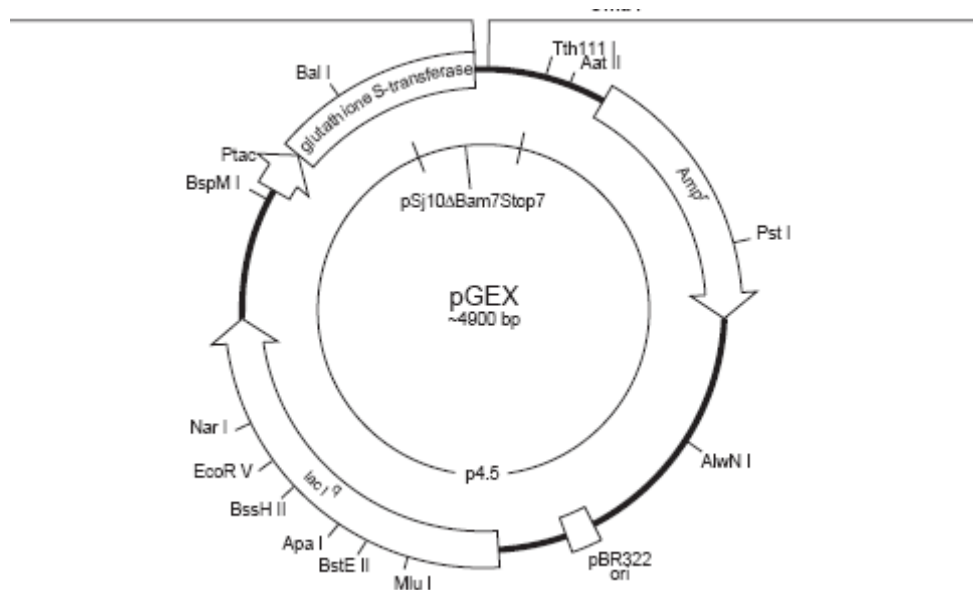
1097 CTGTTCTCA GTTCAAGTTG GCACTTACG AGAAGACCGG TCTTGCTAGA TTCTAATCAA

          3' AOX1 priming site
1157 GAGGATGTCA GAATGCCATT TGCCTGAGAG ATGCAGGCTT CATTTTTGAT ACTTTTTTAT

                    3' polyadenylation site
1217 TTGTAACCTA TATAGTATAG GATTTTTTTT GTCATTTTGT TTC

```

E.2 Vector map of pGEX-4T-2



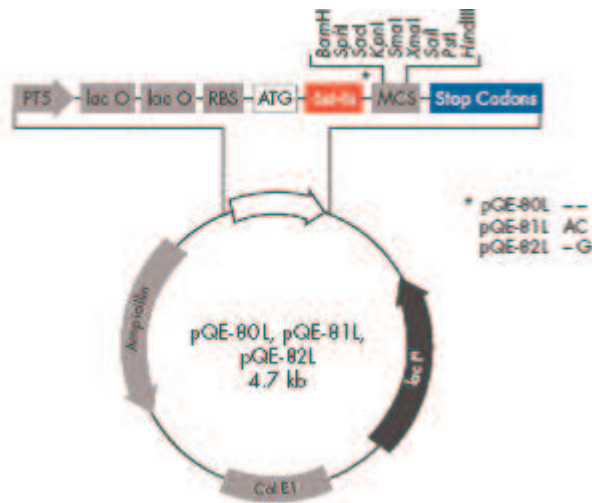
Multiple cloning site of pGEX-4T-2

pGEX-4T-2 (27-4581-01)

Thrombin

Leu	Val	Pro	Arg	Gly	Ser	Pro	Gly	Ile	Pro	Gly	Ser	Thr	Arg	Ala	Ala	Ala	Ser	
CTG	GTT	CCG	CGT	GGA	TCC	CCA	GGA	ATT	CCC	GGG	TCG	ACT	CGA	GCG	GCC	GCA	TCG	TGA
				BamH I		EcoR I		Sma I		Sal I		Xho I		Not I			Stop codon	

E.3 Vector map of pQE-80L

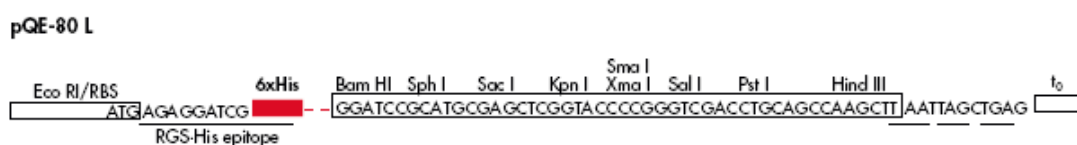


pQE vectors for N-terminal 6xHis tag constructs. **PT5**: T5 promoter, **lac O**: lac operator, **RBS**: ribosome-binding site, **ATG**: start codon, **6xHis**: 6xHis tag sequence, **MCS**: multiple cloning site with restriction sites indicated, **Stop Codons**: stop codons in all three reading frames, **Col E1**: Col E1 origin of replication, **Ampicillin**: ampicillin resistance gene, **lacI_a**, **lacI_r**: repressor gene.

pQE-80L, pQE-81L, and pQE-82L Vectors

Positions of elements in bases	pQE-80L	pQE-81L	pQE-82L
Vector size (bp)	4751	4753	4752
Start of numbering at <i>Xho</i> I (CTCGAG)	1-6	1-6	1-6
T5 promoter/ <i>lac</i> operator element	7-87	7-87	7-87
T5 transcription start	61	61	61
6xHis-tag coding sequence	127-144	127-144	127-144
Multiple cloning site	145-192	147-194	146-193
Lambda <i>t</i> ₀ transcriptional termination region	208-302	210-304	209-303
<i>rrnB</i> T1 transcriptional termination region	1064-1161	1066-1163	1065-1162
<i>lac</i> repressor coding sequence	2333-1252	2335-1254	2334-1253
ColE1 origin of replication	2928	2930	2929
β-lactamase coding sequence	4546-3686	4548-3688	4547-3687

Multiple cloning site of pQE-80L



APPENDIX F

SEQUENCING RESULTS

F.1 Sequencing results of GPA1 and pPICZC+GPA1-2 construct, with *EcoRI* and *XhoI* restriction enzyme sites at 5' and 3' sites, respectively. Alignment starts at the *EcoRI* site and ends at the stop codon of polyhistidine tag of pPICZC.

```

      10      20      30      40      50      60
1  TTGATTTAGGACTTTTAGGAGACTTGAGAAGATGAAAAAGAAGTAATTATTGGAAAAGG
1  pPICZCGPA1
    GPA1

      70      80      90     100     110     120
61 GGAATTGCTCATGGGCTTACTCTGCAGTAGAAGTCGACATCATACTGAAAGATACTGATGA
1  GGAATTGCTCATGGGCTTACTCTGCAGTAGAAGTCGACATCATACTGAAAGATACTGATGA
    pPICZCGPA1
    GPA1

     130     140     150     160     170     180
121 GAATACACAGGCTGCTGAAATCGAAAAGACGGATAGAGCAAGAAAGCAAAGGCTGAAAAGCA
60 GAATACACAGGCTGCTGAAATCGAAAAGACGGATAGAGCAAGAAAGCAAAGGCTGAAAAGCA
    pPICZCGPA1
    GPA1

     190     200     210     220     230     240
181 TATTGGAAAGCTTTTGCTACTTGGTGCTGGGGAATCTGGAAAATCTACAATTTTAAGCA
120 TATTGGAAAGCTTTTGCTACTTGGTGCTGGGGAATCTGGAAAATCTACAATTTTAAGCA
    pPICZCGPA1
    GPA1

     250     260     270     280     290     300
241 GATAAACTTCTATTCCAAAAGGGGATTTGATGAAAGGAGAACTAAAGAGCTATGTTCCAGT
180 GATAAACTTCTATTCCAAAAGGGGATTTGATGAAAGGAGAACTAAAGAGCTATGTTCCAGT
    pPICZCGPA1
    GPA1

     310     320     330     340     350     360
301 GATTGATGCCAATGCTCTATCAGACTATAAAATTATTGCAATGATGGAACAAAAGGAGTTTC
240 GATTGATGCCAATGCTCTATCAGACTATAAAATTATTGCAATGATGGAACAAAAGGAGTTTC
    pPICZCGPA1
    GPA1

     370     380     390     400     410     420
361 TCAAAATGAAAACAGATTCTGCTAAAATATATGTTATCTTCTGAAAAGTATTGCAATTGGGGA
300 TCAAAATGAAAACAGATTCTGCTAAAATATATGTTATCTTCTGAAAAGTATTGCAATTGGGGA
    pPICZCGPA1
    GPA1

     430     440     450     460     470     480
421 GAAACTATCTGAGATTGGTGGTAGGTTAGACTATCCAGCTCTTAGCAAGGACATGGCTGA
360 GAAACTATCTGAGATTGGTGGTAGGTTAGACTATCCAGCTCTTAGCAAGGACATGGCTGA
    pPICZCGPA1
    GPA1

     490     500     510     520     530     540
481 GGGAAATAGAAAACACTATGGAAGGATCCTGCAATCAGGAAACTTGTGCTCGTGGTAATGA
420 GGGAAATAGAAAACACTATGGAAGGATCCTGCAATCAGGAAACTTGTGCTCGTGGTAATGA
    pPICZCGPA1
    GPA1

     550     560     570     580     590     600
541 GCTTCAGGTTCTGATTGTACGAAAATATCTGATGGAGAAGCTTGAAGAGACTATCAGATAT
480 GCTTCAGGTTCTGATTGTACGAAAATATCTGATGGAGAAGCTTGAAGAGACTATCAGATAT
    pPICZCGPA1
    GPA1
```

601 810 820 830 840 850 860 pPIGZGPA1
540 AAATTATATTGCAACTAAGGAGGATGTACTTTATGCAAGAGTTGGCAGAACTGGTGTGGT GPA1
AAATTATATTGCAACTAAGGAGGATGTACTTTATGCAAGAGTTGGCAGAACTGGTGTGGT

661 870 880 890 700 710 720 pPIGZGPA1
600 GGAAATACAGTTGAGCCCTGTGGGAGAGAATAAAAAAAGTGGTGAAGTGTACCGATTGTT GPA1
GGAAATACAGTTGAGCCCTGTGGGAGAGAATAAAAAAAGTGGTGAAGTGTACCGATTGTT

721 730 740 750 760 770 780 pPIGZGPA1
660 TGACGTGGGTGGACAGAGAAATGAGAGGAGCAAAATGGATTTCATCTGTTTGAAGGTGTAACT GPA1
TGACGTGGGTGGACAGAGAAATGAGAGGAGCAAAATGGATTTCATCTGTTTGAAGGTGTAACT

781 790 800 810 820 830 840 pPIGZGPA1
720 AGCTGTGATATTTTGTGCTGCCATCAGCGAGTACGACCAAAAGCGTCTTTGAGGACGAGCA GPA1
AGCTGTGATATTTTGTGCTGCCATCAGCGAGTACGACCAAAAGCGTCTTTGAGGACGAGCA

841 850 860 870 880 890 900 pPIGZGPA1
780 GAAAAACAGGATGATGGAGACCAAGGAATTATTGCACTGGGTGCTGAAAACAACCGTCTTT GPA1
GAAAAACAGGATGATGGAGACCAAGGAATTATTGCACTGGGTGCTGAAAACAACCGTCTTT

901 910 920 930 940 950 960 pPIGZGPA1
840 TGAGAAAACATCCCTTCATGCTGTTCTTGAACAAGTTCCACATATTTGAGAAGAAAAGTTCT GPA1
TGAGAAAACATCCCTTCATGCTGTTCTTGAACAAGTTCCACATATTTGAGAAGAAAAGTTCT

961 970 980 990 1000 1010 1020 pPIGZGPA1
900 TGACGTTCCGTTGAACGTTTGGAGTGGTTGAGAGATTAGCAACCAAGTTTCAAGTGGGAA GPA1
TGACGTTCCGTTGAACGTTTGGAGTGGTTGAGAGATTAGCAACCAAGTTTCAAGTGGGAA

1021 1030 1040 1050 1060 1070 1080 pPIGZGPA1
960 ACAAGAGATTGAGCATGCATACGAGTTTGTGAAGAGAAGTTTGAAGGAGTTATATTACCA GPA1
ACAAGAGATTGAGCATGCATACGAGTTTGTGAAGAGAAGTTTGAAGGAGTTATATTACCA

1081 1090 1100 1110 1120 1130 1140 pPIGZGPA1
1020 GAACACGGCGCCGGATAGAGTGGACAGGGTATTCAAAATCTACAGGACGACGGCTTTGGA GPA1
GAACACGGCGCCGGATAGAGTGGACAGGGTATTCAAAATCTACAGGACGACGGCTTTGGA

1141 1150 1160 1170 1180 1190 1200 pPIGZGPA1
1080 CGAGAAAGCTTGTAAAGAAAAGCTTCAAGCTCGTAGATGAGACACTAAGAAGGAGAAAATTT GPA1
CGAGAAAGCTTGTAAAGAAAAGCTTCAAGCTCGTAGATGAGACACTAAGAAGGAGAAAATTT

1201 1210 1220 1230 1240 1250 1260 pPIGZGPA1
1140 ACTGGAGGCTGGCCTTTTACTCGAGCCGCGCGCGCGCCAGCTTACGTAGAACAAAAACT GPA1
ACTGGAGGCTGGCCTTTTACTCGAGCCGCGCGCGCGCCAGCTTACGTAGAACAAAAACT

1261 1270 1280 1290 1300 1310 1320 pPIGZGPA1
1200 CATCTCAGAAGAGGATCTGAAATAGCGCGGTGGACCATCATCATCATCATGATTGATTTTC GPA1
CATCTCAGAAGAGGATCTGAAATAGCGCGGTGGACCATCATCATCATCATGATTGATTTTC

1321 1330 1340 1350 1360 1370 1380 pPIGZGPA1
1255 TAGGCTTAGACATGACTGTTGCTCAGTTGAAGTTGGCCACTACGAGAAGACCGGCTCTGCT GPA1

1381 AGAT pPIGZGPA1
1255 GPA1

X non conserved
. similar
| conserved
| all match

F.2 Sequencing results of AGB1 and pGEX-4T-2 AGB1 construct

Alignment starts from the *EcoRI* multiple cloning site of the vector and ends at the stop codon of the *AGB1* gene.

```

1   10   20   30   40   50   60   pGEX4T2-AG
1   GGGGGGGCGCGTCTCTCCAAAATCTGGATCTAGGTTCCGCGTGGATCCCAGGAATTCCCAG
1   A
61  70   80   90   100  110  120  pGEX4T2-AG
2   TGTCTGTCTCCGAGCTCAAAGAACGCCACGCCGTCGCTACGGAGACCGTTAATAAACCTCC
2   TGTCTGTCTCCGAGCTCAAAGAACGCCACGCCGTCGCTACGGAGACCGTTAATAAACCTCC
121 130  140  150  160  170  180  pGEX4T2-AG
62  GTGACCAAGCTTAGACAGAGACGCCTCCAGCTCCTCGATACCGATGTGGCGAGGTAATTCAG
62  GTGACCAAGCTTAGACAGAGACGCCTCCAGCTCCTCGATACCGATGTGGCGAGGTAATTCAG
181 190  200  210  220  230  240  pGEX4T2-AG
182 CGGCGCAAGGACGTAAGCTCGGGTGAGCTTCGGAGCAAACGGATCTGGTTTGTGTCGTACTC
182 CGGCGCAAGGACGTAAGCTCGGGTGAGCTTCGGAGCAAACGGATCTGGTTTGTGTCGTACTC
241 250  260  270  280  290  300  pGEX4T2-AG
182 TTCAGGGACACACCGGAAAGGTTTATTCATTAGATTGGACACCGGAGAGAGAAACCGGATTG
182 TTCAGGGACACACCGGAAAGGTTTATTCATTAGATTGGACACCGGAGAGAGAAACCGGATTG
301 310  320  330  340  350  360  pGEX4T2-AG
242 TCAGTGCACTCTCAAGATGGGAGATTAAATCGTGTGGAATGCTCTAACGAGTCAGAAAATCTC
242 TCAGTGCACTCTCAAGATGGGAGATTAAATCGTGTGGAATGCTCTAACGAGTCAGAAAATCTC
361 370  380  390  400  410  420  pGEX4T2-AG
302 ATGCTATTAAACTCCCTTGTGCATGGGTTATGACATGTGCTTCTCTCCAAATGGTCAGT
302 ATGCTATTAAACTCCCTTGTGCATGGGTTATGACATGTGCTTCTCTCCAAATGGTCAGT
421 430  440  450  460  470  480  pGEX4T2-AG
362 CGGTTGCGTGTGGTGGATTAGACAGTGTATGTTCTATCTTTAGCCTTAGCTCAACGGCGG
362 CGGTTGCGTGTGGTGGATTAGACAGTGTATGTTCTATCTTTAGCCTTAGCTCAACGGCGG
481 490  500  510  520  530  540  pGEX4T2-AG
422 ACAAGGATGGAACTGTACCGGTTTCAAGAATGCTCACTGGTCAACAGGGGATATGTTTCGT
422 ACAAGGATGGAACTGTACCGGTTTCAAGAATGCTCACTGGTCAACAGGGGATATGTTTCGT

```

541 550 560 570 580 590 600 pGEX4T2-AG
482 GCTGTCAGTATGTCCTCCAAATGAGGATGCCACCTTATCAACCAATTGAGGTGATCAAACTT
AGB1
GCTGTCAGTATGTCCTCCAAATGAGGATGCCACCTTATCAACCAATTGAGGTGATCAAACTT

601 610 620 630 640 650 660 pGEX4T2-AG
542 GTATCTTATGGGATGTAACCTACTGGTCTCAAAAATTCTGTTTTTGGCGGTGAATTTCAGT
AGB1
GTATCTTATGGGATGTAACCTACTGGTCTCAAAAATTCTGTTTTTGGCGGTGAATTTCAGT

661 670 680 690 700 710 720 pGEX4T2-AG
602 CTGGACATACTGCTGATGTACTAAGCGTCTCAATCAAGTGGATCAAACCCAAACTGTTTA
AGB1
CTGGACATACTGCTGATGTACTAAGCGTCTCAATCAAGTGGATCAAACCCAAACTGTTTA

721 730 740 750 760 770 780 pGEX4T2-AG
662 TATCTGGTTCATGCCGATTCCACAGCACGGTTGTGGGACACTCGTCTGCAAGCCGAGCAG
AGB1
TATCTGGTTCATGCCGATTCCACAGCACGGTTGTGGGACACTCGTCTGCAAGCCGAGCAG

781 790 800 810 820 830 840 pGEX4T2-AG
722 TGCGTACCTTTCATGGTCACGAGGGAGATGTTAATACGGTCAAGTTCTTTCCGGATGGGT
AGB1
TGCGTACCTTTCATGGTCACGAGGGAGATGTTAATACGGTCAAGTTCTTTCCGGATGGGT

841 850 860 870 880 890 900 pGEX4T2-AG
782 ACAGATTGGGACTGGATCAGACGATGGAACATGCAGGCTGTATGACATAAGGACTGGTC
AGB1
ATAGATTGGGACTGGATCAGACGATGGAACATGCAGGCTGTATGACATAAGGACTGGTC

901 910 920 930 940 950 960 pGEX4T2-AG
842 ACCAACTCCAGGTCTATCAGCCACATGGTGATGGTGAGAACGGACCTGTCACTCCATTG
AGB1
ACCAACTCCAGGTCTATCAGCCACATGGTGATGGTGAGAACGGACCTGTCACTCCATTG

961 970 980 990 1000 1010 1020 pGEX4T2-AG
902 CATTCTCTGTGTCAGGGAGACTTCTTTTCGCTGGCTATGCGAGCAACAACACTTGCTACG
AGB1
CATTCTCTGTGTCAGGGAGACTTCTTTTCGCTGGCTATGCGAGCAACAACACTTGCTACG

1021 1030 1040 1050 1060 1070 1080 pGEX4T2-AG
962 TTTGGGATACCCTCTTGGGAGAGGTTGATTGGATTGGGATTACAGCAGGATTCACACA
AGB1
TTTGGGATACCCTCTTGGGAGAGGTTGATTGGATTGGGATTACAGCAGGATTCACACA

1081 1090 1100 1110 1120 1130 1140 pGEX4T2-AG
1022 GGAATAGAAATAAGCTGTTTGGGGTTGTCAGCAGATGGAAAGTCCTTGTGTACAGGAAGTT
AGB1
GGAATAGAAATAAGCTGTTTGGGGTTGTCAGCAGATGGAAAGTCCTTGTGTACAGGAAGTT

1141 1150 1160 1170 1180 1190 1200 pGEX4T2-AG
1082 GGGATTCAAATCTAAAGATATGGCGTTTGGAGGACACAGGAGAGTGATTTGACTCGAGC
AGB1
GGGATTCAAATCTAAAGATATGGCGTTTGGAGGACACAGGAGAGTGATTTGAA

1201 1210 1220 1230 1240 1250 pGEX4T2-AG
1135 GGCCGCATCGTGACTGACTGACGATCTGCCCTCGCGCTTCGGTGAGAATCAAAAA
AGB1

non conserved
 similar
 conserved
 all match

F.3 Sequencing results of AGB1 and pQE-80L AGB1 construct

Sequencing results of forward sequencing primer (QE Type III/IV) and reverse sequencing primer. Alignment starts at RGS-6xhis tag and ends at the stop codon of pQE-80L coding frame.

```

1      10      20      30      40      50      60
1  ATG ..... TCTGTCTCCGAGCTCAAAGAACGC At4g34460
1  ATGAGAGGATCGCATCACCATCAACCATCACGGATCCTCTGTCTCCGAGCTCAAAGAACGC pQE-80

70      80      90      100     110     120
28  CACGCCGTCGCTACGGAGACCCTTAAATAACCTCCGTGACCAGCTTAGACAGAGACGCCCTC At4g34460
61  CACGCCGTCGCTACGGAGACCCTTAAATAACCTCCGTGACCAGCTTAGACAGAGACGCCCTC pQE-80

130     140     150     160     170     180
88  CAGCTCCTCGATAACCGATGTGGCGAGGTAATTCAGCGGCGCAAGGACGTACTCGGGTGAGC At4g34460
121  CAGCTCCTCGATAACCGATGTGGCGAGGTAATTCAGCGGCGCAAGGACGTACTCGGGTGAGC pQE-80

190     200     210     220     230     240
148  TTCGGAGCAAACGGATCTGGTTTGTGTCGTACTCTTCAGGACACACCGGAAAGGTTTAT At4g34460
181  TTCGGAGCAAACGGATCTGGTTTGTGTCGTACTCTTCAGGACACACCGGAAAGGTTTAT pQE-80

250     260     270     280     290     300
208  TCATTAGATTGGACACCGGAGAGGAAACCGGATTGTCAGTGCACTCAAGATGGGAGATTA At4g34460
241  TCATTAGATTGGACACCGGAGAGGAAACCGGATTGTCAGTGCACTCAAGATGGGAGATTA pQE-80

310     320     330     340     350     360
268  ATCGTGTGGAATGCTCTAACGAGTCAGAAAACCTCATGCTATTAAACTCCCTTGTGCATGG At4g34460
301  ATCGTGTGGAATGCTCTAACGAGTCAGAAAACCTCATGCTATTAAACTCCCTTGTGCATGG pQE-80

370     380     390     400     410     420
328  GTTATGACATGTGCTTCTCTCCAAATGGTCAGTCGGTTGCGTGTGGTGGATTAGACAGT At4g34460
361  GTTATGACATGTGCTTCTCTCCAAATGGTCAGTCGGTTGCGTGTGGTGGATTAGACAGT pQE-80

430     440     450     460     470     480
388  GTATGTTCTATCTTTAGCCTTAGCTCAACGGCGGACAAAGGATGGAAGTGTACCGGTTTCA At4g34460
421  GTATGTTCTATCTTTAGCCTTAGCTCAACGGCGGACAAAGGATGGAAGTGTACCGGTTTCA pQE-80

490     500     510     520     530     540
448  AGAATGCTCACTGGTCACAGGGGATATGTTTCGTGCTGTGAGTATGTCCCAAATGAGGAT At4g34460
481  AGAATGCTCACTGGTCACAGGGGATATGTTTCGTGCTGTGAGTATGTCCCAAATGAGGAT pQE-80

```

508 550 560 570 580 590 600 At4g34460
541 GCCCACCTTATCACCAAGTTCAGGTGATCAAACCTTGTATCTTATGGGATGTAACTACTGGT pQE-80
GCCCACCTTATCACCAAGTTCAGGTGATCAAACCTTGTATCTTATGGGATGTAACTACTGGT

568 610 620 630 640 650 660 At4g34460
601 CTCAAAACTTCTGTTTTTGGCGGTGAATTCAGTCTGGACATACTGCTGATGTACTAAGC pQE-80
CTCAAAACTTCTGTTTTTGGCGGTGAATTCAGTCTGGACATACTGCTGATGTACTAAGC

628 670 680 690 700 710 720 At4g34460
661 GTCTCAATCAGTGGATCAAACCCAAACTGGTTTATATCTGGTTCATGCGATTCCACAGCA pQE-80
GTCTCAATCAGTGGATCAAACCCAAACTGGTTTATATCTGGTTCATGCGATTCCACAGCA

688 730 740 750 760 770 780 At4g34460
721 CGGTTGTGGGACACTCGTCTGCAAGCCGAGCAGTGCCTACCTTTCATGGTCACGAGGGA pQE-80
CGGTTGTGGGACACTCGTCTGCAAGCCGAGCAGTGCCTACCTTTCATGGTCACGAGGGA

748 790 800 810 820 830 840 At4g34460
781 GATGTTAATAACGGTCAAGTTCCTTCCGGATGGGTATAGATTTGGGACTGGATCAGACGAT pQE-80
GATGTTAATAACGGTCAAGTTCCTTCCGGATGGGTATAGATTTGGGACTGGATCAGACGAT

808 850 860 870 880 890 900 At4g34460
841 GGAACATGCAGGCTGTATGACATAAAGGACTGGTCACCAACTCCAGGTCTATCAGCCACAT pQE-80
GGAACATGCAGGCTGTATGACATAAAGGACTGGTCACCAACTCCAGGTCTATCAGCCACAT

868 910 920 930 940 950 960 At4g34460
901 GGTGATGGTGAGAACGGACCTGTACCTCCATTGCAATTCCTCTGTGTACAGGGAGACTTCTT pQE-80
GGTGATGGTGAGAACGGACCTGTACCTCCATTGCAATTCCTCTGTGTACAGGGAGACTTCTT

928 970 980 990 1000 1010 1020 At4g34460
961 TTCGCTGGCTATGCGAGCAAACAACACTTGCTACGTTTGGGATACCCCTCTGGGAGAGGTT pQE-80
TTCGCTGGCTATGCGAGCAAACAACACTTGCTACGTTTGGGATACCCCTCTGGGAGAGGTT

988 1030 1040 1050 1060 1070 1080 At4g34460
1021 GTATTGGATTGGGATTACAGCAGGATTCACACAGGAATAGAATAAGCTGTTTGGGGTTG pQE-80
GTATTGGATTGGGATTACAGCAGGATTCACACAGGAATAGAATAAGCTGTTTGGGGTTG

1048 1090 1100 1110 1120 1130 1140 At4g34460
1081 TCAGCAGATGGAAAGTCCTTGTGTAACAGGAAGTTGGGATTCAAATCTAAAGATATGGGCG pQE-80
TCAGCAGATGGAAAGTCCTTGTGTAACAGGAAGTTGGGATTCAAATCTAAAGATATGGGCG

1108 1150 1160 1170 1180 1190 1200 At4g34460
1141 TTTGGAGGACACAGGAGAGTGAATGGAACCCCGGGTCGACCTGCAGCCAAGCTTAATTAG pQE-80
TTTGGAGGACACAGGAGAGTGAATGGAACCCCGGGTCGACCTGCAGCCAAGCTTAATTAG

 non conserved
 similar
 conserved
 all match

F.4 Sequencing results of AGG1 and pGEX-4T-2 -AGG1 construct.

Alignment starts from the forward sequencing primer and ends at the reverse sequencing primer of pGEX-4T-2 vector.

```

      10      20      30      40      50      60
1 1 GGGCTGGCAAGCCACGTTTGGTGGTGGGGACCA TCCTCCAAAATCGGATCTGGTTCCGCG
AGG1
pGEX4T2-AG

      70      80      90      100     110     120
1 1 ATGCGAGAGGAAACTGTGGTTTACGAGCAGGAGGAGTCTGT
-1 TGGATCCCCAGGAATTCCCATGCGAGAGGAAACTGTGGTTTACGAGCAGGAGGAGTCTGT
AGG1
pGEX4T2-AG

     130     140     150     160     170     180
42 TTC TCACGGCGGGGGC AAGCACAGGATCC TTGCAGAGCTTGC CCGCGTTGAACAGGAAGT
60 TTC TCACGGCGGGGGC AAGCACAGGATCC TTGCAGAGCTTGC CCGCGTTGAACAGGAAGT
AGG1
pGEX4T2-AG

     190     200     210     220     230     240
102 CGCTTTCTTGGAGAAA GAGTTGAAGGAGG TCGA GAACACAGATATTGTATCAACCGTGTG
120 CGCTTTCTTGGAGAAA GAGTTGAAGGAGG TCGA GAACACAGATATTGTATCAACCGTGTG
AGG1
pGEX4T2-AG

     250     260     270     280     290     300
162 TGA GGAGCTGCTATCT GTCATCGAGAAA GACCCGATCCTCT GTTGCCACTAACC AATGG
180 TGA GGAGCTGCTATCT GTCATCGAGAAA GACCCGATCCTCT GTTGCCACTAACC AATGG
AGG1
pGEX4T2-AG

     310     320     330     340     350     360
222 ACCTTTGAACTTAGGATGGGACCGGTGGTTTGAAGGACCAAA TGGAGGAGAAAGGCTGCAG
240 ACCTTTGAACTTAGGATGGGACCGGTGGTTTGAAGGACCAAA TGGAGGAGAAAGGCTGCAG
AGG1
pGEX4T2-AG

     370     380     390     400     410     420
282 ATGCTTAATACTTTGA
300 ATGCTTAATACTTTGA CTCGAGCGGGCGCATCGTGACTGACTGACGATCTGCCTCGCGCG
AGG1
pGEX4T2-AG

     430     440     450     460
298 TTTTCGGTGATGACGGTGAAAACCTCTGACACATGCCAGTCCC GG
360 TTTTCGGTGATGACGGTGAAAACCTCTGACACATGCCAGTCCC GG
AGG1
pGEX4T2-AG

```

non conserved
 similar
 conserved
 all match

F.5 Sequencing results of AGG2 and pQE-80L -AGG2 construct

Sequencing results of forward sequencing primer (QE Type III/IV) and reverse sequencing primer (QE terminator) were combined. Alignment starts at RGS-6xhis tag and ends at the stop codon of pQE-80L coding frame.

```

1          10          20          30          40          50          60
1  TACCGTCATTACT ATG . . . . . GAAGCGGGTAG AGG2 (At3g2
1  TACCGTCATTACT ATG AGAGGATCGCATCACCA TCACCATCACGGATCC GAAGCGGGTAG pQE80

          70          80          90          100         110         120
15 CTCCAATTCGTCGGGT CAGCTATCGGGCGGGTGGTTGATACAAGAGGCCAAACACAGGAT AGG2 (At3g2
61 CTCCAATTCGTCGGGT CAGCTATCGGGCGGGTGGTTGATACAAGAGGCCAAACACAGGAT pQE80

          130         140         150         160         170         180
75 TCAAGCTGAACTCAAAAGGCTTGAAACAAGAAGCTCGATTCTTAGAGGAAAGAGCTGGAGCA AGG2 (At3g2
121 TCAAGCTGAACTCAAAAGGCTTGAAACAAGAAGCTCGATTCTTAGAGGAAAGAGCTGGAGCA pQE80

          190         200         210         220         230         240
135 GCTTGAG AAGATGGACAATGCATCAGCATCCTGCAAAGAGTTCTTAGACAGTGTTGACAG AGG2 (At3g2
181 GCTTGAG AAGATGGACAATGCATCAGCATCCTGCAAAGAGTTCTTAGACAGTGTTGACAG pQE80

          250         260         270         280         290         300
195 CAAACCCGATCCTCTTCTTCCCGAAAACAACAGGTCCGGTGAAATGCGACATGGGATCAATG AGG2 (At3g2
241 CAAACCCGATCCTCTTCTTCCCGAAAACAACAGGTCCGGTGAAATGCGACATGGGATCAATG pQE80

          310         320         330         340         350         360
255 GTTCGAAGGCCCTAAA GAAGCAA AACGATGTGGCTGCTCCATTCTT . . . . . AGG2 (At3g2
301 GTTCGAAGGCCCTAAA GAAGCAA AACGATGTGGCTGCTCCATTCTT GGTACCCCGGGTCCG pQE80

          370         380         390         400         410         420
301 . . . . . TGA AGG2 (At3g2
361 ACCTGCAGCCAAGCTTAATTAGCTGA GCTTGGACTCCTGTTGATAGATCCAGTAATGACC pQE80

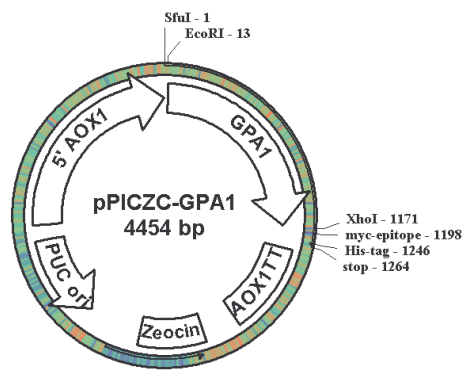
```

non conserved
 similar
 conserved
 all match

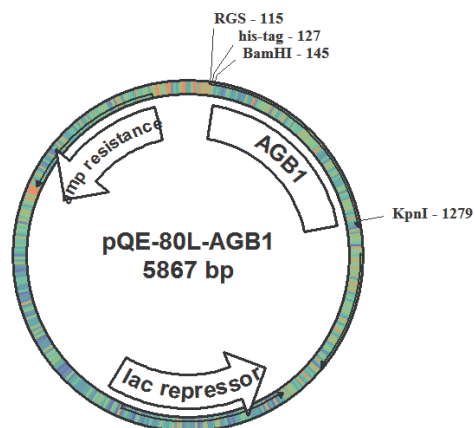
APPENDIX G

CONSTRUCTS

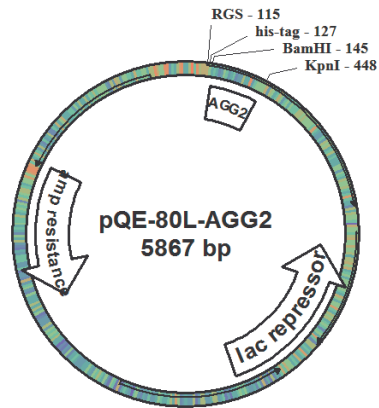
G.1 pPICZC+GPA1



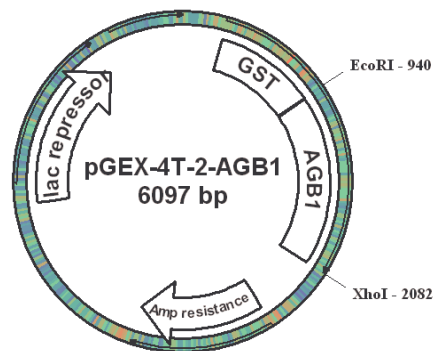
G.2 pQE-80L-AGB1



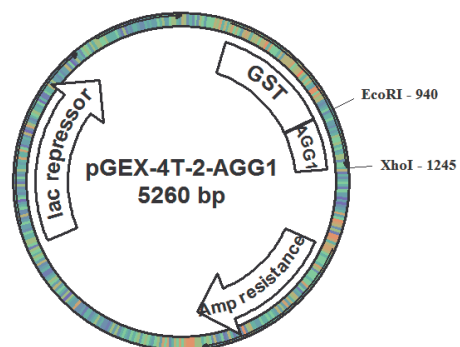
G.3 pQE-80L AGG2



G.4 pGEX-4T-2-AGB1



G.5 pGEX-4T-2-AGG1



APPENDIX H

INDUCTION DATA

Different strains of *Escherichia coli* harboring pGEX-4T-2 or pQE-80L constructs were grown with the given conditions. The cells were analyzed for protein expression, as given in Chapter 4.8.

1. BL21(DE3)

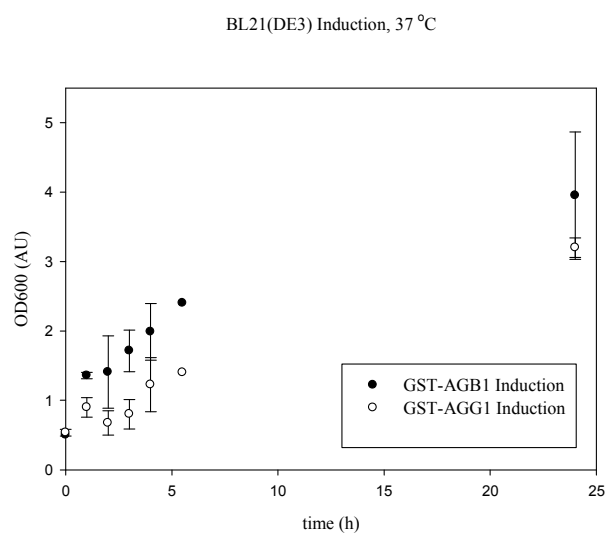


Figure H 1: Growth curves of GST-AGB1 and GST-AGG1 harboring BL21(DE3) cells grown at 37 °C, in LB-amp. 0.5 mM IPTG was given at t=0 to cells.

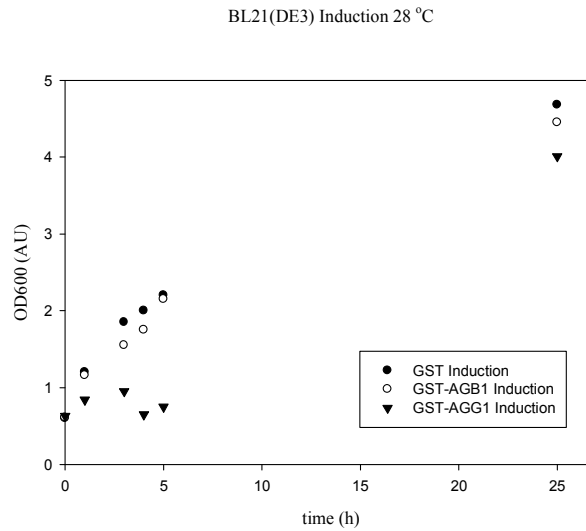


Figure H 2: Growth curves of GST, GST-AGB1 and GST-AGG1 harboring BL21(DE3) cells grown at 28 °C, in LB-amp. 0.5 mM IPTG was given at t=0 to cells.

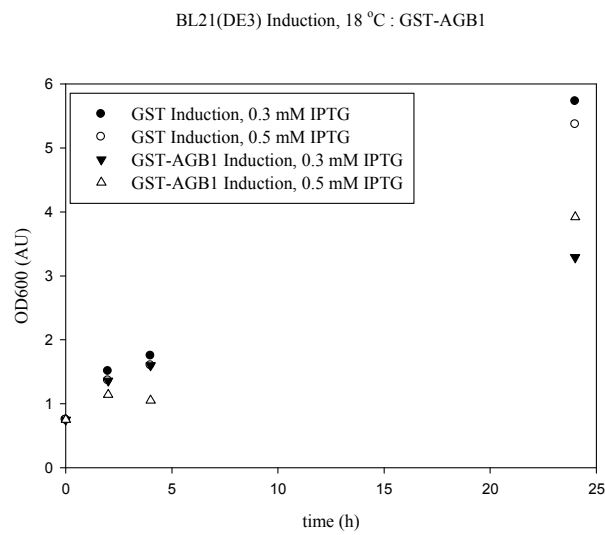


Figure H 3: Growth curves of GST and GST-AGB1 harboring BL21(DE3) cells grown at 18 °C, in LB-amp. 0.3 or 0.5 mM IPTG was given at t=0 for induced cells.

BL21(DE3) Induction, 18 °C : GST-AGG1

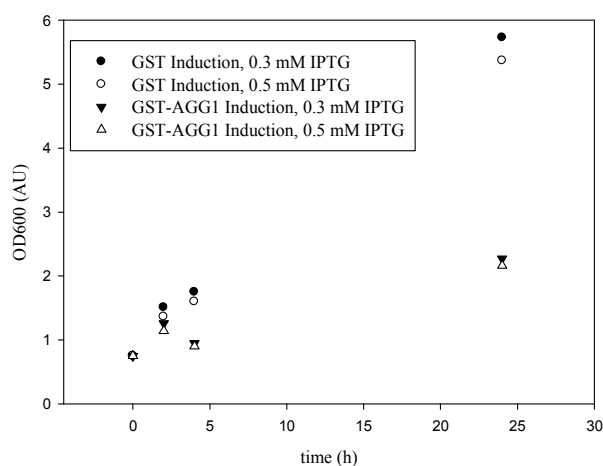


Figure H 4: Growth curves of GST and GST-AGG1 harboring BL21(DE3) cells grown at 18 °C, in LB-amp. 0.3 or 0.5 mM IPTG was given at t=0 for induced cells.

2. BL21(DE3)RIPL

BL21(DE3) RIPL Induction: GST-AGB1

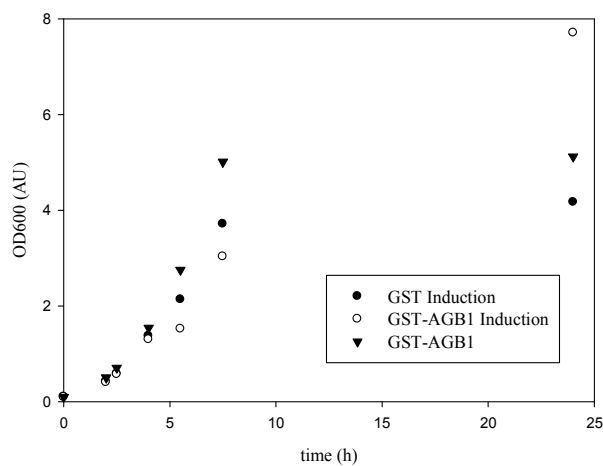


Figure H 5: Growth curves of GST and GST-AGB1 harboring BL21(DE3)RIPL cells grown at 29 °C, in LB-amp. 0.5 mM IPTG was given at t=2.5 for induced cells.

BL21(DE3) RIPL Induction: GST-AGG1

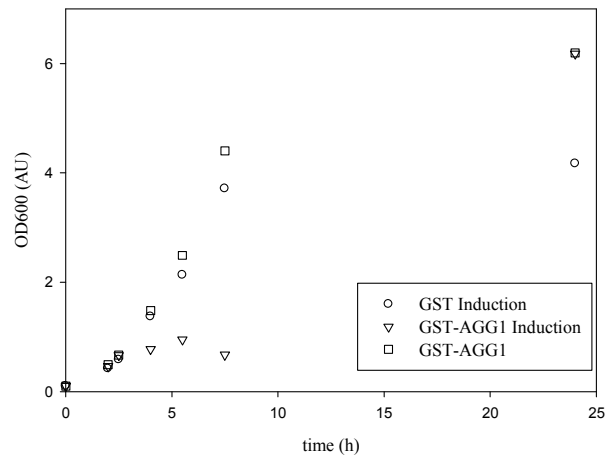


Figure H 6: Growth curves of GST and GST-AGG1 harboring BL21(DE3)RIPL cells grown at 29 °C, in LB-amp. 0.5 mM IPTG was given at t=2.5 for induced cells.

3. TOP10

TOP10 Induction: RGS-his-AGB1

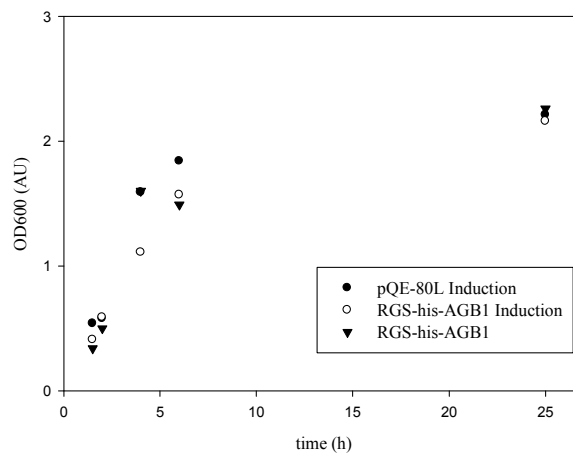


Figure H 7: Growth curves of pQE-80L without insert or RGS-his-AGB1 harboring TOP10 cells grown at 25 °C, in LB-amp. 0.5 mM IPTG was given at t=2 for induced cells.

TOP10 Induction: RGS-his-AGG2

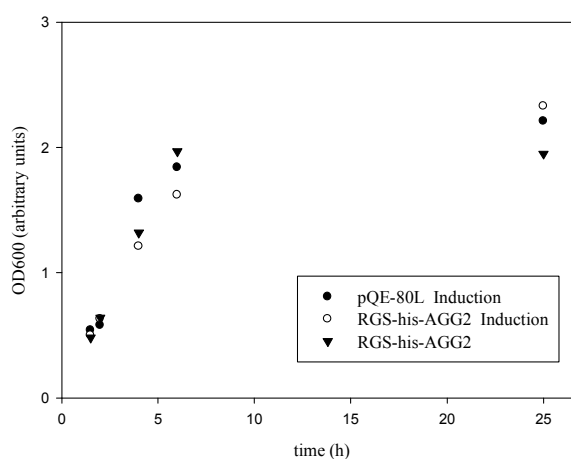


Figure H 8: Growth curves of pQE-80L without insert or RGS-his-AGG2 harboring TOP10 cells grown at 25 °C, in LB-amp. 0.5 mM IPTG was given at t=2 for induced cells.

4. Rosetta 2 (DE3)

Rosetta 2 (DE3) Induction: RGS-his-AGB1 and RGS-his-AGG2

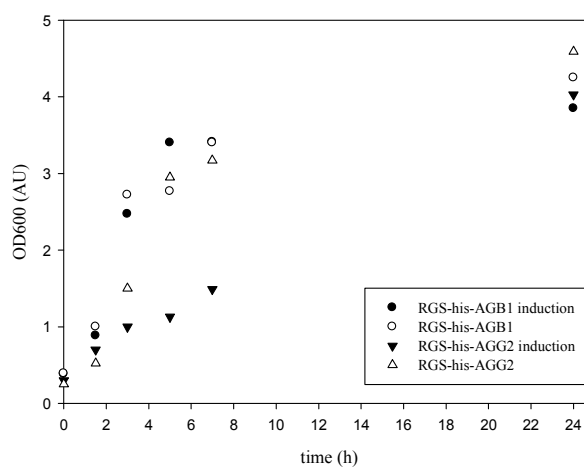


Figure H 9: Growth curves of pQE-80L with RGS-his-AGB1 or RGS-his-AGG2 harboring Rosetta 2 (DE3) cells grown at 29 °C, in LB-amp. 0.5 mM IPTG was given at t=1.5 for induced cells.

APPENDIX I

Amino Acid Sequencing Results and Expected Sequences

A. GPA1-his-myc

- Theoretical Sequence:

MGLLCRSRHHHTEDTDENTQAAEIERRIEQEAKAEKHIRKLLLLGAGESGKSTIF
KQIKLLFQTGFDEGELKSYVPVIHANVYQTIKLLHDGTKFAQNETDSAKYMLS
SESAIGEKLSEIGGRLDYPRLTKDIAEGIETLWKDPAIQETCARGNELQVPDCTK
YLMENLKRLSDINYIPTKEDVLYARVRTTGVVEIQFSPVGENKKSGEVYRLFDV
GGQRNERRKWIHLFEGVTAVIFCAAISEYDQTLFEDEQKNRMMETKELFDWVL
KQPCFEKTSFMLFLNKFDFEKKVLDVPLNVCEWFRDYQPVSSGKQEIEHAYEF
VKKKFEELYQNTAPDRVDRVFKIYRTTALDQKLVKKTFLVDETLRRRNLE
AGLLEPRRPPAYVEQKLISEEDLNSAVDHHHHHH

- Edman Sequencing Result:

(G/X)LLXS

The sequencing results (Figure I 1) verified the presence of expected 4 amino acids. The first glycine was co eluted with an unknown peak, which could be from the blotting buffer or a modification. At position 4 there is only an unknown peak possibly a modified amino acid, e.g. cysteine. Cysteine is destroyed during Edman degradation, so normally it is reduced and carboxamidomethylated before sequencing to get a stable derivative. If it is modified by a fatty acid, it would elute very late or not at all from the reversed-phase HPLC column.

SEQUENCER: ABI 492						Run-Nr 296-5A (5168-1)	
SAMPLE: 1						DATE 08.12.08	
						ID Kaplan	
SUPPORT:	Peptid	Protein	SELEX	PVDF	Glasfaser	Polybren	Blot
		x		x			x
	Main sequence			Minor sequences			
1	G			X			21
2	L						22
3	L						23
4	X?						24
5	S						25
6							26
7							27
8							28
9							29
10							30
11							31
12							32
13							33
14							34
15							35
16							36
17							37
18							38
19							39
20							40
KOMMENTAR							
Position 1: glycine and unknown signal (from blotting buffer?)							
Position 4: unknown signal, maybe cysteine or other modified amino acid							

Figure I 1: N-terminus amino acid sequencing results for GPA1 (stg. 3.2.1).

- MALDI-TOF Result:

The below amino acid sequence was deduced from fragments of pool 3 GPA1. Six amino acid N-terminus fragments could not be assigned to any m/z (mass/ charge). The R/K residues that were not digested by trypsin are highlighted; the unassigned amino acids are underlined, covering 13.28 % of the total sequence. 30% of the sequence was unmatched according to TOPLAB, 17.15% of the sequence was assigned using EXPASY Peptide Mass Server (<http://www.expasy.ch/tools/peptide-mass.html>) using the m/z values.

SRHHTEDTDENTQAAEIERRIEQEAKAEKHIRKLLLLGAGESGKSTIFKQIKLLF
QTGFDEGELKSYVPVIHANVYQTIKLLHDGTKEFAQNETDSAKYMLSS^{ESIAIG}
EKLSEIGGRLDYPRLTKDIAEGIETLWKDPAIQETCARGNELQVPDCTKYLMEN
LKRLSDINYIPTKEDVLYARVRTTGVVEIQFSPVGENKKSGEVYRLFDVGGQRN
ERRKWIHLFEGVTAVIFCAAISEYDQTLFEDEQKNRMMETKELFDWVLKQPCF
EKTSFMLFLNKFDIFEKKVLDVPLNVCEWFRDYQPVSSGKQEIEHAYEFVKKKF
EELYYQNTAPDRVDRVFKIYRTTALDQKLVKKTFKLVD^{ETLRR}RNLLEAGLLL
EPRRPPAYVEQKLISEEDLNSAVDHHHHHH

The below amino acid sequence was deduced from fragments of pool 4 GPA1. N-terminus fragments were assigned correctly. The R/K residues that were not digested by trypsin are highlighted; the unassigned amino acids are underlined, covering 13.3 % of the total sequence. 28% of the sequence was unmatched according to TOPLAB, 15.25% of the sequence was assigned using EXPASY Peptide Mass Server (<http://www.expasy.ch/tools/peptide-mass.html>) using the m/z values.

GLLCSRSRHHTEDTDENTQAAEIERRIEQEAKAEKHIRKLLLLGAGESGKSTIFK
QIKLLFQTGFDEGELKSYVPVIHANVYQTIKLLHDGTKEFAQNETDSAKYMLSS
ESIAIGEKLSEIGGRLDYPRLTKDIAEGIETLWKDPAIQETCARGNELQVPDCTK
YLMENLKRLSDINYIPTKEDVLYARVRTTGVVEIQFSPVGENKKSGEVYRLFDV
GGQRNERRKWIHLFEGVTAVIFCAAISEYDQTLFEDEQKNRMMETKELFDWVL
KQPCFEKTSFMLFLNKFDIFEKKVLDVPLNVCEWFRDYQPVSSGKQEIEHAYEF
VKKKFEELYYQNTAPDRVDRVFKIYRTTALDQKLVKKTFKLVD^{ETLRR}RNLLE
AGLLEPRRPPAYVEQKLISEEDLNSAVDHHHHHH

B. RGS-his-AGB1

- Theoretical Sequence:

MRGSHHHHHHGSSVSELKERHAVATETVNNLRDQLRQRRLQLLDTDVARYSA
AQRTRVSEFGATDLVCCRTLQGHTGKVYSLDWTPERNRIVSASQDGR LIVWNA
LTSQKTHAIKLPCAWVMTCAFSPNGQSVACGGLDSVCSIFSLSSSTADKDGTVPV
SRMLTGHRGYVSCCQYVPNEHAHLITSSGDQTCILWDVTTGLKTSVFGGEFQS
GHTADVLSVSISSNPWFISGSCDSTARLWDTRAASRAVRTFHGHEGDVNTV
KFFPDGYRFGTGSDDGTCRLYDIRTGHQLQVYQPHGDGENGPVTSIAFSVSGRL
LFAGYASNNTCYVWD TLLGEVVL DLGLQQDSHRNRISCLGLSADGSALCTGS
WDSNLKIWAFGGHRRVIGTPGRPAAKLN

- Sequencing Result:

Sample gave a sequence of 15 amino acids, but it contained no His-Tag. The database search identified the main sequence as Lac repressor (*E.coli*, cloning vector). There were traces of minor sequences visible, but not enough for identification.

C. The 60 kDa protein co-purified with RGS-his AGB1

N-terminal sequence AAKDV

Although 5 amino acid residues were not enough to directly identify the protein, this sequence is highly conserved within 60 kDa chaperonin groEL protein family.

D. RGS-his-AGG2

- Theoretical Sequence:

MRGSHHHHHHGSEAGSSNSSGQLSGRVVDTRGKHRIQAELKRLEQEARFLEEE
LEQLEKMDNASASCKEFLDSVDSKPDPLLPETTGPVNATWDQWFEGPKEAKRC
GCSILGTPGRPAAKLN

- Sequencing Result:

The sequence following the 6 histidines is clearly GSEAE, although there is a high lag of the many consecutive histidines and the minor sequence which seems to have an additional F at the N-terminus.

Major sequence: MRGSHHHHHHGSEAE

Minor sequence: FMRGSHHHHHHGSEA

SEQUENCER: ABI 492						Run-Nr 299-5A (5168-4)	
SAMPLE: 4						DATE 10.12.08	
						ID Kaplan	
SUPPORT:	Peptid	Protein x	SELEX	PVDF x	Glasfaser	Polybren	Blot x
	Main sequence			Minor sequences			
1	M			F			21
2	R			M			22
3	G			R			23
4	S			G			24
5	H			S			25
6	H			H			26
7	H			H			27
8	H			H			28
9	H			H			29
10	H			H			30
11	G			H			31
12	S			G			32
13	E			S			33
14	A			E			34
15	E			A			35
16							36
17							37

Figure I 2: N-terminus amino acid sequencing results for RGS-his-AGG2, 14 kDa band.

The 15th residue of RGS-his-AGG2 is supposed to be a G, but the sequencing results is an E. When the chromatogram is analyzed carefully the signal for G is also

increasing at position 15, but the dominating signal is from E, but could be the remainder from E at position 13, while G would possibly increase in cycle 16 and 17, but sample was not sequenced that far.

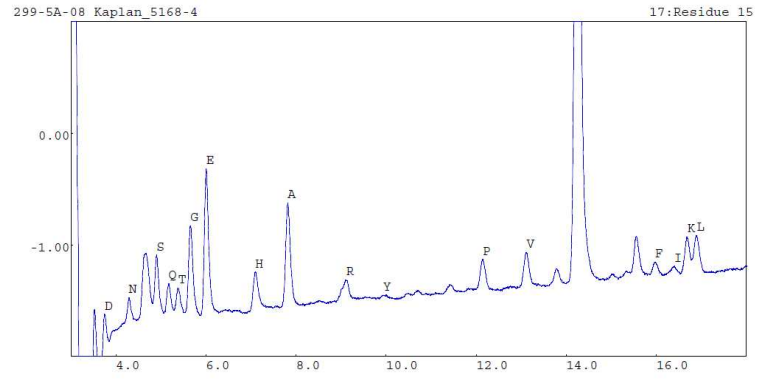


Figure I 3: The chromatogram of 15th amino acid residue of RGS-his-AGG2

APPENDIX J

GPA1-myc-his recombinant protein myristoylation was predicted using NMT - The MYR Predictor (<http://mendel.imp.ac.at/myristate/SUPLpredictor.htm>). Results are given below, server predicts the first glycine as a myristoylation site.

Prediction of potential Myristoylation by NMT (predicted myristoylation site highlighted):

```
MGLLCSRSRH HTEDTDEN TQ AAEIERRIEQ EAKAEKHIRK LLLLGAGESG KSTIFKQIKL
LFQTGFDEGE LKSYVPVIHA NVYQTIKLLH DGTKEFAQNE TDSAKYMLSS ESIAIGEKLS
EIGGRLDYPR LTKDIAEGIE TLWKDPAIQE TCARGNELQV PDCTKYL MEN LKRLSDINYI
PTKEDVLYAR VRTTGVVEIQ FSPVGENKKS GEVYRLFVVG GQRNERRKWI HLFEGVTAVI
FCAAISEYDQ TLFEDQKNR MMETKELFDW VLKQPCFEKT SFMLFLNKFD IFEKKVL DVP
LNVCEWFRDY QPVSSGQEI EHAYEFVKKK FEELYQNTA PDRVDRVFKI YRTTALDQKL
VKKTFKLVE TLRRRNLEA GLLLEPRRPP AYVEQKLI SE EDLNSAVDHH HHHH
```



Figure J 1: 'RELIABLE' myristoylation site predicted, Sequence of the predicted myristoylation signal. Overall score: 0.092. Probability of false positive prediction: 4.66e-03. Parameter set: EUKARYOTA (without FUNGI) plus VIRUSES. All glycines investigated.

GPA1-myc-his recombinant protein palmitoylation was predicted using CSS-Palm 2.0 Online Server (<http://csspalm.biocuckoo.org/online.php>). Server predicts that the cysteine in GLLCSRS motif is a palmitoylation site.

CSS-Palm 2.0 Applet will appear below in a Java 1.4 or later enabled browser.

Predicted sites				
Position	Peptide	Score	Cutoff	Type
5	GLLCSRS	5,191	1	TypeIII: Others

Enter sequence(s) in FASTA format

```
MGLLCSRSRHHHTEDTDENTQAAEIERRIEQEAKAEKHIRKLLLLGAGESGKSTIFKQIKLLFQTGFDEGE
LKSYPVIHANVYQTIKLLHDGTFEFAQNETDSAKYMLSSSIAIGKLEIGGRLDYPRLTKDIAEGIE
TLWKDPAIQETCARGNELQVPDCTKYLMLNKRKLSINYIPTKEDVLYARVRTTGVEIQFSPVGENKKS
GEVYRLFVGGQRNERRKWIHLFEGVTAVIFCAAISEYDQTLFEDEQKNRMMETKELFDWVWKQPCFEKT
SFMLFLNKFDIFEKVLVDVPLNVCEWFRDYQPVSSGKQIEHAYEFVKKKFEELYQNTAPDRVDRVFKI
YRTTALDQKLVKTKFLVDETLRRRNLEAGLLLEPRRPPAYVEQKLISEEDLNSAVDHHHHHH
```

Threshold: High Medium Low All

Console:

Figure J 2: Palmitoylation site predicted using CSS-Palm 2.0 Online Server.

APPENDIX K

Lubrol PX and Triton X-100 Characterization

Triton X-100 and Lubrol-PX were used at different concentrations. The Triton X-100 concentration was 1.5 mM in the lysis buffer and 0.3 mM in the purification buffer. The critical micelle concentration (cmc) for Triton X-100 is 0.25 mM and 0.1 mM for Lubrol PX [119]. Different concentrations of the detergents were prepared in 50 mM Tris, pH 8.0 and 150 mM NaCl. The DLS analysis showed that, below the cmc the solution was heterogeneous but that a homogenous solution with particle diameter 8.5 nm started to form above the cmc for both Triton X-100 (Figure K 2 - Figure K 6) and Lubrol PX (Figure K 7 - Figure K 9).

One major drawback of using Triton-X in buffers is that the detergent itself absorbs at 280 nm, thus interfering with protein concentration estimations. It was not possible to measure the absorbance of 6 mM (0.4 %) and higher concentrations of Triton X-100 (Figure K 10). Lubrol PX, on the other hand, does not have a significant absorbance around 260 and 280 nm even at very high concentrations (Figure K 11).

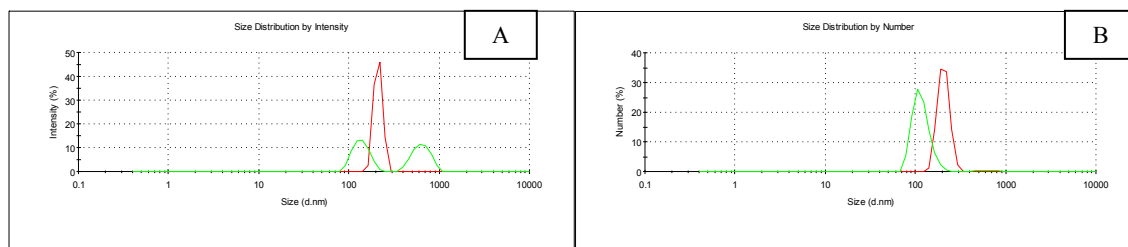


Figure K 1: DLS size distributions by intensity (A) and number (B) of 50 mM Tris, pH 8.0 and 150 mM NaCl.

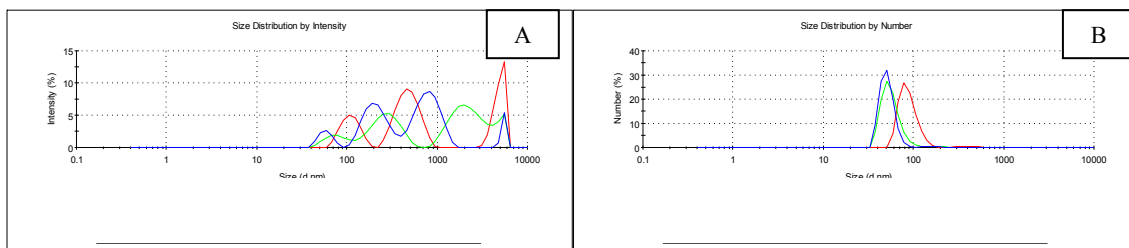


Figure K 2: DLS size distributions by intensity (A) and number (B) of 0.012 % (0.2 mM) Triton X-100.

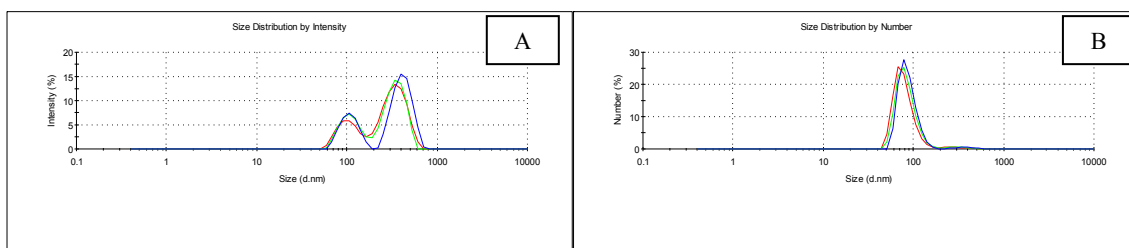


Figure K 3: DLS size distributions by intensity (A) and number (B) of 0.015 % (0.25 mM) Triton X-100.

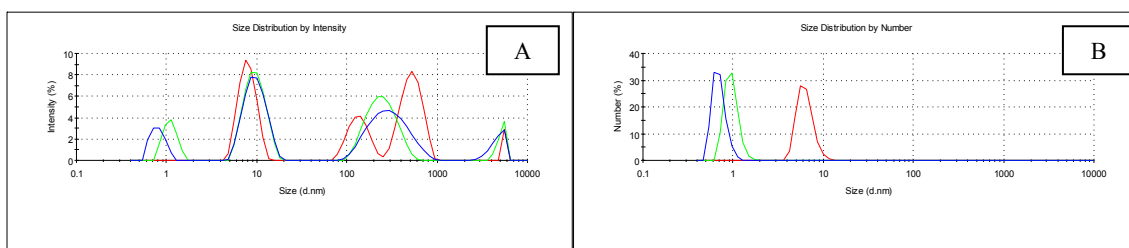


Figure K 4: DLS size distributions by intensity (A) and number (B) of 0.02 % (0.3 mM) Triton X-100.

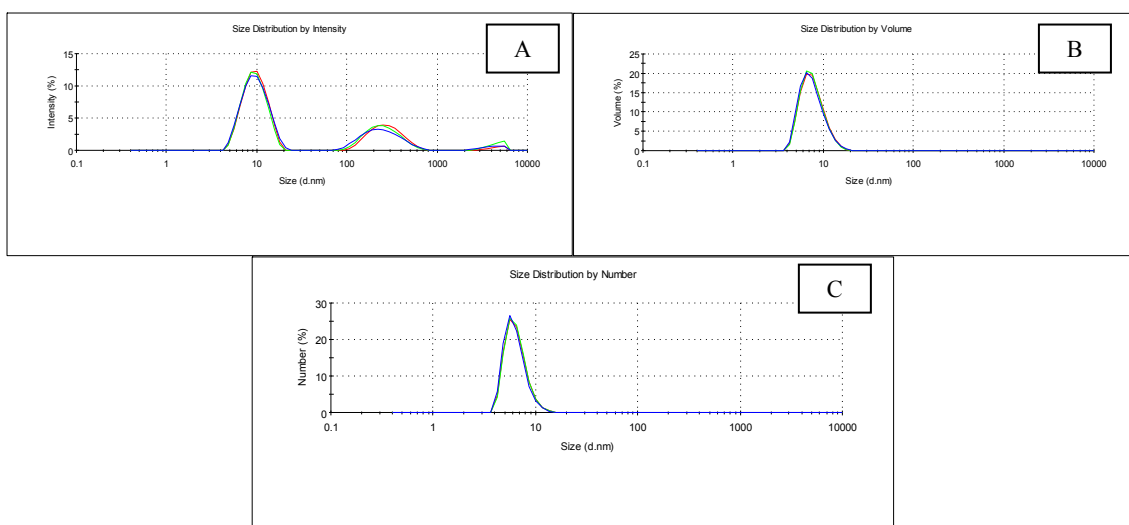


Figure K 5: DLS size distributions by intensity (A), volume (B) and number (C) of 0.1 % (1.5 mM) Triton X-100.

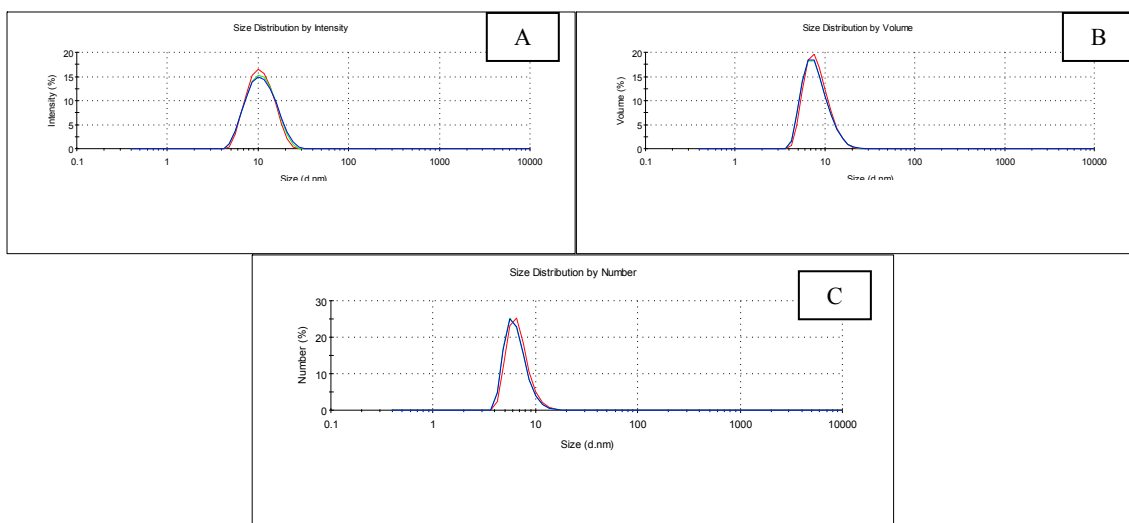


Figure K 6: DLS size distributions by intensity (A), volume (B) and number (C) of 1 % (15 mM) Triton X-100.

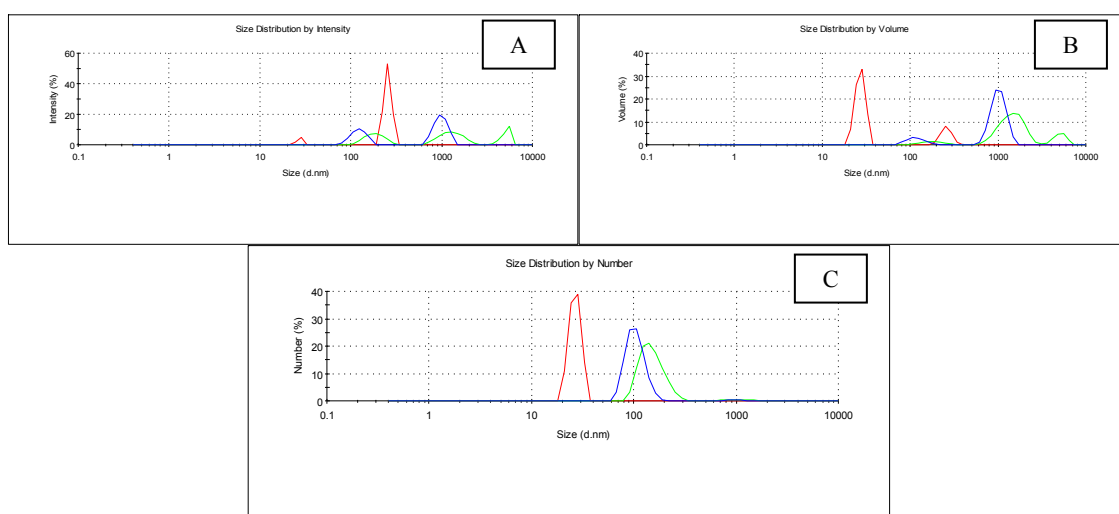


Figure K 7: DLS size distributions by intensity (A), volume (B) and number (C) of 0.0004 % (0.006 mM) Lubrol PX.

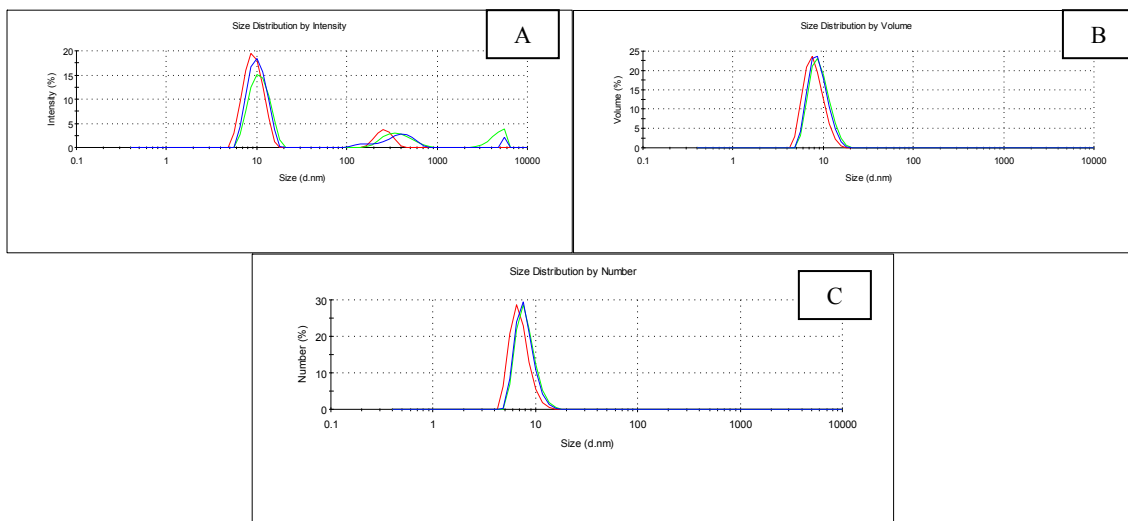


Figure K 8: DLS size distributions by intensity (A), volume (B) and number (C) of 0.1 % (1.7 mM) Lubrol PX.

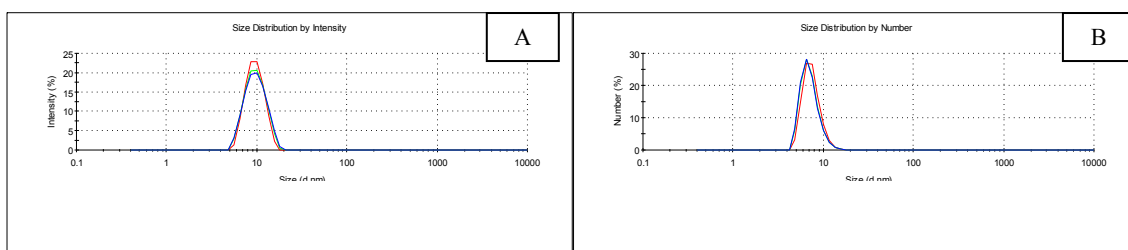


Figure K 9: DLS size distributions by intensity (A), volume (B) and number (C) of 1 % (17 mM) Lubrol PX.

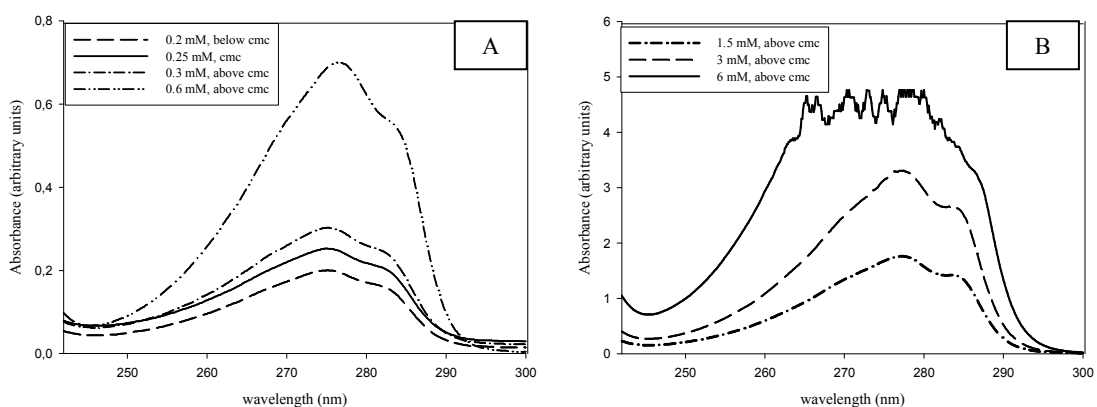


Figure K 10: UV spectra of different concentrations of Triton X-100. A: below the cmc and low concentrations above the cmc, B: High concentrations above the cmc.

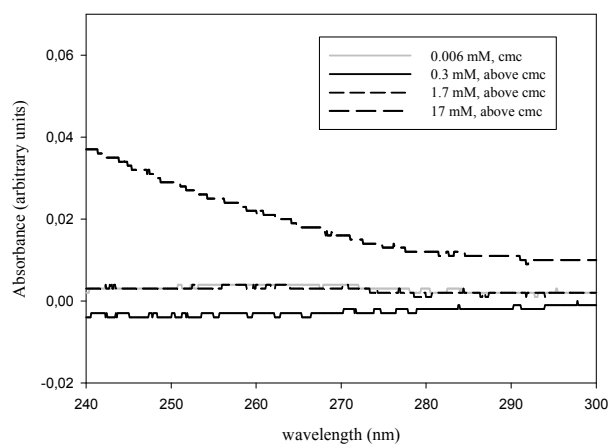


Figure K 11: UV-spectra of different concentrations of Lubrol PX.

CD spectra were recorded for TND buffer, 0.02 % Triton X-100 and 0.1 % Lubrol-PX in TND Buffer. After buffer subtraction the milidegree values were plotted (Figure K 12).

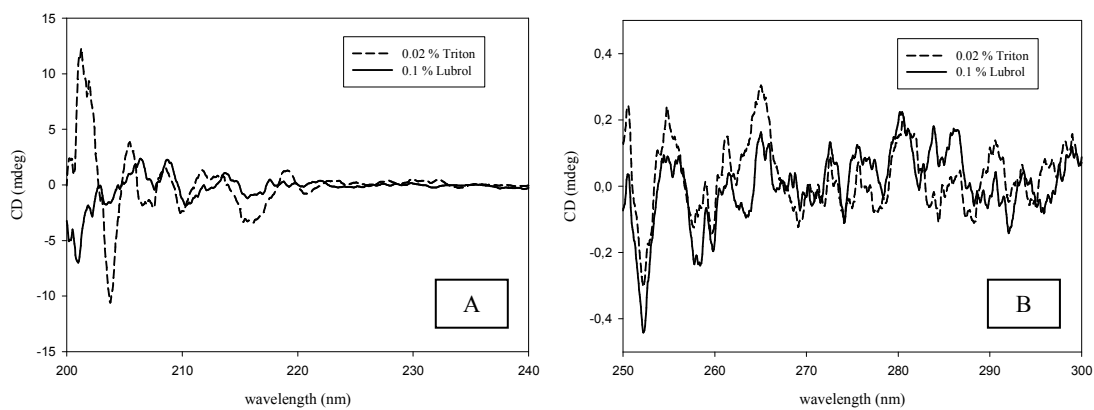


Figure K 12 CD spectra of 0.02 % Triton X-100 and 0.1 % Lubrol-PX in TND buffer, A: Far-UV region, B: Near-UV region.

APPENDIX L

SIZE EXCLUSION COLUMN CALIBRATIONS

- **HiPrep 16/60 Sephacryl S-300 High Resolution Calibration Results**

Standards (Table L1) were prepared in 50 mM Phosphate Buffer pH 7.2, 150 mM NaCl and 200 μ l from each 4 mg/ml solution were combined. Sample was centrifuged and 0.5 ml sample was loaded to S-300 column. Column was run with 50 mM Phosphate Buffer pH 7.2, 150 mM NaCl at 0.5 ml/min and 1 ml fractions were collected (Figure L1).

Void volume of column was calculated from a separate run with 0.5 ml of 1mg/ml blueextran 2000 in 50 mM phosphate 150 mM NaCl pH 8.0 buffer at 0.5 ml/min. The void volume of the column was found 32 ml. Column volume is 120 ml and K_{av} was calculated from $K_{av} = (V_e - V_o) / (V_c - V_o)$; V_o (column void volume), V_c (geometric column volume) and V_e (elution volume).

Table L 1: Standards used in column calibration.

Standards	MW (Da)	Sample amount (mg/mL)
Ribonuclease A	13700	4
Carbonic anhydrase	29000	4
Ovalbumin	43000	4
BSA	67000	4
B-galactosidase	118000	4

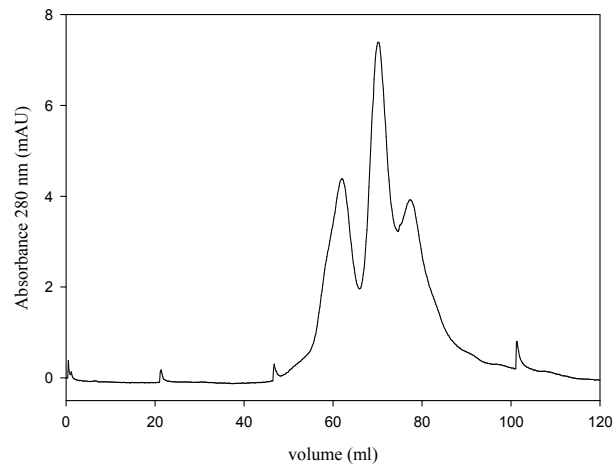


Figure L 1: Elution of standards from S-300 column.

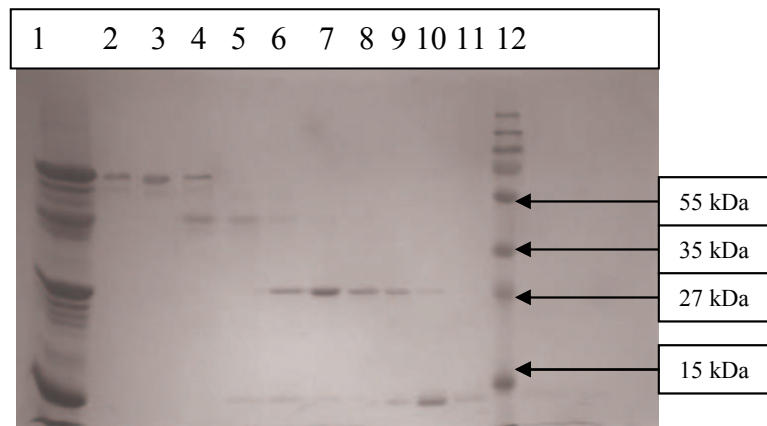


Figure L 2: 12% SDS-PAGE analysis of fractions eluted from S-300 column. Lane 1: column load, lanes 2-11:elution volume; lane 2: 57.5, lane 3: 58.5, lane 4: 61.5, lane 5: 64.5, lane 6: 67.5, lane 7: 69.5, lane 8: 72.5, lane 9: 74.5, lane 10: 77.5, lane 11: 81.5, lane 12: Prestained protein ladder Plus ®. Samples were prepared with 6X SDS loading dye.

The standarts eluted at the indicated volumes in Table L2 and proteins were analyzed by SDS-PAGE (Figure L2). The 118 kDa protein B-galactosidase is not present even in column load, so there was a problem with protein stock.

Table L 2 S-300 column calibration results and calculations. Experimental Log MW calculated from calibration curve equation (Figure L3).

	Range	Ve	Kav	Theoretical		Experimental	
	ml	ml		MW	Log MW	Log MW	MM
BSA	57-61	59	0.306	67000	4.826	4.826	66.988
ovalbumin	61-66	63	0.35	43000	4.633	4.674	47.206
CA	67-74	70	0.43	29000	4.462	4.399	25.061
RNaseA	75-81	78	0.5	13700	4.137	4.158	14.387

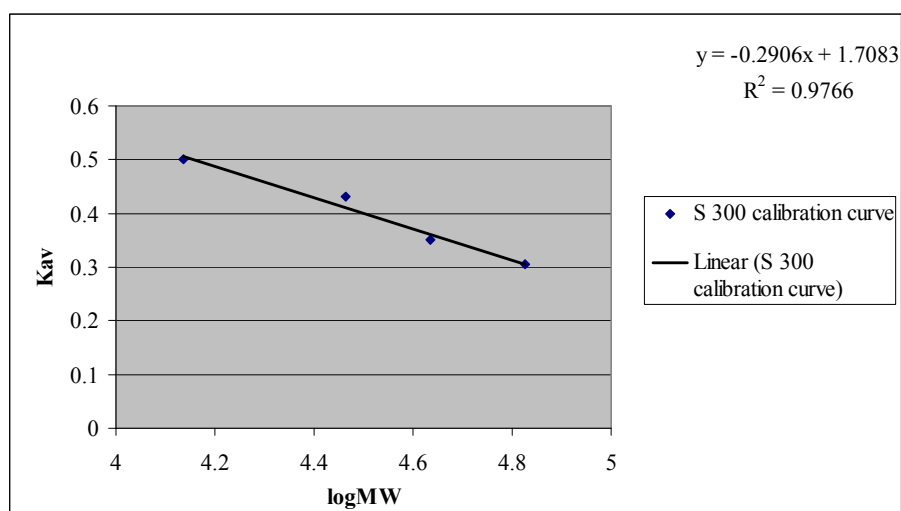


Figure L 3: S-300 column calibration curve

- **HiPrep 16/60 Sephacryl S-200 High Resolution Calibration Results**

Standards (Table L3) were prepared in Buffer D (Table 4.10) and 200 µl from each 4 mg/ml solution were combined. Sample was centrifuged and 0.5 ml sample was loaded to S-300 column. Column was run with Buffer D at 0.5 ml/min and 1 ml fractions were collected (Figure L4).

Void volume of column was calculated from a separate run with 0.5 ml of 1 mg/ml blue dextran 2000 Buffer D at 0.5 ml/min. The void volume of the column was found 32 ml.

Column volume is 120 ml and K_{av} was calculated from $K_{av} = (V_e - V_o) / (V_c - V_o)$; V_o (column void volume), V_c (geometric column volume) and V_e (elution volume).

Table L 3 Standards used in column calibration.

Standards	MW (Da)	Sample amount (mg/mL)
Aprotinin	6 500	3
Ribonuclease A	13 700	3
Carbonic anhydrase	29 000	3
Ovalbumin	43 000	4
Conalbumin	75 000	3

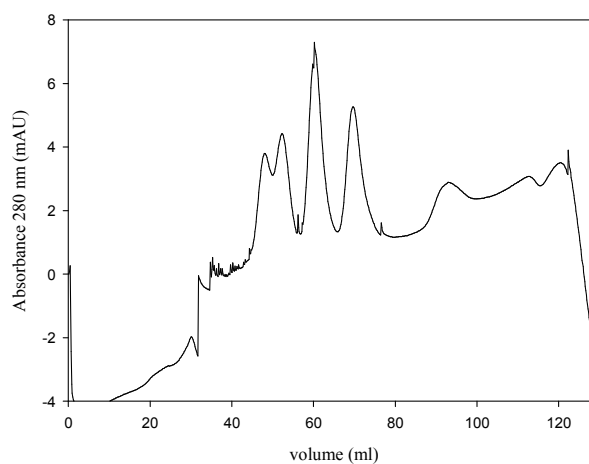


Figure L 4: Elution of standards from S-200 column

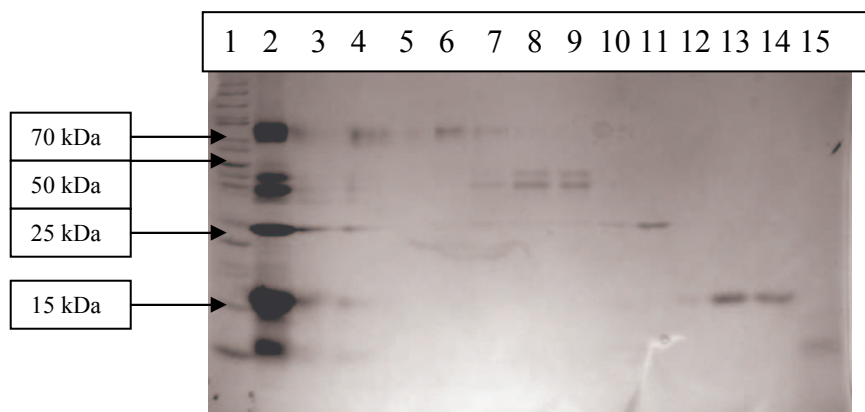


Figure L 5: 12% SDS-PAGE analysis of fractions eluted from S-200 column. Lane 1: Protein ladder®, lane 2: column load, lane 3: overflow, lane 4: 48 ml, lane 5: overflow, lane 6: 49 ml, lane 7: 51 ml, lane 8: 52 ml, lane 9: 54 ml, lane 10: 58 ml, lane 11: 60 ml, lane 12: 67 ml, lane 13: 70 ml, lane 14: 72 ml, lane 15: 92 ml.

The standards eluted at the indicated volumes in Table L4 and proteins were analyzed by SDS-PAGE (Figure L5).

Table L 4: S-200 column calibration results and calculations. Experimental Log MW calculated from calibration curve equation (Figure L6).

	Range	Ve	Kav	Theoretical		Experimental	
	ml	ml		MW	Log MW	Log MW	MM
Conalbumin	46-49	48	0.1818	75000	4.875	4.850	70831
Ovalbumin	51-54	52.2	0.2295	43000	4.633	4.688	48752
CA	58-63	60.2	0.3205	29000	4.462	4.416	26061
RNaseA	67-72	69.7	0.4284	13700	4.137	4.155	14288
Aprotinin	89-98	92.2	0.6841	6500	3.813	3.812	6486

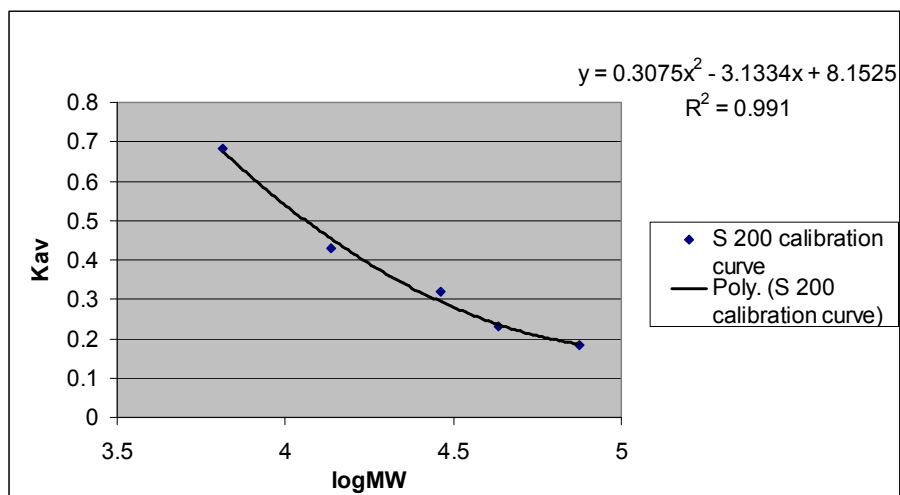


Figure L 6: S-200 column calibration curve

APPENDIX M

CD SPECTRA OF BUFFERS

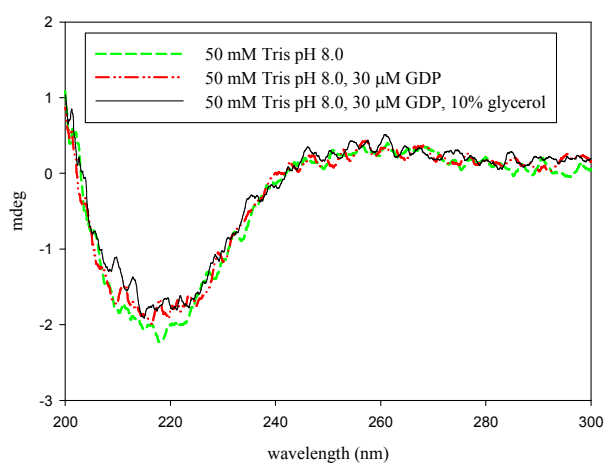


Figure M 1: CD raw data for buffers

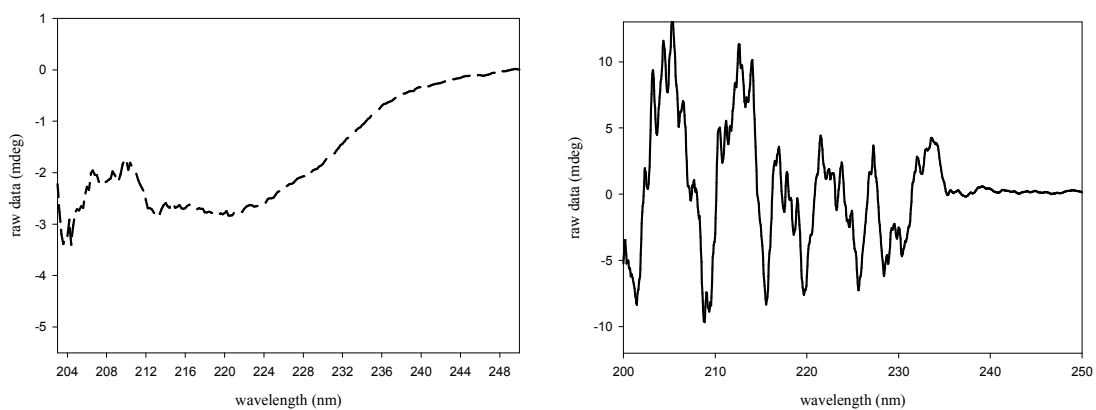
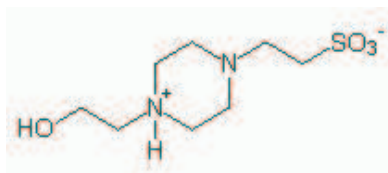


Figure M 2: CD raw data for C48/80, A: spectrum of C48/80 used in assays. B: C48/80 with noisy spectrum. The receptor mimetics compound was tested for noisy spectra before assays.

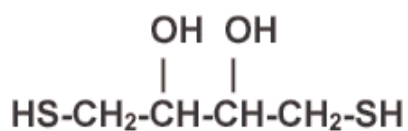
APPENDIX N

CHEMICAL STRUCTURES

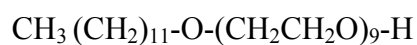
1. HEPES: [4-(2-hydroxyethyl)-1-piperazineethanesulfonic acid, $C_8H_{18}[N_2O_4S]$;
amount in HND; 20 mM



2. DTT: dithiothreitol; amount in HND; 1 mM



3. Lubrol-PX, used 1.7 mM (0.1 %) in affinity purification buffer



4. Triton X-100, used 0.3 mM (0.02 %) in affinity purification buffer

General structure for Octylphenoxypolyoxyethanol is given below, x denotes the length of polyoxyethylene chain. Triton X-100 has on average 9-10 ethylene oxide units

